Genetic and pharmacological exploration of the methyltransferase Ezh2 in different breast cancer subtypes

by

Alison Misa Hirukawa

A thesis submitted to McGill University in partial fulfillment of the requirements of the degree of Doctor of Philosophy

Department of Biochemistry
McGill University
Montreal QC, Canada

April 2017

Table of Contents

Abstract

Over the last decade, several lines of evidence have demonstrated that the transformation of a normal epithelial cell to a malignant phenotype requires the accumulation of multiple events; growing evidence suggests that the acquisition of abnormal chromatin modifications may act in conjunction with genetic aberrations to facilitate dysregulation. Polycomb Group proteins (PcG) are a group of transcriptional repressors that silence genes by modifying chromatin through covalent modification of histones. Enhancer of zeste homology 2 (EZH2) is a PcG protein that, as a part of the multi-protein Polycomb Repressive Complex 2 (PRC2), mediates gene silencing via tri-methylation of lysine 27 on histone 3 ($H3K27me^3$). Interestingly, clinical studies have reported that EZH2 transcript and protein levels are consistently elevated in aggressive human breast carcinomas when compared to normal breast tissue. Immunohistochemical analysis for a range of breast cancer subtypes revealed that high EZH2 levels were associated with shorter disease-free survival and higher probability of death due to breast cancer. The frequent over expression of EZH2 in poor-prognosis breast cancer may indicate that maintaining silencing of key genes through $H3K27me^3$ is important in tumour progression, however, the known spectrum of PRC2 target genes in breast cancer is incomplete and may vary greatly between breast cancer subtypes.

This work has focused on using biologically relevant models of different intrinsic subtypes of breast cancer to explore the necessity of Ezh2 in tumour initiation, maintenance and metastasis. In this work, we identify a mechanism through which EZH2 mediates repression of *FOXC1* to promote metastasis in Luminal B breast cancer. Perhaps most significantly, we demonstrate that pharmacological intervention to inhibit

EZH2 in an immune-competent preclinical mouse model of Luminal B breast cancer completely prevents the formation of distal metastases. We also utilized PDX models, arguably the most relevant existing human preclinical models, to illustrate the significant effect of EZH2 methyltransferase inhibition on spontaneous metastasis in Luminal B but not HER2+ breast cancer. These findings raise the possibility that EZH2 methyltransferase inhibitors may be used in a clinical setting as a neoadjuvant therapy to suppress invasion and metastasis in Luminal B breast cancer patients.

This work also explores the role of Ezh2 in HER2+ breast cancer and the potential for combining Ezh2 methyltransferase inhibition with current HER2 targeted therapy to improve patient response. Loss of Ezh2 in an ErbB2-driven mouse model significantly delayed tumour onset, reduced proliferative capacity of hyperplastic lesions and decreased tumour penetrance from 100% to 20%. The anti-proliferative effects of Ezh2 were recapitulated with pharmacological inhibition of its methyltransferase activity. Interestingly, transcriptional profiling revealed a significant increase in a tumour intrinsic viral-defense signaling pathway, leading us to speculate that modifications can be made to the tumour epigenome that lead to increased vulnerability to detection and destruction by the immune system. Finally, we report that the combination of a pharmacological inhibitor of Ezh2 and HER2 monoclonal antibody synergizes to dampen tumorigenicity in immune competent hosts, increasing apoptosis and the tumour infiltration of cytotoxic immune cell populations.

Taken together, our work demonstrates the context specific function of Ezh2, even within a single disease, and highlights the therapeutic potential of inhibiting PRC2 in breast cancer.

Résumé

Au cours de la dernière décennie, plusieurs éléments de preuve ont démontré que la transformation d'une cellule épithéliale normale en un phénotype malin nécessite l'accumulation d'événements multiples. Il apparaît de plus en plus clairement que l'acquisition d'une modification anormale de la chromatine pourrait agir conjointement avec des aberrations génétiques pour faciliter la dérégulation. Les protéines du Groupe Polycomb (PcG) sont un groupe répresseur de transcription qui rendent silencieux des gènes en modifiant la chromatine à travers une modification covalente des histones. L'amplificateur de l'homologie zeste 2 (EZH2) est une protéine PcG qui, faisant partie du complexe multi-protéines Polycomb Repressive Complex 2 (PRC2), participe à l'inhibition des gènes par tri-méthylation de la lysine 27 sur l'histone 3 (H3K27me^3). Les gènes cibles de la répression opérée par H3K27me^3 incluent des gènes impliqués dans des processus cellulaires fondamentaux tels que la décision du devenir cellulaire, la régulation du cycle cellulaire, la sénescence et la différenciation. De manière intéressante, les études cliniques ont signalé que la transcription Ezh2 et les niveaux de protéines sont constamment plus élevés dans des carcinomes du sein humains agressifs que dans le tissu mammaire normal. L'analyse immunohistochimique pour une gamme de sous-types de cancer du sein a révélé que des niveaux élevés de l'Ezh2 étaient associés à un temps de survie sans récidive plus court et à une plus grande probabilité de décès dû au cancer du sein. La surexpression fréquente de l'Ezh2 dans le cancer du sein à faible pronostic pourrait indiquer que l'inhibition de gènes clés par H3K27me3 joue un rôle important dans la progression de la tumeur. Cependant, le

spectre connu des gènes cibles PRC2 dans le cancer du sein est incomplet et peut varier considérablement entre les différents sous-types de cancer du sein.

Ce travail de recherche s'est focalisé sur les modèles biologiques pertinents de différents sous-types de cancer de tumeurs mammaires afin d'explorer la nécessité de Ezh2 pour l'initiation, la maintenance et le stade métastatique des tumeurs. Nous avons identifié un mécanisme par lequel EZH2 effectue une répression de *FOXC1* pour favoriser le développement des métastases dans les cancers de tumeurs mammaires de sous-type luminale B. Peut-être plus significatif encore, nous avons démontré qu'une intervention pharmacologique pour inhiber EZH2, dans un modèle préclinique murin immuno-compétent de sous-type luminale B de cancer mammaire, prévient complètement la formation des métastases. L'utilisation de modèles PDX (Patient-Derived Xenografts, soit des xénogreffes dérivées de tumeurs de patients) semble être le modèle préclinique humain le plus pertinent pour illustrer l'impact considérable de l'inhibition de l'activité méthyltransférase de Ezh2 sur les métastases spontanées dans les cancers du sein de sous-type luminale B mais pas dans les cancers de type HER2+. La portée de ces résultats suggère que les inhibiteurs de l'activité méthyltransférase de Ezh2 pourraient être utilisés en recherche clinique comme thérapie néoadjuvante afin de supprimer l'invasion et les métastases chez les patientes atteintes d'un cancer du sein de sous-type luminal B.

Nous avons par la suite exploré le rôle de EZH2 dans les cancers du sein de sous-type HER2+ pour évaluer la synergie potentielle de l'inhibition de l'activité methyltransférase de EZH2 en présence d'une thérapie visant HER2 pour améliorer la réponse des patients. La perte de Ezh2 dans le modèle murin de tumeurs mammaires ErbB2 réduit de façon significative le temps de développement des tumeurs, la

prolifération des lésions hyperplasiques ainsi que la pénétrance des tumeurs de 100% à 20%. L'effet anti-prolifératif de Ezh2 est reproduit par l'inhibition pharmacologique de son activité méthyltransférase. De façon intéressante, le profil transcriptionnel révèle une augmentation significative de la voie de signalisation de la défense virale dans la tumeur intrinsèque. Ce résultat nous amène à supposer que les modifications peuvent être effectuées dans l'épigénome de la tumeur créant une vulnérabilité dans la détection et la destruction accomplie par le système immunitaire. Finalement, nous avons identifié que la combinaison pharmacologique de l'inhibition de Ezh2 et d'un anticorps monoclonal de HER2 freine la tumorigenèse et améliore la surveillance immunitaire de leur hôte en augmentant l'apoptose et l'infiltration de cellules immunitaires cytotoxiques.

Considérés dans leur ensemble, ces résultats démontrent le contexte spécifique des fonctions de Ezh2, même dans une seule et même maladie, et souligne le potentiel thérapeutique de l'inhibition de PRC2 dans le cancer du sein.

Acknowledgments

The work was supported by a MICRTP studentship, and a CIHR Systems Biology Training Program studentship.

I would like to thank my thesis supervisor, Dr. William Muller, for allowing me the freedom to pursue the questions I found most interesting. Your belief in the free movement of ideas and materials is an ideal that I hope the scientific community will one day embrace.

I would like to thank the members of my Research Advisory committee, Dr. David Dankort and Dr. Vincent Giguère, who have provided excellent advice and have challenged me during this project.

It has been a pleasure to be a part of the Muller lab and the Goodman Cancer Center, and I thank all those with whom I've crossed paths. Thank you to Chen Ling for your encouragement and advice, to Bin Xiao for your passion for science, to Laura Jones for your friendship and perspective, and to Alexandra Simond for thoughtful conversations, scientific and otherwise. Thank you to Tung Bui for being there for me both in and out of the lab, and as my partner in crime in so many adventures. Thank you to Virginie Sanguin-Gendreau and Dongmei Zuo, for your wisdom and helping me to grow as an individual. I would especially like to thank Dr. Harvey W Smith for being an amazing mentor during my PhD. Your intellect, dedication and talent are impressive, yet you've always had the patience to discuss ideas with me at any moment. You are all talented individuals that I am grateful to call friends, and I look forwards to see what the future holds for each of you.

I would like to thank my parents Linda and Tomio, and my sister Christina, who have always supported me with their enthusiasm, encouragement and a keen interest to understand what I have been working on for the past 6 years.

Merci à Fred. Thank you for your support in absolutely everything I do and for never stifling my creativity. Your confidence in me has shown me the world is my oyster and that together anything is possible.

Preface

This thesis is presented in the traditional format. It is comprised of:

1. Literature Review
2. Results, comprised of three sub-sections addressing different experimental rationale
3. General Discussion that encompasses a discussion of the results, implications, limitations, future directions and brief concluding remarks
4. Experimental Procedures
5. References

Publications arising from this thesis:

Chapter 2.1 is included in the following manuscript:
Alison Hirukawa, Harvey W. Smith, Dongmei Zuo, Catherine R. Dufour, Paul Savage, Nicholas Bertos, Radia M. Johnson, Tung Bui, Guillaume Bourque, Vincent Giguère, Morag Park, and William J. Muller. Targeting EZH2 Reactivates a Breast Cancer Subtype Specific Anti-Metastatic Transcriptional Program. *Under peer review, Nature Communications.*

Chapter 2.2 is included in the following manuscript:
Harvey W. Smith, Alison Hirukawa, Virginie Sanguin-Gendreau, Wafa B'Chir, Catherine Rosa Dufour, Yutian Cai, Dongmei Zuo, Vincent Giguère, Ivan Topisirovic and William J. Muller. An ErbB2/c-Src Axis Drives Mammary Tumorigenesis via Metabolic and Translational Upregulation of Polycomb Repressor Complex 2. *Submitted to Cancer Cell.*

Chapter 2.2 and Chapter 2.3 have been combined to be included the following manuscript:
Alison Hirukawa, Harvey W. Smith, Virginie Sanguin-Gendreau, Dongmei Zuo, Catherine Rosa Dufour, Matt Swiatnicki, Jonn Rennack, Salendra Singh, Vincent Giguère, Vinay Varadan, Lyndsay Harris and William J. Muller. Synergy between $H3K27me^3$ inhibition and HER2 monoclonal antibody therapy to improve therapeutic outcome. *Manuscript in preparation.*

Contributions of Authors

Mouse lines and tissue samples

Dr. Guy Sauvageau provided the $Ezh2^{fl/fl}$ mice (Chapter 2.1, 2.2)
Dr. Alana Welm generated the Luminal B PDXHCI003 (Chapter 2.1)
Dr. Mark Basik and Paul Savage generated the HER2+ PDX GCRC1999 (Chapter 2.1)
Dr. Morag Park and Dr. Nicholas Bertos provided Luminal B patient samples and data
Dr. Sandra O'Toole provided the breast cancer TMA (Chapter 2.3)

Technical assistance

ChIP-Seq analysis was performed by Dr. Johanna Sandoval (Chapter 2.1)
Ingenuity Pathway analysis was performed by Cathy Dufour
Tail vein injections were performed by Vasilios Papvasiliou
Mammary fat pad injections were performed by Cynthia Lavoie
Vasilios Papvasiliou and Cynthia Lavoie performed tumour measurements for the PDX experiments in Chapter 2.1, and the preclinical drug trials in Chapter 2.3
Paraffin-embedding, sectioning and H&E staining was performed by the Goodman Cancer Research Center Histology Core

Figure 2-15: Immunofluorescence staining of human Luminal B tumours was performed by Dongmei Zuo
Figure 2-17: Bioinformatic of TCGA datasets was performed by Dr. Radia M Johnson
Figure 2-23: Staining of human samples was performed by Dr. Dongmei Zuo and quantification of the TMA was conducted by Dr. Sandra O'Toole
Figure 2-26, D: Immunoblot and proliferation assay were done by Dr. Harvey W Smith
Figure 2-38: Tumour volume measurements were performed by Cynthia Lavoie and Vasilios Papvasiliou to ensure that results were blinded. Dr. Harvey W Smith aided with tumour necropsies.
Figure 3-3: Dr. Vinay Varadan performed bioinformatic analysis and generated figure for panel B and C
Figure 3-4: Dr. Dongmei Zuo took the mammospheres images and generated 3D composite images using Volocity Software

List of Figures

List of Abbreviations

4EBP - eukaryotic translation initiation factor 4E binding protein
a.u- arbitrary units
ADC- adenocarcinoma
ADCC- antibody dependent cellular cytotoxicity
Aebp2- Adipocyte Enhancer-Binding Protein
Akt - v-akt thymoma viral oncogene homolog
AML- Acute Myeloid Leukemia
APC - allophycocyanin
ARID1a- AT-Rich Interaction Domain 1A
ATP- adenosine triphosphate
BLBC- basal like breast cancer
BOLERO-3- Breast Cancer Trials of Oral Everolimus-3
BPE - bovine pituitary extract
BRCA1- breast cancer 1
BRDU- bromodioxyuridine
BSA- bovine serum albumin
CCL - Chemokine (C-C motif) ligand
CCR - Chemokine (C-C motif) ligand receptor
CD - cluster of differentiation
CDK- cyclin dependent kinase
ChIP-Seq- chromatin immunoprecipitation followed by sequencing
Chl1- cell Adhesion Molecule L1 Like
CK- cytokeratin
CLEOPATRA- Clinical Evaluation of Pertuzumab and Trastuzumab
CLL - chronic lymphocytic leukemia
CML - chronic myeloid leukemia
Col15a- collagenase 15a
Cre - Cre recombinase
CXCL - Chemokine (C-X-C motif) ligand
CXCR - Chemokine (C-X-C motif) ligand receptor
DAPI- 4',6-diamidino-2-phenylindole
DBC1- deleted in bladder cancer 1
DCIS - ductal carcinoma *in situ*
DFS- disease free survival
DMEM - Dulbecco’s modified Eagle's medium
DMNT- DNA methyltransferase

DMSO- dimethyl sulfoxide
DNA- deoxyribonucleic acid
DOCK8- Dedicator of cytokinesis 8
Dox - doxycycline
dsDNA - double stranded DNA
ECM - extracellular matrix
Eed- embryonic ectoderm development
EGF - epidermal growth factor
EGFR - epidermal growth factor receptor
eIF4A- eukaryotic initiation factor-4A
ELISA- enzyme-linked immunosorbent assay
Elk1- ETS domain-containing protein
EMT - epithelial-mesenchymal transition
ER - estrogen receptor
ErbB2 - v-erbb2 erthroblastic leukemia viral oncogene homolog 2
ERV- endogenous retroviral element
ES - embryonic stem cell
EtOH- ethanol
EZH1- enhancer of zeste 1
EZH2- enhancer of zeste 2
FACS- fluorescence associated cell sorting
FBS- fetal bovine serum
FcRγ – fragment crystallizable receptor gamma
FDA- Food and Drug Administration
FGF - fibroblast growth factor
FGFR - fibroblast growth factor receptor
FISH - fluorescent in situ hybridization
FITC - fluorescein isothiocyanate
FOX- forkhead box
FVB - friend virus B-type
Fwd- forwards
GAPDH - glyceraldehyde 3-phosphate dehydrogenase
GFP - green fluorescent protein
GLI2 - GLI Family Zinc Finger 2
GO - gene ontology
Grb2 - growth factor receptor bound protein 2
GSEA - gene set enrichment analysis
H&E - hematoxylin and eosin
H2A- histone 2 A
H3K27me^3- trimethylation of lysine 27 on histone 3

H3K9me^3- trimethylation of lysine 9 on histone 3
HDAC- histone deacetylase
HER2 - human epidermal growth factor receptor 2
HIF1 - hypoxia-inducible factor 1
HMT- histone methyltrasnferase
HOX- homeobox
HR- hazards ratio
HR+- hormone receptor positive
HRE - HIF response element
Hsp60- heat shock protein 60
IF - immunofluorescence
Ifnα - interferon alpha
Ifnβ - interferon beta
Ifnγ - interferon gamma
IGF - insulin-like growth factor
IGFBP - insulin-like growth factor binding protein
IGFR - insulin-like growth factor receptor
IgG1- immunoglobulin 1
IGV- integrative genome viewer
IHC - immunohistochemistry
IL - interleukin
ILC- invasive lobular carcinoma
i.p- intra-peritoneal
IPA- Ingenuity pathway analysis
IRES - internal ribosome entry site
JAK- janus kinase
JAZF1- Juxtaposed with another zinc finger protein 1
Jmjd3- jumonji domain 3
KRAS- V-Ki-ras2 Kirsten rat sarcoma viral oncogene homolog
Lin- lineage
lncRNA- long non-coding RNA
LPS- lipopolysaccharide
LTR - long terminal repeat
mAb- monoclonal antiboey
MAPK - mitogen activated protein kinase
MAT- *S*-adenosylmethionine synthetase enzyme
MAVS- Mitochondrial antiviral-signaling protein
MBT- malignant brain tumor
MDS- Myelodysplasia syndrome
MEK- Mitogen-activated protein kinase kinase

MMTV - mouse mammary tumour virus
MPN- Myeloproliferative neoplasm
MPNST- malignant peripheral nerve sheath tumours
MSigDB- molecular signature database
mTOR- mammalian target of rapamycin 1
MTS - 3-(4,5-dimethylthiazol-2-yl)-5-(3-carboxymethoxyphenyl)-2-(4-sulfophenyl)-2Htetrazolium
MYC - myelocytomatosis
NDL - Neu deletion
Neu - neuro/glioblastoma derived oncogene homolog
NFkB - nuclear factor kappa B
NGS- next generation sequencing
NIC - Neu-IRES-Cre
NK - natural killer cell
NKT - natural killer T cell
nm- nanometers
NOD-SCID- non-obese diabetic severely combined immunodeficiency
OS- overall survival
p16/INK4A- cyclin-dependent kinase inhibitor 2A
PAM50- prediction of microarray 50
PBS- phosphate buffered solution
PCL- polycomb like
pCR - pathological complete response
PCR - polymerase chain reaction
PD-1- programmed Cell Death 1
PD-L1- programmed Cell Death 1 ligand
PDX- patient derived xenograft
PE - R-Phycoerythrin
pHGG- pediatric high grade gliomas
PI-MEC- parity identified mammary epithelial cells
PI3K - phosphatidylinositol 3'-kinase
PLZF - promyelocytic Leukaemia Zinc Finger
PR - progesterone receptor
PRC1- Polycomb repressive complex 1
PRC2- Polycomb repressive complex 2
PTB- phosphotyrosine binding
PTEN - phosphatase and tensin homolog deleted on chromosome 10
PWWP- Pro-Trp-Trp-Pro domain
PyVMT - polyomavirus middle T antigen
qRT-PCR- quantitative real time PCR

Rag- recombination activating gene
Rb- retinoblastoma
RbAp46/48- Retinoblastoma protein associated protein 46/48
REST- RE1 Silencing Transcription Factor
Rev- reverse
Rgma- repulsive guidance molecule A
RNA- ribonucleic acid
RPM- revolutions per minute
RTK - receptor tyrosine kinase
rtTA - reverse tetracycline transactivator
RXR- retinoid x receptor
SAH- *S*-adenosyl homocysteine
SAM- *S*- adenosyl methionine
SCC-squamous cell carcinoma
S.E.M- standard error of the mean
SET- Su(var)3-9, Enhancer-of-zeste and Trithorax
SH2- src homology 2
ShcA- SHC-Transforming Protein A
SLC35F2- solute Carrier Family 35 Member F2
SLC9a9- solute Carrier Family 9 Member A9
Slfn5- schlafen Family Member 5
SMARCB1- SWI/SNF Related, Matrix Associated, Actin Dependent Regulator of Chromatin
Src- sarcoma
STAT- signal transducer and activator of transcription
SUZ12- suppressor of zeste 12
SWI-SNF- SWItch/Sucrose Non-Fermentable
T-DM1- Ado trastuzumab emtasine
TCGA- the cancer genome atlas
TDLU- terminal ductal-lobular units
TE- tris-EDTA
TEB - terminal end bud
TetO - tet-operator
T_H1-T help type 1
TNF- tumour necrosis factor
TUNEL - terminal deoxynucleotidyl transferase dUTP nick end labeling
UTX- ubiquitously transcribed tetratricopeptide repeat
VEGF - vascular endothelial growth factor

Original Contributions to Knowledge

1) We demonstrate that loss of Ezh2 in a transgenic mouse model of Luminal B breast cancer significantly delays tumour onset. This is the first report of Ezh2 ablation impeding breast cancer initiation, *in vivo*. We then show that loss of Ezh2 significantly impairs spontaneous metastasis and that this is partially due to the reactivation of FoxC1.

2) We show that use of a pharmacological inhibitor of Ezh2 methyltransferase activity in vitro and *in vivo*, recapitulates what was observed with genetic ablation of Ezh2, activating FoxC1 to impair tumour invasiveness and their ability to colonize the lung. We then demonstrate that the anti-metastatic EZH2-FOXC1 axis is breast cancer subtype specific, thus raising the possibility that EZH2 methyltransferase inhibitors may be used in a clinical setting as a neoadjuvant therapy to suppress invasion and metastasis in Luminal B breast cancer patients.

4) We are the first to show that ablation of Ezh2 in a mouse model of HER2+ breast cancer significantly impairs tumour initiation and penetrance. We also show that inhibition of Ezh2 methyltransferase activity impairs cellular proliferation of HER2+ cells and that this may, in part, be due to modulation of the ability of the tumour avoid detection of the immune system.

5) We demonstrate that the inhibition of Ezh2 methyltransferase activity synergizes with HER2 monoclonal antibody therapy to dampen tumorigenicity and propose a novel combination therapy to address the intratumour heterogeneity or HER2 levels.

1 Literature Review

1.1 Incidence of Breast Cancer

Breast cancer is the most common cancer amongst women, with 1 in 9 Canadian women afflicted during her lifetime, and is one of the leading causes for cancer related death, second only to lung cancer(1). While the Canadian Breast Cancer Foundation cites the current overall 5-year survival rate for breast cancer to be 87%, this statistic does not consider the biological complexity of breast cancer. Breast cancer is a heterogeneous disease comprised of several subtypes that possess distinct molecular profiles and can also be distinguished through various histopathological criteria. Importantly, different subtypes are associated with different patient outcomes and therapeutic strategies to achieve the best possible outcome.

1.2 Histopathological Subtypes of Breast Cancer

Most breast cancer cases begin as ductal carcinomas originating from epithelial cells in the mammary ducts or lobules(2). The proliferation of luminal cells gradually fills the ductal lumen and is contained by the basement membrane to form what is clinically designated as ductal carcinoma *in situ* (DCIS). Following a breach of the basement membrane, these cells become invasive and can enter the vasculature of the lymphatic system to disseminate and colonize a distal organ, a process known as metastasis. Based on histological parameters visualized by light microscopy, most invasive breast cancers are classified as invasive ductal carcinoma *in situ* (approximately 55%) or invasive lobular carcinomas (ILC) (approximately 5-10%).

The clinical evaluation of several other parameters can be predictive of prognosis and informative to patient care. These include tumour size, tumour grade, with higher grade tumours associated with aggressive disease and characterized by poorly differentiated cellular morphology, and tumour stage. Tumour stage indicates the extent to which the disease has progressed through the body, with patients with localized disease faring better than those whose disease has spread (metastasized) to secondary sites. For patients who do not present with distal metastases, evaluation of the sentinel lymph nodes adjacent to the breast for tumour cells can also provide further insight into disease progression.

The immunohistochemical detection of specific markers on tumour biopsies is also an integral component of breast cancer diagnosis. These markers include the proliferative marker Ki67, Human Epidermal Growth Factor Receptor (HER2) and the hormone receptors Estrogen Receptor (ER) and Progesterone Receptor (PR). Presence or exclusion of the latter three markers plays a significant role in dictating patient care.

Tumour biopsies that are positive for nuclear staining of estrogen and progesterone receptor are known as Hormone receptor positive (HR+), and constitute the majority of breast cancer cases (75%) (3). While a small subset of these are also positive for HER2, most HR+ patients are negative for HER2 staining(4). HR+/HER- cases have the most optimistic clinical outcome, and are associated with small low grade tumours that are less likely to recur or metastasize distally. These patients receive endocrine therapies, such as tamoxifen(5, 6). HR+/HER2- patients in the advanced stages of disease typically receive aromatase inhibitors, sometimes in combination with everolimus, which inhibits mTOR, a serine/threonine kinase central to cell growth and metabolism. For women with HR+/HER2+ breast tumours, endocrine therapy can be augmented with cyclin dependent kinase inhibitors targeting CDK4/6 to stall the cell cycle, and aromatase inhibitors(7, 8). Breast cancer cases that lack HR and HER2 staining are known as the 'triple negative' subtype. These cases represent approximately 17% of breast cancer bases and are the poorest prognosis(4, 9). The current standard of care for triple negative breast cancer involves cytotoxic chemotherapy, such as anthracycline and taxane. HER2+ patients represent 15-20% of total breast cancer cases and correlate with poor outcome. As subsequent studies confirmed HER2 to be an oncogene that could be over expressed or amplified in patients, immunohistochemical staining and fluorescence in situ hybridization (FISH) are often employed in succession to confirm HER2 positivity(10-12). HER2+ patients receive HER2 targeted therapies, which will be elaborated on in the following section.

1.3 Intrinsic Molecular Subtypes of Breast Cancer

The heterogeneity of breast cancer can also be further refined at the genomic level. With improvements to microarray technologies, large scale unsupervised hierarchical clustering of gene expression data has revealed that breast cancer can be further stratified by unique transcriptional signature. The initial molecular taxonomy of breast cancer by Perou and colleagues identified four intrinsic molecular subsets based on 496 genes that segmented breast cancer into luminal-like, basal-like, HER2-enriched and normal-like (13). Subsequent studies have further distilled the luminal-like into luminal A and B and identified a novel subtype termed claudin-low(14, 15). The original 496 genes have since been streamlined to 50 genes, known collectively as the Prediction of Microarray 50 (PAM50). The PAM50 signature can be employed to classify patients into Luminal A, Luminal B, HER2-enriched or basal-like breast cancer. Interestingly, each subtype is associated with varying risk for progression, response to treatment and survival outcome(16-18). Thus, while molecular subtyping is still primarily used in a research context, diagnostic products are beginning to be commercialized to further inform clinical decisions.

Along with the genetic mutational profile, the tumour cell of origin has also been proposed to be an important determinant in breast cancer heterogeneity (19, 20). Comparisons between the molecular profiled of different intrinsic subtypes of breast and different progenitors of the mammary gland have revealed distinct progenitor cells might give rise to different subtypes (15, 21). For example, the expression profile of the claudin-low breast cancer subtype is most closely aligned with mammary stem cells, while the luminal progenitor population is closely aligned with basal-like breast cancer (22). The cell of origin for both Luminal B and HER2+ breast cancer is still unclear.

1.3.1 Luminal A and B

Most breast cancer cases (between 40-60%) are Luminal A, and this has the best prognosis of all the subtypes due to its low rate of relapse due to its responsiveness to hormone receptor therapies. Luminal A breast cancer is characterized by enrichment for genes associated with the luminal identity, lower

proliferative index and a lower rate of mutations, across the genome compared to other subtypes (23, 24). In contrast, Luminal B cases have a higher expression of proliferative programs, lower expression of markers of luminal identity such as *FOXA1*, lower expression of hormone receptor related genes, and increased incidence of *TP53* mutations. Comprising 15% of breast cancer cases, Luminal B cases are considered to have a poor prognosis.

1.3.2 Basal-like

Basal-like breast cancer are characterized by high expression of genes reflective of basal cell identity, such as *FOXC1* and Keratin 5. They comprise 10-20% of breast cancer cases, are highly proliferative and due to their genomic instability display an abundance of mutations and chromosomal alterations across the genome. Approximately 80% of basal-like breast cancers are HER2-, ER-,PR- and are considered very poor prognosis, characterized by an elevated risk of metastasis and short disease free survival (25, 26).

1.3.3 HER2-Enriched

HER2-enriched tumours comprise 15-20% of cases and show increased levels or amplification of *HER2* (also referred to as *ERBB2*). These tumours are also considered poor prognosis, with elevated risk of metastasis, high levels of mutation across the genome, and high proliferation (13, 18). *HER2* (*ERBB2*) encodes for a receptor tyrosine kinase that homo or heterodimerizes with HER family members to elicit downstream signaling pathways that allow for cell growth, survival and differentiation such as the PI3K/Akt and the Ras/Raf/MEK/MAPK pathways. The identification of HER2 as a proto-oncogene led to the exploitation of its intracellular and extracellular features to develop targeted therapies that selectively perturb tumour cells. Inhibitors targeting the intracellular tyrosine kinase activity of HER2, such as lapatinib, are typically administered to women with advanced disease that has progressed following treatment with previous therapies while monoclonal antibodies (mAb) targeting the extracellular

domain of HER2, in combination with chemotherapy, constitute the standard of care for both early and metastatic HER2+ breast cancer.

1.3.3.1 HER2 monoclonal antibodies (mAbs)

The first HER2 mAb approved for medical use was trastuzumab, a humanized mAb that targets an epitope located near the juxta-transmembrane domain of HER2. Trastuzumab was engineered by inserting antigen binding loops of murine HER2 antibody 4D5 into a human IgG1 framework (27, 28). Several clinical trials have illustrated its efficacy of, as evidenced by improved overall survival (OS) in metastatic breast cancer(29, 30) and improved disease free survival (DFS) in early breast cancer(31, 32). While the prevention of HER2 homodimerziation plays a role in its mechanism of action(33), several other anti-tumour mechanisms have also been proposed, including inhibition of downstream signaling pathways and cell cycle arrest (34-36), induction of apoptosis(37) and inhibition of angiogenesis(38). Recently, the importance of HER mAb mediated anti-tumour immunity has also been demonstrated to be an essential mechanism of action (to be reviewed in greater detail in the following sections).

Currently, the US Food and Drug Administration (FDA) has approved two other HER2 mAbs for treatment of HER2+ metastatic breast cancer. Unlike trastuzumab, pertuzumab binds to the dimerization arm of HER2 and was developed to inhibit HER2 heterodimerization (39). Ado Trastuzumab emtasine (T-DM1) is an antibody drug conjugate in which trastuzumab is linked to a potent microtubule inhibitor. Several clinical trials have demonstrated improved tolerability of T-DM1 compared with current standard therapies and assessed its potential as a frontline therapy for HER2+ breast cancer. The EMILIA trial demonstrated improved PFS and OS with T-DM1 in patients with locally advanced or metastatic breast cancer. However, its use as a frontline drug against HER2+ cancers is unclear, as recent updates from the MARIANNE trial illustrated that T-DM1 did not improve PFS beyond the current standard of care(40).

1.3.3.2 The role of the immune system in HER2mAb therapy

Although HER2 mAbs were initially designed with the aim of interfering with HER2 dimerization, it has become apparent HER2 mAbs are also functioning as an immunotherapy (41, 42). By the virtue of being a monoclonal antibody, HER2 mAbs can engage the immune system through a process known as antibody dependent cellular cytotoxicity (ADCC). ADCC is a mechanism of cell mediated immune defense whereby tumour cells bound by an antibody are targeted for destruction by immune cells such as Natural Killer (NK) cells and macrophages. Studies in animal models have revealed that the therapeutic activity of anti-HER2 mAbs depends on the presence of Fcγ receptors (FcγR) on NK cells and macrophages(41, 43). The adaptive immune system has also been demonstrated as an important contributor to the effects of trastuzumab, as HER2+ tumours in *Rag* $^{-/-}$ (T cell deficient) mice do not respond to a murine version of trastuzumab (44, 45).

1.3.3.3 HER2 Abs in combination with other therapies

Clinically, HER2 mAbs are not used as a monotherapy but rather in the combination with other therapies. The most common combination has been in conjunction with chemotherapy, as several clinical trials have illustrated the superiority of this combination(46-48). Despite the strong affinity of trastuzumab for HER2, many patients are *de novo* resistant or have disease progression within one year of treatment (46). Extensive studies both *in vitro* and *in vivo* have proposed several mechanisms of trastuzumab resistance, leading to a therapeutic strategy in which trastuzumab is combined with therapies targeting some of the identified resistance mechanisms. Proposed major resistance mechanisms include the activation of Src family kinases(49), IGFR(50, 51) and activation of alternative receptor tyrosine kinases such as c-Met(50). Furthermore, as patients only require 10% of tumour cells to stain for HER2 to be considered HER2+, high intra-tumour heterogeneity might also lead to tumours becoming refractory to HER targeted therapies, once the HER2+ cells have been eliminated(52).

To improve the blockage of signal transduction through HER2 and its dimerization partners(53, 54) dual treatment with trastuzumab and pertuzumab two large scale clinical trials, CLEOPATRA(55, 56) and NEOSPHERE (31) were conducted and demonstrated superiority to monotherapy. Activation of a serine threonine kinase that mediates protein synthesis, mammalian target of rapamycin (mTOR) has also been shown to be a mechanism of resistance (57). Considering this, the BOLERO-3 clinical trial combined the mTOR inhibitor Everolimus with Trastuzumab and chemotherapy agents in and determined that the combination significantly prolonged progression free survival in trastuzumab-resistant HER2+ breast cancer patients (58). Resistance via increased Akt activity through the loss of PTEN(59, 60), was addressed in the phase I Neo-PHOEBE in which Trastuzumab was combined with BKM120, an oral pan PI3K inhibitor(61). However, the trial was terminated prematurely due to elevated toxicity.

1.4 The Metastatic Cascade

Despite the availability of different treatment options, the outcome for patients whose disease has spread to other organs is poor, as most patient mortality is due to metastasis to distal organs, not the primary tumour itself. For breast cancer patients, metastatic tumour cells are found in the lymph nodes, brain, bone and lung(62). Metastasis is a highly complex process; tumour cells that successfully achieved dissemination and colonization of a distal organs have evaded numerous barriers. The acquisition of characteristics necessary for metastasis are hypothesized to arise from the accumulation of mutations in cellular populations within a primary tumour. Thus, only a select number of cells from the primary tumour cells are fit enough to undergo metastasis (63).

Like tumour initiation, cellular invasion and metastatic dissemination occurs in a multi-step process. The structural of normal epithelium acts as a barrier to invasiveness, and must first be overcome by tumour cells. Local invasion begins with tumour cells breaching the basement membrane, a component of the extracellular matrix that facilitates structural organization to epithelial tissues. This active proteolysis is typically

driven my matri-metalloproteinases (MMPS), However, for individual cells to dissociate from their neighbors, loss of adherens and tight junctions which must occur, in a process known as EMT((64). EMT programs are orchestrated by a set of well characterized transcription factors including Slug, Snail, ZEB1 and ZEB2. These factors act to repress epithelial markers such as E-cadherin and induce markers of a mesenchymal state (65). With respect to morphology, tumour cells can adopt different cellular programs to facilitate invasion in response to changing environments. These include the 'mesenchymal' and 'amoeboid' invasion programs, each defined by distinct effector proteins (66).

Molecular changes also underlie the ability of tumour cells to traverse the cellular barriers of tumour associated blood vessels. These changes can be mediated by signals from the stromal microenvironment. Following successful intravasation, cancer cells enter the circulation and must withstand several stresses to reach distal organs. Without adhesion and the ECM components, epithelial cells can undergo apoptosis by anoikis. Furthermore, in the circulation they are exposed to hemodynamic shear forces and detection from the immune system.

Once localized to the vasculature of distal organs, tumour cells must extravasate through blood vessels to the parenchyma of a distal tissue. The metastatic cascade is completed upon colonization, proliferation and growth into metastatic lesions in the distal organ(67, 68).

1.5 Genetically Engineered Mouse Models of Breast Cancer

Genetically engineered mouse models have been tremendously informative to our understanding of the molecular mechanisms underlying breast cancer. Transgenic mouse models not only have the benefit of allowing the study of tumour progression and metastasis within the biologically relevant context of a competent immune system, but also enable spatial and temporal control of target genes. The latter two features of control are conferred using tissue specific promoters to facilitate conditional expression, conditional gene targeting technology such as the Cre/LoxP system, and the use of a pharmacologically inducible gene expression system.

1.5.1 Tissue Specific Promoters

Tissue specific promoters confer the ability to express or ablate transgenes in the desired cellular components of a specific tissue, which is particularly useful if manipulating a gene of interest in the germline tissue is embryonically lethal. The Mouse Mammary Tumour Virus long terminal repeat (abbreviated as MMTV-LTR) is a tissue specific promoter that allows for expression or ablation in the mammary epithelium. MMTVLTR is not an endogenous murine promoter, but was discovered as a component of the Mouse Mammary Tumour Virus (MMTV) a milk-transmitted retrovirus which is the causal agent of spontaneous tumours in inbred mice, passed from nursing mothers to their pups(69). Expression from the MMTV promoter begins at 3-4 weeks of age, and it is active in both lactating and virgin mammary glands(70).

*1.5.2 Cre-recombinase/*loxp *System*

The cre-recombinase/*loxP* system is derived from a bacteriophage genetic integration system which has been experimentally co-opted to allow for targeted deletion of a specific gene of interest. In this system, a conditional allele is generated by inserting 34-base pairs palindromic sequences known as the *loxP* around multiple exons of the gene of interest (71). In the presence of the cre recombinase enzyme, the *loxP* sites recombine, allowing for excision of the flanked genomic regions and ablation of the gene of interest. The cre-recombinase/*loxP* system can also be implemented to visually track cells that have expressed cre recombinase using *loxP* flanked stop cassettes. In this system, transcription of reporter genes such as green fluorescent protein (GFP) is blocked by the stop cassettes; presence of cre recombinase excises the stop cassette, driving expression of the reporter gene.

1.5.3 Tetracycline-inducible Promoter

An additional level of temporal control can be conferred by the addition of a tetracycline inducible system. This method can be advantageous if transgene expression or target gene ablation is detrimental to normal development, because it

allows for induction at a physiologically appropriate age. In this system, a reverse tetracycline transactivator (rtTA) transgene is driven by a given tissue specific promoter. Upon supplementation of food or water with doxycycline (a tetracycline derivative) rtTA binds to a tetracycline operon (TetO) in the promoters of appropriately designed transgenes, thus driving their expression.

1.5.4 The murine mammary gland as a model of the adult breast

The anatomy of the murine mammary gland is surprisingly like the human breast, and this similarity has helped to form the basis for using mice as the primary model for human breast cancer. The human breast is comprised of stromal and glandular tissues that form radially organized lobes of mammary ducts, each comprised of several milk producing terminal ductal-lobular units (TDLU) (72), with the equivalent structure in the mouse being the terminal end bud (TEB). In both species, mammary glands are hormone sensitive following the completion of development, and contain multiple progenitor cell populations with different capacities for differentiation. Specific cell surface markers have been identified to distinguish these different progenitor cell populations in the mammary gland and have been of great interest to the field of breast cancer, as disease subtype is dictated by both the genetic/genomic profile of the tumour but also the cell of origin (Figure 1-X).

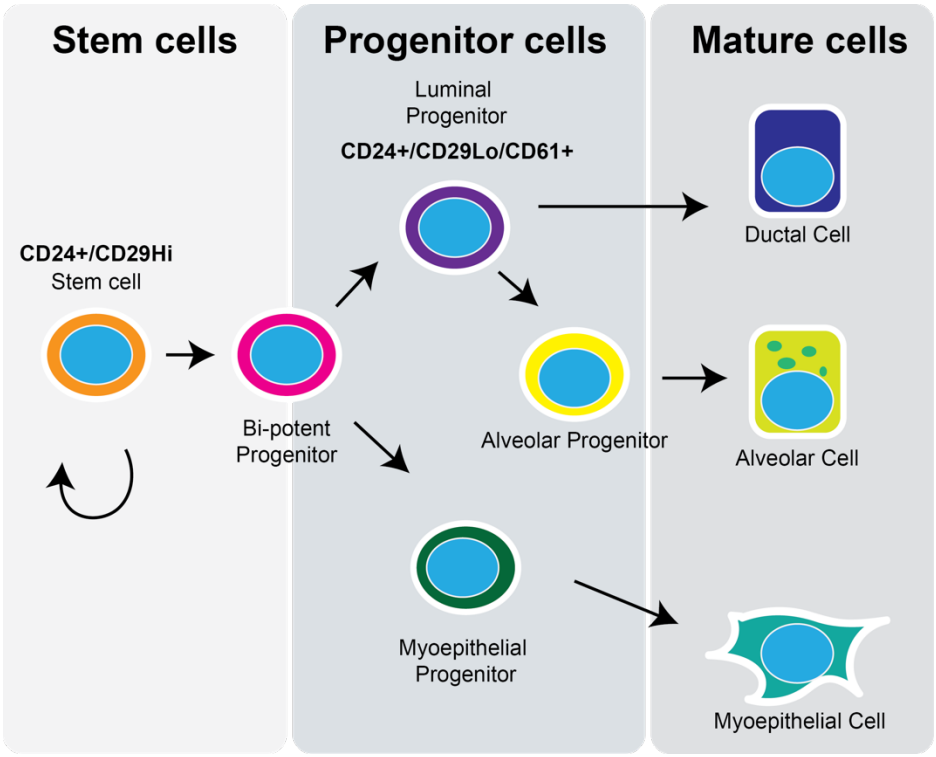

Figure 1-1. Cellular hierarchy of the mouse mammary gland

1.5.5 Neu-driven model reflective of HER2+ luminal breast cancer

Mouse models of tumorigenesis have been generated through the expression of various forms of *Neu*, the rat orthologue of *HER2* (also referred to as *ERBB2*), driven by the MMTV promoter (73). The MMTV-NDL model constitutively expresses a *Neu* mutation (NDL2.5) which was first identified as a somatic mutation that arose in the transgene of MMTV-Neu tumours (74, 75). The mutation creates an imbalance of cysteine residues in the extracellular region of the receptor, promoting homo dimerization and subsequent activation of the receptor (76). To determine the role of a specific gene of interest within the context of the ErbB2 transgenic models, a more recent model features coupled expression of NDL2.5 and Cre recombinase in a bicistronic construct with an internal ribosome entry site (IRES)(77). This is referred to as the MMTV-NIC model. This system allows for ablation of the gene of interested in a cell transformed by ErbB2; Cre recombinase mediated excision of *loxP*-flanked alleles occurs only in the ErbB2-driven mammary epithelial tumour cells. The potent

transforming potential of ErbB2 in the mammary epithelium is thought to be due to its capacity to couple with a number of Src homology 2 (SH2) and phosphotyrosine binding (PTB) domain-containing signaling molecules (8). Following activation of the intrinsic tyrosine kinase activity of ErbB2, specific phosphotyrosine residues within ErbB2 provide binding sites for several such adaptor proteins and signaling effectors including ShcA, Grb2, Src family kinases and the p85 subunit of the phosphadityl inositol 3' kinase (PI-3K) (9). Mouse models driven by activated ErbB2 (reviewed in 1.5.2.1) exhibit solid comedo-adenocarcinoma histology which closely resembles human DCIS(72, 78) (**Figure 1-2A**).

1.5.6 The Inducible Polyoma Virus Middle T model of Luminal B Breast Cancer

Another transgenic mouse model that has been instrumental to our understanding of how tyrosine kinase signaling can direct cellular transformation is the Polyoma Virus Middle T (PyVmT) model, in which PyVmT expression, under the control of the MMTV promoter, is restricted to the mammary epithelium. PyVmT is a membrane anchored protein encoded by the small DNA polyoma virus. While not expressed in human breast cancer tumors, PyVmT functions as a potent oncogene in the mouse because it is able to bind to several key molecules that activate signal transduction pathways driving cell growth and survival, in a manner analogous to the function of receptor tyrosine kinases (10). Although it lacks intrinsic tyrosine kinase activity, PyVmT recruits Src family kinases which phosphorylate specific tyrosine residues that form docking sites for many of the same SH2- and PTB domain-containing proteins that are recruited by ErbB2, including Grb2, Shc and p85. Like ErbB2, mammary specific expression of the PyVmT oncogene results in the rapid induction of metastatic mammary tumors (11) (**Figure 1-2B**).

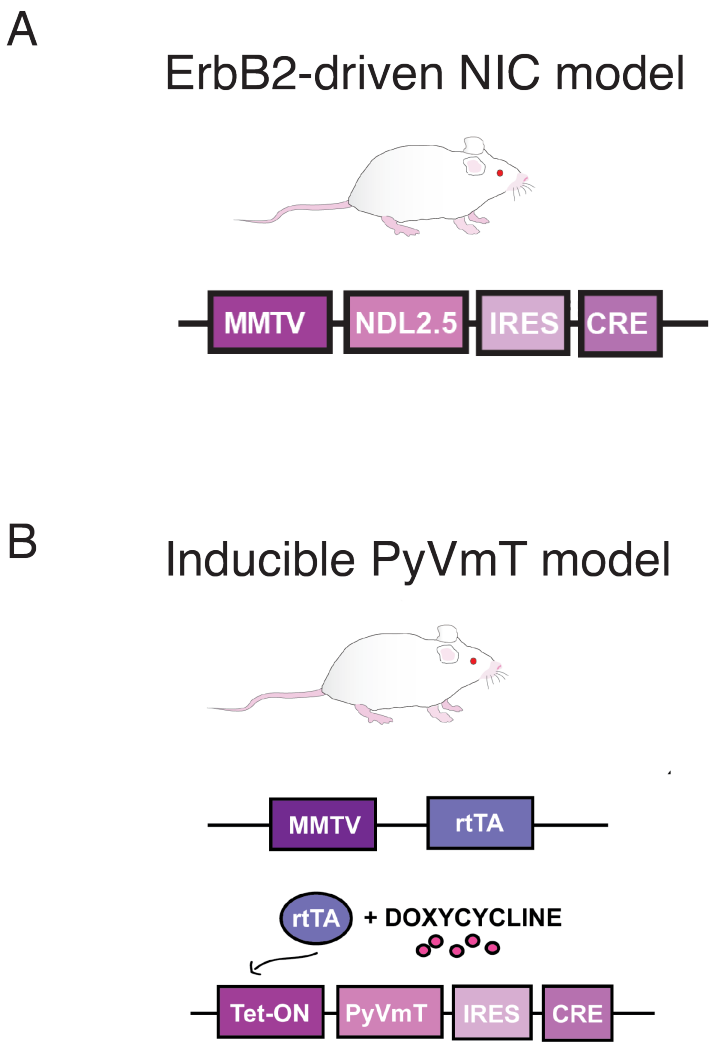

Figure 1-2. Transgenic mouse models of mammary tumorigenesis

1.6 The Role of Chromatin Modifications in Cancer

Epigenetics has traditionally been defined as heritable changes in DNA that are not due to sequence specific alteration, but a modern definition has emerged which applies the term in a broader sense as the study of chromatin biology and is the definition which will be employed in this work. Epigenetic modifiers, processes that regulate chromatin at different levels of organization, include methylation of DNA, post translation modifications of histones and nucleosome remodeling. Numerous studies from developmental biology have revealed the importance of these modifers in the orchestration of cellular identity via their dynamic organization of DNA accessibility.

Since transcriptional dysregulation is a key feature of many diseases, the contribution of epigenetic modifers to disease states has been of great interest.

Progression of cancer is a stepwise process that involves the transformation of a normal cell to a neoplastic state. Hannahan and Weinberg defined a series of traits necessary for cancer cells to achieve malignancy, broadly known as the hallmarks of cancer. They include (1) sustained proliferative signaling, (2) resisting cell death, (3) evading tumour suppressors, (4) vascularization, (5) invasion and metastasis, and (6) replicative immortality(79). Recently four emerging hallmarks have also been added, including (1) deregulation of cellular energetics, (2) evasion of the immune system, (3) genomic instability and (4) pro-tumour inflammation(80). A great deal of work has been undertaken to further understand how these hallmarks emerge in different types of cancer and emerging evidence indicates that aberrations in epigenetic modifers play a key role. Numerous studies have characterized global epigenetic changes in cancer cells, both at the global level and at discrete targets. Furthermore, recent advances in Next Generation Sequencing (NGS) technology have identified an abundance of mutations in different chromatin modifiers across many types of cancers.

1.7 Chromatin Writers, Readers and Eraser Mediate Dynamic Modifications

To accommodate the necessary genetic material in the nuclei of a cell, 147 base pairs of DNA is wound around an octamer of core histone proteins (H2A, H2B, H3, H4) forming nucleosomes. Arrays of nucleosomes are connected by linker histones to form the canonical ‘beads on a string’ structure, and are condensed to form 30-nm chromatin fibers, which is further packed to the chromosome observed during metaphase. In addition to facilitating DNA compaction, histones are also the site of post-translational modifications that can regulate gene expression thus forming an important level of transcriptional regulation. The dynamic process of adding, removing and recognizing covalent modifications on the amino acids at the N-terminal tails of different histones is orchestrated by a legion of chromatin modifying enzymes. Chromatin modifying enzymes can be defined as either chromatin readers, writers or erasers. Writers can

establish covalent histone modifications, the most prominent being lysine or arginine methylation and acetylation as well as serine/threonine phosphorylation. However, advanced mass spectrometry approaches have expanded the catalog of post translational histones modifications to include at least 13 different types (81-83). Chromatin readers are effector proteins recruited to the site of modifications to interpret the histone modifications laid down by the writers. Domains typically associated with chromatin readers include, Chromo, Bromo, Tudor, PWWP, MBT and PHD domains. Chromatin erasers are responsible for removing the marks deposited by the writers, and they include histone deacetylases, and histone lysine/arginine demethylases. The dynamic interactions between these three groups function to coordinate transcriptional programs necessary for maintaining cellular identity (**Figure 1-3**).

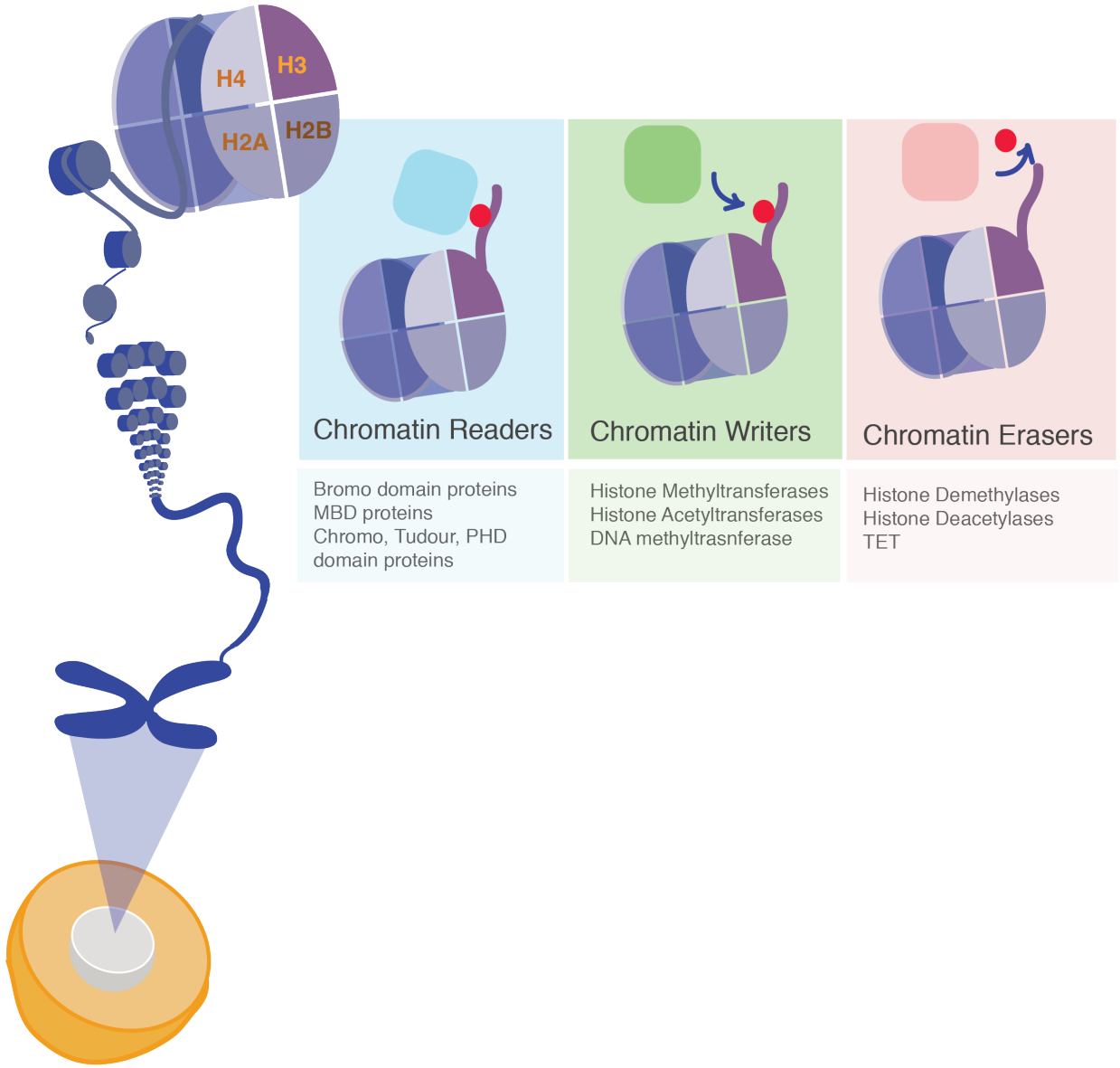

Figure 1-3. Chromatin Reader, Writers and Erasers

1.8 Writing the Repressive Mark: Polycomb Repressive Complex 2 (PRC2)

An important author of transcriptionally repressive chromatin marks is the lysine methyltransferase PRC2. As a multi-subunit protein complex, PRC2 catalyzes di and tri methylation of lysine 27 on the amino acid tail of histone 3 (commonly written as H3K27me^3) (84-87). The exact method whereby deposition of H3K27me^3 results in silencing is unclear, but is hypothesized to be due to (a) steric hindrance or (b)

impairment of transcriptional machinery. Briefly, H3K27me^3 recruits Polycomb Repressive Complex 1 (PRC1) which ubiquitinates lysine 119 of histone 2A and facilitates chromatin compaction to inhibit RNA polymerase II-dependent transcriptional elongation and access to transcription factors (88, 89). However, several studies analyzing Polycomb Group binding across the genome have revealed that PRC1 and PRC2 do not always overlap (90-92) and other studies have illustrated that PRC2 can be recruited to mono ubiquitinylated H2A by non-canonical PRC1 components (93) suggesting that other mechanism might be involved. Other groups have proposed that PRC2 can stall transcriptional activity at target promoters by locking RNA Polymerase II in its poised form (serine 5 phosphorylation) thus preventing the switch to the elongating form (serine 2 phosphorylation) (94, 95). In addition, methylation of H3K27 is incompatible with acetylation of the same residue. Since H3K27 acetylation recruits important transcriptional activators, H3K27me^3 represses transcription by antagonizing acetylation-dependent transcriptional activation. Thus, while the role of H3K27me^3 in modulating transcription is established, there is no consensus on the molecular mechanisms underlying this function.

The arrangement of marks laid by most chromatin writers along a gene is inconsistent, but PRC2 has been observed to deposit H3K27me^3 in one of two patterns; large domains greater than 100 kb(96), or small domains covering a few kb(97-99). In line with its role as in transcriptional repression, along a given silenced locus H3K27me^3 enrichment is typically concentrated around the transcriptional start site (97, 100), but has also been observed at intergenic regions (100, 101), subtelomeric regions (102) and in retro transposable elements(103). Interestingly, up to 10% of annotated genes in ES cells are H3K27me^3, while the levels of the H3K27me^2 mark are approximately 80%(104).

1.8.1 PRC2 is a multi-sub unit complex

PRC2 is a holoenzyme comprised of four core proteins; Ezh2, Suz12, RbAp46/48, and Eed(105) (**Figure 1-4**). While at least Eed and Suz12 are necessary

for PRC2 to function *in vitro*(106), the catalytic machinery is located in the SET domain of Ezh2, enabling the transfer of a methyl group from *S*-adenosylmethionine to a lysine's e-amino group. Ezh1 is 96% homologous to Ezh2 and is enriched in non-proliferative terminally differentiated tissue. Ezh1 also contains a SET domain, but the functional redundancy of Ezh1 with Ezh2 is context specific. In ES cells , Ezh1 was shown to have a lower enzymatic activity than Ezh2 and to target a different subset of genes (107). However, in adult skin cells, Ezh1 able to completely compensate for Ezh2 ablation(108).

The non-catalytic units of PRC2 are important for recruitment and stability. The WD40 domain of Eed binds repressive chromatin marks (H3K9me^3, H3K27me^3, H4K20me^3)(109-111) thus recruiting PRC2 to loci that are already repressed. This recruitment is thought to allosterically activate EZH2 methyltransferase activity and provides a scaffolding function which is thought to underlie the "spreading" of the H3K27me3 mark into its larger, domain-type arrangements(112). Suz12 is required for nucleosome recognition, stability and activity of PRC2 (105, 106). RbAp46/48 plays a role in chromatin binding, containing a WD40 domain that interacts with Suz12 and H3 histones (113, 114). Both Suz12 and RbAp46/48 have been proposed to play a role in detecting active chromatin marks such as H3K4me^3, which inhibit PRC2 activity.

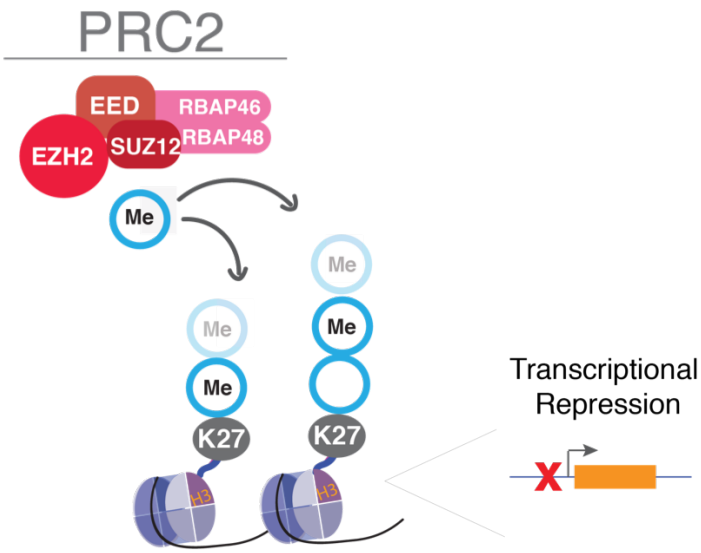

Figure 1-4. Schematic of PRC2

1.8.2 Regulation of PRC2 Activity and the H3K27me^3 mark

Mechanisms of PRC2 and H3K27me^3 regulation can be divided into (1) Inputs from the surrounding chromatin environment, (2) post translational modifications of Ezh2, and (3) variations in PRC2 subunits (**Figure 1-5**).

1.8.2.1 Inputs from the Surrounding Chromatin Environment

The H3K27me$^{2/3}$ mark itself can be diminished by specific chromatin erasers, either the lysine demethylases UTX (115) or Jmjd3(116). Histone marks typically associated with transcriptional activity such as H3K4me^3, and H3K36me^2 have been demonstrated to decrease the catalytic activity of PRC2(113, 117, 118). The acetylation of H3K27 is mutually exclusive and antagonistic to H3K27me^3 mediated silencing(119), and the association of PRC2 with histone deacetylases HDAC1 and HDAC2 in certain contexts may facilitate changes in the chromatin environment that favour the activity of PRC2. Conversely, the presence of compact nucleosomes or H3K27me^2 or me^3 increase PRC2 activity (110, 120). The H3K27me^3 mark has also been implicated in relationships with non-histone modifiers of DNA organization, acting antagonistically to the nucleosome remodeller SWI-SNF and acting in concert with DNA methylation. Numerous *in vivo* genetic studies across different species have established the inverse relationship between PRC2 and the nucleosome remodelling complex SWI-SNF (121, 122). Comprised of 12-15 subunits, SWI-SNF employs ATP hydrolysis to remodel nucleosomes to open chromatin for transcriptional activation. Antagonism between SWI-SNF and PRC2 was first documented in *Drosophila melanogaster*, in which Polycomb group proteins were found to oppose Trithorax group proteins, of which SWI-SNF is an activator, during development (123). In the vertebrates, this antagonism has primarily been documented in the context of disease (section 1.3.5.2 will elaborate on this in the context of cancer). The link between H3K27me^3 deposition and DNA hypermethylation is a more divisive topic in the field. H3K27 has been reported to associate with DNA methyltransferase *in vitro* (124-126) and loss of PRC2 activity has been shown to induce DNA hypomethylation (127, 128). However, another group

demonstrated that Ezh2 depletion does not affect DNA methylation status or the expression of known hyper-methylated loci in a human epithelial osteosarcoma cell line (129) and genome-wide analysis of tumour cells revealed that H3K27me^3 and DNA methylation are mutually exclusive in CpG islands(130). The cross talk between PRC2 and DNA methylation will further investigation.

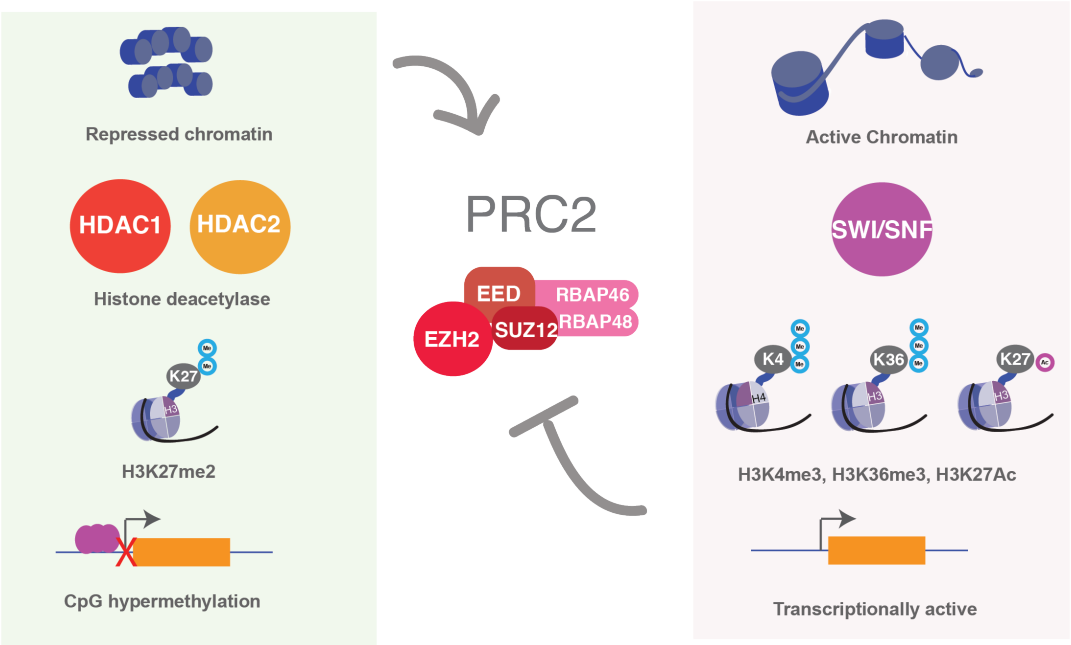

Figure 1-5. Input from the surrounding environment influences PRC2 activity

1.8.2.2 Post-translational Modifications of Ezh2

Post translational modifications on Ezh2 have also been demonstrated to augment or impair the methyltransferase activity of PRC2 (**Figure 1-6**). Phosphorylation of Ezh2 by Akt1 at serine 21 reduces H3K27me^3 activity(131), while JAK2 has also been shown to phosphorylate Ezh2 at tyrosine 641, promoting the degradation of Ezh2(132).

Phosphorylation of Ezh2 by CDK1 and CDK2 at various sites have proposed to elicit different effects. Phosphorylation on threonine 345 promotes the association between Ezh2 and the lncRNA HOTAIR(133), while phosphorylation at threonine 345 and 416 is required for recruitment of PRC2 to certain genetic loci (134). In mesenchymal stem

cells, CDK1 phosphorylation of Ezh2 at threonine 487 induces the dissociation of Ezh2 from PRC2 (135), while phosphorylation of threonine 345 promotes proliferation and migration in prostate cancer cells (134). O-linked N-acetylglucosamine transferase (OGT) can also glycosylate EZH2 at serine 75 to maintain EZH2 stability and activity (136).

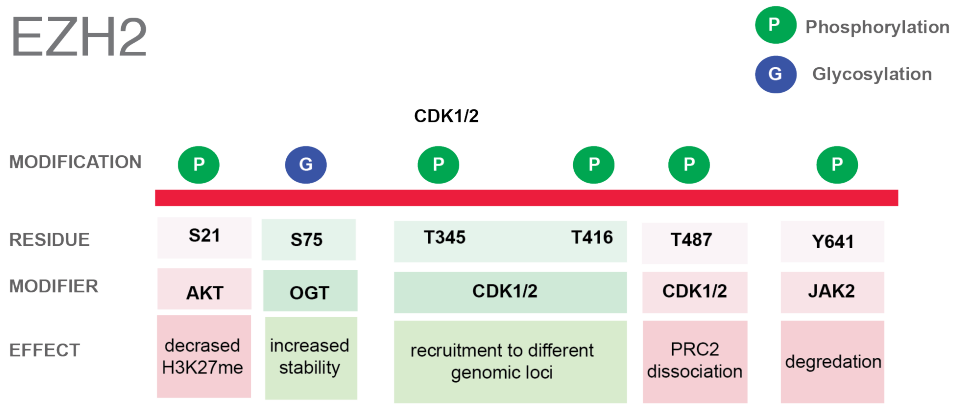

Figure 1-6. Post translational modifications of Ezh2 affect its activity

1.8.2.3 PRC2 Subunit Variability

Core components of PRC2 are highly conserved across species, but subunit composition can vary across different vertebrate cell types and can augment PRC2 activity or recruitment (**Figure 1-7**). Aebp2 is a zinc finger protein that interacts with several components of PRC2 to enhance enzymatic activity of the complex, perhaps due to its ability to bind nucleosomes(137). Polycomb like proteins (PCL1,2 and 3) are differentially expressed in tissues and have been shown to co-occupy PRC2 targets, regulate PRC2 enzymatic activity and can mediate PRC2 recruitment to sites of H3K36 methylation(138-141). In some cell lineages, Jarid2 is a factor that has been co-purified with PRC2 through its interaction with Suz12(87). It has been proposed to contribute to PRC2 recruitment through its DNA-binding motifs(142), and differentially augments on PRC2 methyltransferase activity depending on its association with Ezh2 or Ezh1 (143, 144) and context of the surrounding chromatin (145).

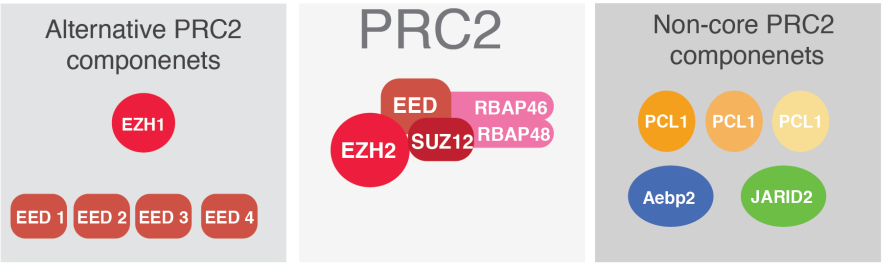

Figure 1-7. PRC2 core and noncore components

1.8.3 Mechanisms of PRC2 Mediated Silencing in the Mammalian Genome

Despite the high degree of conservation between core Polycomb group proteins and their repertoire of targets, the mechanisms underlying PRC2 recruitment differ across phyla. During *Drosophila melanogaster* development, Polycomb groups protein are recruited to *cis*-regulatory elements called Polycomb Repressive Elements (PRE) by transcriptional repressors (146-148). However, the identification of equivalent motifs in vertebrates has been limited(149-157) and cannot account for recruitment to the hundreds of PRC2 targets across the genome. Thus, in vertebrates, alternative PRC2 recruitment mechanisms have been proposed.

1.8.3.1 PRC2 Recruitment and DNA Methylation

PRC2 has been observed to be preferentially recruited to unmethylated CpG islands (1-2 kb regions with a high density of guanine and cytosine repeats) that are transcriptionally silent (158). Artificial reduction of endogenous DNA methylation has been well documented to result in the global redistribution of PRC2 to previously methylated CpG islands (127, 130, 152, 159, 160). However, this phenomenon is not observed for all loci targeted by PRC2, as deletion of CpG islands from the murine *HoxD* locus did not affect recruitment of PRC2 *in vivo* (155). Furthermore, in ES cells, 30 to 40% of CpG islands do not acquire PRC2 even after transcriptional inhibition(154). These observations have led to the discovery of mechanisms to explain recruitment of PRC2 to specific loci that have found to be highly context specific (**Figure 1-8**).

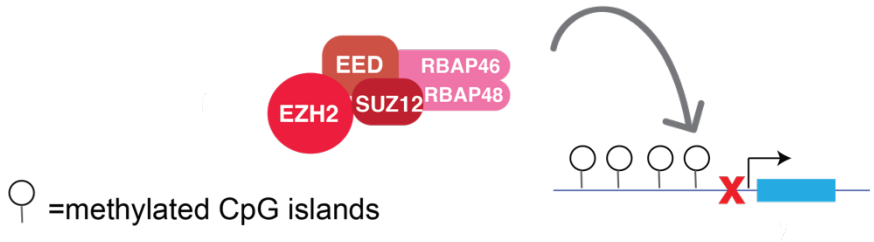

Figure 1-8 Recruitment of PRC2 to DNA regions of methylated CpG islands

1.8.3.2 LncRNA

In addition to transcription factors, long non-coding RNA (lncRNA), sequences of non-coding RNA greater than 200 nucleotides, have also been implicated in PRC2 recruitment (**Figure 1-9**). This phenomenon was first observed in the context of X chromosome inactivation during which lncRNA *Xist* mediates recruitment of PRC2 to facilitate repression(161-164). The lncRNA HOTHAIR has also been demonstrated to silence the *Hox D* locus through PRC2 recruitment (165, 166). PRC2-RNA interactions do not always equate to a meaningful recruitment mechanism, however. Genomic screen have revealed that PRC2 can bind to thousands of RNA species(167, 168) and PRC2 promiscuity is increased by RNA length, irrespective of sequence (169). Furthermore, recently PRC2 was found to preferentially bind to G-rich RNA sequences including G-quadruplexes (170).

Figure 1-9 Recruitment of PRC2 by lncRNAs

1.8.3.3 Inhibition of PRC2 Activity by Actively Transcribed Regions

A recent model that has been developed to explain both the promiscuous binding of Ezh2 to RNA and the complex dynamic epigenetic control across the genome, is the 'genome surveillance' model. In this model, PRC2 is constantly sampling the genome

for regions of low transcriptional activity, and occupies a large fraction of active promoters where it binds to nascent transcripts. This RNA-Ezh2 interaction correlates with a decrease in H3K27me^3 at these promoters; active transcription inhibits H3K27me^3 deposition. Thus, Ezh2 recruitment follows the initial repression of transcription by removal of activating signals or recruitment of repressors (133, 169, 171) (**Figure 1-10**). This model accounts for the observed cooperation of PRC2 with different transcription factors in many different contexts. Furthermore, proteomic studies validating PRC2 complex interactions have failed to find any direct binding between PRC2 and transcription factors, suggestion that direct recruitment by transcriptional factors is unlikely (172).For example, the transcription factor REST has been observed to localize with PRC2 to CpG islands in neural progenitor cells, but not ES cells (156). During epithelial-to-mesenchymal transformation (EMT), a process required to enable metastatic dissemination of the primary tumour, the transcriptional factor Snail1 has been shown to cooperate with PRC2 at specific loci(173).

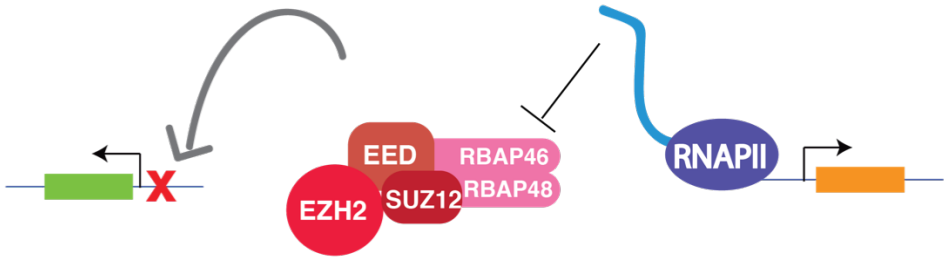

Figure 1-10 Inhibition of PRC2 by actively transcribed regions of the genome

1.8.4 PRC2 Function during Mammalian Development

Polycomb group proteins were first identified as repressors of homeotic (*Hox*) genes important for body segment specification in *Drosophila melanogaster* (174, 175). Analogous functions in mammalian systems were subsequently reported and with improvements to high throughput sequencing technologies, the identification of PRC2 targets across the genome expanded. In the context of adult somatic tissues, PRC2 deposits H3K27me^3 at the promoters of transcription factor and differentiation-associated genes, thus enforcing a given terminally differentiated cell state. For

example, *Eed*$^{-/-}$ hematopoietic stem cell are not able to differentiate into mature lineages(176) and immature B cells require PRC2 to initiate rearrangement of the immunoglobulin heavy locus gene (177). Conversely, in pluripotent Embryonic Stem (ES) cells, H3K27me^3 is enriched at the promoters of key developmental regulators (104, 178, 179). Germline deletion of *Ezh2* (180), *Eed* (181,182) or *Suz12* (183) in mice is embryonically lethal at the post implantation stage. Accordingly, while loss of these factors in ES cells does not completely disturb the ability to self-renew, it significantly affects the capacity to activate certain lineage-specific transcriptional programs (178, 183, 184). These observations have led to the proposition that PRC2 does not dictate differentiation or pluripotency outright, but instead suppresses the expression of genes controlling differentiation into inappropriate lineages. In this capacity, the function or consequences of perturbing PRC2 is dependent on the tissue examined.

1.8.5 Role of PRC2 in Cancer

The importance of PRC2 as a transcriptional regulator also invokes the potential of PRC2 dysregulation driving diseases such as cancer. Mutations or aberrant expression of PRC2 core components or factors in the chromatin landscape that affect PRC2 activity have been documented to contribute to oncogenesis. Interestingly, both gain and loss of PRC2 function have been observed to drive disease, reflecting both context specific repression or de-repression of different types of target genes and the discovery of H3K27me^3 independent functions of PRC2 components. Perhaps even more fascinating is that Ezh2 can act as both a tumour suppressor or oncogene in different cellular compartments of the same tissue (summarized in **Figure 1-11**). For example, *in vivo* genetic studies in the hematopoietic compartment have demonstrated that targeted ablation of Ezh2 in hematopoietic stem cells (HSC) causes spontaneous T cell acute leukemia (185). However, in an AML murine model, Ezh2 loss inhibited cancer cell proliferative capacity and disrupted tumor progression by re-activating EZH2 target genes implicated in myeloid cell differentiation(186). In non-malignant lymphoid progenitor cells, PRC2 has been observed to inhibit proliferation and the capacity to self-renew(187, 188) while ectopic expression of Ezh2 stimulates proliferation of mature

hematopoietic lineages (189-191). Taken together, these observations suggest that PRC2 functions as a tumour suppressor in progenitor cells, but as an oncogene in terminally differentiated cells of the hematopoietic system. Additionally, PRC2 function could also reflect the nature of its interaction with specific oncogenes. For example, in neuroendocrine prostate cancer, the oncogene N-Myc cooperates with Ezh2 to turn off Androgen Receptor signaling and initiate alternative pro-survival pathways (192). In endometrial stromal tumours, chromosomal translocation involving the PRC2 component SUZ12 have been proposed to drive tumorigenesis. These translocations generates the JAZF1-SUZ12 oncogene, comprised of the N-terminus of JAZF1 and the C-terminus of SUZ12, which functions to disrupt PRC2 complexes and diminish H3K27me^3 levels (193) (194).

1.8.5.1 Gain of PRC2 Function

Deep sequencing of human tumour samples revealed that Ezh2 is mutated in 20% of diffuse large B cell lymphomas and in 7% of follicular B cell lymphomas. These mutations are at the Y641 and A677 residues, which reside in the SET domain of Ezh2, and confer increased levels of global H3K27me^3, due to preferential methylation of H3K27me^2 at the expense of H3K27me^0 or H3K27me^1 methylation (195). Thus, these mutations exist in cancer in a heterozygous state, co-operating with the wild-type allele which can still generate H3K27me^1 and H3K27me^2. Gain of function mutations in the SET domain of Ezh2 have also been reported in 3% of melanomas (196) and subsequent functional studies have confirmed that these mutations are drivers of disease (197). How increased levels of global H3K27me^3 drives disease is unclear. Souroullas and colleagues have recently proposed that the Ezh2 Y641 mutation does not uniformly redistribute H3K27me^3, but rather redistributes it to novel locations across the genome (197). In the engineered Ezh2 Y641 mutant mice, H3K27me^3 is favored at gene bodies and intergenic regions at the expense of local peaks near the transcriptional start site at several genetic loci, however the functional consequences in terms of disease development are still unclear.

Indirect PRC2 gain of function has been observed through mutations effecting loss of function in PRC2 antagonists. For example, inactivating mutations affecting the Jumonji C domain of UTX, which is a lysine demethylase that removes methyl groups from H3K27me^2 and me^3, have been observed in multiple myeloma, medulloblastoma, and pancreatic and renal cancers, thus favoring the deposition of H3K27me^3 (198-200). PRC2 is also antagonized by the nucleosome remodeling complex SWI-SNF. In aggressive pediatric rhabdoid sarcomas driven by loss of the SWI-SNF component *SMARCB1*, EZH2 activity promotes tumorigenesis (121, 122). In ovarian cancer xenografts harboring mutations in the SWI-SNF component *ARID1A*, or lung cancer xenografts harboring the SWI-SNF component *BRG1*, inhibition of EZH2 is synthetically lethal, or in the latter case sensitizes tumours to chemotherapy (201, 202).

1.8.5.2 Loss of PRC2 Function

In certain cancers, loss of PRC2 function has been driven by mutations within the core units of PRC2 as well as by mutations in components that govern the chromatin landscape by regulating PRC2 function. A majority of Malignant Peripheral Nerve Sheath Tumours (MPNST) are driven by loss of function mutations in EED and SUZ12 (203, 204) and inactivating mutations in PRC2 components have also been reported in patients with myelodysplastic syndrome (MDS), myeloproliferative neoplasms (MPNs), and both chronic and juvenile myelomonocytic leukemia (205-210). Perhaps of the most interesting mutations conferring loss of PRC2 function are somatic mutations in the histone3 variant H3.3 in ~50% of pediatric high grade gliomas (pHGG)(211, 212). These substitution mutations occur on K27 or G35 of N-terminal amino acid tail of H3.3. The K27M mutation was later found to act in a dominant negative fashion, with the mutant histone variants acting as a competitive inhibitor of Ezh2 (213, 214).

1.8.5.3 Non-canonical Functions

While the function of PRC2 has predominantly been framed in the context of its histone methyltransferase activity, several studies have demonstrated the ability of PRC2 to methylate non-histone protein targets or for Ezh2 to modulate transcription

independent of PRC2. In glioblastoma cancer stem cells Ezh2 methylation of the transcription factor Stat3 promotes tumorigenicity (215). In a castration resistant prostate cancer model, Ezh2 is phosphorylated at serine 21 by Akt1 to inhibit its methyltransferase function and subsequently couples with Androgen Receptor to facilitate transcriptional activation (216). In the context of breast cancer, several PRC2 independent function of Ezh2 have been reported. In the aggressive basal subtype of breast cancer, Ezh2 was reported to expand the pool of tumour initiating cells through activation of Notch1 expression(217). Ectopic expression of Ezh2 in a transgenic mouse model of breast cancer increased tumorigenicity and increased Notch1 expression independent of Ezh2 histone methyltransferase activity. Another group observed that Ezh2 functioned as a transcriptional activator through physical interaction with both the estrogen receptor and Wnt signaling component B-catenin, thus promoting cell cycle progression (218).

1.8.5.4 Overexpression in solid tumours is associated with poor prognosis

PRC2 mutations have not been reported in all cancers but amplification or over-expression of Ezh2 or Suz12 have been associated with decreased survival and aggressive disease in multiple tumour types. High levels of Ezh2 were first correlated with poor outcome in prostate cancer (219). This observation was followed by similar observations in other solid malignancies such as breast, bladder, kidney, and endometrial cancer, as well as melanoma (220-223) and blood malignancies (224, 225). Subsequent functional studies both *in vivo* and *in vitro* have revealed that ectopic expression of Ezh2 in different tissues can induce aberrant cellular proliferation and sometime result in oncogenic transformation. For example, overexpression of Ezh2 in the mammary gland cues hyperplasia but not the development of tumours (226). *In vitro* RNAi of Ezh2 in various breast cancer cell lines reduced proliferation, delayed G2M cell cycle transition and reduced survival in breast cancer xenografts.

With respect to human breast cancer, an immunohistochemical study of Ezh2 expression in over 400 patient samples revealed that high levels of Ezh2 were associated with Basal-like and HER2+ breast cancer, more aggressive subtypes(227).

Interestingly, a recent study demonstrated that in women with a benign breast disease, expression of high levels of EZH2 in if greater than 20% of normal epithelial cells associated with a significantly increased risk of developing breast cancer in the future(228).

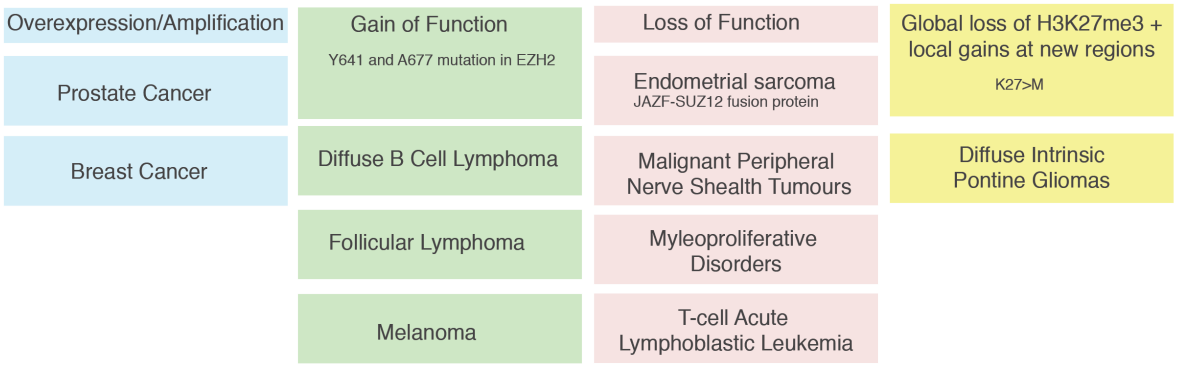

Figure 1-11 Summary of changes to PRC2 components and activity in different types of cancers

1.8.6 Pharmacological Inhibition of PRC2

The discovery of activating mutations in PRC2 components and its overexpression in several cancers has led to the rapid development of potent and selective pharmacological inhibitors that target the enzymatic activity or stability of PRC2 (**Table 1-1**). Initially, the only drug available was the pan lysine methyltransferase inhibitor DZNep(3-deazaneplanocin) which, that in addition to being non-specific to Ezh2, was inappropriate for use *in vivo* and had a short half-life(229, 230). DZNep increases intracellular S-adenosylhomocysteine (SAH) levels by inhibiting the enzyme S-adenosylhomocysteine transferase, leading to a feedback inhibition mechanism that degrades PRC2. High throughput screens have since identified several compounds that function as *S*-adenosyl- L-methionine(SAM) competitive inhibitors, thus blocking the donation of a methyl group to substrates by lysine methyltransferases. Non-competitive SAM inhibitors have also been subsequently identified, as well as peptides that can disrupt PRC2 stability. These inhibitors have proven to be extremely specific in targeting PRC2's catalytic activity and amendable for use in animal models or in clinical trials.

EPZ005687(231), followed by the orally bioavailable EPZ006438, GSK-126 (232) and EI1(233) are SAM-competitive inhibitors that have been demonstrated to selectively inhibit Ezh2 methyltransferase activity. UNC1999 is an orally bioavailable SAM competitive inhibitor and has a 1000-fold selectivity for other methyltransferases except Ezh1 (22-fold selectivity), so it is commonly employed to inhibit both Ezh1 and Ezh2 (234). CPI-1205 and CPI-169 are also a series of SAM-competitive inhibitors that are being investigated. Promisingly, SAM competitive inhibitors are effective against the activity of both wild type Ezh2 and Ezh2 with gain of function mutations. The compound EED226 acts through an allosteric mechanism, binding to the H3K27me3 pocket of Eed to disrupt PRC2 activity and would be appropriate for situations where Ezh1 and Ezh2 inhibition would be necessary(235). Since PRC2 can elicit effects independent of its enzymatic activity, inhibitors targeting PRC2 stability have also been developed. Stabilized alpha-helix of Ezh2 (SAH-Ezh2) is a peptide that disrupts the Ezh2-Eed complex (236).

Inhibitor	Target	Selectivity	Delivery	Clinical Trial Status	Commercial
DZNep	SAH hydrolase	Pan lysine methyltransferase inhibitor, not specific to Ezh2	*In vitro only*	N/A	N/A
EPZ005687	SAM competitive	>500-fold against other HMT 50-fold against EZH1	IP	N/A	Epizyme Inc.
EPZ006438	SAM competitive	>500-fold against other HMT 50-fold against EZH1	Orally Bioavailable	Phase I, II B-cell and follicular lymphomas (NCT01897571) Phase I synovial sarcoma (NCT 02601937)	Epizyme Inc.
EI1	SAM competitive	>10,000-fold against other HMT 90-fold against EZH1	IP	N/A	Novartis
GSK-126	SAM competitive	-fold against other HMT 150-fold against EZH1	IP	Phase I B-cell and follicular lymphomas (NCT02082977)	GSK
GSK-343	SAM competitive	1000-fold against other HMT 60-fold against EZH1	IP	N/A	GSK
UNC1999	SAM competitive	>1000-fold against other HMT 22-fold against EZH1	Orally Bioavailable	N/A	Structural Genomics Consortium
CPI-169	SAM competitive	Unknown	Subcutaneously	N/A	Constellation
CPI-1205	SAM competitive	Unknown	Orally Bioavailable	Phase I patients with B cell lymphoma (NCT02395601)	Constellation
EED226	Allosteric inhibitor	Unknown	Orally Bioavailable	N/A	Novartis
SAH-EZH2	Peptide	Unknown	*In vitro only*	N/A	N/A

SAM= *S*-adenosyl-methionine, SAH= S-adenosyl-homocysteine, HMT= histone methyltransferases, IP= intra-peritoneal injection

Table 1-1. Table of currently available PRC2 inhibitors.

1.8.7 Potential of Targeting PRC2 in Breast Cancer

Given the importance of tissue specificity in dictating PRC2 function, this section will outline the mechanisms of PRC2 activity and regulation framed in the context of breast cancer. With the availability of promising anti-Ezh2 therapies and the correlation between high levels of Ezh2 and aggressive breast cancer, the potential of targeting PRC2 activity in breast cancer has been identified. However, the reality may be a more complex topic than anticipated. Several mechanisms upstream of PRC2 components have been reported to contribute to their documented overabundance in breast cancer. Bracken and colleagues identified that Ezh2 and Eed are targets of E2F, a family of transcription factors that is important for regulation of the cell cycle(220). In normal somatic cells, E2F is controlled by the tumour suppressor Rb, which binds to E2F1 thus restricting it from interacting with transcriptional machinery. In cancer, this regulation is undermined, and phosphorylation of Rb by cyclin-dependent kinases (CDKs) releases E2F, allowing for the transcriptional activation of genes controlling cell cycle and DNA replication. The MEK-ERK-Elk-1 signalling cascade is frequently upregulated in cancer, and Ezh2 has also been demonstrated to harbour several Elk-1 binding sites. Inhibition of Elk-1 or treatment with a MEK inhibitor, significantly decreases transcription of Ezh2 in human breast cancer cell lines (237). Hypoxia in the microenvironment can also drive expression of Ezh2, as a HIF responsive element (HRE) has been identified in the promoter of Ezh2(238). The loss of negative regulators such as micro RNA 101(219) and Micro RNA 214(239) has also been suggested as an additional causes for overexpression of Ezh2 in breast cancer. The prevailing impression in the context of breast cancer has been that elevated levels of PRC2 contribute to disease through the repression of tumour suppressors. Some of the most well-characterized examples

include silencing of the Ink4/Arf tumour suppressor locus(240), Runx3(241), E-cadherin(242) and components of DNA-damage repair pathways(238). However, recent evidence suggests that PRC2 plays differential roles depending on the molecular features of the breast cancer in question. Lee and colleagues provided the first evidence for breast cancer subtype-specific regulation by Ezh2, illustrating that Ezh2 can have opposing functions depending on the estrogen receptor (ER) status of the cell(243). They reported the collaboration of Ezh2 with nuclear factor kappa B (NF-kB) signaling subunits RelA and RelB to activate NF-kB targets in ER-negative cells, but in ER-positive cells, Ezh2 functioned as a part of PRC2 to repress NF-kB targets through H3K27me^3. These observations suggest that some functions of PRC2 are context-dependent and thus and any therapeutic potential in the context of breast cancer will have to be carefully evaluated. A series of studies in which conditional ablation of Ezh2 was performed in different transgenic mouse models of breast cancer has also yielded interesting results that also support the notion of differential PRC2 function. In a *p53* heterozygous *Brca*-deficient mouse model aggressive breast cancer, the conditional ablation of Ezh2 did not significantly affect tumour onset or growth (244) due to the compensation of Ezh1 for Ezh2 methyltransferase activity. In an activated Notch model of mammary tumorigenesis, ablation of Ezh2 increased the penetrance of mammary tumours following multiple rounds of pregnancy (245). The context specificity of PRC2 function and heterogeneity of breast cancer merits careful elucidation of PRC2 function in all breast cancer subtypes.

1.9 Experimental rational

Excess levels of Ezh2 alter the genomic landscape in breast cancer, yet there is a lack of functional genetic evidence supporting how Ezh2 is contributing to tumor initiation and progression. Breast cancer is a heterogeneous disease, and given the context dependent activity of PRC2, it may play different roles in different breast cancer subtypes. With multiple promising Ezh2 methyltransferase inhibitors currently in clinical trials for other indications, we wanted to evaluate the therapeutic potential of targeting the tumour epigenome by abolishing H3k27me^3 levels in HER2+ and Luminal B breast cancer. To this end, we employed a combination of transgenic mouse models and patient derived- xenografts to understand the effect of manipulating Ezh2 levels in a biologically relevant system. Finally, we used immune competent preclinical models to explore the combination of inhibiting Ezh2 methyltransferase activity with HER2 monoclonal antibody therapy to improve therapeutic response.

2 Results

2.1 Targeting EZH2 reactivates a breast cancer subtype-specific anti-metastatic transcriptional program

2.1.1 Experimental rationale

Breast cancer is comprised of a variety of disease entities bearing diverse pathological features, prognostic outcomes and metastatic behaviors. In an effort to unravel the heterogeneity of this disease, global transcriptional profiling has led to the characterization of at least 5 different intrinsic molecular subtypes of breast cancer; HER2+, Luminal A, Luminal B, Normal-like and Basal-like breast cancer (BLBC)(13). The Luminal B subtype has particularly poor survival outcome, partly due to the lack of viable therapeutic options. An important aspect of developing effective therapies consists of defining how distinct transcriptional networks within each subtype are uniquely modulated by genetic and epigenetic mechanisms. Tri-methylation of lysine 27 on histone 3 ($H3K27me^3$) by the methyltransferase Ezh2, as a part of the Polycomb Repressive Complex 2 (PRC2), is an important mechanism of gene silencing. Interestingly, aberrant expression of Ezh2 expression has been widely observed in cancer, with reports of both oncogenic and tumor suppressive functions(246).

With respect to breast cancer, Ezh2 levels are observed to be elevated and increased expression has been associated with poor survival(222). However, functional studies have failed to reach a consensus as to whether Ezh2 plays a causal role in driving disease or is merely a by-product of increased cellular proliferation(245). The context-dependent nature of Ezh2 function has also been proposed to be determined by the cell of origin and/or early transformation events undertaken by a tumor cell(247). Thus, the different developmental origins of intrinsic breast cancer subtypes(15) underscores the importance of evaluating the role of Ezh2 in each molecular subtype. Furthermore, while

significantly higher H3K27me^3 levels are observed in Luminal B compared to BLBC or HER2+, the functional relevance of this increased global histone methylation state is unclear(227).

Given that the behavior of Ezh2 is context-dependent, in this study we investigated the role of Ezh2 specifically in Luminal B breast cancer. To this end, we employed a transgenic mouse model to examine the effects of *Ezh2* ablation at each stage of tumorigenesis from early hyperplastic lesions to invasive metastatic disease. This work led to the identification of a Luminal B-specific anti-metastatic transcriptional program centered on the master transcriptional regulator FOXC1, which is silenced in these tumors in an Ezh2-dependent manner. Notably, pharmacological inhibitors targeting Ezh2 de-repressed *FOXC1* and reactivated this anti-metastatic program in both murine and human pre-clinical models, resulting in a dramatic reduction in both the size and number of metastatic lesions. Thus, our findings have important implications for the treatment of Luminal B breast cancer, where a paucity of options for targeted therapy has significantly hindered progress in improving patient outcomes.

2.1.2 Ablation of Ezh2 in a Luminal B model delays tumour onset

To explore the role of Ezh2 in Luminal B breast cancer, we employed a Polyomavirus Middle T (PyVmT) driven model, in which the rapid development of tumors closely mimics human disease progression(70, 248), and which has been shown to cluster with the human Luminal B intrinsic subtype(249). Since Ezh2 plays an important role in maintaining mammary luminal progenitor cells and is required for mammary alveolargenesis(250, 251), we utilized an inducible PyVmT transgene(252) to circumvent phenotypes arising from impaired mammary development (Tet-ON PyVmT).

This model combines mouse mammary tumor virus promoter (MMTV)-driven expression of the reverse tetracycline-dependent transactivator (rtTA)(253) with a Tet operator-controlled bicistronic transgene encoding the PyVmT oncogene and Cre recombinase. Hence, upon induction with doxycycline, coordinated PyVmT expression and deletion of conditional *Ezh2* allele(s)(184) occur specifically in the mammary epithelium (**Figure 2-1A**). Whereas cohorts of virgin females bearing the wild-type or one conditional allele of *Ezh2* developed measurable mammary tumors after an average onset of 67 and 61 days respectively, *Ezh2*-deficient mice displayed a significant delay in tumor onset to an average of 145 days (**Figure 2-1B**). *Ezh2* deletion and oncogene expression were confirmed by both immunoblot and immunohistochemistry analyses (**Figure 2-2A, B**). Interestingly, Ezh2-deficient tumors assessed for H3K27me^3 by immunofluorescence at endpoint exhibited undetectable levels of H3K27me^3 in the epithelium, indicating that Ezh1 was not able to compensate for the loss of Ezh2 histone methyltransferase activity (**Figure 2-2C**).

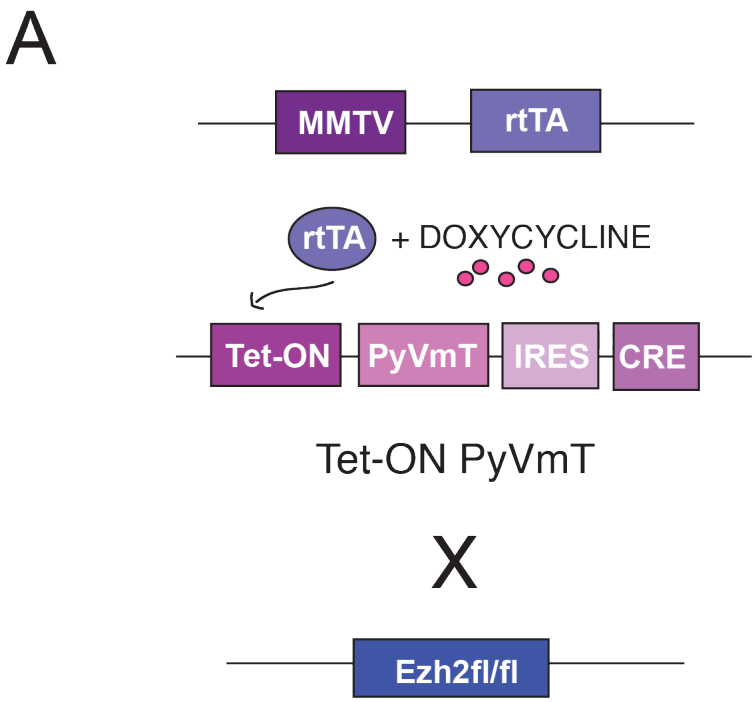

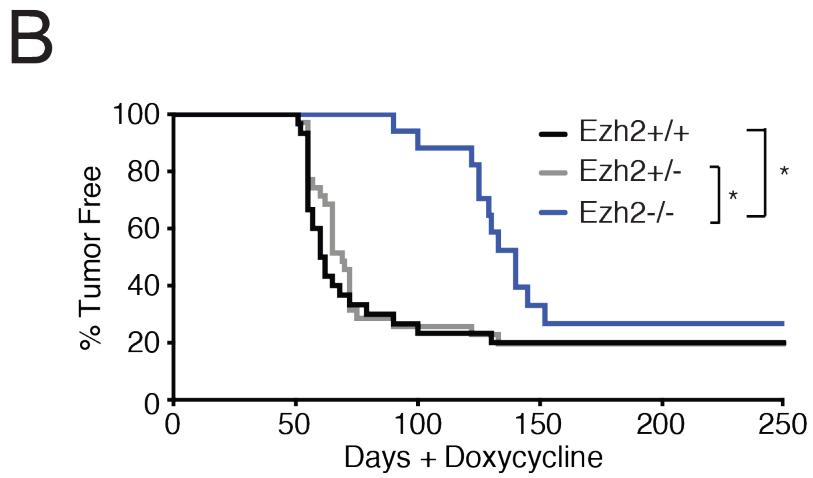

Genotype	t50 (days)	Penetrance	n
Ezh2+/+	**67**	**81%**	**27**
Ezh2+/-	**61**	**80%**	**20**
Ezh2-/-	**145**	**76%**	**25**

Figure 2-1. Loss of Ezh2 significantly alters breast cancer latency

(**A**) Schematic of the transgenic mouse model. (**B**) Kaplan-Meier survival curve of mammary tumor onset in Tet-ON PyVmT mice with wild-type ($Ezh2^{+/+}$), heterozygous ($Ezh2^{+/-}$) or homozygous ($Ezh2^{-/-}$) Ezh2 conditional alleles. *p<0.05.

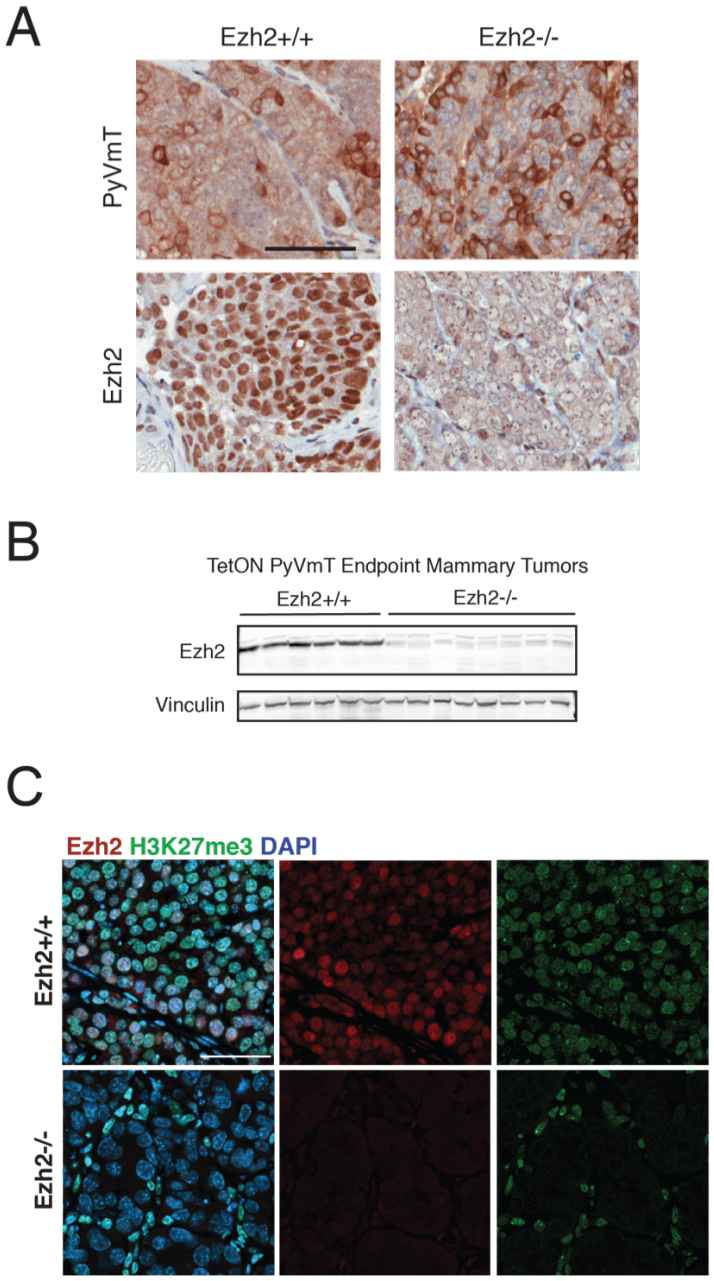

Figure 2-2. Loss of Ezh2 is retained in endpoint tumours and is accompanied by global loss of H3K27me^3

(**A**) Representative images of paraffin-embedded sections of endpoint Tet-ON PyVmT tumors stained by immunohistochemistry for Ezh2 and PyVmT levels. Scale bars are 300μm. (**B**) Immunoblot of endpoint Ezh2$^{+/+}$ or Ezh2$^{-/-}$ Tet-ON PyVmT tumors assessed for protein levels of Ezh2 and PyVmT. Vinculin was used a loading control. (**C**) Immunofluorescence staining of endpoint Ezh2$^{+/+}$ or Ezh2 $^{-/-}$ Tet-ON PyVmT tumors for Ezh2, H3K27me^3 or the nuclear stain DAPI. Scale bar is 50μm.

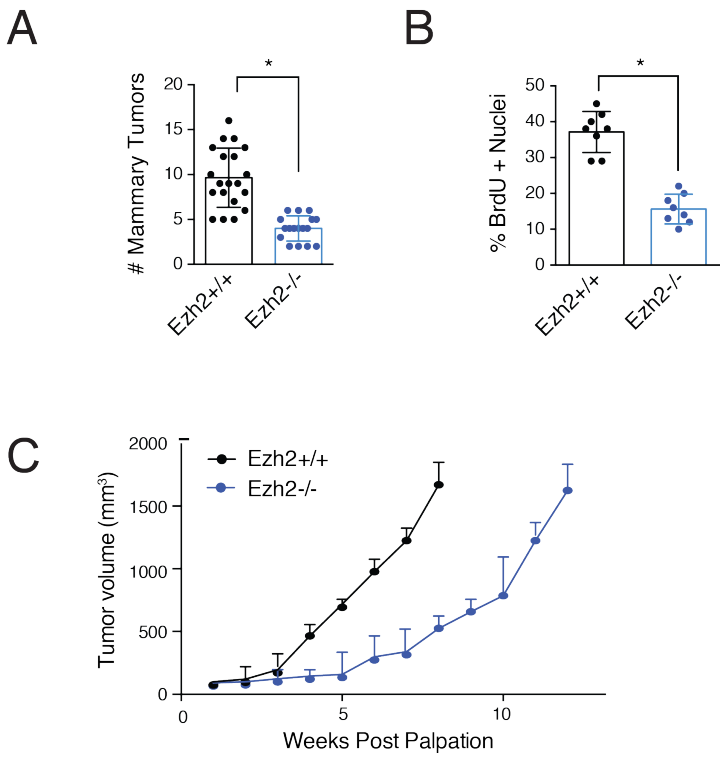

Figure 2-3. Loss of Ezh2 reduces tumour focality and proliferation

(**A**) Quantification of the total number of mammary tumors per mouse, for each genotype. (**B**) Percentage of BrdU positive nuclei in endpoint Tet-ON PyVmT tumors. All mice were injected with BrdU (0.05mg/gram) and sacrificed after 2 hours to allow for BrdU incorporation into cells. N=20 mice per genotype. (**C**) Total tumor volume of $Ezh2^{+/+}$ or $Ezh2^{-/-}$ Tet-ON PyVmT tumors. N=20 mice per genotype. *p<0.05.

2.1.3 Ablation of Ezh2 significantly delays metastasis to distal organs

An important, clinically relevant feature of the PyVmT model is its capacity to metastasize to the lungs with high efficiency. Since complete ablation of *Ezh2* reduced tumor focality and proliferation (**Figure 2-3A, B, C**), animals were sacrificed at an endpoint defined by total tumor volume to confirm that metastatic phenotypes were exclusive of the reduced proliferative capacity of Ezh2-null tumors. Histological

examination of lung tissue sections for the presence of metastatic lesions revealed that mice lacking Ezh2 exhibited a significant reduction in both the size and number of lesions (**Figure 2-4A, B**). To further establish that the observed impact on metastasis was independent of differences in tumor burden and to gain insight into how loss of Ezh2 impairs the metastatic cascade, cells from freshly dissociated wild-type and Ezh2-null tumors were injected into the tail vein of athymic nude mice. Following 8 weeks of doxycycline induction, mice were sacrificed and lungs were assessed. The results demonstrated that loss of Ezh2 significantly impairs the ability of cells to colonize the lung (**Figure 2-4C**).

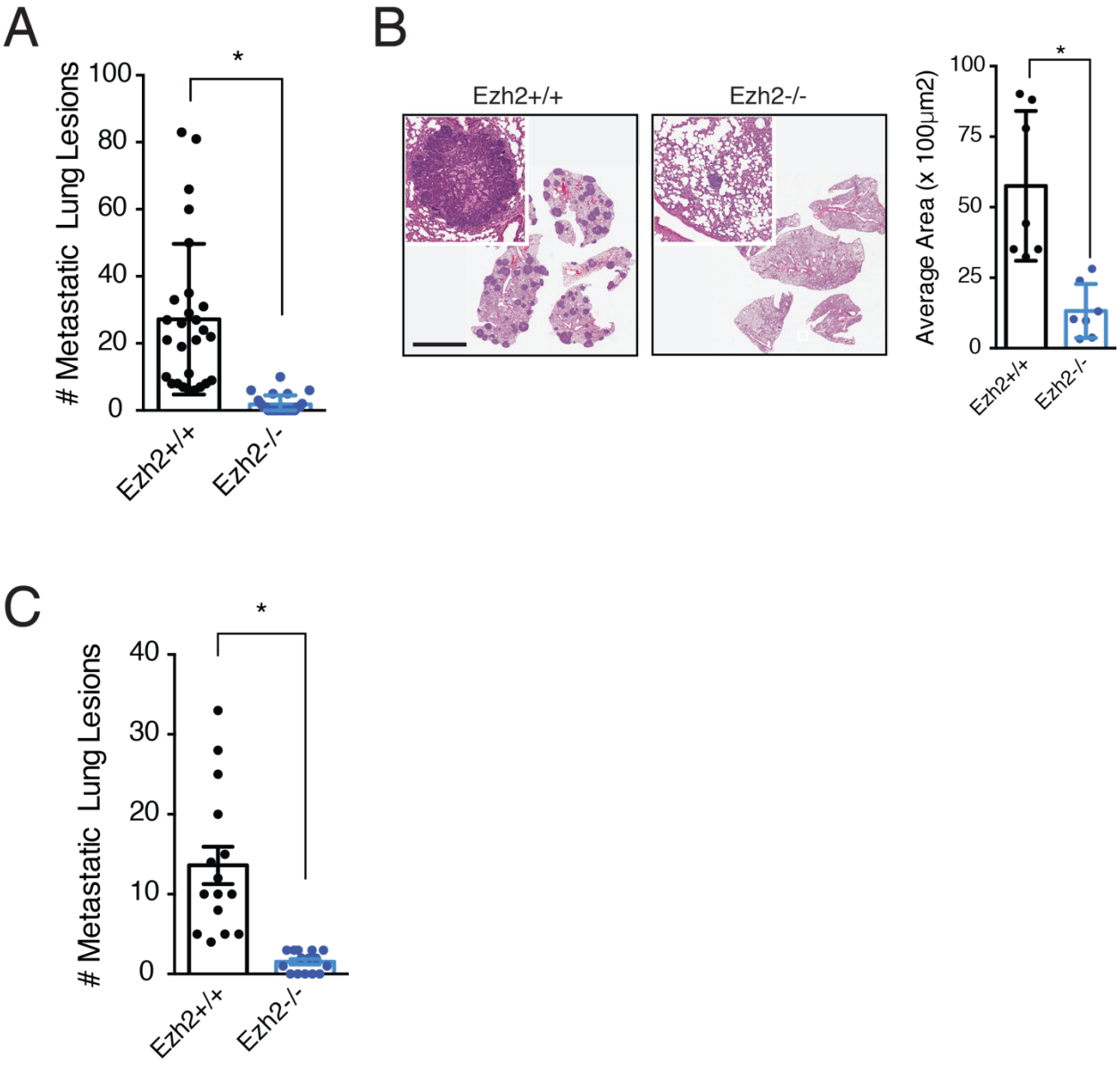

Figure 2-4. Loss of Ezh2 significantly impairs spontaneous metastasis

(**A**) Average number of metastatic lung lesions from tumor burden endpoint Tet-ON PyVmT mice. (**B**) Representative images of hematoxylin and eosin stained sections of paraffin embedded lungs from Tet-ON PyVmT mice at tumor burden endpoint. Scale bar is 5mm. Average area of lung lesions per genotype. (**C**) Quantification of lung lesions following tail vein injections of freshly dissociated cells from $Ezh2^{+/+}$ or $Ezh2^{-/-}$ Tet-ON PyVmT tumors into athymic nude hosts. Mice were sacrificed after 8 weeks and maintained on water supplemented with doxycycline for the duration of the experiment. *$p<0.05$.

2.1.4 Pharmacological inhibition of Ezh2 methyltransferase activity recapitulates genetic perturbation of PRC2

In light of our genetic studies indicating that loss of Ezh2 impairs metastasis, we wished to explore the clinical relevance of these observations further and also establish whether they were directly related to the methyltransferase activity of Ezh2. Several pharmacological inhibitors developed to target PRC2 activity have already shown clinical response in early phase trials in leukemia(254, 255). To test the hypothesis that Ezh2 is a druggable anti-metastatic target, we treated immune-competent mouse models reflective of different clinical situations with the Ezh2 methyltransferase inhibitor GSK-126(232). Previous characterization of the Tet-ON PyVmT model has shown that hyperplastic lesions in the mammary gland can rapidly form following induction with doxycycline for 2 weeks, while progression to invasive adenocarcinoma with metastasis to the lungs occurs upon 6 weeks of doxycycline administration. Thus, to recapitulate a neoadjuvant therapy scenario following the detection of early mammary lesions, we induced Tet-ON PyVmT mice with doxycycline for 2 weeks to allow for palpable lesions to form, and then treated mice with either GSK-126 or vehicle for 4 weeks to determine the effect on the progression of these lesions (**Figure 2-5A**). The efficacy of GSK-126-mediated inhibition was confirmed by immunohistochemical analysis of H3K27me^3 levels (**Figure 2-5B**). Consistent with the genetic ablation of *Ezh2*, we observed a dramatic decrease in the induction of mammary hyperplasias and early adenomas (**Figure 2-5C**) and a complete block in the formation of lung metastases in GSK-126-treated cohorts (**Figure 2-5D**). To further support the concept that the anti-metastatic effect of GSK-126 was due to its effect on the tumor cells, we examined the presence of spontaneous metastatic lung lesions in cohorts of wild-type and Ezh2-null Tet-ON

PyVmT mice induced with doxycycline for 6 weeks. In line with our observations using GSK-126, metastatic lung lesions were detectable in all wild-type Tet-ON PyVmT mice, but not observed in any of the Ezh2-null Tet-ON PyVmT mice (**Figure 2-5D**).

Given that Ezh2 has effects on both tumor initiation and metastasis in our model, we next determined whether GSK-126 administration can alter the metastatic potential of established PyVmT tumor cells. To accomplish this, PyVmT cells were orthotopically implanted into the mammary fat pad of immune-competent hosts, and allowed to grow to a palpable size, at which point mice were treated with GSK-126 or vehicle (**Figure 2-6A**). Loss of H3K27me^3 due to GSK126 administration demonstrated a modest effect on primary tumor growth rate that did not reach statistical significance (**Figure 2-6B, C**). However, like genetic ablation of *Ezh2*, GSK-126 treatment resulted in a dramatic reduction in metastatic burden (**Figure 2-6D**). Collectively, these observations demonstrate that the catalytic activity of Ezh2 is directly required to facilitate dissemination of established Luminal B breast cancer cells.

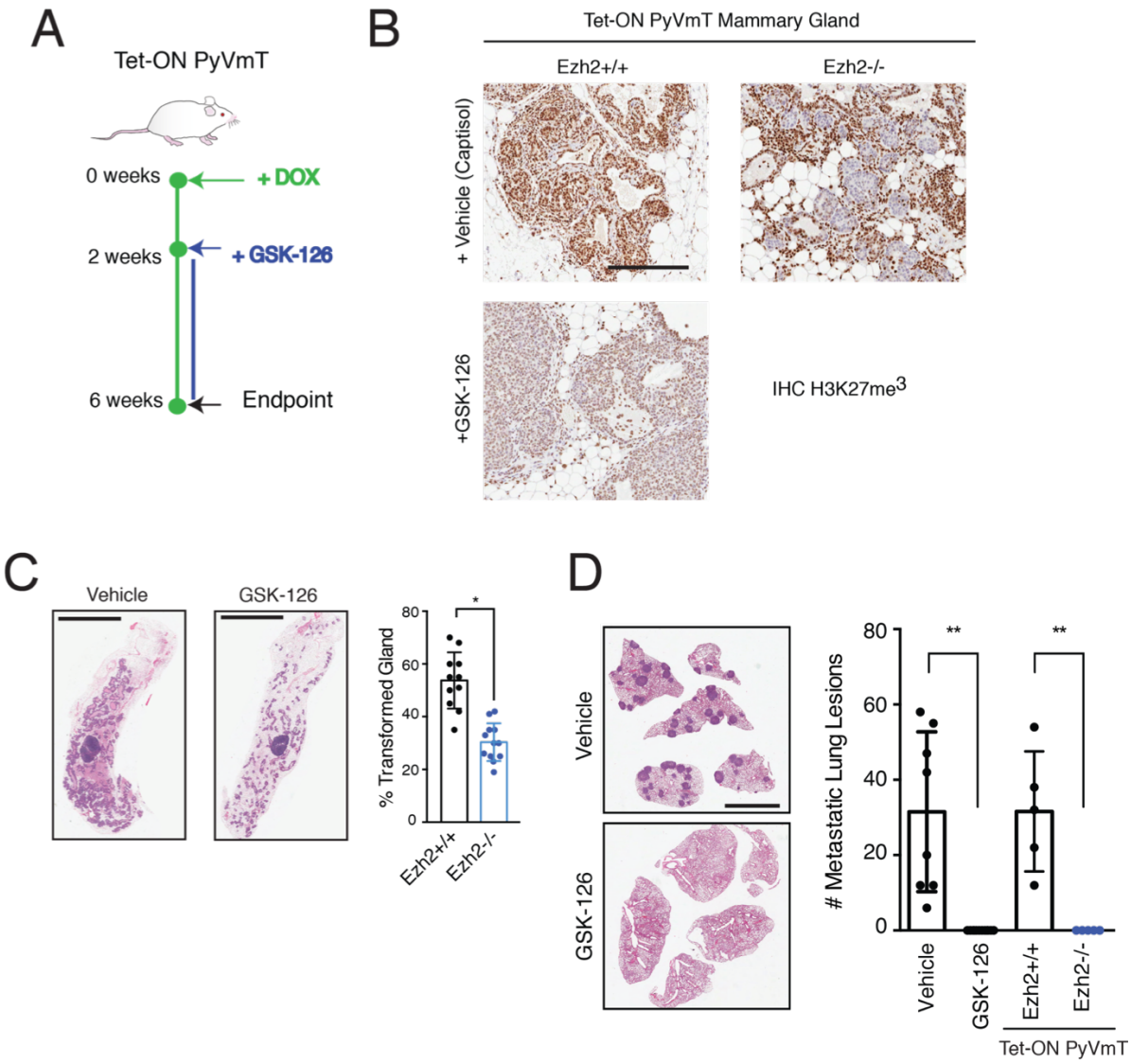

Figure 2-5. Pharmacological inhibition of Ezh2 inhibits metastasis *in vivo*

(A) Schematic of the preclinical model. (B) Representative images of hematoxylin and eosin stained paraffin embedded lungs from mice treated with vehicle control (Captisol) or GSK-126 (150mg/kg) via intraperitoneal injection, 3 times a week. Mice were sacrificed after 6 weeks on water supplemented with doxycycline. Enumeration of metastatic lung lesions in drug treated cohorts as outlined in the schematic, or in $Ezh2^{+/+}$ or $Ezh2^{-/-}$ Tet-ON PyVmT mice induced with doxycycline for 6 weeks. Scale bar is 5 mm.

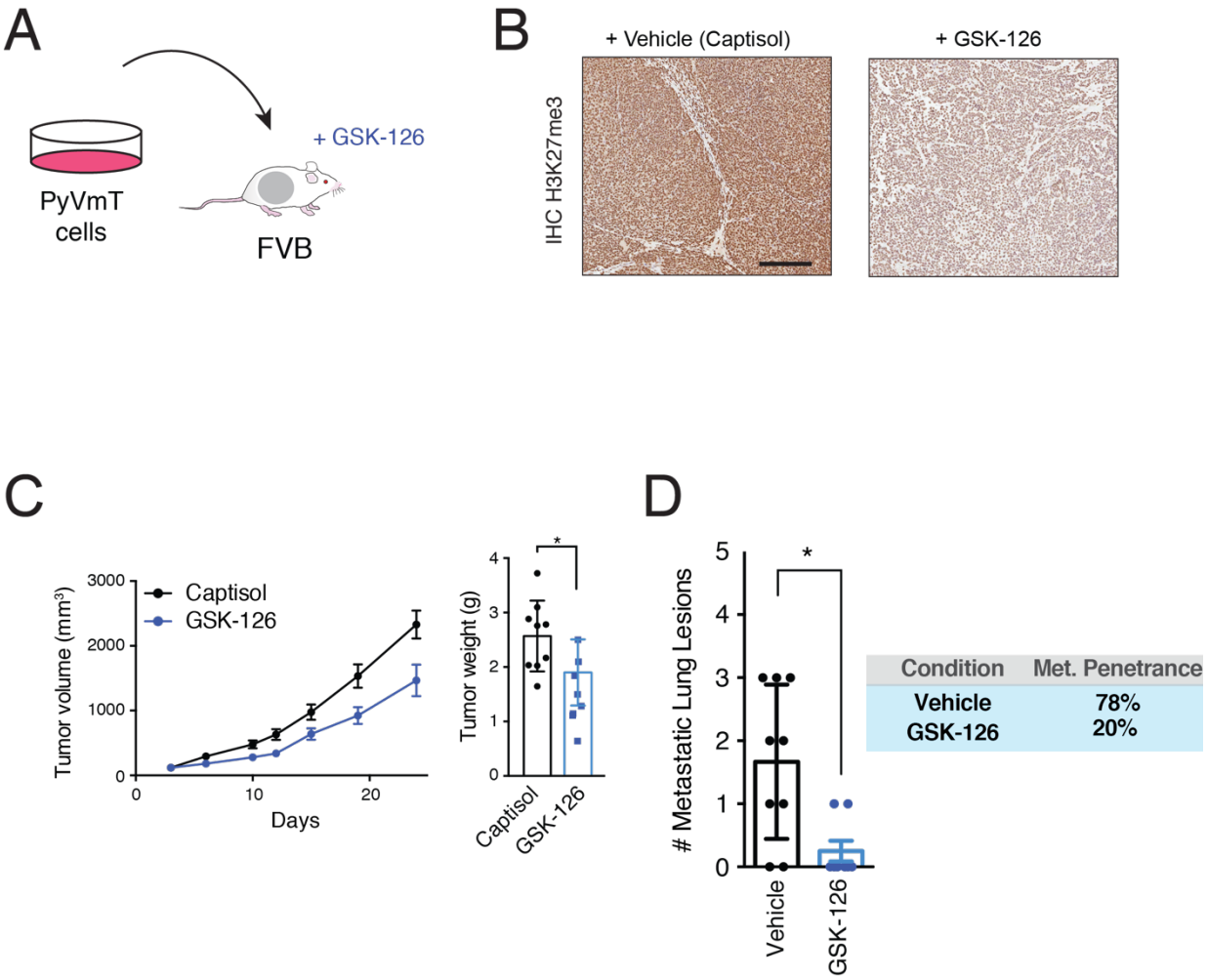

Figure 2-6. Inhibition of Ezh2 impairs metastasis of transformed tumour cells

(A) Schematic of orthotopically injected PyVmT cells in an immune-competent FVB strain host. GSK-126 or Captisol vehicle control treatment commenced when tumors reached 5mmx5mm. (B) Paraffin-embedded sections of tumors from PyVmT cells orthotopically injected into the mammary fat pad of FVB hosts, and treated with GSK-126 or vehicle for 3 weeks. Scale bars are all 1mm. (C) Tumor growth of mice treated with GSK-126 or vehicle control. Quantification of tumor weight after 3 weeks of drug treatment. * $p<0.05$.(**D**) Enumeration of lung lesions from mice treated with GSK-126 or vehicle for 24 days. * $p< 0.05$ **$p<0.01$. Met. Penetrance= Penetrance of Metastatic lung lesions.

2.1.5 Transcriptional profiling of Ezh2 ablated tumours

To further evaluate the effect of loss of Ezh2 on the transcriptome of PyVmT tumors, gene expression profiling of Ezh2 proficient and deficient Tet-ON PyVmT endpoint tumors was conducted (**Figure 2-7A**). Ingenuity Pathway Analysis (IPA) was used to reveal functional pathways and functions activated in the absence of Ezh2. The functional analysis uncovered a significant number of differentially regulated genes in the Ezh2 knock-out mice associated with cellular differentiation and axonal guidance (**Figure 2-7B**).

Notably, Ezh2 has been reported to be necessary for Epithelial to Mesenchymal Transformation (EMT), a process critical to metastatic disease progression(256). However, functional enrichment analysis using IPA identified EMT as a biological pathway up-regulated in Ezh2-null Tet-ON PyVmT tumors (**Figure 2-7B**), suggesting that a block in EMT is unlikely to explain the impaired metastatic capacity of these tumor cells. To independently validate the pathways identified by IPA, we also used Gene Set Enrichment Analysis (GSEA) to analyze our microarray dataset. Similar to the IPA analysis, GSEA identified up-regulation of pathways related to ECM organization and Axon Guidance in $Ezh2^{-/-}$ tumors (**Figure 2-7C**).

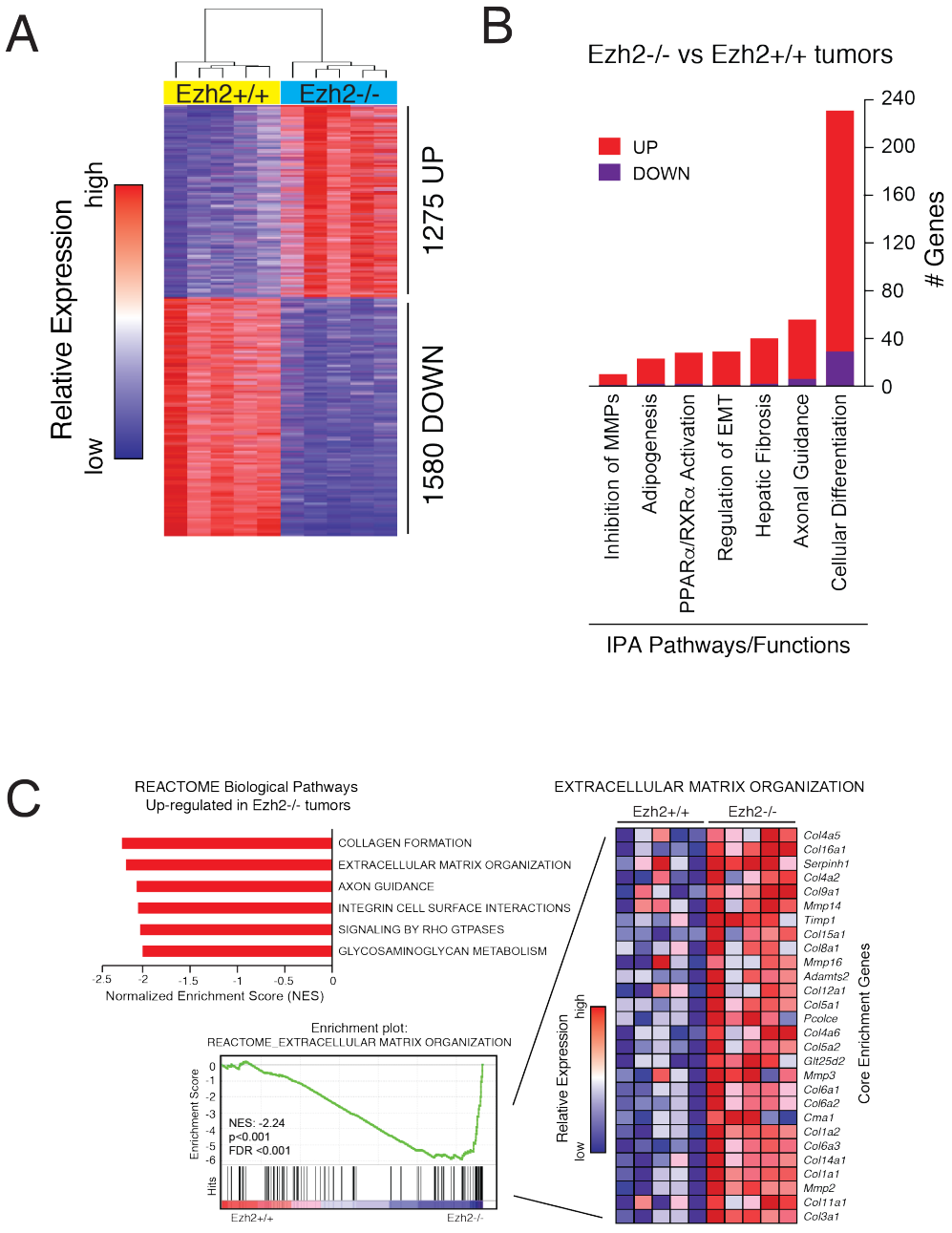

Figure 2-7. Functional genomics of Ezh2$^{-/-}$ vs Ezh2$^{+/+}$ endpoint tumours

(A) Hierarchical clustering of genes differentially expressed between Ezh2$^{+/+}$ and Ezh2$^{-/-}$ Tet-ON PyVmt tumors (n=5) using p-value < 0.05 and fold change > 1.5 cutoffs. Red and blue indicate high and low expression of genes, respectively. (B) Schematic of a subset of over-represented pathways and functions identified by IPA analysis of genes found differentially expressed in Ezh2 null tumors. (C) GSEA identification of significantly up-regulated Reactome biological pathways in Ezh2$^{-/-}$ tumors. A representative plot and heatmap illustrating the increased expression of genes associated with ECM organization in Ezh2 null tumors are shown.

2.1.6 ChIP-Seq analysis of H3K27me^3 marks in the inducible PyVmT model

We speculated that the metastatic impairment observed might be due to the activation of novel transcriptional programs in the absence of Ezh2-mediated repression. To explore this idea, we performed chromatin-immunoprecipitation coupled with deep sequencing (ChIP-seq) of H3K27me^3 on 5 endpoint tumors per genotype. As anticipated, we observed a global decline in binding peak events across the genome including at the transcriptional start sites of genes in Ezh2-null tumors (**Figure 2-8A, B**).

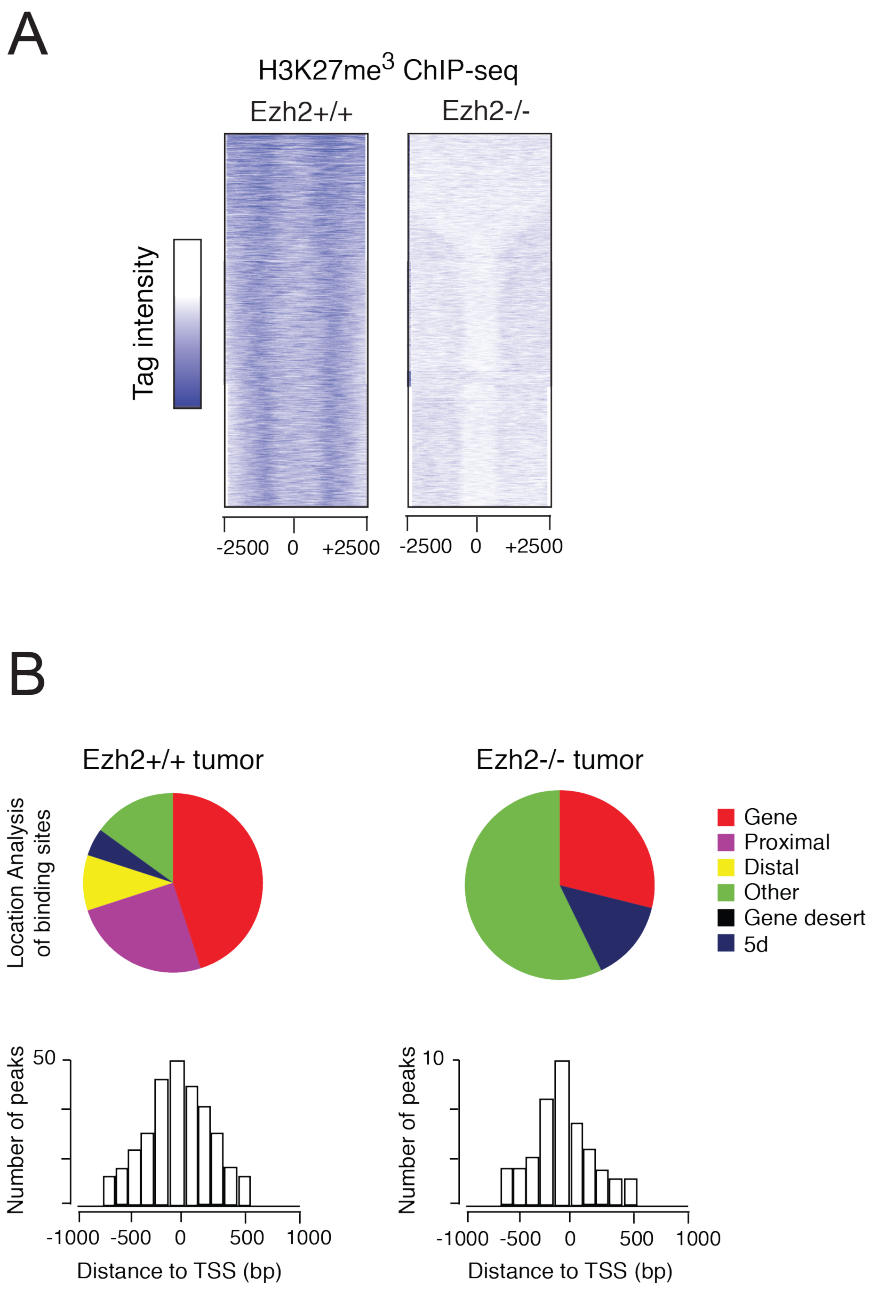

Figure 2-8. H3K27me3 ChIP-Seq analysis of Ezh2$^{-/-}$ vs Ezh2$^{+/+}$ endpoint tumours

(A) Heatmaps of signal intensity illustrating H3K27me^3 ChIP-seq genomic mapping in a window of ± 2.5kb from the TSS identified in Ezh2$^{+/+}$ and Ezh2$^{-/-}$ Tet-ON PyVmt tumors. ChIP-Seq data is a cumulation of 5 samples per genotype combined. (B) Pie chart and histogram showing ChIP-seq H3K27me^3 mapping across the genome.

2.1.7 Identification of a novel Foxc1-driven anti-metastatic cascade

Next, we intersected our transcriptomic and ChIP-seq datasets to identify genes directly regulated by Ezh2. Our cross-examination revealed that approximately 22% of differentially up-regulated genes in Ezh2-null Tet-ON PyVmT tumors were H3K27me^3 targets (**Figure 2-9A**). Transcription factor motif enrichment analysis of this 328 gene subset was performed (**Figure 2-9B**). One candidate master regulatory factor, Forkhead Box C1 (Foxc1) was of interest, as we identified it as a direct target gene of Ezh2-mediated H3K27me^3 (**Figure 2-10A**) and confirmed to be up-regulated in the tumor epithelium of Ezh2-null tumors (**Figure 2-10B**). Of note, tumors lacking Ezh2 did not have altered expression of other Forkhead box family members (**Figure 2-10C**). Consistent with the notion that *Foxc1* was a target of transcriptional silencing by Ezh2, immunofluorescence revealed that Ezh2 and Foxc1 did not co-localize in endpoint Tet-ON PyVmT tumors (**Figure 2-10D**). As observed with the genetic loss of Ezh2, inhibition of Ezh2 activity with GSK-126 resulted in a specific increase in *Foxc1* transcript levels (**Figure 2-11A**) coinciding with loss of H3K27me^3 in the promoter region of *Foxc1* determined by ChIP-qPCR (**Figure 2-11B**).

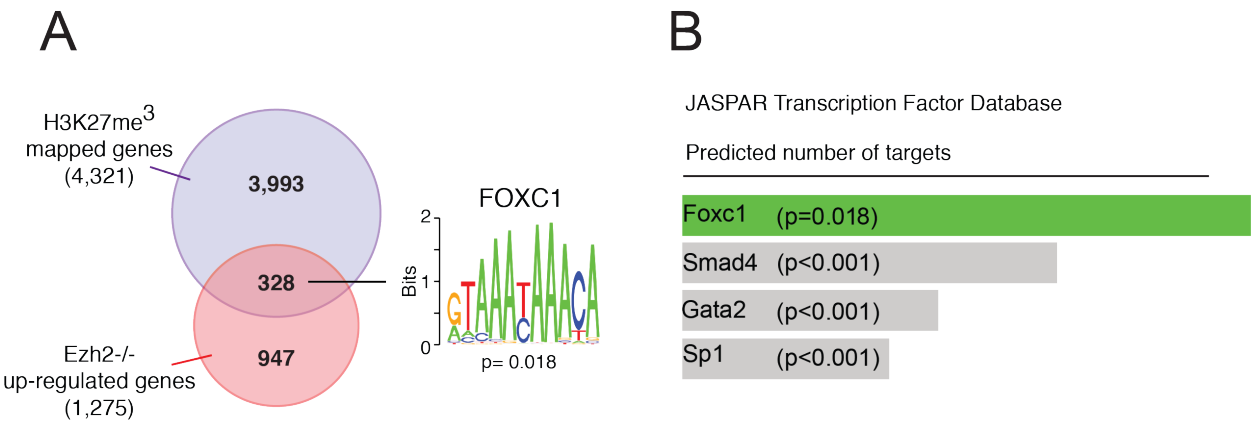

C

GO biological pathway enrichment in H3K27me^3 target genes found up-regulated in Ezh2-/- tumors

GO: Biological Pathway	p Value
Neuron Projection & Guidance (GO: 00974695)	0.03
Axon Guidance (GO: 0007411)	0.03
Extracellular Matrix Organization (GO:0030198)	0.04
Neural Crest Cell Development (GO:00143032)	0.05
Tissue Morphogenesis (GO:00061667)	0.05

Figure 2-9. Overlay of microarray and ChIP-Seq data and identification of FoxC1

(A) Overlap between differentially up-regulated genes in Ezh2$^{-/-}$ endpoint Tet-ON PyVmT tumors and genes identified by ChIP-seq to be targeted by H3K27me^3. (B) Transcription factor enrichment for genes up-regulated in the Ezh2-null mammary tumors that were also identified as being targets of H3K27me^3. (C) Gene Ontology (GO) terms most significantly enriched in genes differentially upregulated in Ezh2$^{-/-}$ endpoint tumors, that were also H3K27me^3 targets.

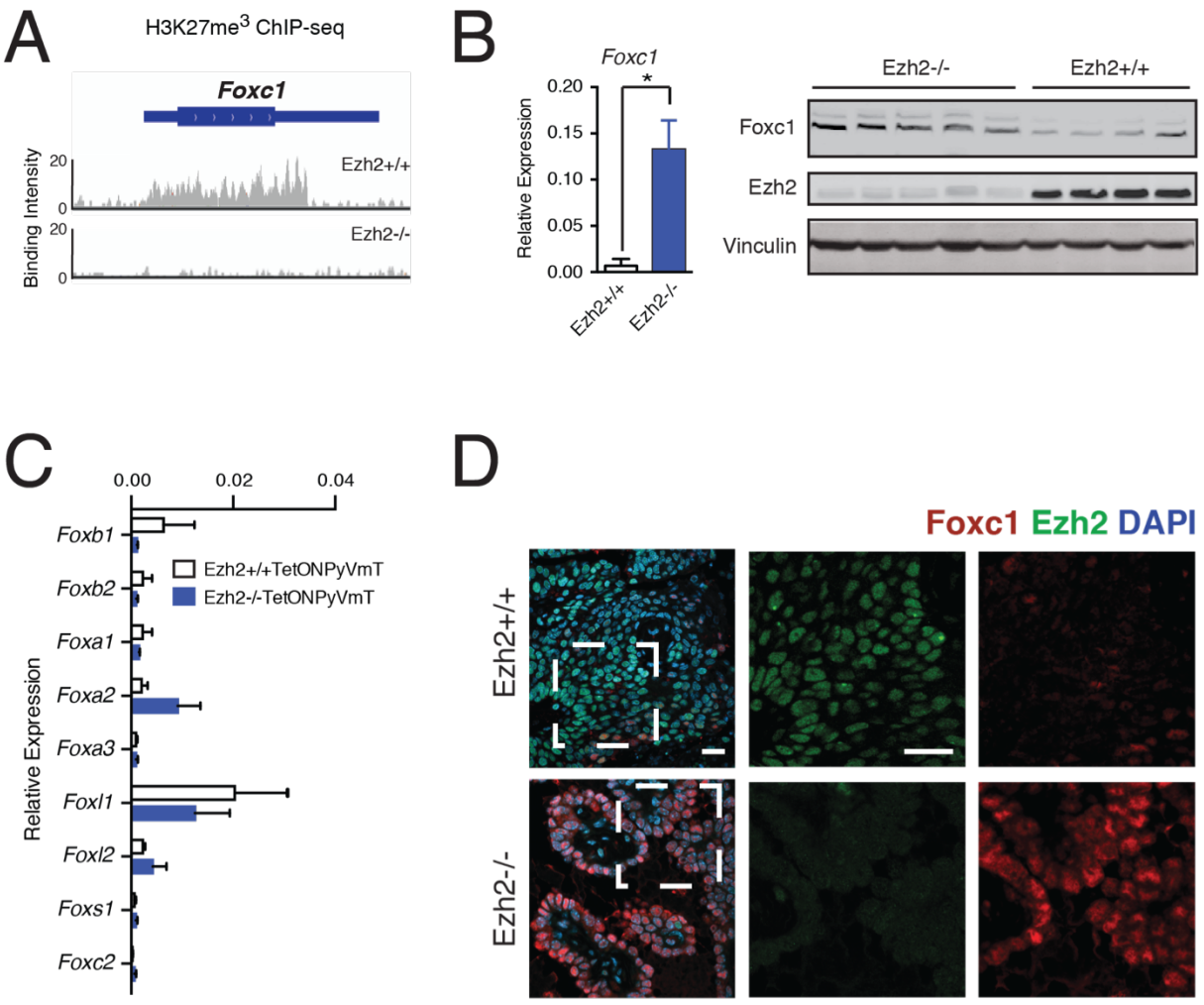

Figure 2-10. Confirmation of Foxc1 as a PRC2 target

(A) Differential H3K27me^3 levels in the upstream promoter region of *Foxc1* in Ezh2$^{+/+}$ vs. Ezh2$^{-/-}$ endpoint Tet-On PyVmT tumors. Image from the IGV browser. (B) Left- Significant up-regulation of Foxc1 mRNA in Ezh2$^{-/-}$ Tet-ON PyVmT endpoint tumors compared to wild-type tumors. Right- Immunoblot of Ezh2$^{+/+}$ or Ezh2$^{-/-}$ Tet-ON PyVmT endpoint tumors for Foxc1 and Ezh2 levels. Vinculin loading control. (C) qRT-PCR screen of Forkhead box family members in tumors lacking Ezh2. (D) Immunofluorescence staining of Foxc1 and Ezh2 in endpoint Ezh2$^{+/+}$ or Ezh2$^{-/-}$ Tet-ON PyVmT tumors. Scale bars are 50μm.

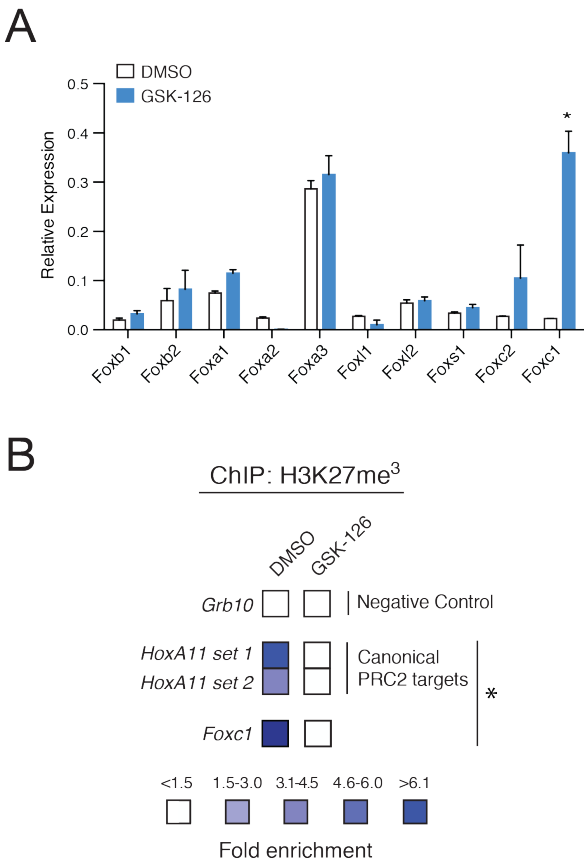

Figure 2-11. Validation of the PRC2-FoxC1 locus in GSK-126 treated cells

(A) PyVmT cells treated with GSK-126 (2μM, 72 hours) significantly up-regulated the Forkhead box family member, *Foxc1*, compared to DMSO control treated cells. (B) Chromatin-immunoprecipitation enrichment of H3K27me^3 at canonical PRC2 targets and the *Foxc1* promoter in DMSO treated PyVmT cells which is lost in GSK-126 treated cells.

Given that Foxc1 acts a pioneer transcription factor that can independently regulate its own target genes, we next assembled a set of 23 putative Foxc1 target genes (derived from the JASPAR database) that were both upregulated in the Ezh2$^{-/-}$ mice and enriched for H3K27me^3 binding in the ChIP-Seq dataset (**Figure 2-12A**). Then, to understand the pathways downstream of the identified Foxc1 targets, we used Gene Ontology (GO) terms to organize Foxc1 targets found up-regulated in the context of Ezh2 deletion (**Figure 2-12B**). Several of these genes clustered with cellular processes related to neuronal function and ECM organization, and were reflective of the primary programs identified by IPA and GSEA in the broader Ezh2$^{-/-}$ upregulated gene set. Interestingly, the overexpression of several of these targets has been reported to be anti-metastatic. The ECM matrix components *Col4a6*(257) and *Col15a1*(258) maintain basement membrane integrity to prevent tumor migration, and are lost prior to tumor invasion. Facilitators of axon guidance and cell adhesion *Slfn5*(259), *Rgma*(260, 261) and *Chl1*(262) are also down-regulated during breast cancer progression. To establish that the effects of *Foxc1* de-repression could be recapitulated with a pharmacological inhibitor, we validated the transcriptional up-regulation of 13 Foxc1 target genes following treatment with GSK-126 (**Figure 2-12C**). Next, ChIP-qPCR was employed to validate that Foxc1 is indeed recruited to its candidate targets upon global reduction of H3K27me^3 in the absence of Ezh2 methyltransferase activity. Foxc1 occupancy in the promoter regions of 4 different genes in the set of Foxc1 targets (*Rgma, Chl1, Slc9a9, Col15a1*) was confirmed only in the presence of GSK-126 (**Figure 2-12D**).

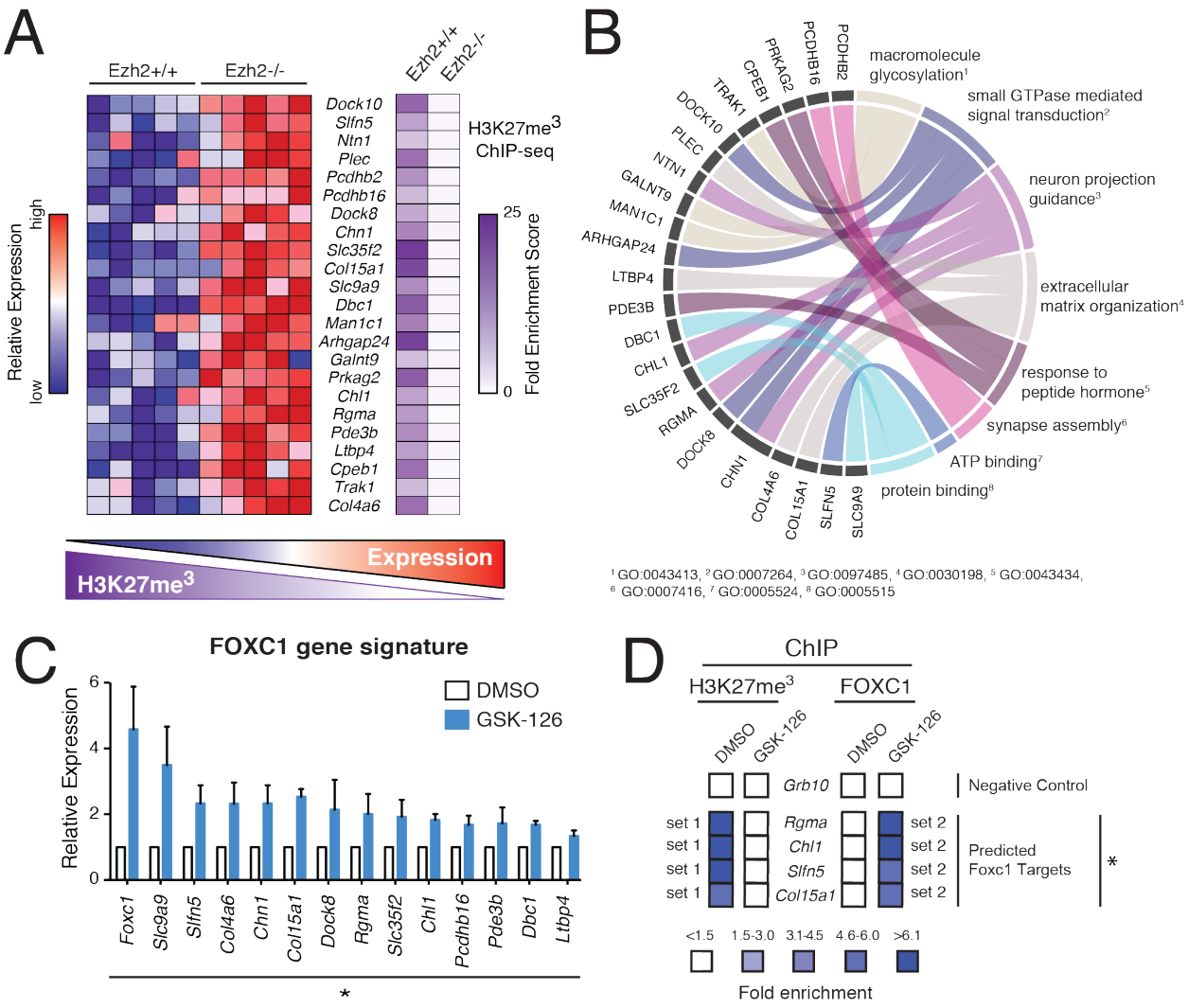

Figure 2-12. Identification of anti-metastatic targets repressed by Ezh2

(A) Increased expression of Foxc1 predicted target genes coincides with reduced H3K27me^3 enrichment status in Ezh2$^{-/-}$ versus Ezh2$^{+/+}$ tumors. (B) Chord diagram of up-regulated Foxc1 targets and their associated GO Biological Terms. The ChIP experiment is reflective of 3 different PyVmT cell lines. (C) Quantitative RT-PCR analysis of Foxc1 targets in PyVmT cells treated with GSK-126 (2μM for 72 hours) or DMSO (vehicle). Data is an average of experiments performed in three different PyVmT cell lines. *p<0.05 (D) Chromatin-immunoprecipitation of H3K27me^3 or Foxc1 in the presence or absence of Ezh2-mediated H3K27me^3 profiles. 3 different PyVmT cell lines were treated with or without GSK-126 (2μM, 72 hours) or DMSO. Specific primers to detect binding by H3K27me^3 and Foxc1 were designed. *p<0.05

2.1.8 Functional validation of the anti-metastatic capacity of Foxc1

Many of the validated downstream targets of Foxc1 exert their anti-metastatic effects through impairment of cellular motility and invasiveness. Thus, to test the contribution of Foxc1 to the metastatic cascade, we generated PyVmT cells stably expressing Foxc1 and assayed invasiveness. Interestingly, while ectopic expression of Foxc1 significantly impaired the ability of cells to invade across a basement membrane matrix (**Figure 2-13A**), it did not alter cellular proliferation (**Figure 2-13B**). In addition, the capacity of cells to colonize the lung was also dramatically diminished upon exogenous Foxc1 expression (**Figure 2-14A**). Given these results, we sought to ascertain the extent of the contribution of Foxc1 to the metastatic defect induced by global reduction of H3K27me^3 profiles. To this end, lentiviral-mediated RNA interference was used to knock-down expression of *Foxc1* in PyVmT cells, which were then treated with GSK-126 or DMSO (vehicle). Expression of shRNAs targeting *Foxc1* significantly blunted the de-repression of Foxc1 by Ezh2 inhibition (**Figure 2-14B**). Remarkably, the loss of Foxc1 almost completely restored the invasiveness of the GSK-126-treated cells to the level of control cells (**Figure 2-14B**) indicating that transcriptional repression of *Foxc1* is a critical molecular component of the pro-metastatic effect facilitated by H3K27me^3-mediated silencing.

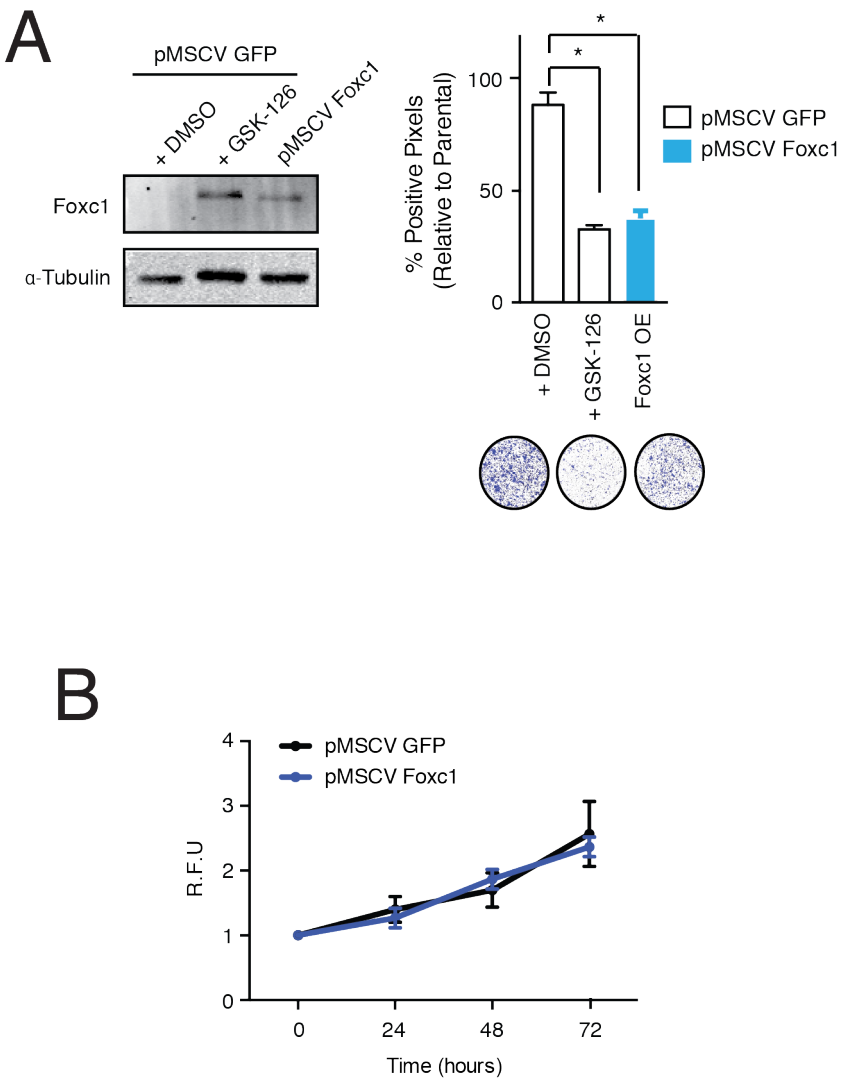

Figure 2-13. Ectopic expression of Foxc1 alters invasion but not proliferation

(A) Transwell invasion assay of PyVmT cells expressing exogenous Foxc1 or GFP. Experiments were performed three times, and results are displayed relative to untreated parental cell. (B) CyQUANT assay measuring cellular proliferation of PyVmT cells expressing exogenous GFP or Foxc1. R.F.U= relative fluorescence units. Data were normalized to the fluorescence values at time=0.

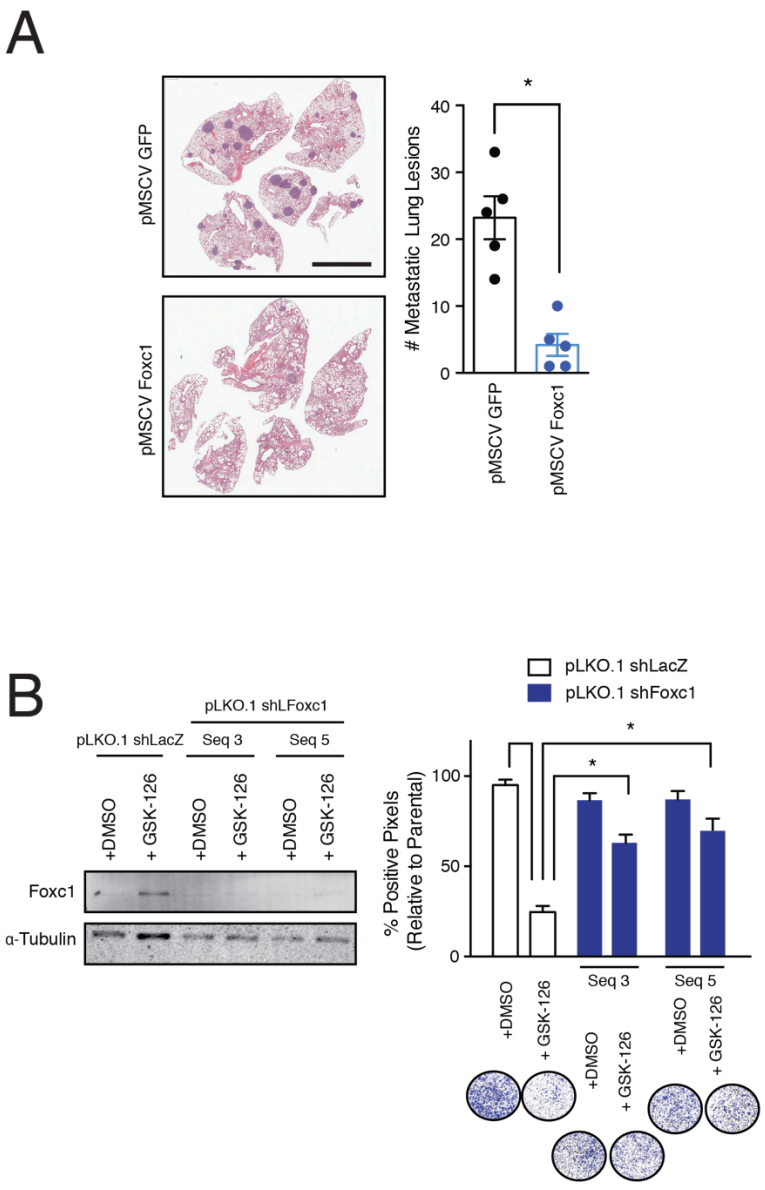

Figure 2-14. Ectopic expression of Foxc1 impairs metastasis

(A) Enumeration of lung lesions following the injection of PyVmT cells expressing exogenous Foxc1 or GFP in the tail vein of athymic nude mice. *p<0.05. Scale bar is 5 mm. (B) Left- Representative immunoblot showing Foxc1 expression in cells stably transduced with a control shRNA (shLacZ) or two independent shRNAs targeting *Foxc1* and treated with DMSO or GSK-126 (2μM for 72h). α-Tubulin was used as a loading control. Right- Transwell invasion assay of PyVmT cells infected with shRNA targeting LacZ (control) or two different sequences targeting Foxc1. Cells were pre-treated with DMSO or GSK-126 (2μM) for 72 hours and assayed for their capacity to invade through Matrigel. All assays were performed in triplicate. * p<0.05.

2.1.9 Elevated FOXC1 *levels associates with different outcomes across breast cancer subtypes*

Having established that FOXC1 can drive an anti-metastatic program, we sought to confirm the relevance of this finding in a clinical context using both publicly available breast cancer patient data sets and human patient specimens.

To validate the relationship between EZH2 and FOXC1, we first quantified FOXC1 protein levels in 20 Luminal B patient tumor samples via immunofluorescence staining of breast tissue biopsies. We confirmed significant positive correlation with matched *FOXC1* mRNA expression levels (r=0.57, p=0.004) (**Figure 2-15A**). Importantly, we observed an inverse correlation between EZH2 and FOXC1 protein levels in this Luminal B cohort (**Figure 2-15B**). This observed mutual exclusivity supported the mechanism of EZH2-mediated FOXC1 repression in Luminal B breast cancer.

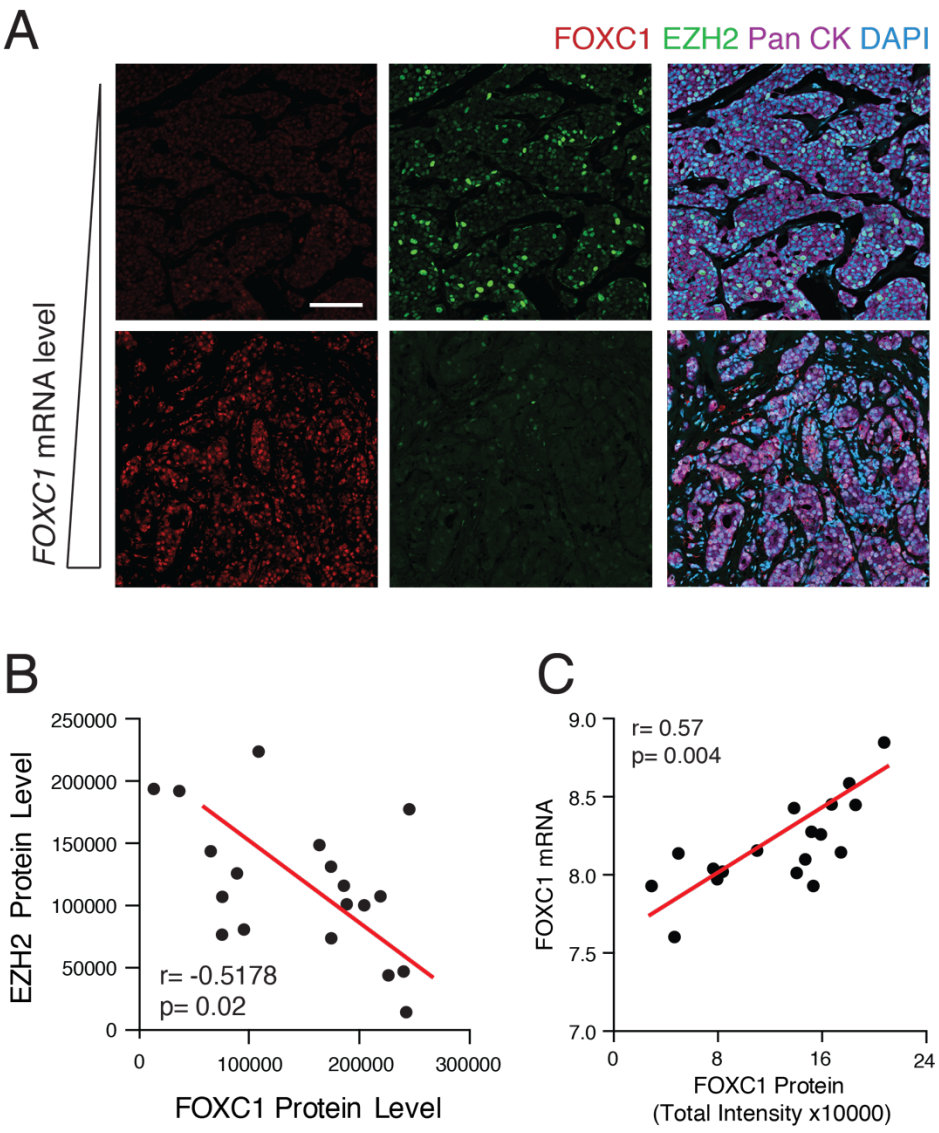

Figure 2-15. Breast Cancer subtype specificity of the EZH2/FOXC1 metastatic axis

(A) Representative images of formalin fixed paraffin embedded tissue samples from human Luminal B tumors stained for FOXC1 and EZH2. Scale bar is 100µm. (B) Significant negative correlation between FOXC1 transcript levels and EZH2 protein levels (Total intensity) quantified by immunofluorescence in human Luminal B patient samples (r=-0.52, p=0.02). 8 different fields taken with a 20x objective were quantified per sample. (**C**) Significant positive correlation between FOXC1 transcript levels derived from microarray profiling of Luminal B patient tumor samples and protein levels as assessed by immunofluorescence staining (r= 0.57, p=0.004).

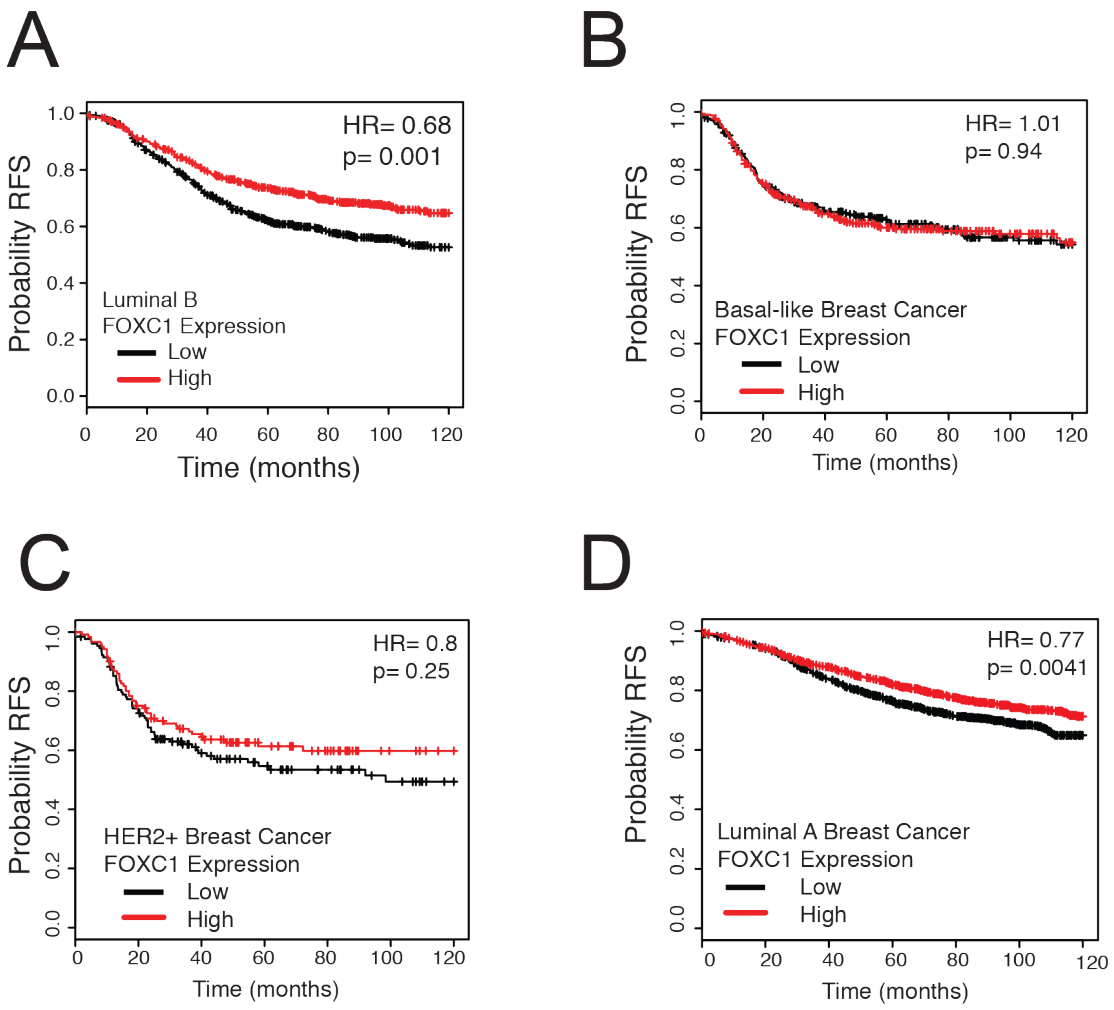

Figure 2-16. High FOXC1 levels are associated with good outcome in luminal B breast cancer

(A) Kaplan-Meier survival curve of relapse free survival (RFS) of 1142 luminal B tumors with high or low FOXC1 (log rank p=0.001). Patient samples were split into two groups according to carious quantile expression of FOXC1. Hazards Ratio (HR) are calculated with a 95% confidence interval. (B) Kaplan-Meier survival curve of relapse free survival of 618 BLBC patients with high or low FOXC1 (no significant difference). (**C**). Kaplan-Meier survival curve of relapse free survival of 335 HER2+ patients with high or low FOXC1 (no significant difference, but trend towards higher levels of *FOXC1* conferring better outcome, p=0.25). (D) Kaplan-Meier survival curve of relapse free survival of 2504 Luminal A patients with high or low FOXC1 (p=0.004).

To next address the prognostic value of FOXC1 levels across different subtypes, we interrogated a large breast cancer clinical dataset available through KM plotter (263). We observed that higher expression of *FOXC1* was associated with increased relapse-free survival in Luminal B patients (**Figure 2-16A**), but not in BLBC (**Figure 2-16B**). Interestingly, there was a trend towards increased relapse-free survival in HER2+ patients with increased *FOXC1* levels, and a significantly increased probability in Luminal A patients (**Figure 2-16C, D**). Taken together, these data suggested that FOXC1 plays a tumor suppressive role in non-BLBC subtypes and we hypothesized that the previously identified FOXC1 targets might facilitate this anti-metastatic program. To confirm this hypothesis, we interrogated the TCGA database using the previously validated FOXC1 13-gene signature (**Figure 2-12A**). As expected, our analysis identified a positive correlation between *FOXC1* transcript levels and the FOXC1 multi-gene signature in Luminal B patients (**Figure 2-17A**) as well as the HER2+ and Luminal A subtypes, but not in the BLBC cohort **(Figure 2-17B-D).** This observation for BLBC patients is consistent with previous findings, as *FOXC1* has gained notoriety in breast cancer as a key marker for BLBC(264) dictating aggressiveness of the subtype through various mechanisms(265). Hence, activation of an anti-metastatic gene signature by FOXC1 would not be expected in this subtype.

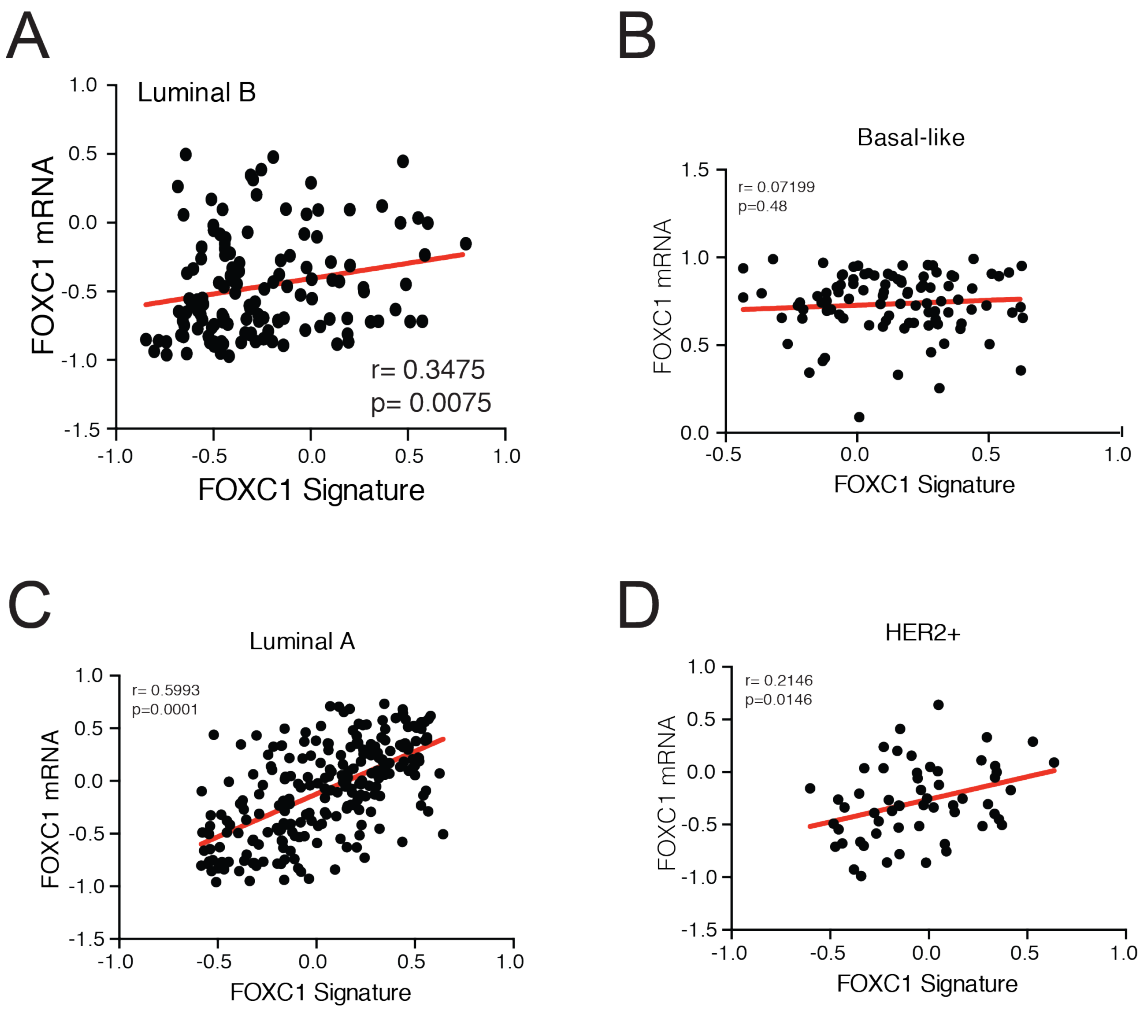

Figure 2-17. Correlation between FOXC1 and the FOXC1 signature across different breast cancer subtypes

(A) Correlation between FOXC1 mRNA levels and the FOXC1 Signature in a cohort of 385 Luminal B patients from publicly available TCGA Breast Cancer data set. (B) No correlation between the *FOXC1* gene signature and *FOXC1* transcript levels in Basal-like patients from the TCGA Breast Cancer database (r=0.07, p=0.48). (**C**) Significant positive correlation between the *FOXC1* gene signature and *FOXC1* transcript levels in HER2+ patients from the TCGA Breast Cancer database (r=0.21, p=0.015). (D) Significant positive correlation between the *FOXC1* gene signature and *FOXC1* transcript levels in Luminal A patients from the TCGA Breast Cancer database (r=0.6, p=0.0001).

2.1.10 EZH2-mediated repression of an anti-metastatic program is specific to the Luminal B subtype

To establish the prognostic importance of the FOXC1 gene signature, we revisited KM plotter to analyze the effect of the FOXC1 signature levels across different breast cancer subtypes. Interestingly, higher expression of the FOXC1 signature conferred a significantly greater probability of relapse free survival in only the Luminal B (**Figure 2-18A**) and HER2+ breast cancer patients (**Figure 2-18B,C**).

While FOXC1 may operate as an anti-metastatic factor in non-BLBC breast cancer subtypes, it was unclear if EZH2 mediated repression of an anti-metastatic program through suppression of FOXC1 was subtype specific. To explore if this, we first analyzed *EZH2* and *FOXC1* transcript levels in a large cohort of breast cancer patient data from The Cancer Genome Atlas (TCGA) database. Notably, we observed that higher levels of *EZH2* mRNA reads coincided with lower levels of *FOXC1* read counts only in the Luminal B and HER2+ subtypes (**Figure 2-19A,** Luminal B r=, HER2 r=). Given that we observed this inverse association in both Luminal B and HER2+ patient samples, next we functionally validated that EZH2-mediated H3K27me^3 repression of *FOXC1* was unique to the Luminal B subtype. First, we treated a panel of human breast cancer cell lines representing 4 different molecular subtypes with GSK-126. Subsequent analysis of transcript levels demonstrated that only the Luminal B cell line showed significant up-regulation of *FOXC1* upon reduction of global H3K27me^3 levels (**Figure 2-19B**).

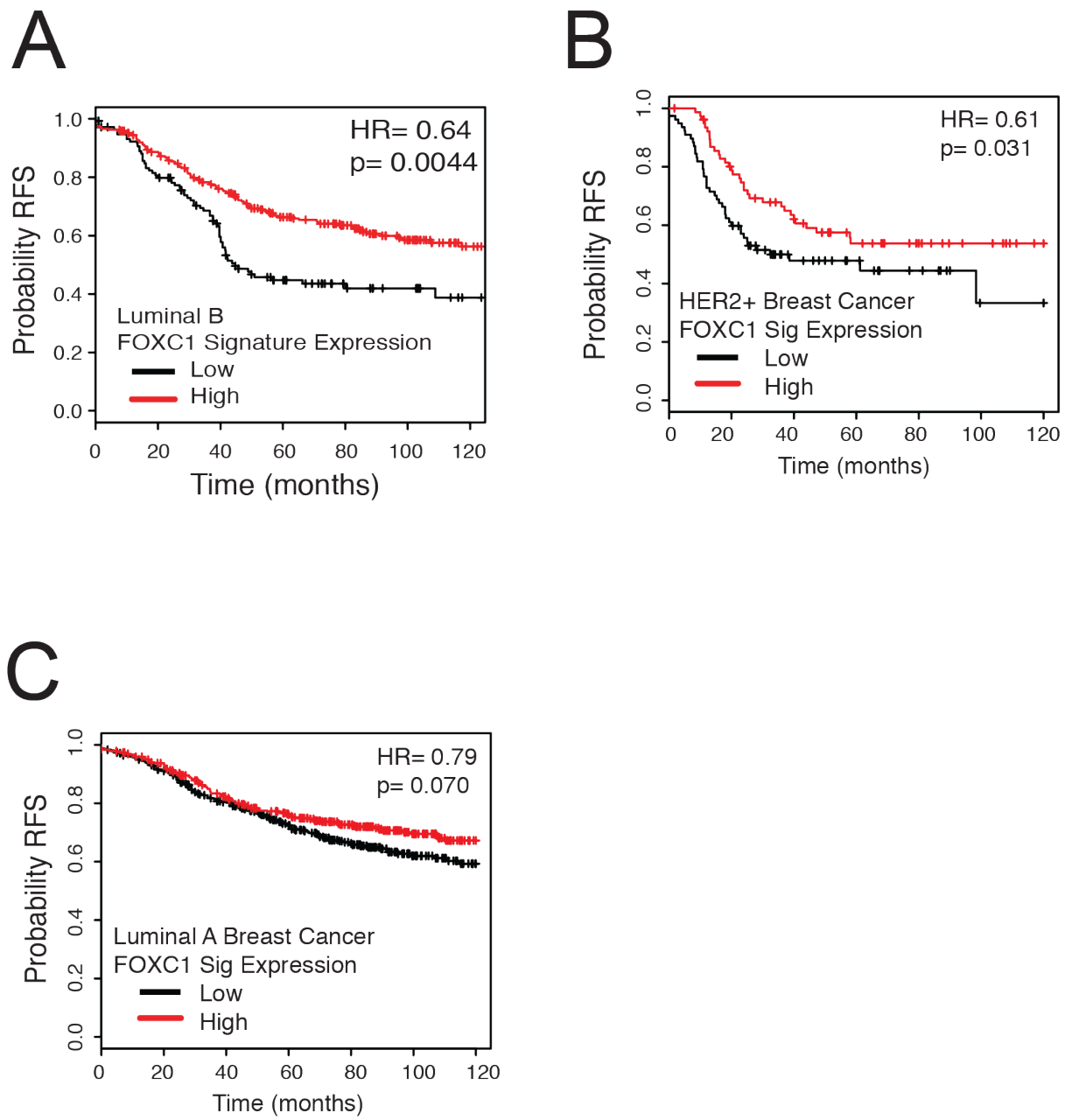

Figure 2-18. Survival of patients with FOXC1 signature ^{High} across different breast cancer subtypes

(A) Kaplan-Meier analysis of relapse free survival of 1142 Luminal B tumors with high or low FOXC1 gene signature expression (log rank p=0.0044).(B) Kaplan-Meier survival curve of relapse free survival of 335 HER2+ patients with high or low FOXC1 signature (p=0.031). (C) Kaplan-Meier survival curve of relapse free survival of 2504 Luminal A patients with high or low FOXC1 signature (p=0.07).

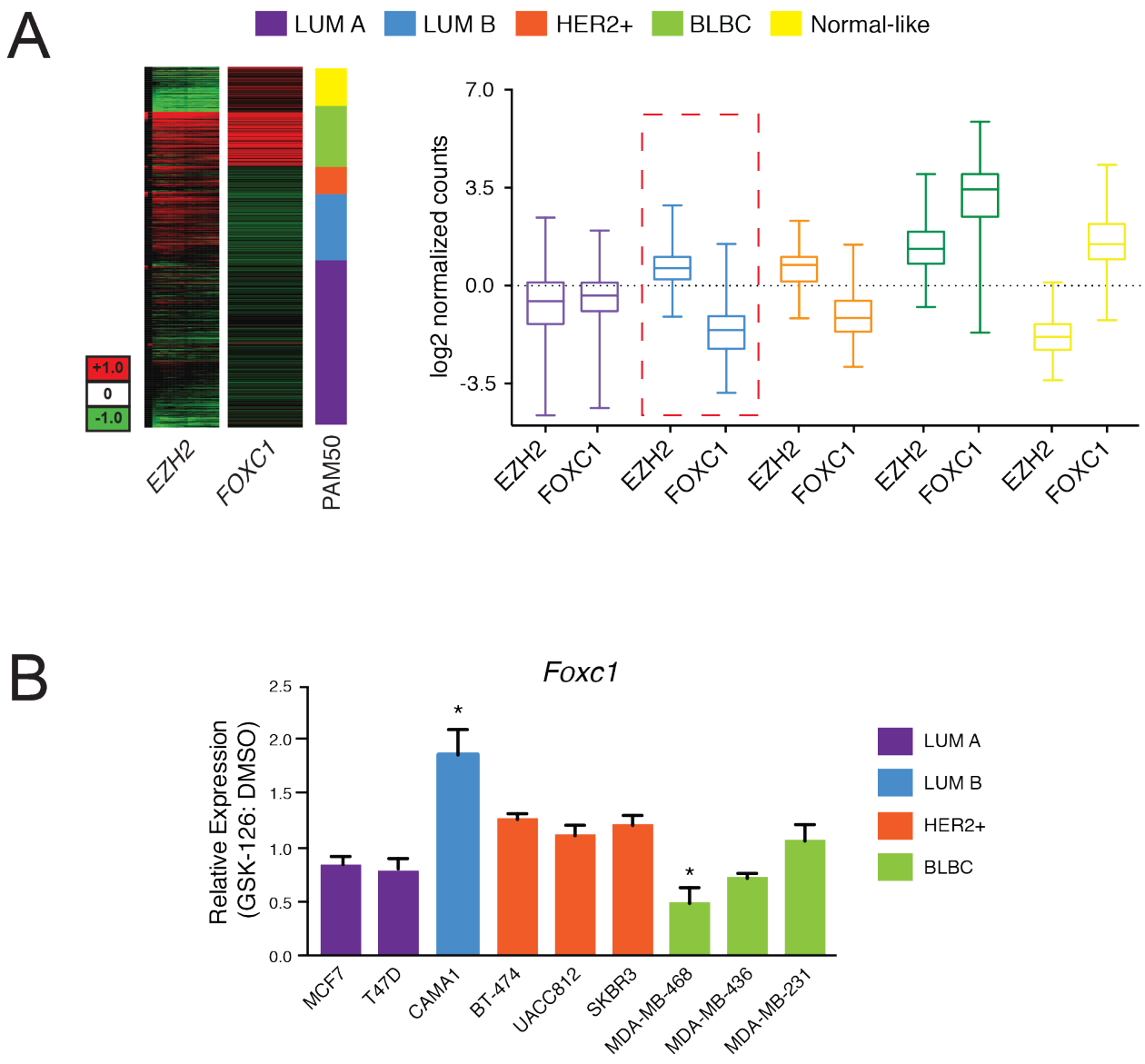

Figure 2-19. Correlation between FOXC1 and the EZH2 across different breast cancer subtypes

(A) *FOXC1* or *EZH2* transcript levels across different PAM50 subtypes of breast cancer represented in a heat map. Turkey box plots showing median EZH2 or FOXC1 levels across different breast cancer subtypes. Data is from the TCGA Breast Cancer data set, publicly accessible via the XENA UCSC Cancer Genome Browser. (B) qRT-PCR analysis of FOXC1 levels in different breast cancer cells lines following 72 hours of treatment with GSK-126 (2μM) or DMSO (vehicle) for 72 hours. Samples were assayed in triplicate, and *FOXC1* expression was normalized to the housekeeper gene *ACTB.*

Next, to validate the anti-metastatic effect of EZH2 inhibition in distinct molecular subtypes of human breast cancer *in vivo*, we orthotopically transplanted two different patient-derived xenografts (PDX) established from Luminal B (HCI003)(266) or HER2+ (GCRC1991) samples into the mammary fat pads of immune compromised hosts and treated mice with either GSK-126 or vehicle for 5 weeks. The presence of spontaneous lung metastases in hosts transplanted with the Luminal B PDX was quantified via a combination of human-specific pan cytokeratin immunohistochemical staining and enlarged nuclear morphology (**Figure 2-20A**), and HER2 positive immunohistochemical staining in the HER2 PDX (**Figure 2-20B**). Strikingly, in the Luminal B PDX, we observed only a 40% penetrance of lung metastases in the GSK-126 treated cohort (n=2/5), compared to 100% in the vehicle control group (n=5/5). There was also a significant decrease in the number of lung lesions per mouse in the GSK-126 treated cohort, compared to mice treated with the vehicle control in the Luminal B, but not the HER2 PDX hosts (**Figure 2-20C**). Of the lung metastases that did appear in GSK-126 mice, 7% were defined as overt metastases greater than 10 cells (1/14 total enumerated lesions) (**Figure 2-20D**). However, in vehicle treated hosts, 30% of metastatic lesions were identified to be overt metastases greater than 10 cells (33/109 total enumerated lesions). In the context of the HER2+ PDX, there were no significant differences in the penetrance or number of lung metastases between treatment groups. Furthermore, no difference in the relative proportions of micro (<10 cells) or overt metastases were observed in differentially treated HER2+ PDX hosts (**Figure 2-20D**). While we observed a pronounced effect of GSK-126 on lung metastasis in the Luminal B PDX, we did not observe any significant effect on tumor growth (**Figure 2-20E**). These findings are in line with our results generated from preclinical mouse studies in

which we utilized transformed tumor cells and indicate that the loss of global H3K27me^3 levels directly perturbs the metastatic cascade rather than primary tumor growth in the Luminal B subtype.

Lastly, to confirm that *FOXC1* levels were indeed elevated in Luminal B but not HER2+ PDXs treated with GSK-126, we performed qRT-PCR on breast tumor samples at endpoint and confirmed a significant upregulation of *FOXC1* transcript levels in GSK-126 treated Luminal B but not HER2 PDXs (**Figure 2-21A**). Additionally, we observed the significant upregulation of 4 genes previously confirmed to be FOXC1 targets, in Luminal B PDXs treated with the Ezh2 inhibitor (**Figure 2-21B**)**.**

Taken together, these data provide compelling evidence that pharmacological intervention targeting the EZH2-dependent repression of a FOXC1-dependent transcriptional program can hinder the metastatic properties of human Luminal B breast cancer (**Figure 2-22**).

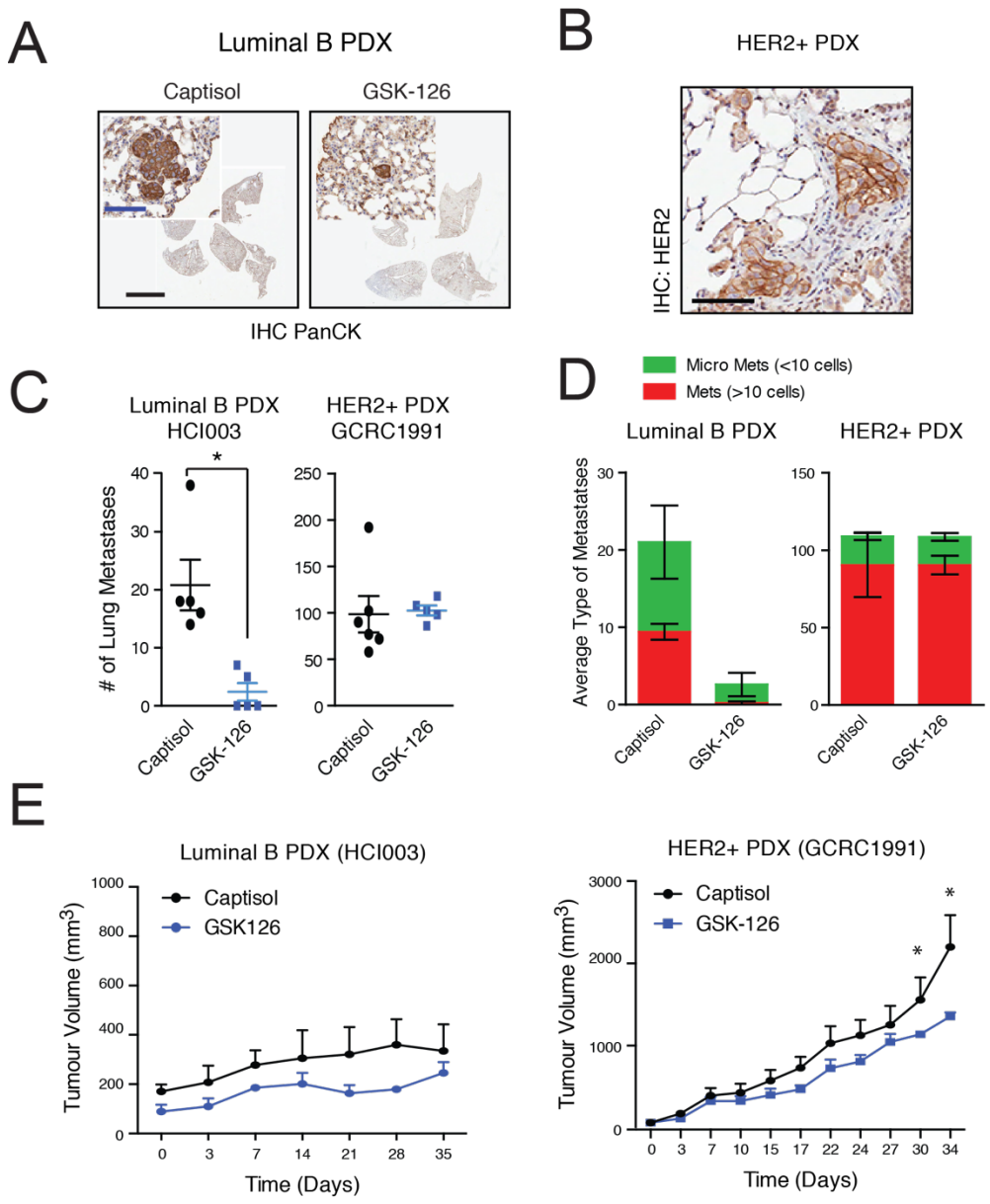

Figure 2-20. Metastasis is significantly impaired in human Luminal B but not HER2+ PDX

(A) Representative images of paraffin embedded sections of lung stained with pan cytokeratin (pan CK). Lung lesions were identified by pan CK positivity and enlarged nuclei. Top scale bar is 200 µm. Bottom scale bar is 5mm. (B) Representative staining of lung lesion for HER2 by immunohistochemistry. Scale bar=100µm. (C) Quantification of total numbers of lung lesions in each PDX, as identified by HER2 or panCK staining. (D) Characterization of micro metastases or overt metastases in each PDX. (E) Tumour growth was assessed for each PDX line during drug treatment. n= 6 per PDX. *=p<0.05. Error bar= S.E.M.

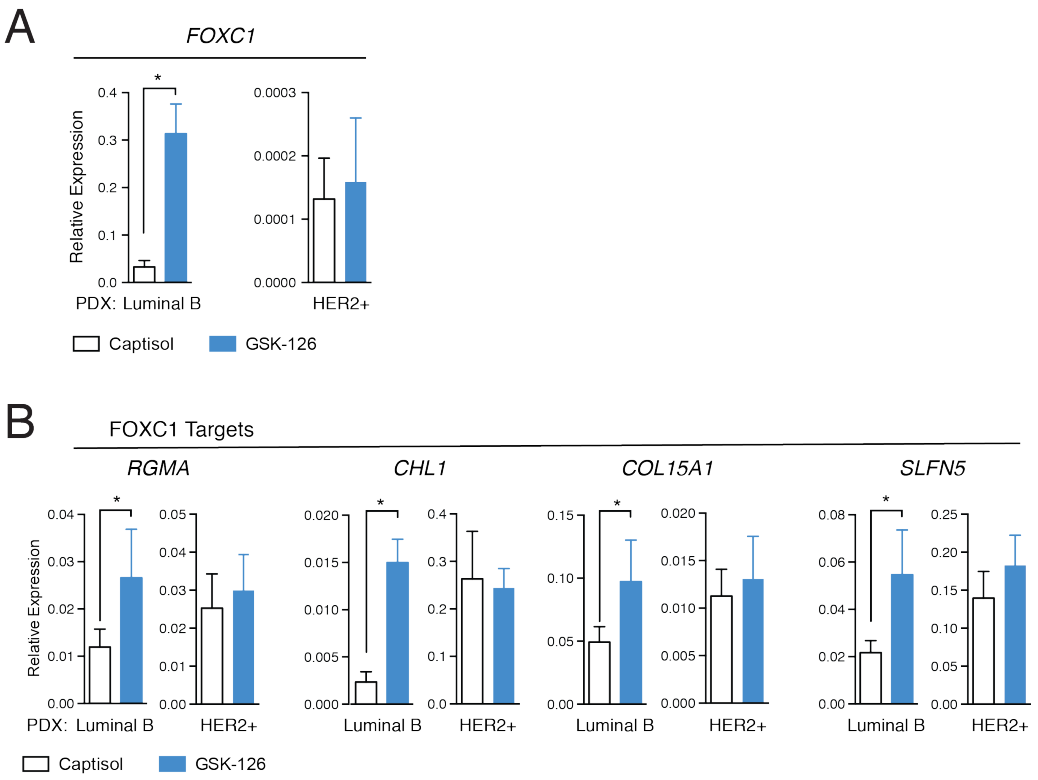

Figure 2-21. Expression of FOXC1 and FOXC1 targets is significantly elevated in GSK126 treated Luminal B but not HER2+ PDX

(A) qRT-PCR analysis of *FOXC1* transcript levels in endpoint Luminal B (n=4 per condition) or HER2+ (n=4 per condition) PDX tumors treated with GSK-126 or vehicle long term *in vivo*. * p<0.05. (B) qRT-PCR analysis of 4 FOXC1 targets in in endpoint Luminal B (n=4 per condition) or HER2+(n=4 per condition) PDX tumors treated with GSK-126 or vehicle long term *in vivo*. * p<0.05.

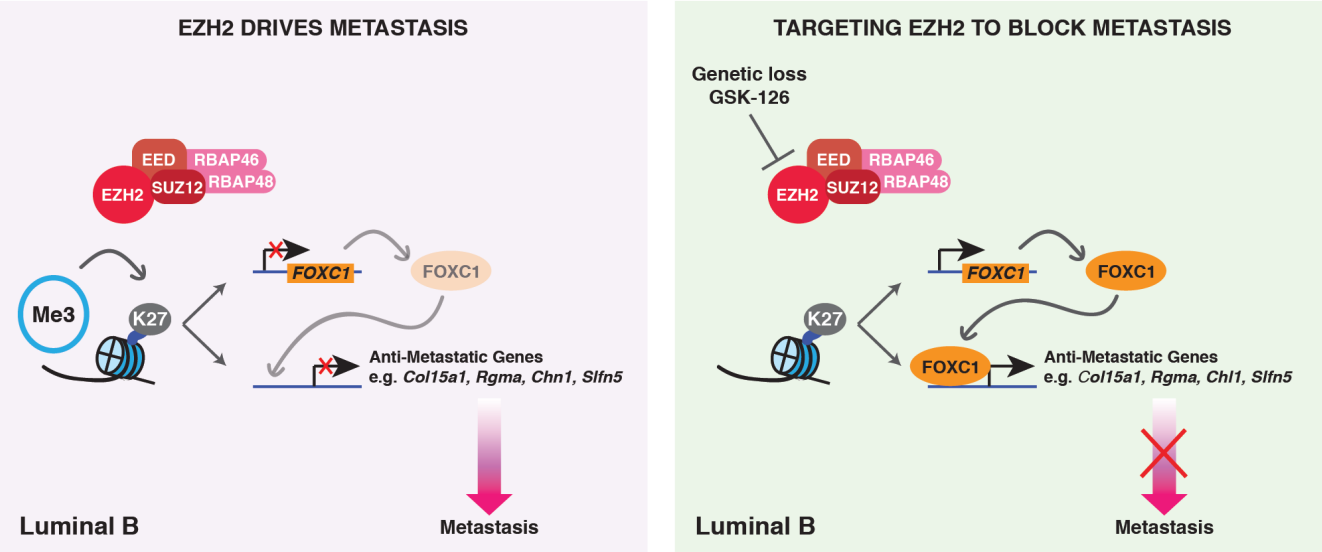

Figure 2-22. Schematic illustrating repression of FOXC1 by EZH2 and its effect on the metastatic cascade in Luminal B breast cancer

2.2 Ezh2 is necessary for HER/ErbB2-driven tumour initiation and maintenance

2.2.1 Experimental Rational

In the previous section (2.1), we discovered that inhibition of Ezh2 methyltransferase activity could be exploited as an anti-metastatic therapy, but only in a specific subtype of breast cancer. Given the context specific nature of PRC2 function, we next sought to understand the role of PRC2 in other intrinsic molecular subtypes of breast cancer. In this chapter, we explored the role of PRC2 in HER2-driven breast cancer within the context of tumour initiation, tumour maintenance, and assessed the therapeutic implications of our findings.

Immunohistochemical staining of EZH2 across a variety of human breast cancer subtypes has revealed that high EZH2 levels are correlated with basal-like and HER2+ breast cancers (227). Fujii and colleagues reported transcriptional control of Ezh2 downstream of HER2 via the MEK-ERK signal transduction pathway, thus linking elevated Ezh2 levels to amplification or overexpression of HER2(241). The relevance of Ezh2 overexpression has been supported by *in vivo* functional work in which overexpression of Ezh2 in a mouse model of breast cancer driven by activated HER2 has been shown to significantly accelerate tumour latency (217). The authors of this study attributed this phenotype to the role of Ezh2 in the expansion of the tumour initiating cell population, emphasizing the importance PRC2 in the earlier stages of tumour initiation. Functional *in vivo* studies, however, have not yet examined the necessity of Ezh2 in tumour initiation in a HER2/ErbB2-driven model.

2.2.2 Characterization of EZH2 across different breast cancer subtypes

We first sought to confirm if EZH2 levels associated with specific intrinsic subtypes of breast cancer. In line with what other groups have reported(227), evaluation of EZH2 levels by immunohistochemistry in a large cohort of human breast cancer tissues confirmed that higher nuclear EZH2 levels associated with subtypes poor outcome; Luminal B, HER2+ and Triple Negative Breast Cancer cases each had significantly higher levels of EZH2 than Luminal A (**Figure 2-23A**). High EZH2 levels also associated with hormone receptor negativity, increased histological grade and higher proliferative index, as evidenced by a greater percentage of Ki67 positive cells (**Figure 2-23B**).

While previous studies have associated high Ezh2 levels with aggressive subtypes such as HER2+ breast cancer, we wished to further understand if high EZH2 levels significantly correlated with other histopathological parameters within HER2 breast cancer cases. To this end, a Tissue Microarray (TMA) comprised of 132 HER2+ breast cancer biopsies was stained and quantified for nuclear EZH2 levels. Interestingly, patients with the highest EZH2 levels were significantly enriched in the hormone receptor negative, high grade HER2+ breast cancer cases with high mitotic index (**Figure 2-23C**).

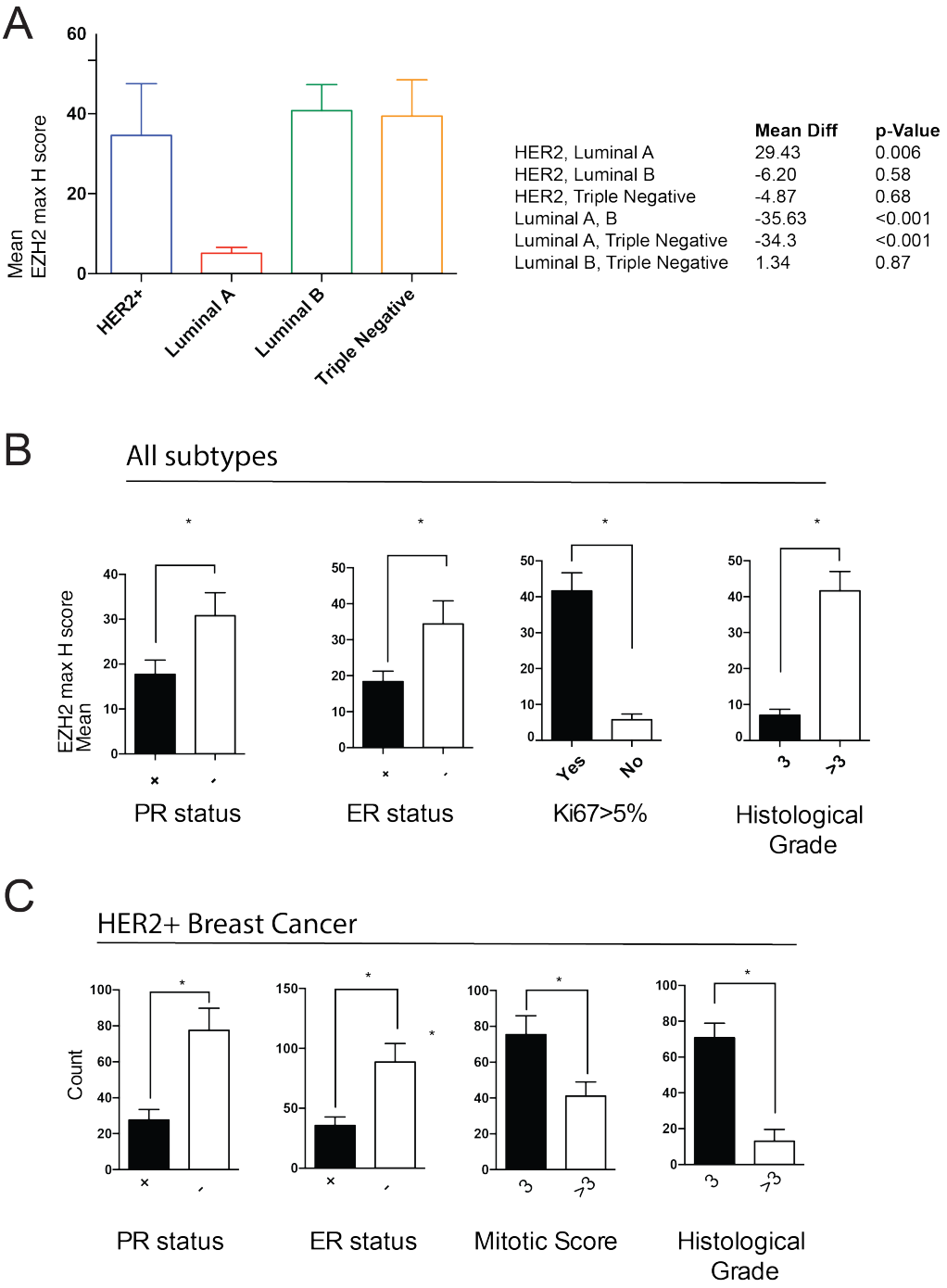

Figure 2-23. Evaluation of EZH2 levels in a human breast cancer cohort

(A) Quantification of the number of samples with high nuclear EZH2 levels, across different subtypes from a TMA. (B) EZH2 H score per core including all subtypes, clustered by of different features (C) Quantification of HER2+ breast cancer samples with high EZH2, clustered by of different features. *=p<0.05. H score= histological score for the core= (1*% $Ezh2^{lo}$ cells) + (2*% $EZH2^{mid}$ cells)+ (3*% $EZH2^{Hi}$ cells).

2.2.3 Genetic ablation of Ezh2 in transformed ErbB2-driven tumour cells reduces cellular proliferation

To study the role of Ezh2 function in the context of HER2+ breast cancer, we selected the NIC mouse model of activated ErbB2 as it recapitulates many of the features of $EZH2^{High}$HER2+ breast cancer cases. The NIC model is highly proliferative and hormone receptor negative, and forms comedo-adenocarcinomas similar to those found to arise from human DCIS(73). To assess the role of Ezh2 in transformed tumour cells we used RNA interference (RNAi) in primary cell lines established from NIC mammary gland tumours using two different shRNA sequences to knock down Ezh2 (**Figure 2-24A**). The proliferative capacity of these cells was significantly reduced *in vitro* (**Figure 2-24B**), and *in vivo* upon orthotropic injection in the mammary fat pad of athymic nude hosts (**Figure 2-24C, 2-24D**). Due to the difficulty in maintaining shEzh2 NIC cell lines in culture, to complement our RNAi we also employed a genetic method to establish Ezh2 null Neu/ErbB2-driven tumour cells lines. In this strategy, we interbred mice harboring mammary gland specific activated ErbB2 uncoupled from cre (MMTV-NDL2-5) with mice harboring the floxed Ezh2 allele. Upon the formation of mammary tumours, we established primary cells lines and employed Adenovirus Cre *in vitro* to delete Ezh2 (**Figure 2-25A, B**). In accordance with our previous results using shRNA against Ezh2, the proliferative capacity of Ezh2 null cells was also significantly affected (**Figure 2-25C**).

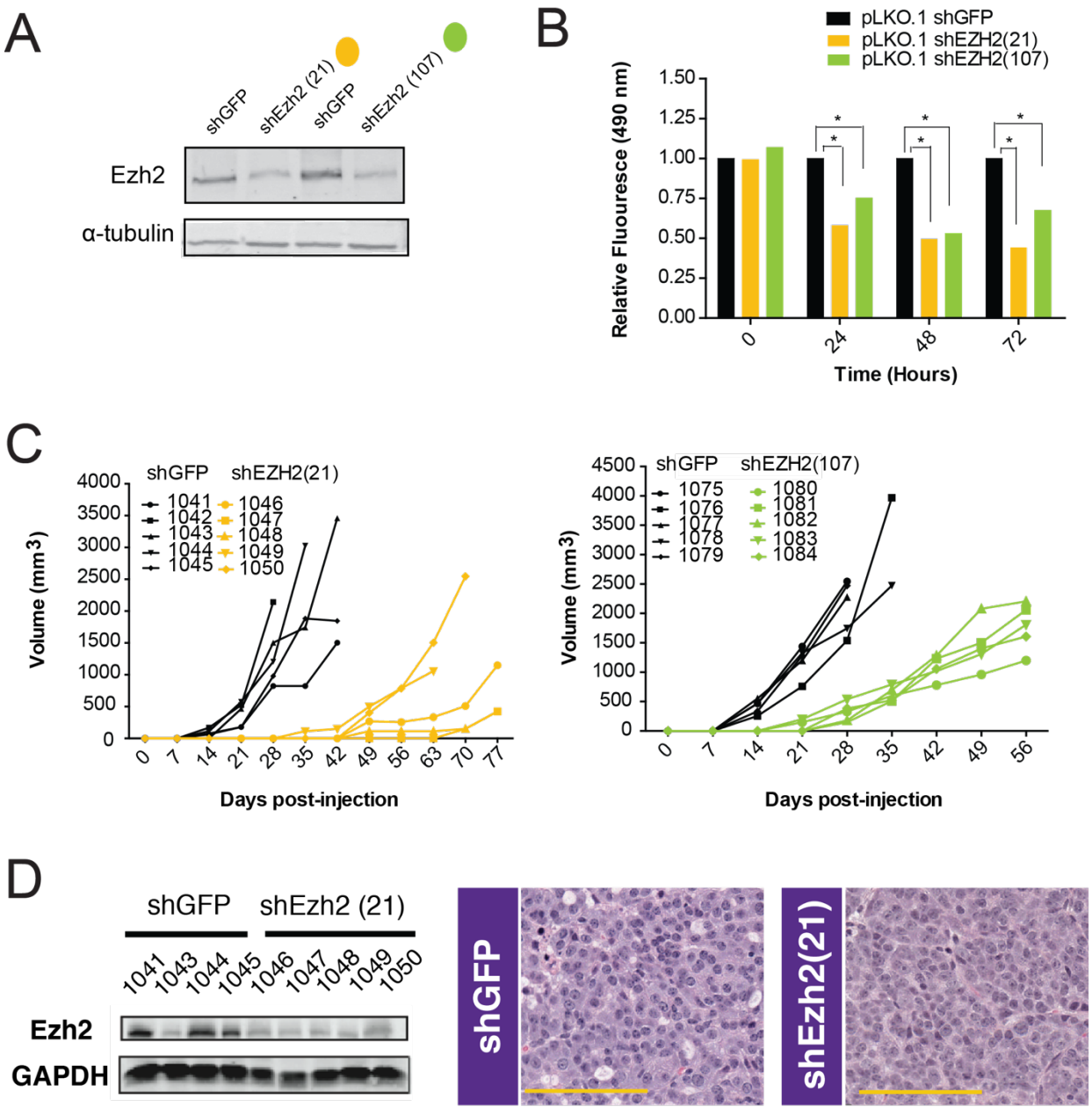

Figure 2-24. RNAi mediated knock down of Ezh2 in primary tumour cells lines derived from ErbB2-driven mouse mammary tumours

(A) Immunoblot analysis confirms knock down of Ezh2 with 2 independent shRNA sequences in an NIC cell line. (B) MTS proliferation assay reveals that reduction of Ezh2 significantly affects cellular proliferation. (C) shEzh2 or shGFP NIC cells were injected orthotopically into athymic nude hosts and tumour outgrowth was assessed. (D) Endpoint tumours maintained loss of Ezh2 but were histologically similar to controls as evidenced by H&E staining. Scale bars= 100μm.

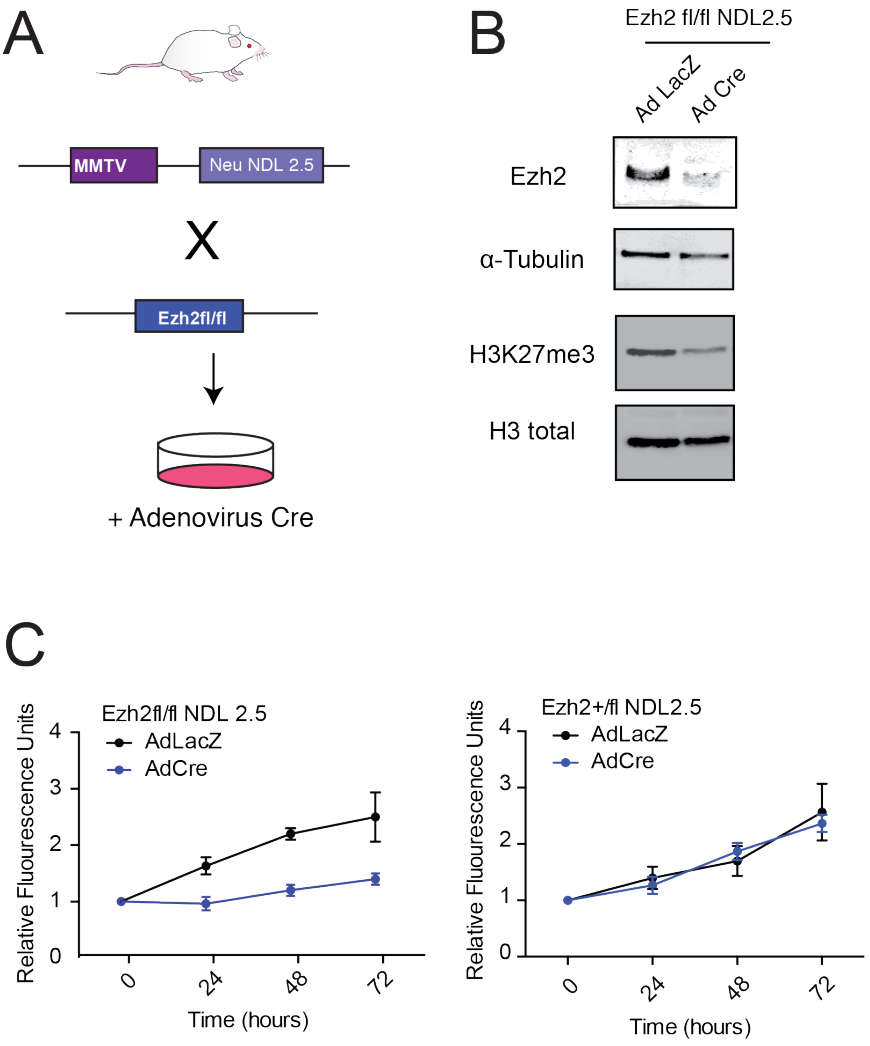

Figure 2-25. Complete ablation of Ezh2 in primary cells lines established from Neu/ErbB2-driven mouse mammary tumours

(A) Schematic illustrating the generation of Ezh2$^{fl/fl}$ NDL (Neu/ErbB2-driven) cell lines. (B) Immunoblot confirming the loss of Ezh2 and a reduction in global H3K27me3 levels in Ezh2$^{fl/f}$NDL+ AdCre compared to controls. (C) Proliferative capacity of Ezh2$^{fl/f}$NDL+ AdCre compared to AdLacZ, and Ezh2^{fl+}NDL+ AdCre or Ad LacZ. AdCre= Adenovirus Cre, AdLacZ= Adenovirus LacZ.

2.2.4 Pharmacological inhibition of Ezh2 methyltransferase activity affects proliferation

Next, we wished to determine if pharmacological impairment of Ezh2 catalytic activity could recapitulate the anti-proliferative phenotype observed in our genetic experiments. To this end, we first used GSK-126, a high specific SAM competitive inhibitor of Ezh2 methyltransferase activity and observed that changes to global H3K27me^3 of NIC cells were visible even after 24 hours of GSK-126 treatment (**Figure 2-26A**). Immunofluorescence staining of cells treated with 2μM GS-126 further confirmed complete loss of H3K27me^3 by 72 hours (**Figure 2-26B**). Interestingly, the MTS assay revealed that significant changes to proliferation only began after 72 hours of treatment with GSK-126 (**Figure 2-26C**). This observation is in line with what other have reported upon inhibiting Ezh2 methyltransferase activity in tumour cells, and is speculated to be due to the necessity of several cell divisions to complete dilute the methyl marks established by PRC2 (231, 232).

To validate our results in an independent inhibitor, we also employed EPZ6438, another SAM competitive inhibitor of Ezh2 methyltransferase activity. Following pretreatment of NIC cells with 2μM GSK-126 or EPZ6438 for 72 hours, we observed a significant decrease in cellular proliferation with either inhibitor and complete loss of H3K27me^3 (**Figure 2-26D**).

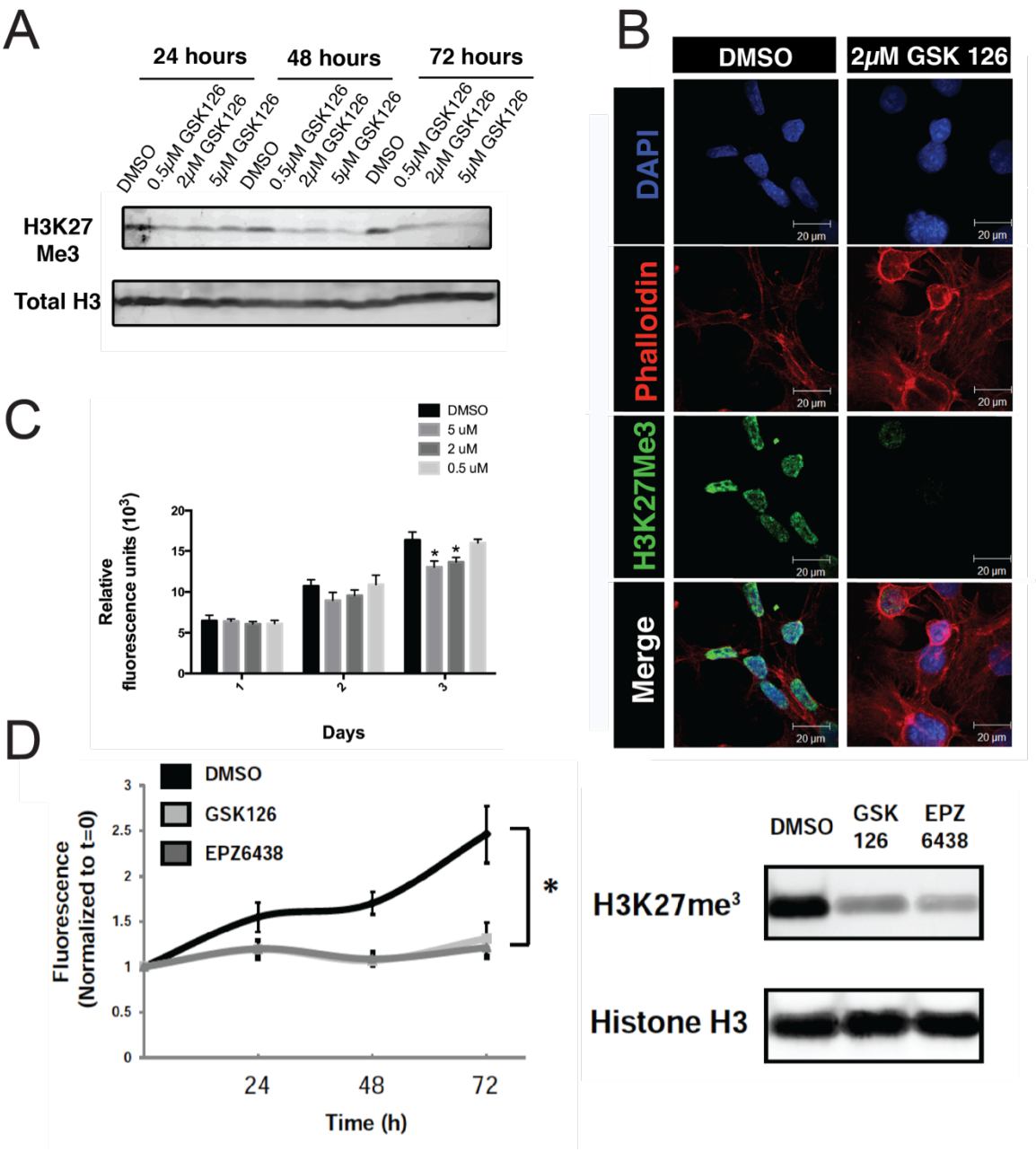

Figure 2-26. Inhibition of Ezh2 methyltransferase activity significantly impairs cellular proliferation in transformed ErbB2-driven tumour cells

(A) Immunoblot confirming loss of global H3K27me3 at different time points and at different concentrations of GSK-126. (B) Immunofluorescence staining of NIC cells treated with 2μM GSK-126 for 72 hours. (C) MTS proliferation assay of GSK-126 treated cells at different concentrations over 3 days. (D) Comparison of the proliferative capacity of NIC cells pretreated with 2μM GSK or 2μM EPZ6438 for 72 hours, as assessed by CyQuant. Immunoblot illustrating global loss of H3K27me3 with either inhibitor, after 72 hours of treatment. *p<0.05.

2.2.5 Inhibition of Ezh2 methyltransferase activity upregulates transcriptional programs involved in extracellular matrix organization and the anti-viral immune response

Since the canonical role of PRC2 is to repress transcription via H3K27me^3, we next sought to identify transcriptional targets that would be upregulated in response to acute inhibition of Ezh2 methyltransferase activity. To this end, transcriptional profiling was performed on established primary cultures of ErbB2-driven mouse mammary tumour cells treated with GSK-126 or vehicle (DMSO) for 72 hours. Employing a stringent p value ($p<0.02$) and a 1.5-fold cut off, analysis of GSK-126 treated cells revealed the upregulation of 165 genes (**Figure 2-27A**). To identify biological programs enriched in these upregulated genes, we used Reactome transcriptional pathway analysis and observed a significant enrichment for genes involved in the extracellular matrix (ECM) organization and in the Interferon alpha/beta response IFN α/β are members of the Type 1 IFN family, which are responsible for activating intracellular antimicrobial programs to influence the innate and adaptive immune system(267, 268). Type 1 IFN, such as IFN α/β, can be produced in most cell types in response to a variety of stimuli. A heat map of targets that clustered with the Type 1 immune response was generated to visualize the upregulation of these genes upon induction of H3K27me3 (**Figure 2-27B**).

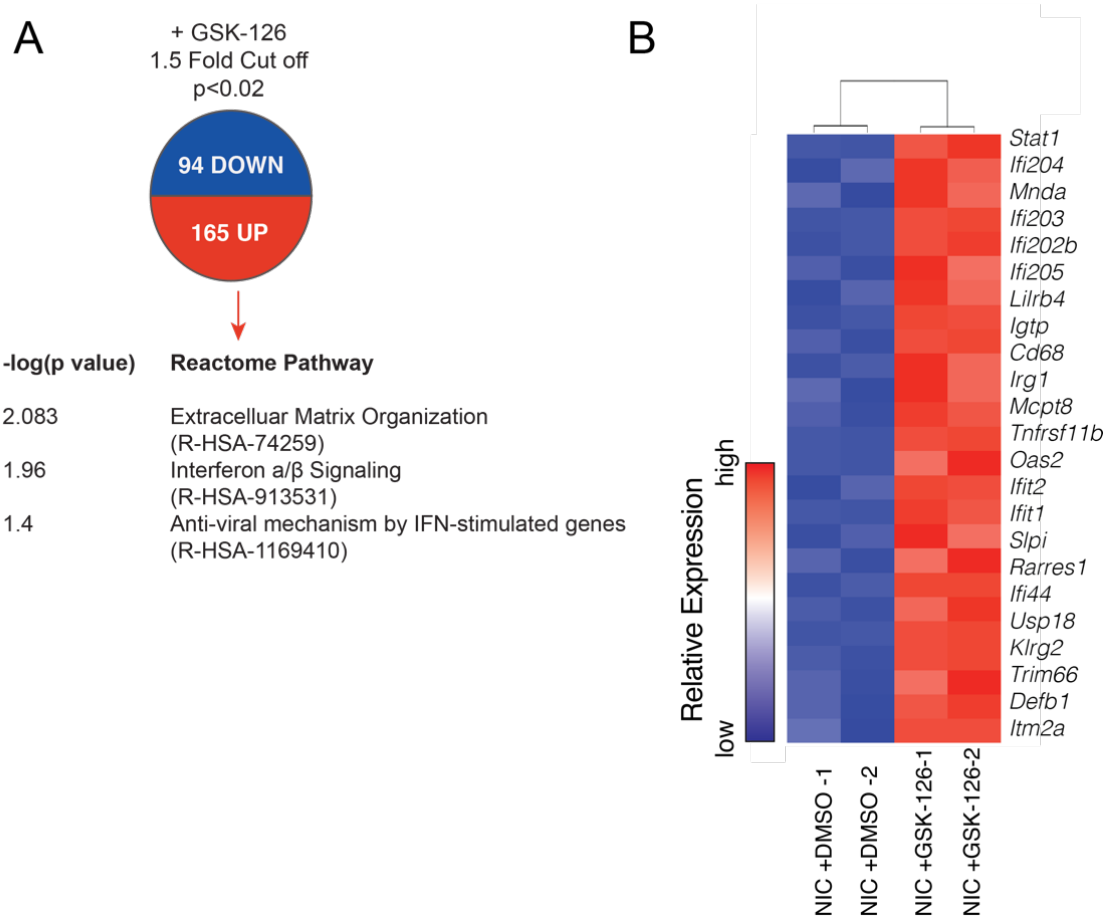

Figure 2-27. Inhibition of Ezh2 methyltransferase upregulates distinct transcriptional programs

(A) Schematic of the differentially regulated genes in GSK-126 treated Neu/ErbB2-driven cells compared to DMSO treated controls. Cells were treated with 2μM GSK-126 for 72 hours (± 1.5-fold change, p<0.02). (B) Heat map illustrating only the differential expression of targets downstream of Interferon α/β pathway following treatment with 2μM GSK-126 for 72 hours. Microarrays were performed with two technical duplicates of NIC cells lines treated with either inhibitor or DMSO control. A stringent p value of 0.02 was selected for

2.2.6 Characterizing the Type 1 IFN response in ErbB2-driven tumours upon reduction of global H3K27me^3 levels

To validate the upregulation of an IFN α/β gene program, we selected the 4 most differentially upregulated genes (>1.8 fold) identified to be part of the IFN α/β pathway, and performed qRT PCR in 3 different ErbB2-driven mouse mammary tumour cells lines treated with vehicle or one of two different SAM competitive inhibitors of Ezh2 methyltransferase activity (GSK-126 or EPZ-6438). qRT PCR analysis confirmed the significant upregulation of all IFN α/β related genes following acute treatment with either inhibitor in comparison to DMSO treated cells (**Figure 2-29A**).

To confirm the transcriptional changes at the protein level, we next looked at the activation of signal transduction pathways downstream of IFN α/β upon inhibition of Ezh2 methyltransferase activity. The canonical signaling pathway elicited downstream of IFN α/β involves the Janus kinases (JAK) signal transducer and nuclear localization of Stat transcription factors. Upon engagement by IFN α/β, JAK1 and tyrosine kinase 2 (TYK2) bind to the intracellular domain of dimerized IFNA1/2 receptors. Phosphorylation of these kinases results in the recruitment of Stat1, 2 or 3, which in turn result in their phosphorylation, dimerization, nuclear translocation and activation of distinct gene expression programs. We assessed JAK1 and Stat1 activation, as evidenced by their phosphorylation status, in a panel of different ErbB2-driven cells lines treated acutely with one of two different methyltransferase inhibitors. Interestingly, we observed that GSK-126 or EPZ-6438 significantly increased phosphorylation of JAK1 and Stat1, as evidenced by immunoblot (**Figure 2-29B**), confirming that signaling pathways downstream of IFN α/β were indeed upregulated upon loss of global H3K27me^3 levels.

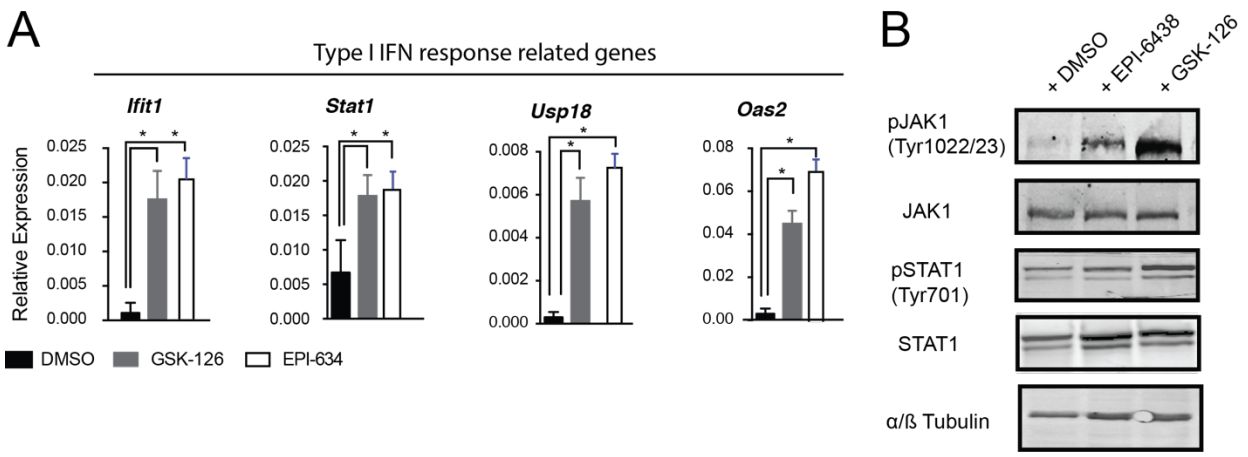

Figure 2-28. Inhibition of Ezh2 methyltransferase upregulates IFN α/β signaling

(A) q-RT PCR analysis of different targets of Interferon α/β identified in the microarray. Targets were assessed in 3 biologically distinct NIC cell lines, treated with 2μM GSK-126 or DMSO for 72 hours. (B) Immunoblot analysis of JAK-STAT signalling in NIC tumour cell lines treated with 2μM GSK-1262μM EPZ 6438 or DMSO for 72 hours.

Recently, two groups have independently shown that in tumour cells, acute treatment with DNA methyltransferase inhibitors induces an anti-viral IFN α/β response through the production of double stranded RNA (dsRNA) (269, 270). PRC2, like DNMT, is associated with transcriptionally silent regions. We hypothesized that Ezh2 methyltransferase inhibition may be functioning in a similar fashion. To test this, we assessed if pattern recognition receptors that detect dsRNA, and their associated signaling pathways were upregulated in cells with decreased global H3K27me^3 levels. Immunoblots of NIC cells treated with Ezh2 methyltransferase inhibitors revealed the upregulation of MDA5, a receptor that function to detect dsDNA. Phosphorylation of IRF3, which lies upstream of IFN α/β production, was also upregulated in NIC cells treated with EPZ6438 (**Figure 2-29A**). Since the mitochondrial localization of MAVS, a signaling adaptor, is an important feature of anti-viral signaling, we also assessed its cellular localization. Interestingly, we have observed co-localization of MAVS with

Hsp60 in GSK-126 treated NIC cell lines, further confirming the induction of an anti-viral response upon loss of global H3K27me^3 levels (**Figure 2-29B**). Taken together, our preliminary data suggest that PRC2 may be functioning to silence the production of dsRNA from genomic repeat regions.

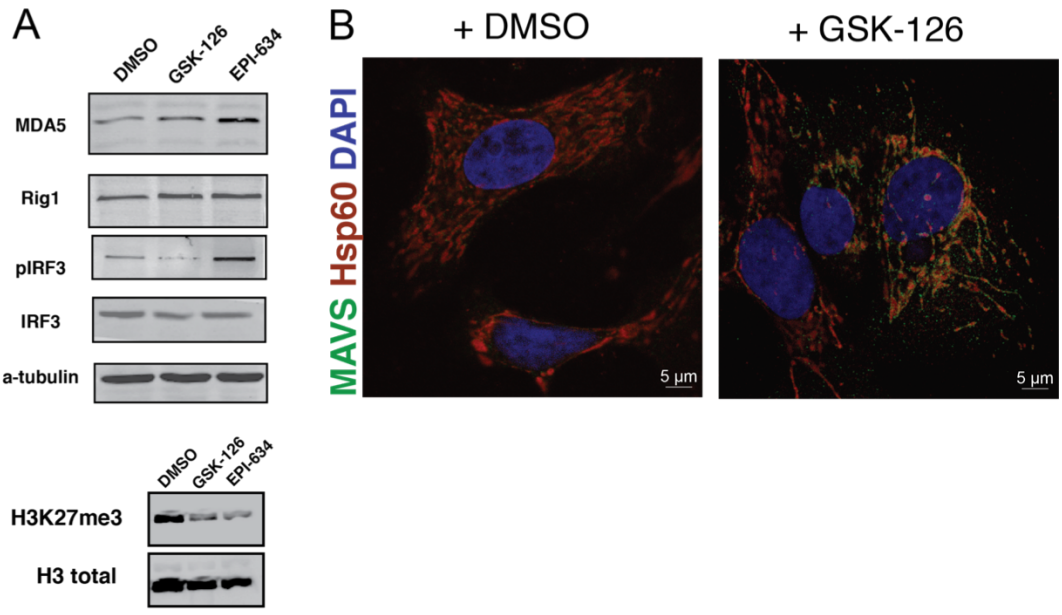

Figure 2-29. Inhibition of Ezh2 methyltransferase upregulates Rig1/MDA5/IRF3 signaling

(A) Immunoblot analysis of Rig1-IRF3 signaling in NIC cells treated with 2μM GSK-1262μM EPZ 6438 or DMSO for 72 hours. (B) Immunofluorescence of NIC cells treated with 2μM GSK-1262μM EPZ 6438 or DMSO for 72 hours.

2.2.7 PRC2 components are significantly upregulated in tumour epithelial cells during progression, compared to normal mammary epithelial populations

We established therapeutic potential for targeting PRC2 in transformed cells, we also wanted to explore how impairment of PRC2 would affect tumour initiation and progression in our NIC model *in vivo*. However, prior to this, we wished to confirm that PRC2 components were upregulated during the early stages of tumorigenesis in the

NIC model. Since the earliest stages of tumorigenesis in the NIC model are difficult to evaluate by histopathological means, we employed a fluorescent reporter transgene and fluorescent associated cell sorting (FACS) to isolate and quantify tumour cells at the early stages of disease. To visualize mammary epithelial cells positive for activated HER2, we crossed a GFP reporter to the NIC model generating a mouse. In this scenario, conditional expression of GFP is activated with the excision of the flanking STOP cassette by cre recombinase linked to activated HER2 driven by the MMTV promoter (**Figure 2-30A**). Single cell suspension of dissociated MMTV-NIC/GFP mammary glands from different time points during tumour progression were sorted using fluorescence associated flow cytometry. We enriched for the epithelial compartment by staining for CD24 positive cells, a cell surface marker for epithelial cells, and excluded stromal and immune cells based on negativity for CD31, Ter119 and CD45 staining (**Figure 2-30B**). Histograms of GFP levels gated on purified epithelial cells revealed an increase in GFP+ epithelial content over time, in accordance with the expansion of the tumour population (**Figure 2-30C**). Both GFP+ and GFP- epithelial populations were retained and assessed for expression levels of activated HER2 (*NeuNT*), and PRC2 components (**Figure 2-30D**).

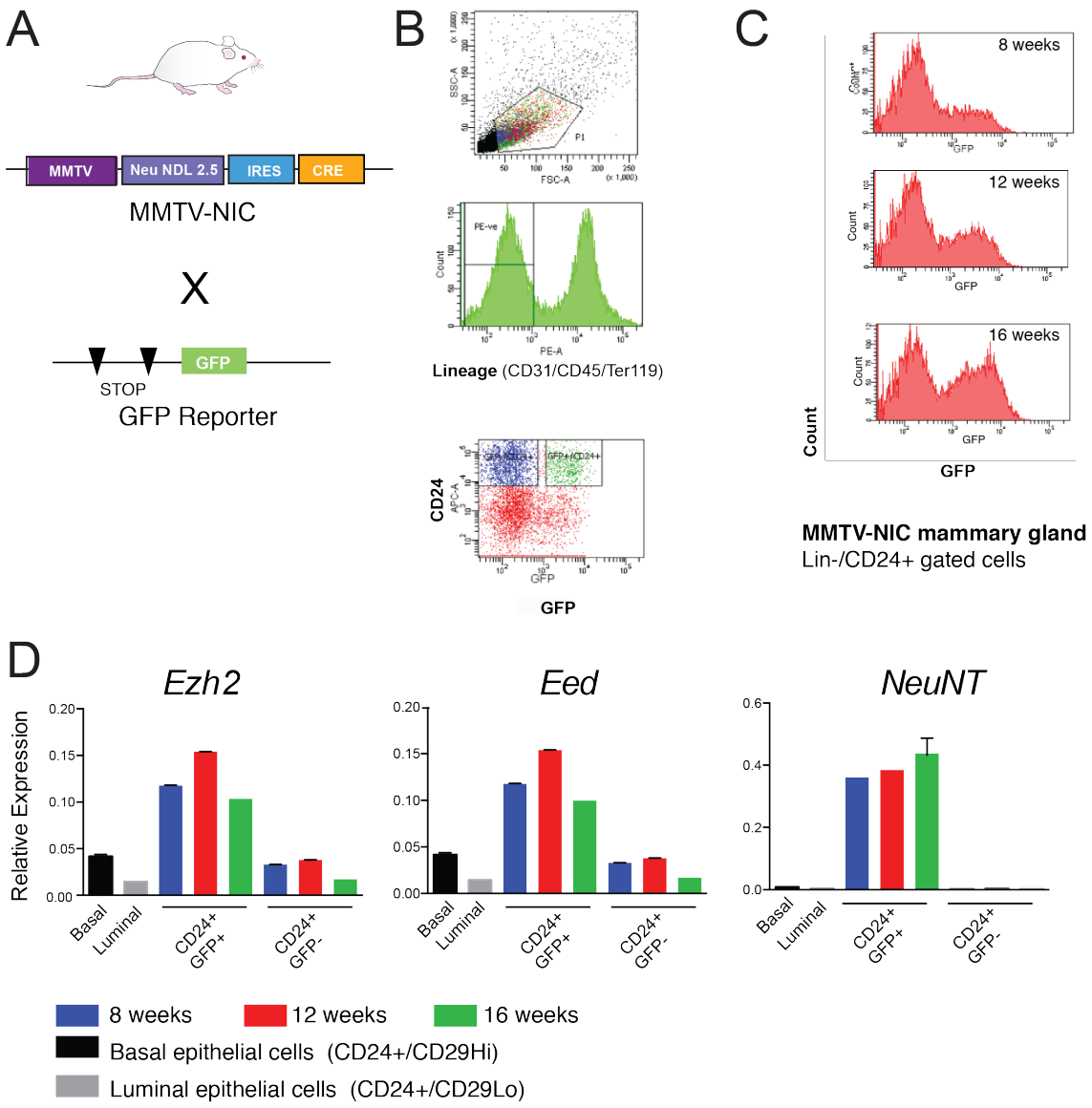

Figure 2-30. PRC2 components are upregulated in ErbB2+ mammary epithelial cells during transformation, compared to normal mammary gland progenitor populations

(A) Schematic of MMTV-NIC mice interbred with a GFP reporter transgene such that in the presence of cre recombinase the STOP cassette is excised, allowing for GFP expression in the mammary gland simultaneously with activated ErbB2 expression. (B) Dot plots illustrating the gating strategy for GFP+ epithelial cells from dissociates MMTV-NIC/GFP mammary glands. (C) Histograms illustrating the enrichment of GFP+ epithelial cells during the progression of tumorigenesis. (D) qRT-PCR analysis of PRC2 components and activated ErbB2 (NeuNT) at different time points during progression, compared to different mammary progenitor cells isolated from normal age 8-12-week-old mammary glands. N=5 per time point.

2.2.8 Dramatic decrease in tumour latency in NIC mice lacking both Ezh2 alleles

To facilitate the simultaneous expression of activated HER2 and genetic ablation of Ezh2 in the mammary gland, we crossed the MMTV-NIC model to the Ezh2 conditional allele (**Figure 2-31A**) and generated cohort of mice homozygous, heterozygous and wild type for Ezh2 and monitored for tumour formation. Immunoblot analysis of endpoint tumours confirmed the expected levels of Ezh2 for each genotype, establishing that $Ezh2^{-/-}$ NIC tumours retained ablation of Ezh2 (**Figure 2-31B**). While mice carrying wild type or the heterozygous allele of Ezh2 developed palpable tumours at an average of 116 and 129 days respectively, the average time of onset was significantly delayed in mice homozygous for Ezh2 (320 days). Furthermore, the tumour penetrance of $Ezh2^{-/-}$ NIC mice was also dramatically reduced from 100% to 20% (**Figure 2-31C**). To determine if loss of Ezh2 also resulted in a loss of $H3K27me^3$ levels, we employed multi-colour immunofluorescence of endpoint tumours. Interestingly, $H3K27me^3$ was also completely absent from the Erbb2 tumour population in $Ezh2^{-/-}$NIC mice (**Figure 2-31D**). The presence of $H3K27me^3$ positive Erbb2 negative cells surrounding and infiltrating the tumour are likely tumour associated fibroblasts, as these cells have been observed to express high levels of $H3K27me^3$, mediated by Ezh1 not Ezh2.

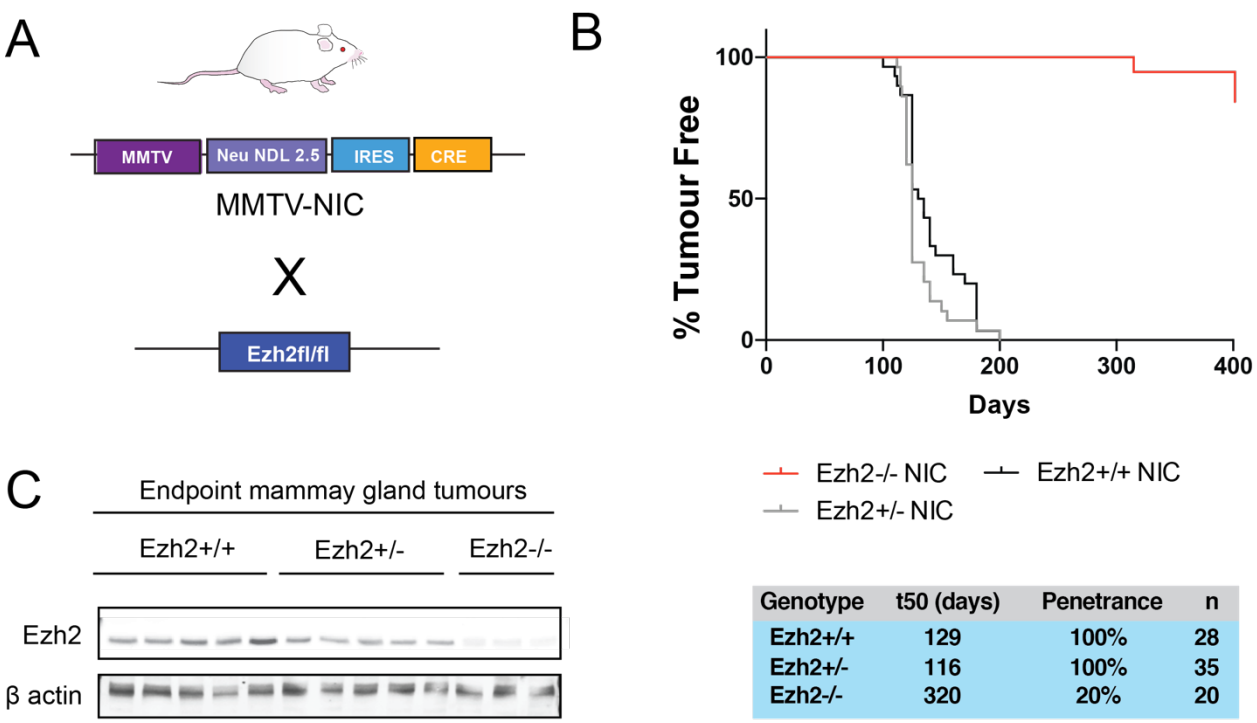

Figure 2-31. Ablation of Ezh2 in the ErbB2-driven NIC significantly delays tumour onset

(A) Schematic of the MMTV-NIC interbred with floxed Ezh2. (B) Immunoblot of endpoint tumours evaluating Ezh2 levels. (C) Tumour onset of Ezh2$^{-/-}$ $^{+/-}$ and $^{+/+}$ NIC mice as evaluated by bi-weekly palpation of the mammary gland. (D) Immunofluorescence staining of endpoint tumour comparing H3K27me3, Ezh2 and ErbB2 levels between different genotypes. Scale bars are 20μm.

2.2.9 *Expression profiling of endpoint Ezh2$^{-/-}$ NIC tumors reveals the repression of transcriptional pathways modulating the extracellular matrix and the immune response*

To understand the transcriptional changes elicited by loss of Ezh2, we performed transcriptional profiling of endpoint Ezh2$^{-/-}$ NIC and Ezh2$^{+/+}$ NIC tumours. Our analysis revealed 697 genes to be significantly upregulated and 667 to be significantly downregulated upon loss of Ezh2 (**Figure 2-32A**) (1.25-fold change, $p<0.05$). To determine if the differentially regulated genes were involved in specific biological processes, we performed Ingenuity Pathways Analysis, comparing the wildtype to the Ezh2$^{-/-}$NIC endpoint tumours. Transcriptional programs related to ECM modulation and the immune response were identified as significantly enriched (**Figure 2-32B**). This was interesting, as previous transcriptional analysis of NIC cells treated with GSK-126 for 72 hours also revealed transcriptional programs associated with the ECM and immune response to be differentially regulated (**Figure 2-27**). However, in contrast to the acute pharmacological decrease in global H3K27me3 levels, in the transgenic model most genes associated with the ECM and immune response were *downregulated*.
Since the downregulation of programs related to the ECM were most strongly enriched in the IPA analysis, we first explored if transcriptional changes were focused in one aspect of the ECM. The ECM is a complex organization of different proteins that provides biophysical and biochemical signals to regulate various cellular processes, thus we speculated that changes genes related to the ECM might alter its composition. To do this end, we employed the 'matrisome' signature, a characterization and classification of different components of the ECM (271). Interestingly, we observed that

loss of Ezh2 uniformly downregulated genes across all categories of the matrisome (**Figure 2-33**).

Given the induction of a strong immune phenotype we previous observed upon treatment with GSK-126 (**Figure 2-27**), we were also interested in further examining which immune regulated pathways were downregulated in the $Ezh2^{-/-}$ NIC tumours. Interestingly, we found all programs to be linked to inflammation, suggesting that the endpoint $Ezh2^{-/-}$ NIC tumours have suppressed inflammation, perhaps as part of a compensatory mechanism. Diapedesis is the process through which blood cells migrate in response to inflammation, while leukotrienes are potent mediators of inflammation. The acute phase response denotes systemic changes that occur in response to inflammatory stimuli. Typically occurring in the early stages in response to infection, the acute phase response is an innate immune response that releases inflammatory cytokines such as TNF-α and IL-1. This occurs in response to pattern-recognition receptors of macrophages and leukocytes bind the pathogen associated molecular patterns present on bacterial microorganisms, fungal cell walls, or viral double stranded RNA.

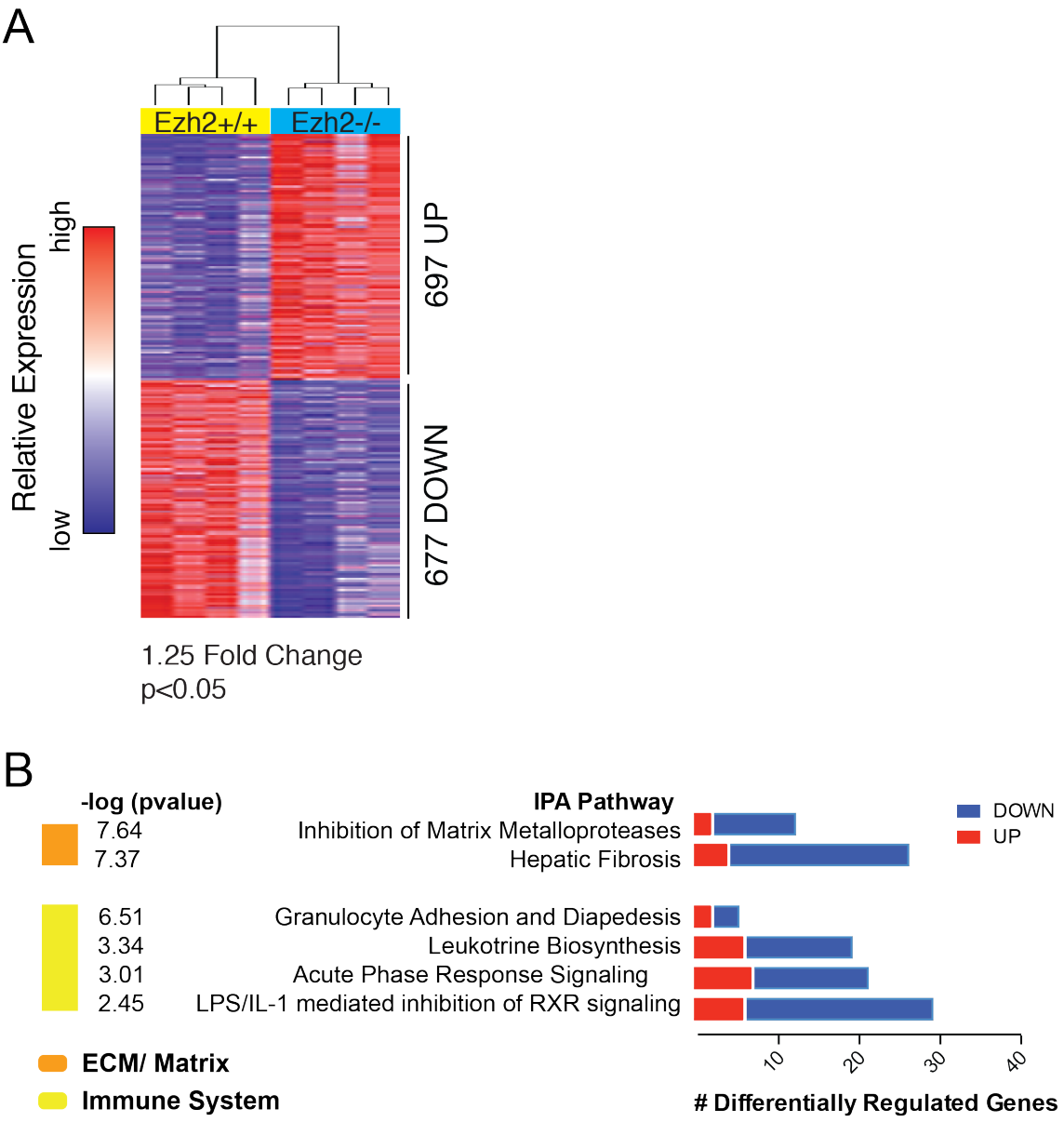

Figure 2-32. Loss of Ezh2 represses transcriptional programs control Extracellular matrix organization and the immune system

(A) Heat map illustrating the genes differentially expressed between Ezh2$^{-/-}$ and Ezh2$^{+/+}$ endpoint NIC tumours (±1.2- fold change, p<0.05). (B) Ingenuity Pathways Analysis of gene differentially regulated in Ezh2$^{-/-}$NIC mice reveal significant changes in pathways related to ECM organization and the immune response. Organization of genes in each pathway by the direction in which they move reveals the suppression of these programs in Ezh2$^{-/-}$NIC endpoint tumors.

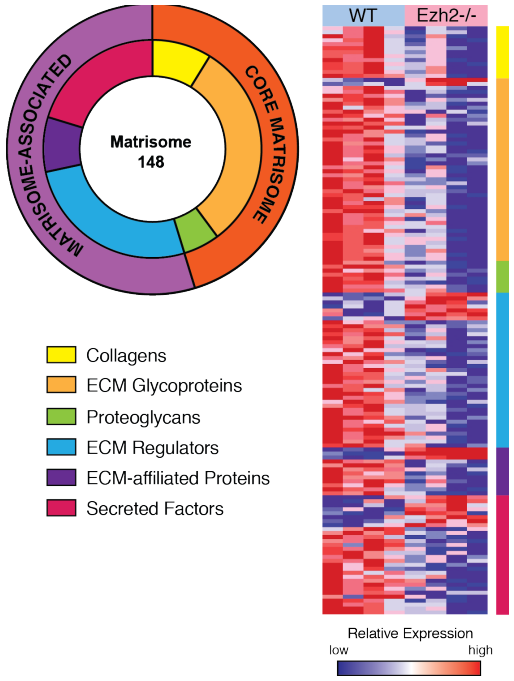

Figure 2-33. Loss of Ezh2 suppresses components of the matrisome

Heat map illustrating the distribution of differentially regulated genes involved in the matrisome across $Ezh2^{-/-}$ and $Ezh2^{+/+}$ endpoint NIC tumours.

2.2.10 Proliferation of early hyperplastic lesions of $Ezh2^{-/-}$ NIC mice is reduced

Examination of an early time point during tumorigenesis just prior to tumour palpation was conducted to determine the nature of the differences between $Ezh2^{-/-}$ and wild type NIC. The mammary glands of 16-week-old mice were first assessed for Ezh2 levels, and then evaluated for the presence of pre-neoplastic lesions. $Ezh2^{-/-}$ NIC mice displayed complete mammary ducts but closer histological examination revealed the presence of small hyperplastic lesions compared to wild type controls. Immunofluorescence analysis of mammary glands isolated from $Ezh2^{-/-}$ NIC mice demonstrated the presence of Ezh2-/ErbB2+ hyperplastic lesions (**Figure 2-34A**). Interestingly, these hyperplastic lesions were rarely positive for staining of Ki67, a

marker of proliferation, whereas prominent Ki67 staining was observed in ErbB2-positive, Ezh2-expressing cells in age-matched control NIC mammary glands (**Figure 2-34B, C**). Flow cytometry was also employed to enumerate the number of ErbB2+ epithelial cells in 16 week mammary glands from both genotypes. In accordance with the histological data, we observed a significantly lower number of ErbB2+ epithelial cells in the mammary glands of Ezh2$^{-/-}$NIC mice (**Figure 2-35 A, B**).

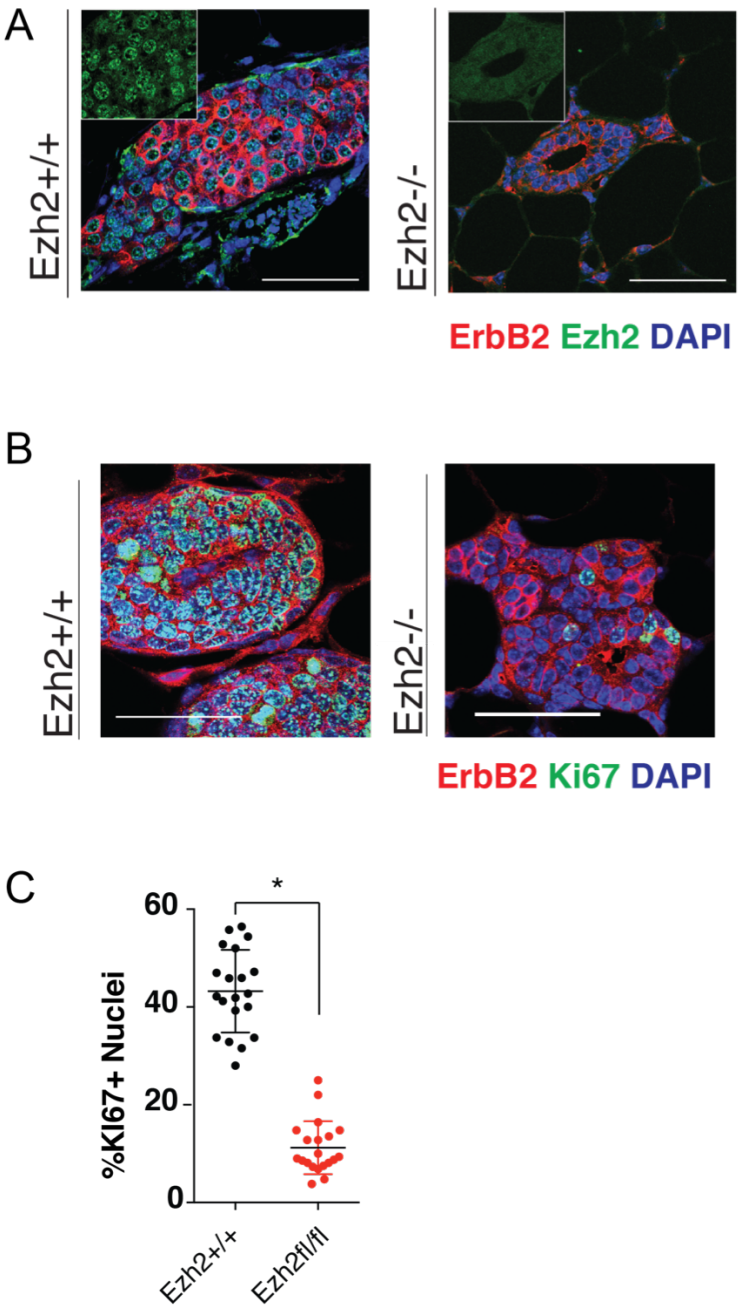

Figure 2-34. Immunohistochemical evaluation of preneoplastic lesions in 16 weeks Ezh2$^{-/-}$ or Ezh2$^{+/+}$ NIC mammary gland

(A) Immunofluorescence analysis of ErbB2 and Ezh2 expression in mammary glands from 16-week-old Ezh2$^{+/+}$ and Ezh2$^{-/-}$ NIC mice. (B) IF analysis of ErbB2 and Ki67 expression in mammary glands from 16-week-old Ezh2$^{+/+}$ and Ezh2$^{L/L}$ NIC mice. (C) Quantification of Ki67-positive nuclei in ErbB2-expressing cells in mice of both genotypes (mean + S.E.M). Data represent analyses of 4 independent mice per genotype, 5 fields of view per mammary gland. All scale bars represent 50 μm.

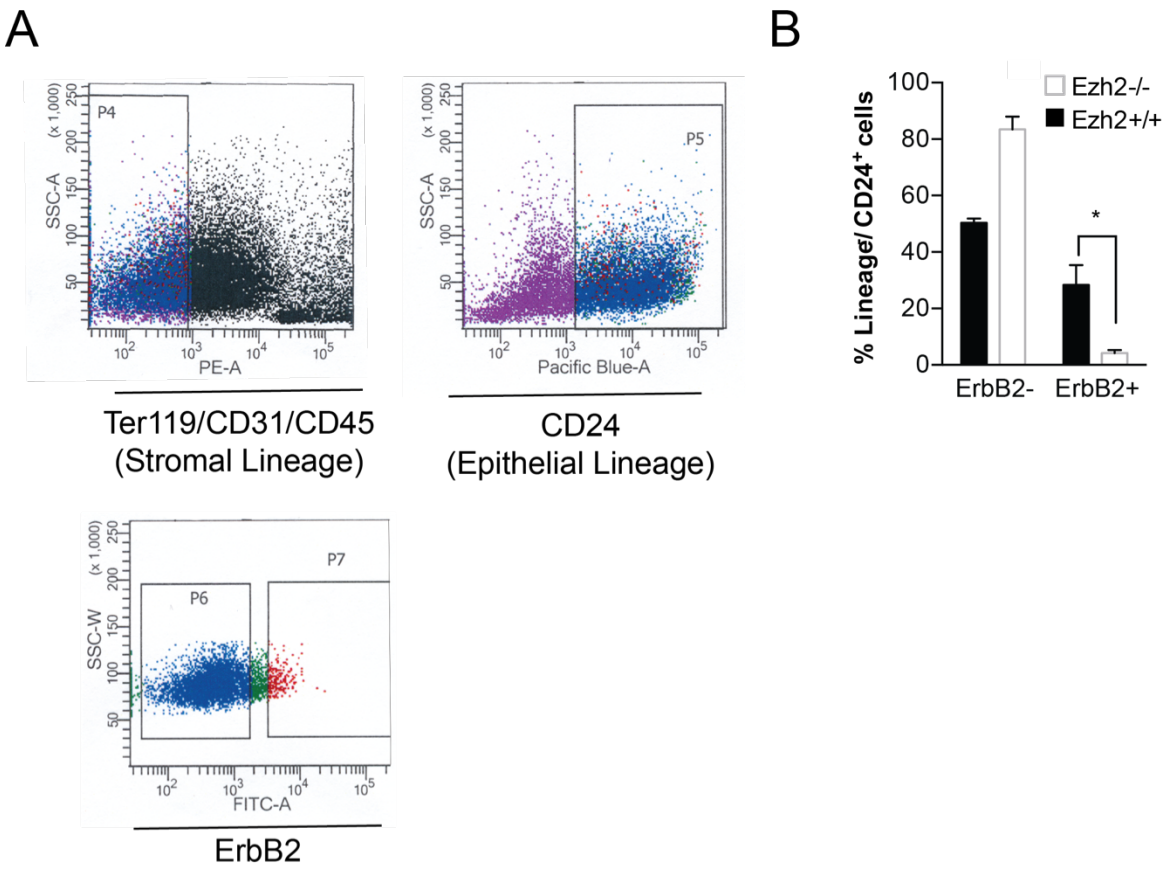

Figure 2-35. Flow cytometric analysis of 16 week mammary glands for ErbB2+ cells epithelial cells, prior to tumour palpation

(A) Example of Flow cytometry gating strategy to detect ErbB2 + and ErbB2- epithelial cells in dissociated mammary gland from mice 14-16 weeks of age. (B) Quantification of ErbB2+ and ErbB2- negative epithelia cells between different genotypes. *=p<0.05. Error bars are S.E.M.

2.2.11 Loss of Ezh2 in the mammary gland does not affect ductal tree outgrowth

One caveat to using the NIC model is that ablation of Ezh2 begins upon expression of MMTV (typically 3-4 weeks of age) before the mammary gland has completely formed. To establish if Ezh2 loss affected mammary gland development, we crossed the Ezh2 conditional mouse to MMTV-Cre mice and monitored ductal tree outgrowth. While we observed an initial defect in outgrowth of $Ezh2^{-/-}$ mice, this phenotype was rescued by 12 weeks of age (**Figure 2-36**). This result is consistent with

previous studies using mice on mixed genetic backgrounds, where Ezh2 depletion caused only a transient delay in mammary development during puberty, with more prominent effects during alveolargenesis and lactation(244, 250, 251).

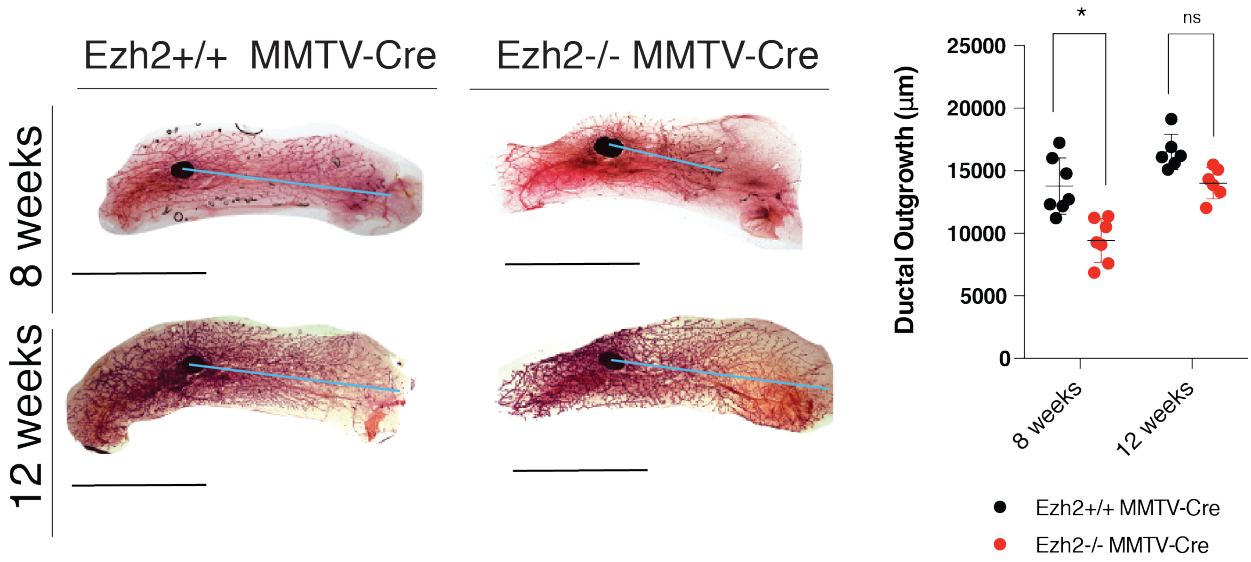

Figure 2-36. Loss of Ezh2 dampens early ductal tree outgrowth but is restored by 12 weeks of age
Whole mount inguinal mammary glands of mice taken at 8 and 12 weeks of age were stained with hematoxylin to determine ductal outgrowth. The blue line indicates the distance from the middle of the lymph node to the end of the most distal terminal end bud. This distance was quantified for both 8 and 12-week-old mice, revealing a significant difference at 8 weeks, but not 12 weeks. 8-10 mice were assayed per time point. *=$p<0.05$, n.s= not significant. Error bars are S.E.M.

2.3 The therapeutic potential of inhibiting Ezh2 methyltransferase activity in combination with HER2 monoclonal antibody therapy

2.3.1 Experimental rationale

In the previous section (2.2), we ascertained that Ezh2 plays a key role in tumour initiation of HER2-driven tumours. Furthermore, we identified two tumour intrinsic transcriptional programs that became upregulated upon global loss of H3K27me^3; ECM organization and an anti-viral immune response. Given the importance of the immune system to the efficacy of the HER2mAb trastuzumab, we were particularly interested in the induction of the latter transcriptional program and potential therapeutic implications for HER2+ breast cancer. We hypothesized that administration of trastuzumab combined the with inhibition of Ezh2 methyltransferase activity would have an additive anti-tumour effect through enhanced engagement of the immune system.

Administration of trastuzumab is currently part of the standard therapy regimen for women with HER2+ breast cancer, and is listed on the World Health Organizations list of essential medicines (272). While several mechanisms of action have been proposed, several lines of evidence suggest that it employs the immune system to mount an anti-tumour response. Data from transgenic models have emphasized the importance of immune cells equipped with Fcγ receptors and adaptive immunity to mediating an anti-tumour antibody dependant cellular cytotoxic response to HER2 mAbs (44). Anti-HER2 mAbs incapable of binding to FcRγ are ineffective against HER2+ xenografts(41). Furthermore, retrospective analysis of the CLEOPATRA clinical trial, in which pertuzumab or placebo was combined with the current standard of care (trastuzumab in combination with chemotherapy) and administered to HER2+ patients, reported a significant correlation between tumour infiltrating lymphocytes and patient

outcome (273). Interestingly, regardless of the treatment group, higher levels of tumour infiltrating lymphocytes were significantly associated with improved overall survival, thus supporting the importance of HER2 mAbs in eliciting an anti-tumour immune response.

HER2mAbs in combination with chemotherapy are the standard of care for HER2+ breast cancer patients, however, some patients are *de novo* resistant and many acquire resistance within one year of therapy(274). Thus other therapeutic strategies have been devised to improve patient outcomes, amongst them a combinatorial approach whereby the existing HER2 targeted therapies are co-administered with more generalized anti-cancer therapies. Immunotherapy, defined as treatment that harnesses the host's immune system to combat the tumour, has emerged as a compelling strategy to extend the survival of cancer patients. Amongst the most promising immunotherapies are immune checkpoint blockades, such as antibodies against Programmed Cell Death 1 (PD-1), a checkpoint protein expressed on the surface of T cells that guards against autoimmunity. Tumours typically express high levels of the PD-1 ligand PD-L1, allowing them to evade immune attack by engaging the PD-1 receptor on T cells thus inducing down regulation of the immune system(275). Therapeutic cancer vaccines have been another active segment of immunotherapy, and include the use of oncolytic viruses and immunization of patients with autologous antigen presenting cells challenged with fragments of HER2 protein (276).

Considering HER2 mAb engagement of the immune system, several preliminary studies have explored the potential of combining HER2 targeted therapies with therapies that stimulate the immune system. Studies in an immune competent HER2-activated transgenic mouse model demonstrated that a murine form of trastuzumab can collaborate with a Neu/Erbb2 vaccine to enhance the effect of cytotoxic CD8+ T cells

and dampen tumorigenicity (277, 278). Subsequent Phase 1 and 2 clinical trials have confirmed that this combination is associated with minimal toxicity and prolonged antigen-specific immune response in treated patients (279, 280). Studies in preclinical models have also revealed that the combination of PD-1 blocking antibodies with HER2 mAbs are significantly more effective than monotherapy (281), while clinical data from HER2+ breast cancer trials has correlated high PD-1 levels with poor response to HER2mAb therapies (282). Finally, in a preclinical model, combination of trastuzumab with IL-12, a cytokine that activates cytotoxic lymphocytes and NK cells, decreased disease progression and increased necrosis compared to monotherapy(283). In accordance with these results, preliminary results from a subsequent Phase 1 clinical trial have also demonstrated that trastuzumab with IL-12 increases NK cell activation and achieves better clinical responses(284).

In this section, we employed immune competent preclinical models to assess synergy between murine equivalent of trastuzumab (7.16.4 Ab) and pharmacological inhibition of Ezh2 methyltransferase activity using GSK-126. We observe a significant change in the profile of tumour infiltrating lymphocytes, accompanied by increased apoptosis in tumours treated with the combination therapy.

2.3.2 Inhibition of Ezh2 methyltransferase activity synergizes with 7.16.4.Ab

To investigate the potential for inhibition of global H3K27me^3 levels to collaborate with anti-HER mAb therapy we used the anti-ErbB2 mAb clone 7.16.4 (285). 7.16.4 mAb recognizes the extracellular domain of murine ErbB2, and allows for recognition of the mouse mAb by the host immune system. We employed primary ErbB2-driven tumour cell lines established from wild type NIC mice and orthotopically injected them

into the mammary fat pads of adult hosts. Due to the immunogenicity of cre recombinase expressed by the NIC cell lines, MMTV-Cre mice were used as hosts. Once a tumours reached dimensions of 5mm by 5mm, mice were treated with one of the following condition; (1) GSK-126+pAb101 (IgG control), (2) 7.26.4Ab+ Captisol, (3) Captisol (vehicle) + pAb101 (IgG control), or (4) GSK-126+ 7.6.4 Ab (**Figure 2-37A**). Following 5 weeks of treatment, the final weight of combination treated tumours were significantly smaller (**Figure 2-37B**). We observed that 7.16.4Ab in combination with GSK-126 significantly elicited the greatest reduction tumour growth. This was observed across two different preclinical trials, employing two different NIC cell lines (**Figure 2-37C, D**).

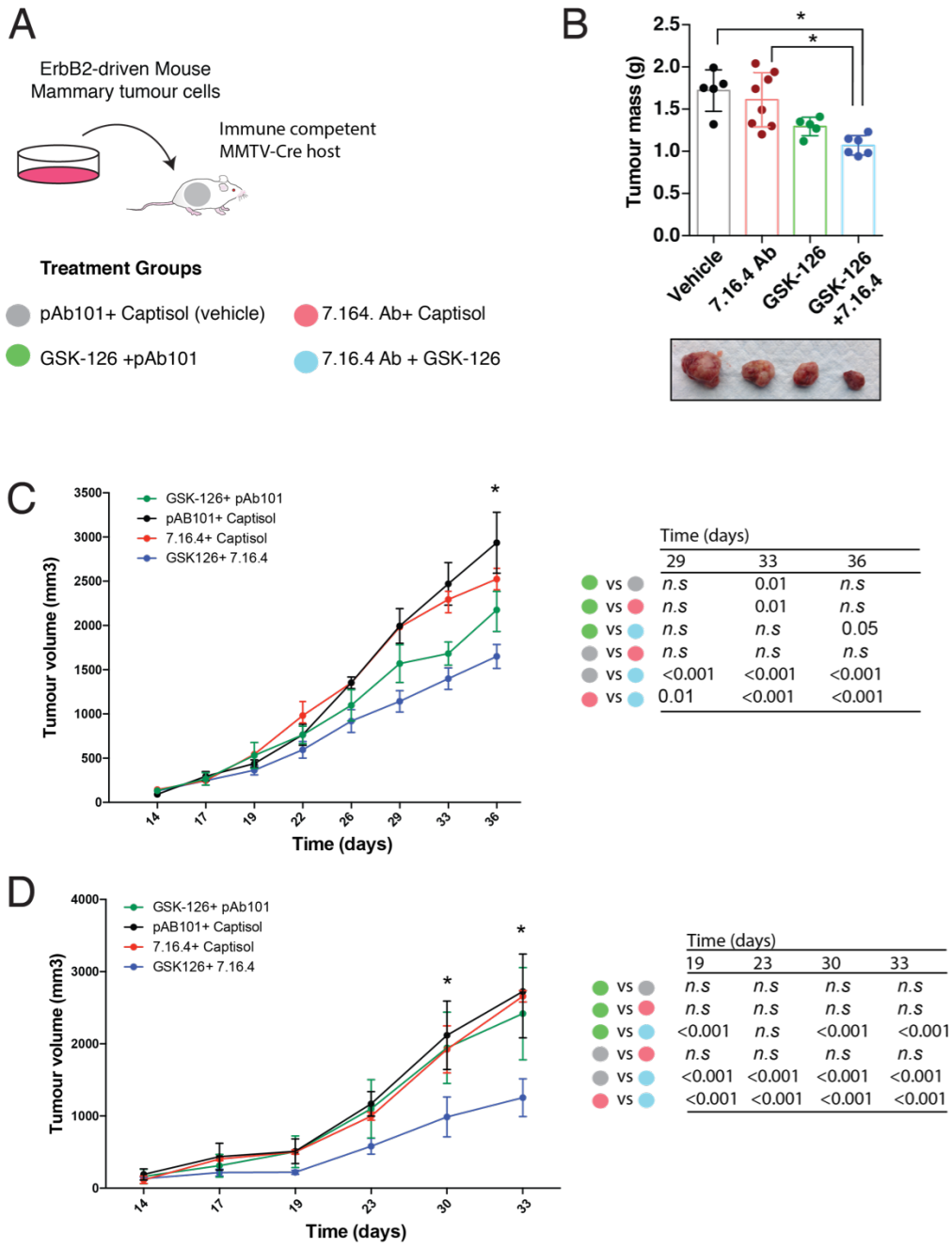

Figure 2-37. GSK-126 synergizes with 7.16.4Ab to reduce tumorigenicity

(A) Schematic of the preclinical model and treatments groups. For all experiments, $1X10^6$ NIC cells were injected into the mammary fat pat of MMTV-Cre mice and treated with 100μg of 7.16.4Ab or control IgG (pAb101), GSK-126 (300mg/kg) or Captisol vehicle, i.p. every other day. (B) Average endpoint tumour weights for the NIC cell line 6113 cohorts. (C) Tumour growth of each treatment group injected with the NIC cell line 6113. (D) Tumour growth of each treatment group injected with the NIC cell line 5567. n=5-6 per treatment groups for all trials. *= $p<0.05$. Statistics were performed using the individual t-tests between two groups, at each time point. *n.s* = not significant. Tables report p values.

2.3.3 Combination treatment of GSK-126 and 7.16.4 Ab does not significantly alter ErbB2 signaling pathways or proliferation

Since Trastuzumab can bind to the extracellular domain of HER2 to limit its ability to activate intrinsic tyrosine kinase, we first evaluated how treatment with GSK-126 and 7.16.4Ab affected important signal transduction pathways downstream of ErbB2. To this end, primary NIC tumour cell lines were evaluated via immunoblot for changes in the PI3K and MAPK/ERK signaling pathways (**Figure 2-38A**). No significant differences between treatment groups was observed. The proliferative status of endpoint tumours from the preclinical trials was also evaluated by immunohistochemistry staining for nuclear Ki67, but no significant differences between treatment groups was observed (**Figure 2-38B**).

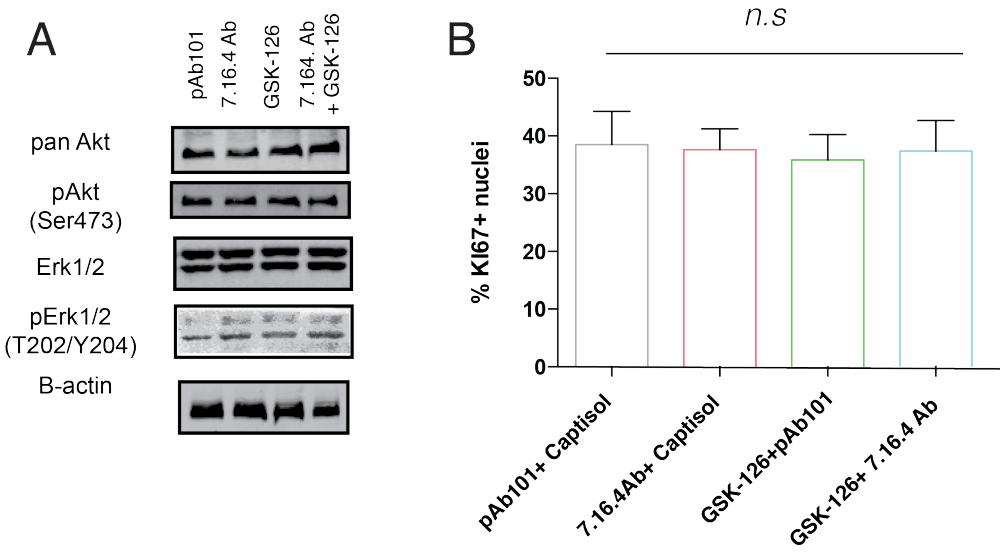

Figure 2-38. Combination treatment does not impact cellular proliferation or signaling pathways downstream of ErbB2

(A) Immunoblot of major signaling pathways downstream of ErbB2 activation in NIC cells treated with 7.16.4 Ab, 2μM GSK-126, or a combination of the two for 5 days. (B) Quantification of nuclear Ki67 immunohistochemical staining in endpoint tumours. Histology from 2 independent clinical trials were pooled and assessed, with each trial comprised of between 5-7 mice per condition. *n.s* = not significant. Error bars denote S.E.M.

2.3.4 Immunophenotyping of endpoint tumours reveals increased infiltration of NK and NKT cells in the combination treatment cohort

The absence of an anti-proliferative effect and no attenuation of signaling downstream of ErbB2 in tumours treated with GSK-126 and 7.6.4 Ab, led us to hypothesize that the anti-tumour effects observed in combinatorial treatments might be elicited from the stromal micro environment. The immune system has been demonstrated to play a key role in anti-tumour defense and must be subverted for the tumour to progress. Interestingly, studies across different types of cancers have demonstrated that increased recruitment of T, NK, and NKT cells correlate with better patient outcome(286, 287). Thus, we performed immunophenotyping of endpoint tumours to better understand the landscape of tumour infiltrating immune populations across different treatment groups. All tumours were harvested at the same time and stained with a panel of different fluorescent cell surface markers, and analyzed by flow cytometry to identify the distribution of CD45 positive immune cells (**Figure 2-39A**). Interestingly, the only immune cell populations in which a significant change was observed were Natural Killer (NK) and Natural Killer T (NKT) cells (**Figure 2-39B, C**) in the combination treated group. While the presence of NKT cells was limited to <1% in almost all the treatment groups, 15.3% of CD45+ immune cells in tumours treated with GSK-126 + 7.16.4Ab were NKT cells (CD3+/CD49b+). Interestingly, infiltration of NK cells was also significantly increased in GSK-126 + 7.16.4Ab treated tumours (21.1%), and GSK-126 treated tumours (16.7%), compared to other treatment groups (6.8%, 7.2%).

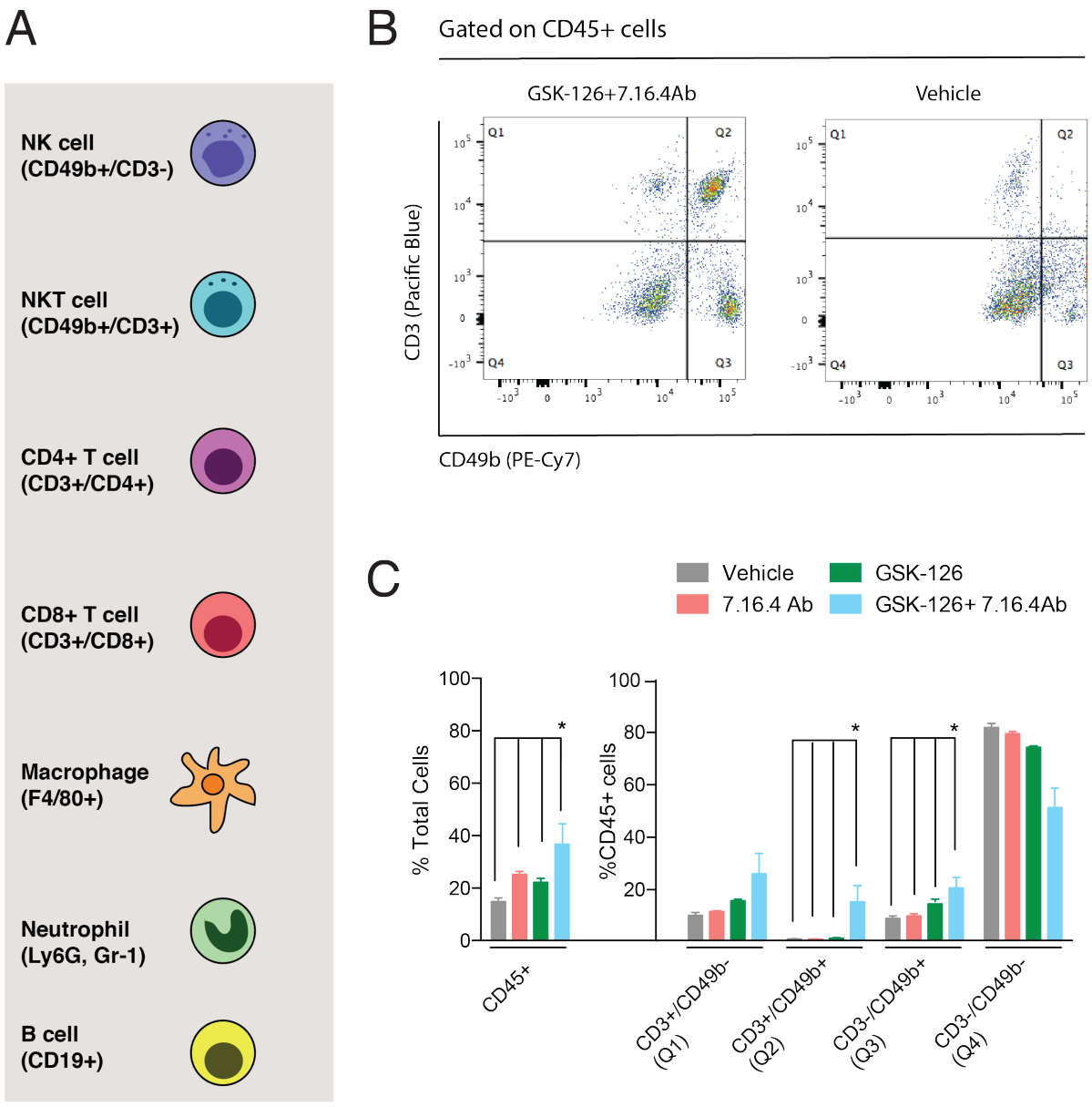

Figure 2-39. Immunophenotyping of endpoint tumour reveals changes in the profiles of tumour infiltrating lymphocytes amongst treatment groups

(A) Schematic of immune cells and the markers employed to sort them using FACS. (B). Example of dot plots of CD45+ gated immune cells stained for CD3 and CD49b in vehicle vs combination treated endpoint tumours. (C) Quantification of total CD45+ immune cells in the endpoint tumours, as well as the % of CD45+ immune cells positive for the T cell marker CD3 only (Q1), CD3 and CD49B (NKT cells Q2), CD49b only (NK cells, Q3) or neither marker (other immune cells, Q4). Q= quadrant, and correspond to the dot plot in panel B. For each condition, the endpoint tumours of 5 different mice were assessed per treatment condition. Error bars indicate S.E.M.

2.3.5 Combination treated tumour have significant elevated levels of the apoptosis marker cleaved caspase 3 and IFNγ

Our immunophenotyping analysis revealed significant infiltration of NKT cells and NK cells in tumours treated with combination therapy, implying that these subsets were part of the observed anti-tumour phenotype. NK cells play a role analogous to cytotoxic T cells, and in response to tumour detection can trigger cytokine release, cell lysis and apoptosis. NKT cells are a subset of T cells that possess a T cell receptor, and do not detect antigens presented by MHC molecules, but lipids presented by CD1d. Bridging the adaptive and innate immune system, NKT can be classified as type 1 or 2, with each subtype playing contrasting functions in the context of cancer. Type I NKT cells are associated with anti-tumour immunity, secreting IFNγ that in turn recruits NK and cytotoxic T cells. Conversely, Type 2 NKT cells primarily inhibit immune surveillance of the tumour. To determine if there might be increased levels of IFNγ in combination treated tumour, and may be contributing to the anti-tumour effect of the therapy, we performed an enzyme-linked immunosorbent assay (ELISA) to detect IFNγ levels in endpoint tumours. Interestingly we detected a significantly increased IFNγ levels in both GSK-126 treated conditions (**Figure 2-40A**). To confirm that tumour cells might be undergoing apoptosis, perhaps due to the presence of increased NK and NKT cells, we stained endpoint tumours from our preclinical trials with the apoptotic marker Cleaved Caspase 3. Quantification of staining revealed a significantly higher presence of staining in combination treated tumour (**Figure 2-40B**).

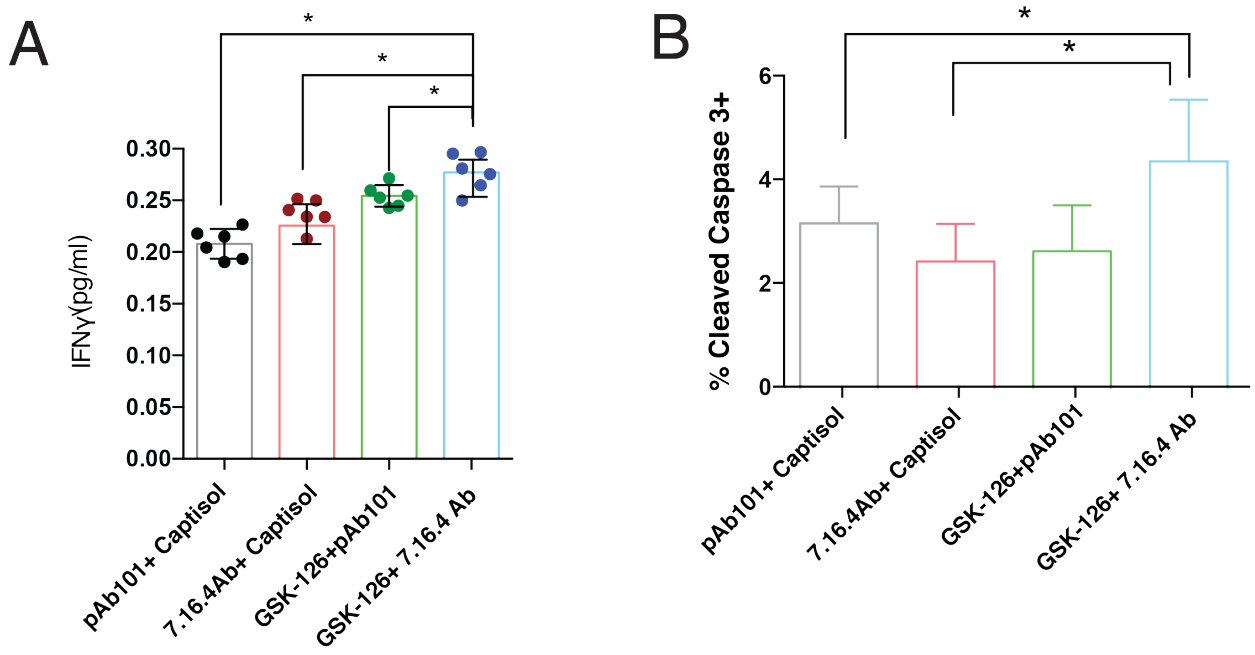

Figure 2-40. Evaluation of IFNγ and apoptosis in endpoint tumours

(A) Endpoint tumour lysates from the first preclinical trial was quantified for levels of IFNγ via ELISA. n=6 per condition. (B) Quantification of Cleaved Caspase 3 staining in endpoint tumours from the preclinical trial. n= 6 tumours per treatment condition. Histology from 2 independent clinical trials were pooled and assessed, with each trial comprised of between 5-7 mice per condition. *n.s* = not significant. Error bars denote S.E.M. *=p<0.05.

3 Discussion

3.1 Summary

While elevated levels of Ezh2 have been observed to correlate with more aggressive subtypes of breast cancer and poor survival outcome, the potential of translating these of these observations into therapeutic strategies has been unclear. An unresolved question has been whether EZH2 targets are universally essential for breast cancer transformation or whether PRC2 mediated transcriptional changes are specific to the intrinsic subtype.

To address this, we first explored the effect of Ezh2 ablation in a transgenic mouse model reflective of the Luminal B subtype of breast cancer. We established that loss of Ezh2 significantly affected metastasis, and established that this phenotype could be recapitulated with the use of pharmacological inhibitors that inhibited Ezh2 methyltransferase activity. We then identified an anti-metastatic transcriptional program that is reactivated upon loss of global H3K27me^3 levels, and demonstrated that this program is driven by the transcription factor FOXC1. Finally, we demonstrated that the EZH2 mediated repression of the FOXC1 anti-metastatic cascade was specific to Luminal B breast cancer, a finding that has important therapeutic implications.

Since we observed differential effects on metastasis between Luminal B and HER2+ breast cancer, we next explored the effect of Ezh2 ablation on tumour initiation and maintenance in a mouse model of HER2 luminal breast cancer. We observed a significant delay in tumour onset, which was likely due to the reduced proliferative capacity of hyperplastic lesions in mice lacking both Ezh2 alleles, and a reduction in tumour penetrance from 100% to 20%. With respect to tumour maintenance, we observed that ablation of Ezh2 or inhibition of Ezh2 methyltransferase activity inhibited

cellular proliferation. Interestingly, transcriptional profiling revealed a significant increase in a tumour intrinsic viral-defense signaling pathway, leading us to speculate that modifications can be made to the tumour epigenome that lead to increased vulnerability to detection and destruction by the immune system.

The current standard of care for HER2+ breast cancer patients are monoclonal antibodies that target the extra-cellular domain of HER2 (HER2 mAbs), but patient response can be poor due to the cellular heterogeneity of the tumour. Considering that a vital mechanism of HER2 mAbs is through engagement of the immune system, we hypothesized that combination of GSK-126 with HER2mAbs would synergize to dampen tumorigenicity in an immune competent system. Interestingly we report that a combination of the two therapies increased apoptosis and the infiltration of anti-tumour immune cell populations such as NK cells and NKT cells.

3.2 An EZH2-FOXC1 anti-metastatic axis in Luminal B Breast Cancer

3.2.1 PRC2 function is dictated by breast cancer subtype

Our interest in pursuing the striking metastatic phenotype observed upon *Ezh2* ablation was driven by clinical knowledge that patient mortality is predominantly a consequence of distal metastasis. Interestingly, while our approach of using *in vivo* transgenic models allowed us to test progression of the metastatic cascade in a biologically relevant way, it also uncovered novel insights into the role of Ezh2 in tumor onset and progression. We observed that deletion of *Ezh2* in a PyVmT-driven model significantly delayed tumor onset, thus indicating that Ezh2 plays an important role in breast cancer progression. This directly contrasted with findings from two recent studies that have utilized other transgenic mouse models to dissect the role of Ezh2 in breast cancer. Woo and colleagues employed a p53 heterozygous *Brca*-deficient mouse model of BLBC and speculated that the absence of any phenotype was due to compensating methyltransferase activity by Ezh1(244). This was not the case in our transgenic model, as evidenced by global depletion of H3K27me^3 in the tumor epithelium. Wassef and colleagues utilized an activated Notch model of mammary tumorigenesis(245) and observed that ablation of *Ezh2* increased the penetrance of mammary tumors following multiple rounds of pregnancy. The combination of our work with what is known about the role of Ezh2 in other transgenic models of breast cancer, indicate that PRC2 can play different roles in different intrinsic subtypes of breast cancer.

3.2.2 Reactivation of a key determinant of Basal-Like Breast Cancer in Luminal B

Like EZH2, we also found that FOXC1 functions in a context-specific manner. In contrast to previous studies that have emphasized the **contribution** of FOXC1 to cancer severity, our functional studies demonstrate that elevated expression of FOXC1 is **detrimental** to the metastatic cascade, and that higher *FOXC1* levels significantly correlate with good prognosis in non-BLBC subtypes of breast cancer.

We were particularly surprised to discover that FOXC1 drove an anti-metastatic program in Luminal B breast cancer, because several publications have reported FOXC1 to be an important determinant of Basal-like Breast Cancer (BLBC) (264, 265, 288, 289). Consistently high FOXC1 expression has been associated with BLBC in multiple analysis of human data sets and an increased risk of metastasis, due to the activation of an EMT related program (264, 290, 291). Consistent with these published data, the anti-metastatic transcriptional program associated with FOXC1 in our study does not correlate with FOXC1 expression in BLBC.

FOXC1 has been implicated in various stages during developmental (292). Interestingly, an EZH2-FOXC1 regulatory axis has also been reported in the hematopoietic system, whereby FOXC1 regulates a cellular differentiation program rather than a mesenchymal phenotype. Somerville and colleagues observed that treatment of adult cord blood cells (CD34+) with EZH2 methyltransferase inhibitors was sufficient to increase transcription of *FOXC1*, leading the authors to conclude that *FOXC1* is typically repressed by PRC2. Furthermore, they reported that *FOXC1*, expressed in 20% of Acute Myeloid Leukemia (AML) cases, blocks differentiation thus enhancing the clonogenic potential of malignant cells(293). Interestingly, our characterization of the targets activated by FOXC1 in the Luminal B context revealed

that these genes were associated with neuronal development. Given the importance of H3K27me^3-dependent silencing during cell lineage decisions and differentiation events(112), it is possible that the absence of EZH2 may have allowed for an inappropriate differentiation program to be induced; one that incidentally also has anti-metastatic capacities.

3.2.2.1 Epigenetics can drive lineage plasticity

We also speculate that the expression of FOXC1, a factor predominantly associated with BLCB, in a Luminal subtype of breast cancer upon loss of Ezh2, might also be indicative of lineage plasticity regulated by epigenetic mechanisms. Numerous publications from the field of developmental biology have highlighted the function PRC2 plays in regulating cellular identity, and how loss of PRC2 can subvert the lineage decisions of epithelial cells (294) (308). Interestingly, recent studies have further illustrated how lineage plasticity can be modulated by epigenetic mechanisms in the context of cancer. Ku and colleagues recent demonstrated that prostate cancer cells escape androgen deprivation therapy through differentiation from a luminal to a basal identity. This lineage change was accompanied by an increase in Ezh2, and perhaps most strikingly, they demonstrated that sensitivity to androgen could be restored by inhibition of Ezh2 methyltransferase activity (295). Complementary to the findings by Ku and colleagues, in a model of KRAS+ lung adenocarcinomas (ADC) another group demonstrated the plasticity of KRAS+ ADC to develop into squamous cell carcinoma (SCC) by undergoing differentiation into another cell lineage (296). A hallmark of the transition from ADC to SCC was the depression of SCC genes through loss of PRC2 mediated H3K27me^3.

3.2.3 Breast cancer subtype specific reactivation of FOXC1

We observed that that high *FOXC1* can function as a prognostic marker for positive outcome in both HER2 and Luminal B subtypes. Furthermore, higher collective expression of multiple FOXC1 targets was also predictive of favorable prognosis across both subsets, suggesting that the identified downstream targets of FOXC1 are tumor suppressive, which also agrees with the findings of multiple functional studies investigating these genes (257-262). However, we found that pharmacological inhibition of EZH2 methyltransferase activity only reactivated FOXC1 and downstream anti-metastatic targets in the Luminal B, but not HER2, PDX. Interestingly, while H3K27me^3 enrichment at the FOXC1 locus has not been previously reported, quantitative DNA methylation analysis identified hypermethylation of CpG islands near the *FOXC1* locus in ductal carcinoma *in situ* (DCIS), an early stage of breast cancer (297).

DNA methylation and H3K27me^3 are two important epigenetic silencing mechanisms that have been closely associated with each other(126), yet the precise mechanism through which this occurs and its relevance during tumorigenesis is unclear. Indeed, during tumorigenesis it has been proposed that DNA methylation patterns affect the affinity of PRC2 binding and can drive the redistribution of H3K27me^3(298). Furthermore, genome wide analyses have suggested that DNA methylation can prevent H3K27me^3 deposition locally and at a megabase scale(130). Thus, it is conceivable that different tumor types, including different subtypes of breast cancer, can adopt DNA methylation or H3K27me^3-based mechanisms of silencing *FOXC1*. Interestingly, the examination of FOXC1 DNA methylation status across a large cohort of breast cancer subtypes from the TCGA data set indicates that the average DNA methylation probe

intensity for FOXC1 is significantly lower in Luminal B breast cancer samples than HER2+ and Luminal A breast cancers (**Figure 3-1**).

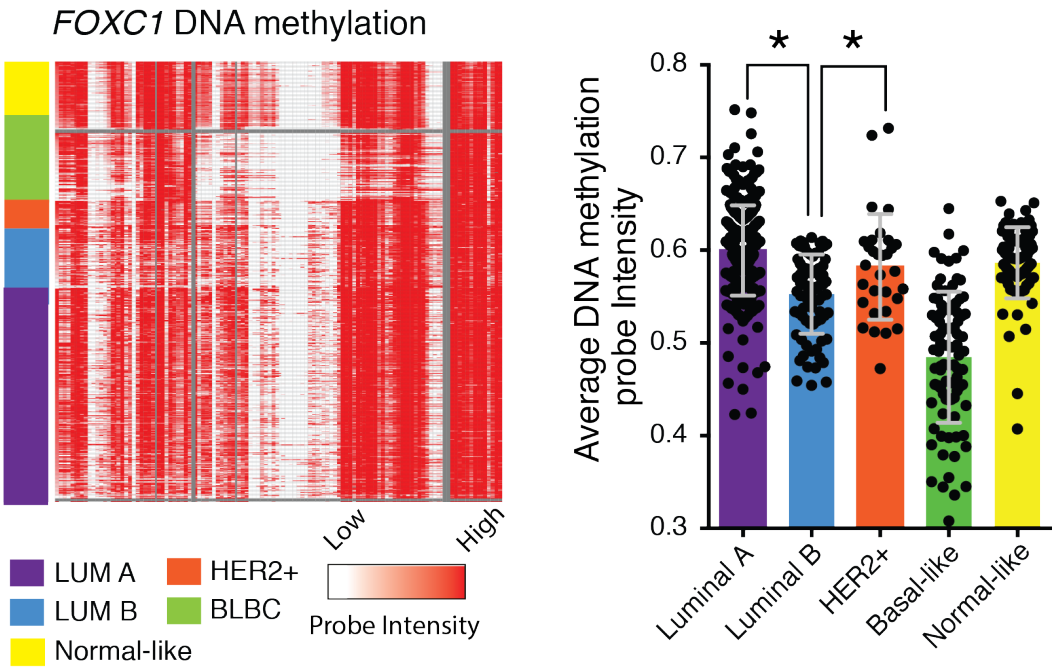

Figure 3-1. DNA methylation of the FOXC1 locus across different breast cancer subtypes

A heatmap illustrating data from the TCGA Breast cancer database (Illumina DNAmethylation450k) for probes along the *FOXC1* locus. Right hand panel is a bar graph of the average DNA methylation probe intensity for the FOXC1 locus, across different breast cancer subtypes. *= $p<0.05$.

We therefore speculate that other mechanisms, such as DNA hypermethylation, might be in place to silence the FOXC1 locus in Luminal A and HER2 breast cancers, whereas Luminal B tumors employ H3K27me^3 for this purpose. Alternatively, since loss of an epigenetic repressive mark does not necessarily guarantee expression of a given locus, a transcription factor milieu intrinsic to the Luminal B subtype might promote the active transcription of FOXC1 in the absence of repressive epigenetic marks.

3.3 The role of Ezh2 in Neu/ErbB2-driven models of HER2+ breast cancer

Given the subtype specific effects PRC2, next we employed pharmacological and genetic techniques to assess the effects of PRC2 in HER2+ tumour cell maintenance and initiation. Both RNAi and the use of a transgenic model coupled with *in vitro* administration of Adenovirus Cre demonstrated that Ezh2 ablation impairs cellular proliferation in transformed tumour cells. These anti-proliferative effects were recapitulated with the use of two different highly specific inhibitors of Ezh2 methyltransferase activity. To understand how transcriptional programs changed upon loss of Ezh2 methyltransferase activity and how this might contribute to the observed proliferation defect, gene expression profiling was performed. Interestingly, ErbB2-driven tumour cells acutely treated with GSK-126 upregulated a significant number of genes related to organization of the Extracellular Matrix (ECM) and the anti-viral IFN α/β immune response. This result was particularly interesting, as gene expression profiling of endpoint $Ezh2^{-/-}$ NIC tumours revealed the repression of transcriptional pathways governing ECM and the immune response, suggesting a compensatory mechanism was employed in the transgenic models to repress these programs to facilitate tumorigenesis.

3.3.1 The role of Ezh2 in tumour initiation of nee/ErbB2-driven tumours

Perhaps the most striking phenotype reported in the NIC mice was the decreased tumour penetrance and significantly delayed tumour onset in Ezh2 deficient NIC mice. Intriguingly, the examination of mammary glands prior to tumour palpation revealed the presence of ErbB2+ early lesions in $Ezh2^{-/-}$ NIC, though these structures were significantly smaller and less proliferative compared to controls. While we did not

determine how loss of Ezh2 contributed to such a pronounced phenotype in ErbB2-driven mouse models of breast cancer, we propose three possibilities; (1) the inability to repress tumour suppressors during transformation, (2) defective mammary gland development or (3) changes to IFN α/β signaling during the early stages of tumorigenesis.

3.3.1.1 Activation of tumour suppressors during initiation

PRC2 has been long understood as an 'epigenetic gatekeeper' during tumour initiation, exercising its repressive capacity to ensure that tumour suppressors are not expressed during transformation. The most renown example involves *p16/INK4A* which plays an important role in cell cycle regulation, decelerating progression from G1 phase to S phase. Silencing of this locus has been observed during the pre-invasive stages of different types of cancer(299-301) and several studies have demonstrated PRC2 is required for repression of this tumour suppressor in different tissue types(302-305). It would be interesting to compare p16/INK4A levels by immunohistochemistry in Ezh2$^{-/-}$ vs wildtype NIC mammary glands during the early stages of tumorigenesis, prior to tumour palpation to determine if de repression of this locus contributes to the delay in tumour initiation.

3.3.1.2 Developmental defects contribute to impaired tumorigenesis

One caveat of the NIC model is that expression of activated ErbB2 and cre recombinase are coupled to the MMTV promoter, the expression of which begins as early as 3-4 weeks of age. Thus, if a gene of interest plays an important role in normal mammary gland development or homeostasis, its ablation during development may

inadvertently hinder disease progression. Recent studies have reported that Ezh2 may play a role in luminal lineage differentiation to mature progenitors; two independent studies have shown that Ezh2 is required for alveolargenesis and lactation in the mouse mammary gland (250, 251). Interestingly, the lactation defect did not affect the expression level of genes related to alveolargenesis, but rather reflected the activation of an unscheduled gene program related to keratinocyte function(250).

In line with observations that PRC2 might be important to luminal lineage identity, the recent epigenomic profiling of different human breast epithelial cell lineages has revealed increased deposition of $H3K27me^3$ in the promoter region of genes in luminal progenitors compared to basal progenitor cells (306).

While no markers have been defined, the tumour initiating cell (TIC) of MMTV-ErbB2 models are proposed to arise from the luminal epithelial cell lineage; ErbB2-induced cancers have been suggested to be initiated by a subpopulation of parity identified mammary epithelial cells (PI-MECs) within the luminal epithelial cell population (307) and two independent groups have reported using the luminal epithelial marker CD61 to enrich for TIC in neu/ErbB2-driven tumours (308, 309).Thus, given that the TIC in the model we employed may originate from the luminal epithelial lineage, it is possible that loss of Ezh2 in the developing mammary gland influences tumour initiation. In our development studies we observed that $Ezh2^{-/-}$ MMTV-Cre mice displayed significantly reduced ductal tree outgrowth, but by 12 weeks of age this difference was no longer detectable. These results, however, do not eliminate the possibility that perturbations to mammary gland development influenced tumour initiation.

3.3.1.3 The contribution of elevated IFN α/β signaling

Finally, considering the observation of increased IFN α and β signaling in response to inhibition of Ezh2 methyltransferase activity, it would also be interesting to quantify IFN α and β levels in hyperplastic mammary glands. Increased IFN α and β levels influence the cell cycle of breast cancer cells (310, 311) and may explain the reduced proliferative capacity of $Ezh2^{-/-}$ NIC hyperplastic lesions and delayed tumour onset. Furthermore, given the immuno-stimulatory effects of cytokines, histological examination of early lesions to profile the immune infiltrate and would be an interesting way to further explore if clearing of the early hyperplastic lesions is also contributing to the observed delay in onset.

3.3.2 Remodeling the tumour epigenome to modulate the stromal microenvironment

Our observation that targets associated with the anti-viral IFN α/β immune response were upregulated upon acute inhibition of Ezh2 methyltransferase activity was of great interest, given some recent revelations in the literature. Recently, two independent papers have demonstrated that a low dose treatment with the DNA methyltransferase (DNMT) inhibitor 5'Azacytdatine can invoke an anti-tumour immune response in ovarian or colon cancer cells (269, 270). The mechanism of action through which this occurs is by the demethylation of endogenous retroviral elements (ERV), which induces the transcription of double stranded RNA, thus triggering the host to mount a viral defense mechanism that includes a Type I IFN response. Given that $H3K27me^3$, like DNA methylation, functions to transcriptionally silence loci, we speculate that a similar mechanism could be occurring in HER2+ tumour cells exposed to GSK-126.

3.3.2.1 Epigenetic silencing of genomic repeat regions

Endogenous retroviral elements (ERV) are a subclass of transposons found abundantly in vertebrate genomes. Originating from retroviruses that integrated themselves into the host genome of a germline cell, ERV have acquired inactivating mutations and are no longer capable of forming virus. As they can be deleterious to the organism, they are transcriptionally silenced by repressive heterochromatin domains. In mouse somatic cells, DNA methylation has been shown to be vital to maintaining transcriptional silencing of ERV(312).

Interestingly, an equivalent role for PRC2 in mediating genomic repeat regions through H3K27me^3 has been investigated in the context of developmental biology. Several studies have demonstrated that DNMT are dispensable for the silencing of ERV in mouse ES cells (313, 314). PRC2 has also been demonstrated to play a role in silencing some types of ERVs in mouse ES cells (103, 315), though this effect is thought to be indirect, as the identified ERVs were not bound by H3K27me^3. However, in an ES cell model of gradual DNA hypomethylation, H3K27me^3 has been demonstrated to compensate for ERV silencing at select types of ERVs (316).

Strikingly, in the context of cancer, Ishak and colleagues have recently reported that Ezh2 can be recruited to repetitive DNA elements, such as ERV, to facilitate H3K27me^3 mediated transcriptional repression in tumour cells (317). They report the indiscriminate recruitment of Ezh2 by retinoblastoma protein (Rb) to areas of genomic repeat sequences, and posit that the use of Ezh2 inhibitors in Rb positive cancers will sensitize the tumours to immune surveillance and immunotherapies.

We speculate that the observed IFN α/β response observed is a byproduct of

de-repression of ERV and other genomic repeat elements, due to the global loss of H3K27me^3. To test this hypothesis, we have performed Chromatin immunoprecipitation followed by next generation sequencing (ChIP-Seq) to determine the global binding and enrichment profiles of H3K27me^3 of primary mouse mammary tumour cells isolated from ErbB2-driven tumours. Additionally, we have performed RNA-Seq of ErbB2-driven mouse tumour cells acutely treated with DMSO, GSK-126 or Epizyme 6348. Hybridization based microarrays are limited by the probes that are contained on the chip; the Affymetrix Mouse 2.0 microarray we have employed in this work only has a select number of probes against retro transposable elements. Thus, the use of RNA-Seq will enable the more robust detection of changes to ERV transcription, and when overlaid with ChIP-Seq H3K27me^3 enrichment profiles will reveal if there is enrichment of H3K27me^3 along these regions in the genome of ErbB-2 driven tumours (**Figure 3-2**).

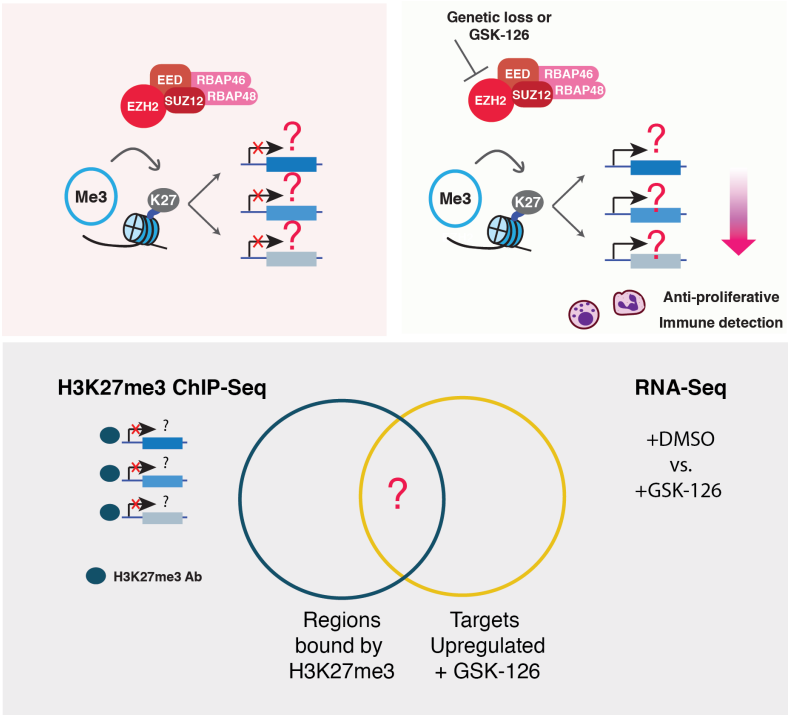

Figure 3-2. Identification of H3K27me3 regions in ErbB2-driven tumour cells

3.4 Combining PRC2 inhibition with HER2 mAb therapy

We explored the potential of combining a HER2 mAb with an inhibitor of Ezh2 methyltransferase activity in immune competent preclinical models. Interestingly, we observed a significant reduction in tumour volume and growth in animals treated with both therapies, which was accompanied by an influx of infiltrating cytotoxic immune cell populations such as NKT cells and NK cells, and elevated apoptosis in the endpoint tumours. While combination therapy influenced the host immune system to elicit anti-tumour effects, further steps should be taken to explore the contribution of tumour intrinsic effects inhibiting Ezh2 methyltransferase activity.

3.4.1 Tumour intrinsic effects of inhibiting Ezh2 methyltransferase activity

A recent study in ovarian cancer cells determined that epigenetic modifications can be utilized by the tumour to silence responsiveness to IFNγ and immunotherapy (318). Peng and colleagues identified the H3K27me^3 mediated repression of T help type 1 (T_H1) cytokines CXCL9 and CXCL10 in tumour populations, thereby influencing T cell trafficking to the tumour microenvironment. Treatment with inhibitors against DMNT and Ezh2 methyltransferase activity increased T cell infiltration and interrogation of a large cohort of human data revealed that EZH2 and DNMT1 levels were inversely correlated with patient survival.

We speculate that there are tumour intrinsic epigenetic silencing mechanisms to avoid detection of the immune system. Earlier, we identified the activation of a tumour intrinsic transcriptional program related to the IFN α/β response, the cause of which was speculated on in the previous section. While we have not confirmed that GSK-126 treated tumour increase production of IFN α and or β, the production of these cytokines

would certainly synergize with immunotherapies. IFN are a family of cytokines that can be produced by both the tumour cells and stromal cells, and have effects on a wide range of cellular populations. Type 1 IFN, which encompasses IFN α and β, have been recognized for their contribution to anti-tumour immunity; they activate the cytotoxicity of NK cells (319) and can inhibit cell cycle progression and apoptosis in malignant cells through activation of IFNAR signaling(281, 320, 321). Several groups have demonstrated that IFN α and β induction can be coupled to immunotherapies to enhance therapeutic response (269, 281, 322).

3.4.2 Tumour extrinsic effects of inhibiting Ezh2 methyltransferase activity

PRC2 has been well documented to play an important role in regulating the development and reactivity of different immune cell populations, and it is also conceivable that and the systemic administration of GSK-126 contributed to anti-tumour effects through inhibition of Ezh2 methyltransferase activity in the stromal microenvironment.

In our preclinical trials, immunophenotyping revealed the significant upregulation of NKT and NK cells in combination treated tumours. NKT cells are non-conventional T cells that develop in the thymus, and are important for mediation of the innate immune response. Capable of generating a range of different cytokines, the expansion of NKT cells can activate the adaptive immune system and are typically considered anti-tumour (323, 324). An important regulator of NKT cell identity, PLZF, has recently been shown to be targeted for degradation via methylation by PRC2. The condition ablation of Ezh2 resulted in an expansions of NKT cells via accumulation and stabilization of PLZF (325).

An independent study has also reported that Ezh2 ablation in the T cell compartment expands the NKT cell population(326).

NK cells play a key role in tumour immune surveillance, and presence of NK cells has been positively correlated with cancer patient outcome (327). Interestingly, the importance of Ezh2 methyltransferase activity to NK cell development has also been reported(328). Loss of Ezh2 has been shown to increase the development of mature NK cell progeny from mouse and human hematopoietic stem cells. Furthermore, loss of Ezh2 not only expanded NK cell populations but also increased the cytotoxicity of these cells towards tumour cells.

Since the administration of GSK-126 is systemic, the observed expansion of NKT and NK cells in combination treated tumours might be a direct consequence of Ezh2 methyltransferase inhibition in these stromal cell populations. This idea is further supported by the significantly increased levels of apoptosis and IFNγ, a cytokine predominantly produced by NK and NKT cells during the innate immune response, we observe in endpoint tumour treated with combination therapy.

3.4.2.1 Impaired Ezh2 activity may deplete anti-tumour T cell populations

Given that we observed increased levels of IFNγ in combination treated tumours, we were surprised that this increase did not coincide with increased infiltration of CD8+ cytotoxic T-cells; our results reflected no significant difference in CD4+ and CD8+ T cell populations across treatment groups. One possibility is that global loss of Ezh2 is adversely affecting the anti-tumour component of the immune system. Ezh2 has been reported to be an important determinant of T cell differentiation and survival (329, 330). A recent study found that Ezh2 was critical to the maintenance of polyfunctional CD8+ T cells, and that the increased infiltration of this cell type in tumours is associated with

better prognosis (331). The potential effect of systemic epigenetic manipulation on all immune cells should be taken into consideration, as the individual effects might not always be anti-tumour.

3.4.3 Implications for tumour heterogeneity in HER2+ breast cancer

One of the most interesting implications of the work performed in this chapter pertains to improving patient outcomes for patients with high intra-tumour heterogeneity of HER2 gene amplification. Breast cancer heterogeneity exists at both at the inter-tumour level and the intra tumour levels, where different sub populations of clones have been understood to influence disease progression. In the context of HER2+ breast cancer, cellular heterogeneity of HER2 levels within the tumour have been extensively reported and patients with higher levels of HER2 heterogeneity are significantly associated with poor response to trastuzumab (332) (333). HER2 genetic heterogeneity has been clinically defined as tumours with HER2 immunohistochemical signal ratios greater than 2.2 or HER2 FISH signals greater than 6, present on greater that 5% but less than 50% of tumour infiltrating cells (334, 335). Thus, while trastuzumab might elicit responses from the HER2+ populations, this might be masked if most cells do not express HER2, or result in the expansion of HER2- populations during drug holidays, intervals when patients are taken off a therapy to allow for recovery from the systemic toxic effects of the therapy. Combination of GSK-126 with trastuzumab might be a strategy to elicit initial anti-tumour immune recruitment and response through engagement of the HER2+ population. The addition of GSK-126 would serve to amplify the reactivity and presence of anti-tumour immune cells to the tumour and via a bystander effect, indiscriminately destroy both HER2+ and HER2- tumour cells.

3.4.4 The prognostic value of EZH2 in assessing patient response to trastuzumab

While the therapeutic implications of our work are promising, we wondered if there were prognostic aspects that could also be leveraged; specifically, if EZH2 levels could predict HER2 patient outcome. To this end, we formed a collaboration with a group that had recently evaluated a preoperative brief exposure paradigm to examine the effects of a loading dose of trastuzumab, pre-and post-administration, in HER2+ breast cancer patients (Dr. Vinay Varadan, Case Western University and Dr. Lyndsay Harris, National Institute of Health) (336).

3.4.4.1 A multi-site trial of HER2+ breast cancer patients prior and post Trastuzumab

Our collaborators recently evaluated a multicenter preoperative trial that administered a single dose of trastuzumab prior to combination with chemotherapy to explore changes to tumours (336). The study was designed such that tumour biopsy samples were attained prior and following administration of trastuzumab (**Figure 3-3A**) to patients with stage I-II HER2+ breast cancer. In addition, the authors performed RNA-Seq to acquire transcriptomic data of samples at both the 'Baseline' time point (pre-trastuzumab), and 'post' treatment (2 weeks following a single loading dose of trastuzumab). They also evaluated the pathological complete response (pCR (reflective of long-term recurrence free survival (337)) 12 weeks after patients began a combination of both trastuzumab and chemotherapy.

3.4.4.2 Do EZH2 levels predict pathological Complete Response (pCR)?

We hypothesized that high EZH2 levels might function to silence targets that could attract an anti-tumour immune response. Thus, we first wanted to examine if transcriptional levels of *EZH2* were significantly correlated with pCR in samples at

baseline or post Trastuzumab exposure. No significant correlation between *EZH2* transcript levels was observed (**Figure 3-3B**). However, transcription of a locus is not always indicative of protein synthesized. Preliminary data from our lab shows that *EZH2* translation is dependent on mTORC1-mediated 4EBP phosphorylation (Dr. Harvey Smith, unpublished data) and another group has reported that EZH2 is sensitive to pharmacological inhibition of eIF4A(338). We are now currently assessing if 'Baseline' nuclear protein levels of EZH2 correlate with pCR, via immunohistochemical staining.

3.4.4.3 Viral defense gene signature

Tumours must evolve to bypass detection by the immune system, and process that can involve changes to epigenetic modifiers. As mentioned previously, two independent groups observed that DNA demethylation increased expression of dsDNA production, thus invoking an anti-viral immune response in tumour cells (269, 270). Chiappinelli and colleagues also generated a signature of significantly upregulated genes upon inhibition of DNA methyltransferase activity, termed a 'Viral defense signature', and observed that the signature was predictive of melanoma patient response to immunotherapy(269).

Since RNA-seq data is available for both the 'baseline' and 'post-Trastuzumab' time points, we were also interested in extending our bioinformatic analysis to determine if response to Trastuzumab can be predicted by a 'Viral gene defense' signature. Interestingly, the 22 gene Viral Defense Gene signature was significantly higher 'Post-treatment' vs 'Baseline', but only in patients that showed pCR (**Figure 3-3C**). This preliminary data indicates that induction of genes in response to anti-viral immune programs are indicative of response to Trastuzumab. Further work will need to be conducted to confirm if this observation is linked to EZH2.

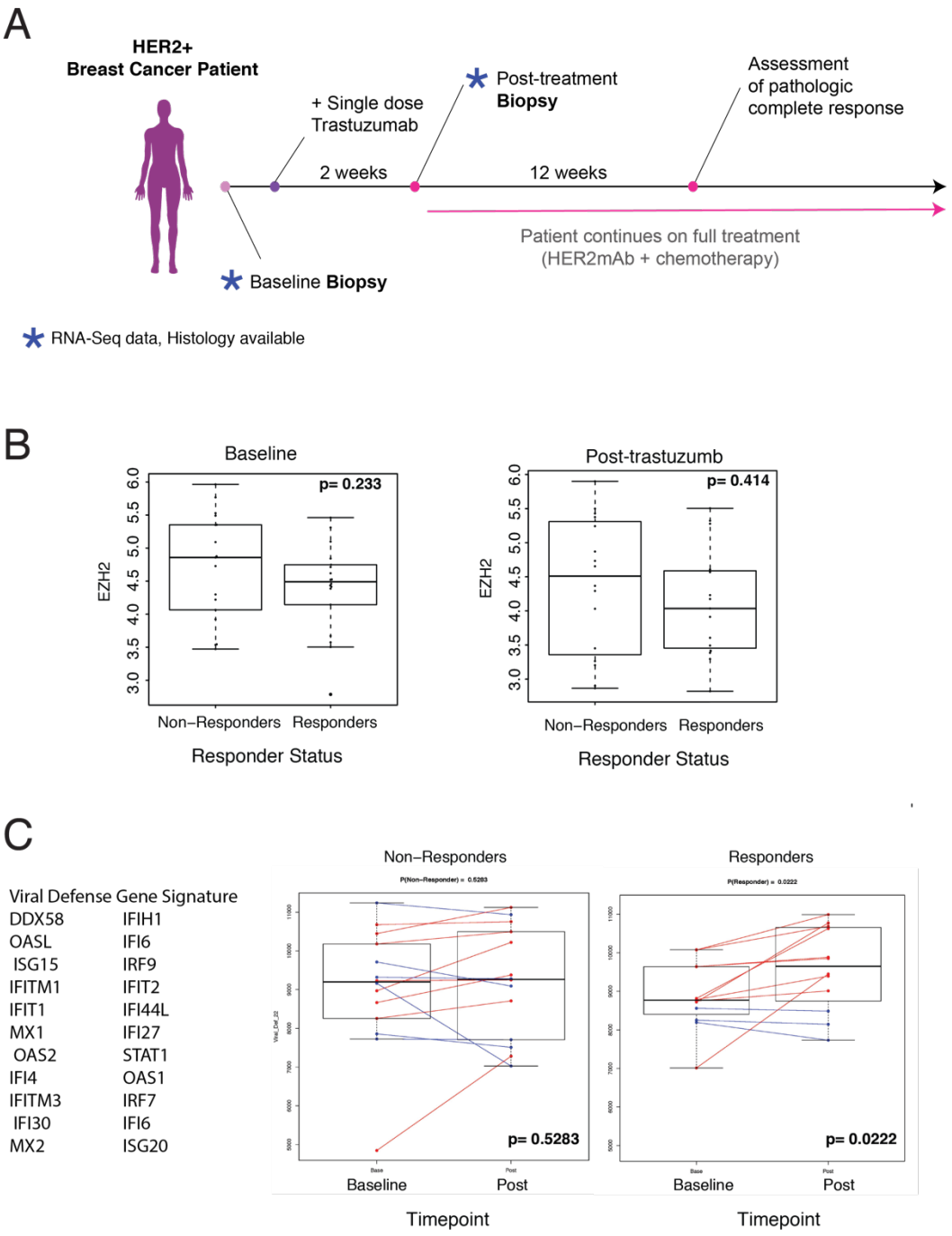

Figure 3-3. Schematic detailing the window of opportunity trial and preliminary data

(A) Schematic of the window of opportunity trial in which patient samples were collected before and after a single dose of trastuzumab. (B). *EZH2* levels do not correlate with pathological complete response to trastuzumab, following 12 weeks of therapy. (C). Patients who respond to trastuzumab significantly increase expression of a previously defined Viral Defense Signature(269) following acute treatment with trastuzumab, compared to baseline levels.

3.5 Experimental Limitations

As with any experiments, there are limitations to our work, some of which have been detailed below.

Exploration of methyltransferase independent effects of Ezh2 was not thoroughly assessed. A survey of the literature reflects that there is no single methyltransferase independent function of Ezh2, and examples of both a co activator or co repressor have been observed. The most complete way to assess the contribution of Ezh2 methyltransferase independent activity to tumorigenesis would be to interbreed mice with the Ezh2 Δ SET domain transgene (177) with the various mouse models employed in this work. Secondly, we did not consider the possibility of histone independent function of Ezh2 methyltransferase activity. Finally, delineating the tumour intrinsic and extrinsic effects of Ezh2 inhibition is another limitation of this work. While GSK-126 and 7.16.4mAb synergized to dampen tumorigenicity, we did not establish the tumour intrinsic vs. extrinsic effects of this combination. We speculate that the ChIP-Seq experiment outlined in **Figure 3-2** will shed some light on this issue, however, to functionally address this issue, $Ezh2^{-/-}$ deficient ErbB2-driven cells lines (such as the $Ezh2^{fl/fl}$ NDL AdCre developed in **Figure 2-25**) could be orthotopically injected into host mice, and treated with the murine version of trastuzumab, 7.16.4Ab.

3.6 Implications and Future Directions

3.6.1 Comparing the epigenetic landscape across different breast cancer subtypes

The most compelling result from this work can be distilled into the concept that PRC2 plays different roles in different subtypes of breast cancer during different stages of tumorigenesis. The clinical implications of this, are that suitability of an Ezh2 methyltransferase inhibitor is not only dictated by breast cancer subtype, but also during a defined window of opportunity. Thus, the natural progression of thought is to more clearly understand what underlies the differences between subtypes and processes that could influence H3K27me^3 deposition and PRC2 activity.

As outlined in the literature review, several factors contribute to recruitment of PRC2 to a given loci. Recent studies have revealed the enrichment of specific lncRNA species in each intrinsic subtype of breast cancer (339) (340), however, the number of species discrete to each subtype is low and does not account for the breadth of H3K27me^3 deposition across the genome. Since the basis of the classification of different intrinsic molecular subtypes are their distinct transcriptional signatures, perhaps the most suitable theory to be applied is the idea of PRC2 constantly surveilling the genome for areas of low transcriptional activity to deposit the H3K27me^3 mark, thus reinforcing transcriptional repression. This would account for differences in H3K27me^3 enrichment and silencing across different tissues and subtypes. To our knowledge, no comprehensive comparison of the reference epigenomes across different breast cancer subtypes have been published.

3.6.1.1 The metabolic wiring of a cell influences chromatin modifications

While the transcriptional profile of a given tumour cell may dictate PRC2 binding and activation of derepressed regions, we speculate that there are other factors

inherent to different subtypes that could contribute to differential sensitivity to inhibition of Ezh2 across different tissues or cell types.

Another parameter that plays an important role in shaping histone methyltransferase activity relates to cellular metabolism, as the production of histone methyltransferase cofactors is dependent on the cellular energy status of the cell. *S*-adenosyl methionine (SAM) is the universal methyl donor from which histone and DNA methyltransferases transfer a methyl group to a given substrate, producing *S*-adenosyl homocysteine (SAH) as a byproduct. The production of SAM itself relies on the *S*-adenosyl methionine transferase (MAT) catalyzed reaction involving methionine and ATP. Thus, production of the donor methyl group is not only tied to the ATP cellular energy status of the cell, but also a large network of amino-acid and nucleotide metabolic pathways known cumulatively as One-Carbon metabolism.

The modulation of SAM and One-Carbon metabolism can have physiological consequences. Recent work has revealed that the status of methionine metabolism is sufficient to influence the levels of histone methylation by modulating SAM and SAH. In fact, the ratio between these two metabolites plays a role in modulating HMT activity, as SAH can inhibit HMT and DNMT(341). Interestingly, studies have revealed that different HMT and DNMT might elicit different reactions to SAM levels, in different cellular contexts**.** For example, several studies in somatic and human ES cells have demonstrated that the H3K4me^3 marks is exquisitely sensitive to shifts in SAM levels (341, 342). However, in mouse embryos, perturbation in SAM levels affected H3K27 and H3K36 but not methylation of H3K4 (343).

We speculate that perhaps different intrinsic breast cancer subtypes have different requirements and reactions to methionine metabolites. A study conducted in a

panel of human cells lines representative of different intrinsic subtypes of breast cancer reported that expression of serine-metabolism associated proteins were increased in the Triple Negative cell lines compared to Luminal A, and that expression of glycine-metabolism associated proteins was highest in HER2 enriched cell lines(344). However, further metabolic flux analysis will need to be performed to understand the methionine and One-Carbon metabolism profiles of different breast cancers, and how this integrates into the epigenomic profiles of these different intrinsic molecular subtypes.

3.6.2 Mapping the changes to the chromatin environment during different stages of tumorigenesis

Studies from developmental biology have reinforced the notion that PRC2 is important for cellular identity during the process of differentiation. With respect to cancer biology, most studies have focused on endpoint tumour or transformed tumour cells lines. This approach, however, fails to capture the dynamic changes to the chromatin environment that occur during tumorigenesis or transition into metastatic lesions. Furthermore, since our results highlight the importance of Ezh2 in tumour initiation, it would be interesting to explore this concept further. To this end, I propose the epigenomic profiling of an *in vitro* model of tumour initiation.

We have observed that if the mammary glands of TetON PyVmT/rtta/GFP mice are harvested, dissociated and plated in non-adherent tissue culture plate to form mammospheres, induction of GFP and the oncogene PyVmT can be elicited by the addition of doxycycline to the cell culture media. This transformation is accompanied filling of the lumen and increased cellular proliferation (**Figure 3-4**). The benefit of this *in vitro* system would be the ease with which it could be manipulated; different

pharmacological inhibitors or cell media conditions could be explored to mimic different environments, and would also be easier to scale up to facilitate enough material ChIP-Seq analysis.

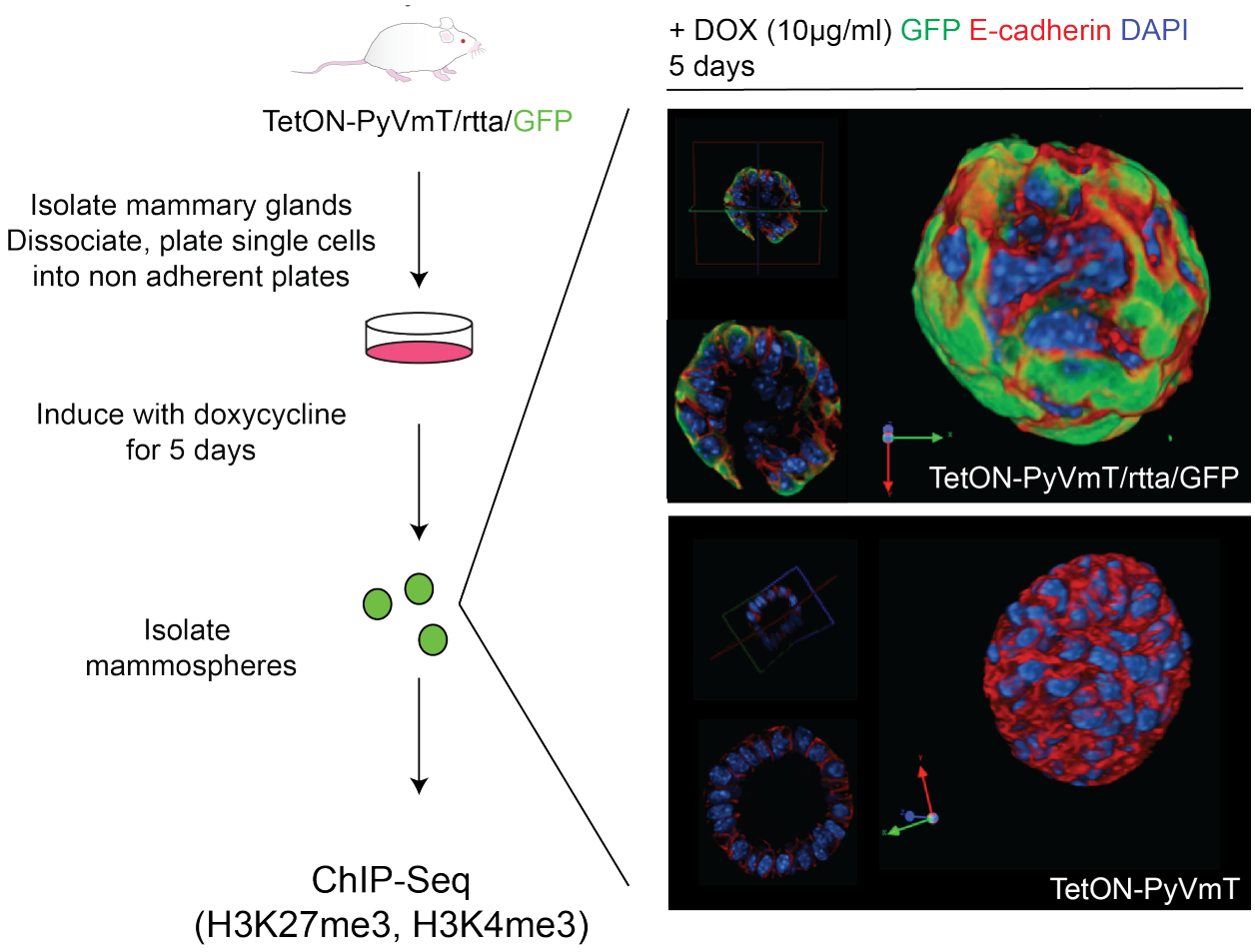

Figure 3-4. Characterization of the epigenetic landscape during tumour transformation

Schematic of an *in vitro* system of tumour initiation using the inducible PyVmT mouse model, wherein *ex vivo* cultures of mammospheres are induced with doxycycline to express GFP and PyVmT. Tumour spheres could then be harvested and assessed by ChIP-Seq for different chromatin marks and compared to normal mammospheres.

3.7 Concluding Remarks

Our work highlights the context specificity of PRC2 function, even within breast cancer. We identify that EZH2 methyltransferase inhibitors could be appropriate in a clinical setting as a neoadjuvant therapy to suppress invasion and metastasis specifically in Luminal B breast cancer patients. In HER2+ breast cancer, we demonstrate the impact of ablating Ezh2 function on cellular proliferation and tumour initiation, thus illustrating the different effects of targeting PRC2 during disease progression. Finally, we speculate that altering the tumour epigenome can modulate the stromal microenvironment, and that this could be leveraged to enhance situations in which the standard of care includes therapy that engages the immune system. Interestingly, Epizyme, a clinical-stage biopharmaceutical company has recently announced that it will begin Phase 1 clinical trials to that combines its Ezh2 methyltransferase inhibitor EPI6438 (Tazemostat) with an anti-PD-1 antibody (Atezolizumab). It will be interesting to see if inhibition of EZH2 has a priming effect on the immune system to improve the activity of checkpoint inhibitors, and how this will translate into improved breast cancer therapies.

4 Experimental Procedures

4.1 Animal Work

4.1.1 General animal husbandry

All mouse manipulations were performed in accordance with the McGill Facility Animal Care Committee and the Canadian Council on Animal Care. All strains were housed in the animal facility at the Goodman Cancer Research Center and back crossed onto a FVB/N genetic background. The Tet-ON PyVmT model(252), MMTV-NIC model((77), MMTV-NeuNDL2.5 model(75), GFP reporter (345) and Ezh2 conditional model(184) have been described previously. For the transgenic animal experiments in Chapter 1, 8-12-week old WT, $Ezh2^{+/-}$ or $Ezh2^{-/-}$ Tet-ON PyVmT mice were induced with water supplemented with Doxycycline (200mg/ml, Wisent).

4.1.2 Tumour monitoring

Mammary tumor formation was monitored by twice weekly palpation and tumor growth was measured by twice weekly caliper measurements. Tumour volumes were calculated using the following formula: $(4/3)x\ (\pi)x(length/2)x\ (width/2)^2$. Transgenic mice were sacrificed when total tumour volume reached 4-5c m^3 or when a single tumour reached 2.5cm^3 as according to animal care guidelines.

4.1.3 Necropsy Protocol

Mice were euthanized and mammary glands or tumour were excised. In most cases, material was frozen in liquid nitrogen, or was fixed in 10% neutral buffered formalin and embedded in paraffin wax. Fix and embedded materials were sectioned at 4μm thickness and stained with hematoxylin and eosin or further process as indicated.

Four hematoxylin and eosin stained lung sections taken at 50μm step section intervals were examined by microscope to assess metastatic lung lesions.

4.1.4 Mammary gland wholemount

Inguinal mammary glands were excised, mounted on glass slides and processed through acetone and stained with Harris Modified Hemotoxlyin (Fischer) overnight. Glands were then destained in 70% EtOH with 1% HCl for several hours, dehydrated in

4.1.5 In vivo drug studies

GSK-126 (Merca Chem) was reconstituted in 20% Captisol (Medchem Express), and brought to a pH of 4.5 with 10M potassium hydroxide, to create a working stock of 150mg/ml. Mice were weighed weekly, and administered 300mg/kg of GSK-126 or an equal volume of vehicle via intra-peritoneal injection, 3 times a week. Tumor growth was assessed in a blinded fashion, with twice weekly caliper measurements. For experiments involving 7.16.4 Ab (Genentech), mice were weighted weekly, and administered 100μg of 7.16.4Ab or an equal volume of pAb101 (vehicle) via intra-peritoneal injection, 2 times a week.

4.1.6 Orthotopic transplantation of cells into hosts

For orthotopic transplantation, 500,000 cells from established PyVmT or NIC cell lines were suspended in 30ul PBS and injected unilaterally into the inguinal fat pads of 8-12-week old immune-competent FVB mice.

4.1.7 Tail vein injections

For tail vein experiments, 250,000 cells were suspended in 100ul PBS and injected in the tail vein of athymic nude mice. Mice injected with cells from freshly dissociated wild-type or Ezh2-null Tet-ON PyVmT tumors were maintained on water supplemented with doxycycline (200mg/ml, Wisent) for the duration of the experiment (8 weeks). Mice injected with PyVmT cells expressing GFP or Foxc1 were sacrificed after 4 weeks.

4.2 Cell culture

4.2.1 Derivation of primary tumour cell lines

Primary mouse tumor cell lines were established from PyVmT, NDL2.5 or NIC tumors by physical dissociation with a McIlwain Tissue Chopper, followed by incubation with DMEM supplemented with 2mg/ml each of collagenase B/ Dispase II (Roche) for 1 hour in at 37C. Primary mouse cells were maintained in Complete Media (DMEM, 10% FBS, 5ng/ml EGF, 1ug/ml Hydrocortisone, 5ug/ml Insulin, 35 ug/ml Bovine Pituitary Extract. All components were from Wisent, except the Bovine Pituitary Extract, which was from Hammond Cell Tech). All human cell lines were purchased from ATCC and maintained in DMEM supplemented with 10% FBS. For $Ezh2^{-/-}$NDL2.5 cell lines, Ezh2 was excised with the addition or Adenovirus Cre or Adenovirus LacZ (University of Iowa) at an MOI of 25.

4.2.2 Viral transduction and lentiviral mediated shRNA silencing

Exogenous Foxc1 expression in mouse cells was performed using the blasticidin selectable retroviral vector pMSCV-GFP (Gift from Dr. Peter Siegel). Foxc1 cDNA

(MR208772, OriGene Gene Tech) was cloned into the vector. pMSCV-Foxc1 or pMSCV-GFP was transfected into Phoenix (obtained from the ATCC) cells using Lipofectamine 3000 (Invitrogen). Supernatants were collected 48 and 72 hr post-transfection, passed through a 0.45 μm nitrocellulose filter and applied to target cells with polybrene (5 μg/ml, Sigma). Cells were re-infected the next day and selected with blasticidin for 72 hr (10μg/ml, Invitrogen). Five days after infection, cells were transferred to 10 cm dishes and maintained for experimental purposes. Foxc1 targeted knock-down was performed using the Sigma MISSION pLKO.1 mouse Foxc1 shRNAs (clone ids TRCN0000085452 and TRCN0000085449), LacZ shRNA (MFC07785395) of GFP shRNA. Ezh2 shRNA sequences (**Table 2-1**) were cloned into the pLKO.1 vector. Each shRNA vector was co-transfected into HEK293T cells with the lentivirus packaging plasmids PLP1, PLP2, and PLP-VSVG (Invitrogen) using Lipofectamine 3000 (Invitrogen). Supernatants were collected 48 and 72 hr post- transfection, passed through a 0.45 μm nitrocellulose filter and applied on target cells with polybrene (5μg/ml, Sigma). Cells were re-infected the next day and selected with puromycin for 48 hr (1μg/ml, Sigma). After 48 hr post-infection, cells were transferred to 10 cm dishes and maintained for experimental purposes.

shRNA name	Oligo Sequences
Ezh2 sh(107)	TGCTGTTGACAGTGAGCGCGCAAAGTACTGTAACAGTAATTAG TGAAGCCACAGATGTAATTACTGTTACAGTACTTTGCATGCCT
Ezh2 sh(21)	TGCTGTTGACAGTGAGCGATCTCTGAAACAGCTGCCTTAGTAG TGAAGCCACAGATGTACTAAGGCAGCTGTTTCAGAGAGTGCCT ACTGCCTCGGA

Table 2-1. Table of Ezh2 shRNA sequences

4.2.3 In vitro *proliferation assays*

The CyQUANT proliferation assay (ThermoFischer Scientific) and MTS proliferation assay (Promega) was performed in accordance with the manufacturer's protocols using 2,500 cells per well in 96-well optical-bottom plates (Nunc). Samples were assayed in quadruplicate for each time point and condition.

4.2.4 In vitro *invasion assay*

Media containing chemotactic factors (Complete Media) was plated in the bottom of a 24-well plate (BD Falcon) and Boyden chambers (8µm pore, BD Falcon) pre-coated at 37°C for 1 hour with DMEM containing 5% growth factor-reduced Matrigel (VWR) were placed on top of the complete median in a 24-well plate. A total of $5x10^5$ cells were re-suspended in DMEM in the absence of chemotactic factors and added to the upper level of the Boyden chambers. Plates were incubated at 37°C for 24 hours after which cells were fixed in a solution of 10% neutral-buffered formalin for 20 minutes. Boyden chambers were counterstained using Crystal Violet solution (Sigma) for 20 to 30 minutes and cells that remained on the upper level of the Boyden chambers were manually removed and chambers were dried overnight. Three representative images of each Boyden chamber were taken and positive-pixel area was calculated using the ImageJ software. Experiments were performed in triplicate and the average values are reported (± S.E.M.).

4.2.5 Primary cell dissociation for flow cytometric analysis

Mammary glands or tumours were excised, and finely chopped using the McIlwain Tissue Chopper and dissociated in DMEM (Wisent) containing 320µL Liberase

(160µg/mL, Roche) and 200µL of DNAse (200mg/mL) for 45 minutes at 37°C, with constant agitation. The cell suspensions were incubated for 3 minutes with Lysis Buffer (NH4Cl solution) and two times in PBS with centrifugation at 3500RPM for 5 minutes at room temperature. For flow cytometry analysis cell suspensions were resuspended in PBS and filtered through 100µm mesh and resuspended in 500µL FACS Buffer (PBS with 5% FBS).

4.2.6 Flow cytometry protocol

Dissociated cell samples were incubated with fluorescently-conjugated antibodies listed in **Table 4-2**, for 30 minutes at 4ºC and washed in PBS. Samples were run using the BD FACS CantoII and data from 100,000-250,000 events were collected from samples. Data was analyzed using FloJo Software. For FACS, the BD FACS ARIA was used.

Antibody	Dilution	Catalogue Number	Supplier
CD3- efluor450	1:100	48-0032-82	eBioscience
CD4- efluor780	1:100	47-0042-82	eBioscience
CD8-V500	1:200	560776	BD Pharmingen
CD11c-PeCy5.5	1:100	560584	eBioscience
CD11b- efluor450	1:100	48-0112-80	BD Pharmingen
CD19-APC	1:100	17-0193-80	eBioscience
CD45-PE	1:300	17-0193-80	BD Pharmingen
F4/80- PeCy7	1:100	25-4801-82	eBioscience
Gr1-FITC	1:100	11-5931-82	eBioscience
CD24-Pacific blue	1:300	101814 clone m1/69	BioLegend
CD29-PeCy7	1:300	25-0291-82	eBioscience
CD49b- PeCy7	1:100	25-5971-81	eBioscience
Ter119-PE	1:300	116207	BioLegend
CD31-PE	1:300	102507	BioLegend

Table 4-2. Table of fluorescent conjugated antibodies used for flow cytometry experiments

4.2.7 Enzyme-linked immunosorbent assay (ELISA)

The Enzyme-linked immunosorbent assay (ELISA) was performed using the eBioscience mouse IFNg kit (MIF00). The protocol was followed as described in the technical manuals from the company, with a few exceptions: protein lysates from mammary glands were used at 50μg total protein concentration and the sample incubation was performed overnight at 4ºC.

4.3 DNA analyses

4.3.1 DNA extraction

Genotyping was performed using tail pieces digested in 500μl of tail buffer (10mM Tris, 100mM NaCl, 10mM EDTA, 0.5% SDS) containing 5 μl of proteinase K (20mg/ml) and incubated at 55°C overnight. Tail DNA was extracted by adding 200 μl of 5M NaCl, and centrifuged at 13,000 RPM for 5 minutes. Supernatant was transferred to a new tube and precipitates by adding two volumes of 70% EtOH and centrifuged at 13,000 RPM for 10 minutes at 4°C. Supernatant was discarded and the DNA pellet was resuspended in 500μl of TE buffer (10mM Tris, 0.5mM EDTA, pH7.8).

4.3.2 PCR genotyping

Genotyping was performed using 1μl of tail DNA in a 25μl volume reaction containing NEB Easy taq DNA polymerase, 10x buffer, 5mM dNTPs and 10μM of the following primers for the following Thermocycler programs shown on **Table 4-3**.

Gene	Primer Sequence (5' to 3')	Thermocycler Program
Cre	**FWD**-GCTTCTGTCCGTTTGCCG **REV**-ACTGTGTCCAGACCAGGC	(1) 94°C - 2 minutes, (2) 94°C - 30 seconds, (3) 58°C - 45 seconds, (4) 72°C - 1 minute, (5) repeat steps 2-4 for an additional 29 cycles, (6) 72°C - 4 minutes, (7) 4°C Hold.
GFP	**FWD**-AAGTTCATCTGCACCACCG **REV**-TGCTCAGGTAGTGGTTGTCG	
Neu	**FWD**-TTCCGGAACCCACATCAGGCC **REV**-GTTTCCTGCAGCAGCCTACGC	
rtTA	**FWD**-ACCGTACTCGTCAATTCCAAGGG **REV**-TGCCGCCATTATTACGACAAGC	
PyVmT	**FWD**-GGAAGCAAGTACTTCACAAGGG **REV**-GGAAAGTCACTAGGAGCAGGG	
Ezh2	**FWD**- CCCATGTTTAAGGGCATAGTGACATG **REV**- TGCAGGTCAGTCAGCAACTTC AG **CEN**- TCGAGGGACCTAATAACTCGTATAGCA	(1) 94° C-3 min (2) 94° C-30 s (3) 62° C-30 s (4) 72° C-30 s (5) repeat steps 2-4 for an additional 35 cycles (6) 72°C - 7 minutes, (7) 4°C Hold.

Table 4-3. Table of PCR genotyping primer sequences

4.3.3 Chromatin immunoprecipitation (ChIP)

For chromatin immunoprecipitation studies, 5µg of anti-H3K27me^3 or rabbit anti-IgG antibody, or 3µg of anti-Foxc1 or rabbit anti-IgG antibody was immobilized overnight at 4°C on 20µl of Magna ChIP Protein A+G magnetic beads (Millipore) diluted in 250µL of PBS + 0.5% BSA and then washed 3 times with PBS + 0.5% BSA. For cell lines, cells in 15 cm plates were fixed with a 1% final concentration of formaldehyde for 10 min at room temperature and then lysed and sonicated. For tumor tissue, 0.5g of tumor was briefly thawed and then homogenized using a tissue homogenizer in 1% final concentration of formaldehyde and let to fix for 10 minutes after which the samples were lysed and sonicated. Equal amounts of chromatin from different treatment conditions or

genotypes were diluted in 2.5X ChIP dilution buffer (EDTA 2 mM, NaCl 100 mM, Tris 20 mM, Triton 0.5%) + 100 µL of PBS+0.5% BSA and added to the antibody-bound beads and left to rotate overnight at 4°C. Next, beads were washed 3 times for 3 min at 4°C with 1 mL LiCl buffer (Tris 100mM, LiCl 500 mM, Na-desoxycholate 1%) then once with 1 mL TE buffer. DNA was eluted with 150 µL of elution buffer (0.1M NaHCO3, 0.1% SDS) overnight at 65°C. Chromatin-immunoprecipitated DNA was purified using a QIAquick PCR purification kit (Qiagen) and eluted in 35µL of elution buffer. FoxC1 primers were designed based on ChIP-seq data from a previous study (346). Primers used in this study are listed in **Table 4-4**.

Name	**Sequences**	**ChIP Ab**
Grb10	F- GGGTTCTCGGTTATAGTGTGGGGACTTC R- GGAACTAAGCTGATTCATGTGCCTCCAG	H3K27me^3, Foxc1
Rgma set 1	F- GATGGTATTTCGGTGCCTCG R- CTGTCCGCGCTTACCTTG	H3K27me^3
Chl1 set 1	F- GAGGGAGGTGGAAGGAAATC R- AAATCCAGCCTTAGCCACCT	H3K27me^3
Slfn5 set 1	F- GCAGACCAAAGAAGCAGGTC R- ATTTCCCAGGCACGACAAAC	H3K27me^3
Col15a1 set 1	F- CACAAGGCAAGCGATGAGAA R- CCCTCACTGTTCACTGGCTA	H3K27me^3
Foxc1	F- GCCCGAACTCTCTAGCTCTT R- GATGGTATTTCGGTGCCTCG	H3K27me^3
HoxA11 set 1	F- CCCTTCTCGGCGTTCTTGTC R- CTATAGCACGGTGGGCAGGAAC	H3K27me^3
HoxA11 set 2	F- CCAGGTTCCAACACAGCCATTC R- CCCATGTGACTCTTTCTAGTCTCCCTTG	H3K27me^3
Rgma set 2	F- TCCACAGAGAAGCGTTTGTTC R- ACAGACCGGGGATTTAAGCT	Foxc1
Chl1 set 2	F- TGCTCTTGCTGGTGGTATTCT R- AGAGAAGATCTTTCCTCTCAGTACA	Foxc1
Slfn5 set 2	F- TGTCTGTCGGTGAATGCTCT R- CACCATTGACTGAGGCAGAA	Foxc1
Col15a1 set 2	F- GGAGATGGGAGTTGAAGAAGG R- CCCAACGGTACAGGAAACAC	Foxc1

Table 4-4. Table of candidate ChIP primer sequences

4.3.4 ChIP-Seq analysis

ChIP-seq was performed at the McGill University and Genome Quebec Innovation Centre. For ChIP-sequencing, five individual ChIPs for each genotype (IgG and H3K27me^3) were pooled following the same protocol described above. A total of 50 ng of DNA was provided per each ChIP-seq to the Génome Québec Innovation Centre for DNA library preparation using the TruSeq DNA sample preparation kit according to Illumina recommendations. The ChIP DNA libraries were sequenced as single 50 bp reads (tags) using the Ilumina Hiseq 2000 sequencer (Illumina). Raw reads were trimmed for length (n>=32), quality (phred score >= 30) and adaptor sequence using fastx v0.0.13.1. Trimmed reads were (pools of 5 different tumors per genotype) then aligned to the mouse reference genome mm10 using BWA v0.5.9 (347). Broad peaks were called using MACS v1.4.1 software (mfold=10,30; bandwith=300; pvalue cutoff=1E-5) using sequenced libraries of matched IgG DNA as control (348). The fragment length used was the one predicted by the program. Peak list intersections were done using BEDTools v2.12.0 (349). Binding peaks were considered overlapping if at least 1 base of the peaks overlapped. Annotations were obtained using HOMER v3.1 (350).

4.4 RNA analyses

4.4.1 RNA isolation, cDNA synthesis and qRT-PCR

Total RNA was extracted from flash frozen mammary tumor or cell lines using an RNeasy Midi Kit (Qiagen). cDNA was prepared by reverse transcribing isolated RNA using M-Mulv Reverse Transcriptase, Oligo-dT(23VN) and murine RNase inhibitor (New England Biolabs). Real time quantitative PCR was performed using SYBR Green

Master Mix (Roche) and Light Cycler 480 instrument. Samples were run in duplicate and normalized to the internal control, *β-Actin*. All primer sequences are listed **Table 4-5** and **Table 4-6**.

Gene	Sequences
RGMA	F- CCTCAGGACTTTCACCGACC R- CGTTCTTAGAGCCATCCACGAA
SLFN5	F- GAGTGTGTTGTAGATGCAGGAA R- ACTGCTCGCAGGATGATTTCA
COL15A1	F- CTGCCCTCGTCCGTATCCT R- CTGATGGCGAAGTCCCTGA
CHL1	F- ATGGAGCCGCTTTTACTTGGA R- GGCAACTTGGACTTTTGACTGT
B ACTIN	F- AGAGCTACGAGCTGCCTGAC R- AGCACTGTGTTGGCGTACAG
FOXC1	F- CGCAGCCCAAGGACATGGTG R- GATGCCGTTCAGGGTGATCTTC

Table 4-5. Human qPCR primer sequence

Gene	Sequences	Gene	Sequences	Gene	Sequences
Slc9a9	F- GGTTTACGTCAGGGAAGGATG R- AGAAGCGGAATCGGTGATTTTT	*Foxa3*	F- CTACATGACCTTGAACCCACTC R- GGGCTACATACCCGGAAGC	*Foxl2*	F- ACAACACCGGAGAAACCAGAC R- CGTAGAACGGGAACTTGGCTA
Col4a6	F- ATCGGATACTCCTTCCTCATGC R- CCAGGGGAGACTAGGGACTG	*Foxa2*	F- CCCTACGCCAACATGAACTCG R- GTTCTGCCGGTAGAAAGGGA	*Foxl2*	F- GAGCAGAGGGTCACACTGAAC R- CTTCCTGCGCCGATAATTGC
Col15a1	F- CCCAGGGAAGAATGGAGAAGT R- CCAGAGCCTTCAATCTCAAATCC	*Foxa1*	F- ATGAGAGCAACGACTGGAACA R- TCATGGAGTTCATAGAGCCCA	*B Actin*	F- TCCATCATGAAGTGTGACGT R- GAGCAATGATCTTGATCTTCAT
Dbc1	F- AGCGCCCTATCCCATGTATCA R- AGCTTGTAGCCCTTATTGCAG	*Foxc1*	F- CGCAGCCCAAGGACATGGTG R- GATGCCGTTCAGGGTGATCTTC	*Ltbp4*	F- CTGGGTGTCGCTATTGGTG R- GTTGTGACAGATCAAGGGACAT
Chl1	F- TCCGCCAGGAAACCTTCAC R- ACAATGTACTCGCTGATTTTGCT	*Foxs1*	F- GTTATGGCGGATGCTGTTTTG R- CTATCCAGAGTTCACCGGGTC	*Pde3b*	F- AAAGCGCAGCCGGTTACTAT R- CACCACTGCTTCAAGTCCCAG
Chn1	F- GCAGCCAGGAACGTACACTTT R- ATCAGTCACCAGATCGTGGAT	*Foxb1*	F- TTCCTACAGCGACCAAAAGCC R- CCGAGGGATCTTGATGAAACAG	*Pcdhb16*	F- GGGAACTGAGGCGCTATTCTG R- TTAGCAAGCATGGCTCTGTATG
Slfn5	F- AAGGGAGGAAATGGATACCACA R- CTCAACCCTGACCACTCCG	*Foxb2*	F- TTCCTACAGCGACCAAAAGCC R- CCGAGGGATCTTGATGAAACAG	*Rgma*	F- AGAGGACCTTATGAGCCAGCA R- GCAGTGAGTGTAGTTGGGGG
Dock8	F- GTGGAAATACGTCCAGTACCTG R- CGATGGGTCAATCGAGGGTG	*Foxc2*	F- GCGTAGCTCGATAGGGCAG R- AACCCAACAGCAAACTTTCCC	*Stat1*	F- TCACAGTGGTTCGAGCTTCAG R- GCAAACGAGACATCATAGGCA
Slc35f2	F- CTGGGTACGGTGGACAGTATC R- GCATCAACGTGTAAACCAGGA	*Ifit1*	F- CTGAGATGTCACTTCACATGGAA R- GTGCATCCCCAATGGGTTCT	*Usp18*	F- TTGGGCTCCTGAGGAAACC R- CGATGTTGTGTAAACCAACCAGA
Ezh2	F- AGTGACTTGGATTTTCCAGCAC R- AATTCTGTTGTAAGGGCGACC	*Eed*	F- GCACTCAGATCCGTATGGAGG R- GTTGTTTCCCAAGACACTTCTCT	*Oas2*	F- TTGAAGAGGAATACATGCGGAAG R- GGGTCTGCATTACTGGCACTT

Table 4-6. Mouse qPCR primer sequences

4.4.2 Microarray analysis and acquisition

Total RNA was extracted from 7 wild-type and 5 $Ezh2^{-/-}$ Tet-ON PyVmT tumors at tumor burden endpoint, or 2 NIC cell lines treated with GSK-126 or DMSO for 72 hours, and quantified using a NanoDrop Spectrophotometer ND-1000 (NanoDrop Technologies, Inc.). RNA integrity was assessed using a Bioanalyzer 2100 (Aglient Technologies). Sense-strand cDNA was synthesized from 100ng of total RNA and fragmentation and labelling were performed to produce ssDNA with the GeneChip WT Terminal Labeling Kit according to manufacturer's instructions (Affymetrix). After fragmentation and labeling, 3.5µg of labeled DNA was hybridized on GeneChip Mouse Gene 2.0 ST arrays (Affymetrix) and incubated at 45°C in the Genechip Hybridization oven 640 (Affymetrix) for 17 hours at 60 rpm. GeneChips were then washed in a GeneChips Fluidics Station 450 (Affymetrix) using Hybridization Wash and Stain kit according to the manufacturer's instructions (Affymetrix) and scanned using a GeneChip Scanner 3000 (Affymetrix). All procedures were performed at the Genome Quebec Innovation Center, McGill University. Raw data were first processed to perform gene-level normalization and quality control using Affymetrix Expression Console software (Affymetrix). Processed data were next subjected to Gene Level Differential Expression Analysis using Affymetrix Transcriptome Analysis Console software. Differentially expressed genes with ANOVA p-value <0.05 were considered in further analyses.

Ingenuity Pathways Analysis (IPA) was performed on differentially expressed genes between $Ezh2^{-/-}$ and $Ezh2^{+/+}$ tumors using IPA software (Ingenuity Systems). Significance of the overrepresented canonical pathways as well as functions and diseases were determined using Fischer's exact test to calculate p-values. GSEA software was used to identify the enrichment of genes in Ezh2 null tumors within pre-defined gene datasets from the Molecular Signature Database (MSigDB). Gene datasets from the c2.cp.reactome.v5.1 were analyzed using gene sets containing 15 to 2000 genes and the false discovery rate was estimated using 1000 permutations of the data sets. Gene Ontology and JASPAR transcription profile analyses were performed

using the EnrichR online tool (www.enrichr.com) (351). Hierarchical clustering of the gene expression profiles of $Ezh2^{+/+}$ and $Ezh2^{-/-}$ Tet-ON PyVmt tumors (n=5) was generated using the HierarchicalClustering module and Euclidean distance measure within the GenePattern software (http://software.broadinstitute.org). The tumor expression dataset was first filtered using the parameters p-value < 0.05 and fold change > 1.5 within Affymetrix TAC software. Probes with no mapped gene or probes mapped to the same gene with bi-directional expression were removed.

4.5 Protein analysis

4.5.1 Immunoblot

Freshly excised mouse tumor tissue was flash frozen in liquid nitrogen, crushed with a mortar and pestle and allowed to thaw briefly before lysing in ice-cold RIPA buffer (50mM Tris-HCl pH 7.4, 150mM sodium Chloride, 1% NP-40, 1% sodium deoxycholate, 0.1% SDS, 2mM EDTA, 0.5mM AEBSF, 25mM β-glycerophosphate, 1 mM sodium orthovanadate, and 10 mM sodium fluoride). Cultured cells were also lysed in RIPA buffer. Protein concentration was determined by Bradford Assay (Bio-Rad) and 30µg of total protein was analyzed by immunoblot using the Odyssey CL-X imaging system (LI-COR Biosciences). All antibodies used are listed in the **Table 4-7**.

Antibody	**Catalog #**	**Supplier**	**Use**	**Application**
Ezh2 (D2C9) XP	5246	Cell Signaling	H,M	IHC, IF, IB, ChIP
H3K27me3 (C36B11)	9733	Cell Signaling	H,M	IHC, IF, IB
PyVmT (762)	NA	Gift from Dr. Steven Dilworth	M	IHC, IF, IB
PanCK	760-2135	Ventana	H,M	IF
FoxC1	NB100-1268	Novus Biologicals	M	IHC, IF, IB, ChIP
FOXC1	HPA040670	Sigma	H	IHC, IF

Rabbit IgG	2729	Cell Signaling	NA	ChIP
α/β tubulin	2148	Cell Signaling	H,M	IB
Vinculin	4650	Cell Signaling	H,M	IB
BrdU	5292	Cell Signaling	H,M	IHC
HER2 (4B5)	790-2991	Ventana	H	IHC
IRDye 800 CW Donkey anti-rabbit	926-32213	LI-COR Biosciences	NA	IB (secondary)
IRDye 680 CW Donkey anti-mouse	926-68072	LI-COR Biosciences	NA	IB (secondary)
ErbB2	A0485	DAKO	H,M	IB, IF
Jak1	3344	Cell Signaling	H,M	IB
pJak (Tyr1007/8)		Cell Signaling	H,M	IB
Stat1	14994	Cell Signaling	H,M	IB
pStat1 (Tyr701)	8062	Cell Signaling	H,M	IB
IRF3	11904	Cell Signaling	H,M	IB
pIRF3(Ser396)	4947	Cell Signaling	H,M	IB
MDA5	5321	Cell Signaling	H,M	IB
MAVS	3993	Cell Signaling	H,M	IF
Rig-1	3743	Cell Signaling	H,M	IB
Hsp60	12165	Cell Signaling	H,M	IF
ERK1/2	4695	Cell Signaling	H,M	IB
Pan Akt	4685	Cell Signaling	H,M	IB
pAkt(Ser 473)	4070	Cell Signaling	H,M	IB
pERK1/2 (T202/Y204)	4370	Cell Signaling	H,M	IB

IHC= immunohistochemistry, IF= immunofluorescence, IB= immunoblot, ChIP= chromatin immunoprecipitation H= Human, M= Mouse, NA= not applicable

Table 4-7. Table of antibodies used in all immunohistochemistry, immunoblot, ChIP and immunofluorescence experiments

4.5.2 Immunohistochemistry and immunofluorescence

Tumors or mammary glands were fixed in 10% neutral buffered formalin overnight and embedded in paraffin for sectioning. Sections were cut at 4*μ*m, de-paraffinized in

xylene and antigen retrieval was performed with 10mM Citrate Buffer (pH 6) using a pressure cooker. Sections were then blocked with 10% Power Block (BioGenex) in PBS for 10 minutes at room temperature. Sections were incubated with primary antibody at 4°C overnight. For immunofluorescence, sections were incubated with secondary antibodies (Invitrogen) for one hour at room temperature, followed by DAPI for 15 minutes, washed three times in PBS and mounted in ImmuMount (Thermo Scientific). Immunostained samples were imaged using a Zeiss LSM800 confocal microscope and analyzed with ZEN software.

For immunohistochemistry (IHC), sections were de-paraffinized and blocked as above, endogenous peroxidase activity was quenched by incubation in 3% hydrogen peroxide for 20 minutes. Sections were incubated with primary antibody overnight at 4°C, washed three times in PBS, and incubated with biotinylated secondary antibodies (Vector Elite). After three further washes in PBS, IHC staining was visualized using the Vectastain ABC kit (Vector Laboratories) according to the manufacturer's instructions. Sections were then counterstained with hematoxylin, dehydrated, and mounted with Clearmount (Invitrogen). Images were acquired using an Aperio-XT slide scanner (Leica Biosystems). All antibodies used for imaging are listed in Table 2-7**.**

4.6 Human samples

4.6.1 Samples from Luminal B patients

Samples were collected from patients undergoing breast surgeries at the McGill University Health Centre (MUHC) between 1999 and 2015 who provided written, informed consent (MUHC Research Ethics Board protocols SDR-99-780 and SDR-00-966). Transcriptional profiles for the human patients from which histology was used, was previously published (352). PAM50 classification of samples was performed using the *genefu* R package (version1.16.0) (15) to identify Luminal B patients, and formalin fixed and paraffin-embedded blocks (FFPE) for the appropriate patients was drawn from the archive. Sections were stained with the immunofluorescence protocol earlier described. For quantification of FOXC1 staining, images of 8 different fields for each sample were acquired with a 20x objective with a LSM 800 confocal microscopy (Leica).

'Image J for Microscopy Software' package for ImageJ software was the used to quantify the total intensity levels of nuclear FOXC1 per sample, as previously reported (353).

4.6.2 Patient derived xenografts

A single fragment of fresh or frozen tumor (~8 mm^3), or 1 × 10^6 cells in Matrigel, into cleared inguinal mammary fat pads of 3–4-week-old female NOD-SCID mice. Interscapular estrogen pellets were also subcutaneously implanted in mice transplanted with HCI003 fragments. HCI003 was established as cited previously (266).

4.6.3 Tissue Microarray from different human breast cancer subtypes

A total of 18 tissue microarrays (TMA) containing 2 cores of each tumor sample were constructed from the formalin-fixed, paraffin-embedded tumor material from each patient in the cohort as previously reported(354). TMAs were produced using the MTA-1 Manual Tissue Arrayer (Beecher Instruments, Woodland, CA, USA).

4.6.4 Human data from publicly available data sets

Transcriptional data for human data sets from The Cancer Genome Atlas (TCGA) was accessed from the UCSC Xena web interface (https://xenabrowser.net/) (355). Kaplan Meier survival graphs were generated from data available on KM Plotter (356). Probes for each gene are listed in **Table 2-8**.

Gene	**Probe ID #**
FOXC1	213260_at
RGMA	223468_s_at
DBC1	205818_at
SLC9A9	227791_at
PDE3B	222317_at
CHL1	204591_at
DOCK8	232843_s_at
SLFN5	238430_x_at

COL15A1	203477_at
CHN1	212624_s_at
SLC35F2	218826_at
COL4A6	213992_at
PCDHB16	232099_at
LTBP4	204442_x_at

Table 2-8. Probes used for KM plotter analysis

4.7 Statistics

Data was exported to Prism software (Graphpad, San Diego, CA), in which graphical figures were made and statistical analysis was performed. Unless indicated otherwise, a two-tailed unpaired Student's t-test was used. The error bars shown in all figures are indicative of S.E.M, unless otherwise noted.

Statistical significance of tumour onset curves was determined using a Rank log (Mandel Cox) test.

For analysis of microarray data, GSEA was performed using the Kolmogorov-Smirnow statistic to generate a nominal p value.

For the TMA, the chi-square test was applied when the variables were dichotomous, the Mann–Whitney test was applied when one variable was dichotomous and the other continuous and the Spearman Rank correlation was applied when both variables were continuous. Statview version 5.0 was used for the analysis (Abacus Systems, Berkeley, CA).

5 References

1. Donepudi MS, Kondapalli K, Amos SJ, Venkanteshan P (2014) Breast cancer statistics and markers. *J Cancer Res Ther* 10(3):506–511.

2. Tarver T (2012) Cancer Facts & Figures 2012. American Cancer Society (ACS). *Journal of Consumer Health On the Internet* 16(3):366–367.

3. Nadji M, Gomez-Fernandez C, Ganjei-Azar P, Morales AR (2005) Immunohistochemistry of Estrogen and Progesterone Receptors Reconsidered. *American Journal of Clinical Pathology* 123(1):21–27.

4. Lin NU, et al. (2012) Clinicopathologic features, patterns of recurrence, and survival among women with triple-negative breast cancer in the National Comprehensive Cancer Network. *Cancer* 118(22):5463–5472.

5. Saphner T, Tormey DC, Gray R (1996) Annual hazard rates of recurrence for breast cancer after primary therapy. *Journal of Clinical Oncology* 14(10):2738–2746.

6. Anderson WF, Chatterjee N, Ershler WB, Brawley OW (2002) Estrogen Receptor Breast Cancer Phenotypes in the Surveillance, Epidemiology, and End Results Database. *Breast Cancer Research and Treatment* 76(1):27–36.

7. Hare SH, Harvey AJ (2017) mTOR function and therapeutic targeting in breast cancer. *Am J Cancer Res* 7(3):383–404.

8. Finn RS, Aleshin A, Slamon DJ (2016) Targeting the cyclin-dependent kinases (CDK) 4/6 in estrogen receptor-positive breast cancers. *Breast Cancer Research* 18(1):17.

9. Kaplan HG, Malmgren JA (2008) Impact of Triple Negative Phenotype on Breast Cancer Prognosis. *The Breast Journal* 14(5):456–463.

10. Slamon D, et al. (1987) Human breast cancer: correlation of relapse and survival with amplification of the HER-2/neu oncogene. *Science* 235(4785):177–182.

11. Sjögren S, Inganäs M, Lindgren A, Holmberg L, Bergh J (1998) Prognostic and predictive value of c-erbB-2 overexpression in primary breast cancer, alone and in combination with other prognostic markers. *Journal of Clinical Oncology* 16(2):462–469.

12. Stenzinger A, et al. (2012) Quantitative Analysis of Diagnostic Guidelines for HER2-Status Assessment. *The Journal of Molecular Diagnostics* 14(3):199–205.

13. Perou CM, et al. (2000) Molecular portraits of human breast tumours. *Nature* 406(6797):747–752.

14. Sørlie T, et al. (2003) Repeated observation of breast tumor subtypes in

independent gene expression data sets. *Proceedings of the National Academy of Sciences* 100(14):8418–8423.

15. Prat A, Perou CM (2010) Deconstructing the molecular portraits of breast cancer. *Molecular Oncology* 5(1):5–23.

16. Wu Q, et al. (2017) Breast cancer subtypes predict the preferential site of distant metastases: a SEER based study. *Oncotarget*. doi:10.18632/oncotarget.15856.

17. Smid M, et al. (2008) Subtypes of breast cancer show preferential site of relapse. *Cancer Research* 68(9):3108–3114.

18. Parker JS, et al. (2009) Supervised risk predictor of breast cancer based on intrinsic subtypes. *J Clin Oncol* 27(8):1160–1167.

19. Visvader JE, Stingl J (2014) Mammary stem cells and the differentiation hierarchy: current status and perspectives. *Genes & Development* 28(11):1143–1158.

20. Polyak K (2007) Breast cancer: origins and evolution. *Journal of Clinical Investigation* 117(11):3155–3163.

21. Lim E, et al. (2009) Aberrant luminal progenitors as the candidate target population for basal tumor development in BRCA1 mutation carriers. *Nature Medicine* 15(8):907–913.

22. Shehata M, et al. (2012) Phenotypic and functional characterisation of the luminal cell hierarchy of the mammary gland. *Breast Cancer Research* 14(5):747.

23. Prat A, et al. (2013) Prognostic significance of progesterone receptor-positive tumor cells within immunohistochemically defined luminal A breast cancer. *J Clin Oncol* 31(2):203–209.

24. Cancer Genome Atlas Network (2012) Comprehensive molecular portraits of human breast tumours. *Nature* 490(7418):61–70.

25. Nielsen TO, et al. (2004) Immunohistochemical and clinical characterization of the basal-like subtype of invasive breast carcinoma. *Clin Cancer Res* 10(16):5367–5374.

26. Rakha EA, et al. (2006) Basal phenotype identifies a poor prognostic subgroup of breast cancer of clinical importance. *European Journal of Cancer* 42(18):3149–3156.

27. Carter P, et al. (1992) Humanization of an anti-p185HER2 antibody for human cancer therapy. *Proceedings of the National Academy of Sciences* 89(10):4285–

4289.

28. Nahta R, Esteva FJ (2006) Herceptin: mechanisms of action and resistance. *Cancer Letters* 232(2):123–138.

29. Slamon DJ, et al. (2001) Use of Chemotherapy plus a Monoclonal Antibody against HER2 for Metastatic Breast Cancer That Overexpresses HER2. *New England Journal of Medicine* 344(11):783–792.

30. Eiermann W, on behalf of the International Herceptin Study Group (2001) Trastuzumab combined with chemotherapy for the treatment of HER2-positive metastatic breast cancer: pivotal trial data. *Annals of Oncology* 12(suppl 1):S57–S62.

31. Gianni L, et al. (2012) Efficacy and safety of neoadjuvant pertuzumab and trastuzumab in women with locally advanced, inflammatory, or early HER2-positive breast cancer (NeoSphere): a randomised multicentre, open-label, phase 2 trial. *Lancet Oncol* 13(1):25–32.

32. Piccart-Gebhart MJ, et al. (2005) Trastuzumab after Adjuvant Chemotherapy in HER2-Positive Breast Cancer. *New England Journal of Medicine* 353(16):1659–1672.

33. Hudis CA (2007) Trastuzumab — Mechanism of Action and Use in Clinical Practice. *New England Journal of Medicine* 357(1):39–51.

34. Yakes FM, et al. (2002) Herceptin-induced inhibition of phosphatidylinositol-3 kinase and Akt Is required for antibody-mediated effects on p27, cyclin D1, and antitumor action. *Cancer Research* 62(14):4132–4141.

35. Junttila TT, et al. (2009) Ligand-Independent HER2/HER3/PI3K Complex Is Disrupted by Trastuzumab and Is Effectively Inhibited by the PI3K Inhibitor GDC-0941. *Cancer Cell* 15(5):429–440.

36. Lane HA, et al. (2000) ErbB2 potentiates breast tumor proliferation through modulation of p27(Kip1)-Cdk2 complex formation: receptor overexpression does not determine growth dependency. *Molecular and Cellular Biology* 20(9):3210–3223.

37. Mohsin SK, et al. (2005) Neoadjuvant Trastuzumab Induces Apoptosis in Primary Breast Cancers. *Journal of Clinical Oncology* 23(11):2460–2468.

38. Izumi Y, Xu L, di Tomaso E, Fukumura D, Jain RK (2002) Tumour biology: Herceptin acts as an anti-angiogenic cocktail. *Nature* 416(6878):279–280.

39. Franklin MC, et al. (2004) Insights into ErbB signaling from the structure of the

ErbB2-pertuzumab complex. *Cancer Cell* 5(4):317–328.

40. Ellis PA, et al. (2011) MARIANNE: A phase III, randomized study of trastuzumab-DM1 (T-DM1) with or without pertuzumab (P) compared with trastuzumab (H) plus taxane for first-line treatment of HER2-positive, progressive, or recurrent locally advanced or metastatic breast cancer (MBC). *Journal of Clinical Oncology* 29(15_suppl):TPS102–TPS102.

41. Clynes RA, Towers TL, Presta LG, Ravetch JV (2000) Inhibitory Fc receptors modulate in vivo cytotoxicity against tumor targets. *Nature Medicine* 6(4):443–446.

42. Petricevic B, et al. (2013) Trastuzumab mediates antibody-dependent cell-mediated cytotoxicity and phagocytosis to the same extent in both adjuvant and metastatic HER2/neu breast cancer patients. *J Transl Med* 11(1):307.

43. Spiridon CI (2004) A Comparison of the in Vitro and in Vivo Activities of IgG and F(ab')2 Fragments of a Mixture of Three Monoclonal Anti-Her-2 Antibodies. *Clin Cancer Res* 10(10):3542–3551.

44. Park S, et al. (2010) The therapeutic effect of anti-HER2/neu antibody depends on both innate and adaptive immunity. *Cancer Cell* 18(2):160–170.

45. Mortenson ED, Fu Y-X (2013) Adaptive Immune Responses and HER2/neu Positive Breast Cancer. *Curr Pathobiol Rep* 1(1):37–42.

46. Romond EH, et al. (2005) Trastuzumab plus Adjuvant Chemotherapy for Operable HER2-Positive Breast Cancer. *New England Journal of Medicine* 353(16):1673–1684.

47. Slamon D, et al. (2014) Phase III Randomized Trial Comparing Doxorubicin and Cyclophosphamide Followed by Docetaxel (AC→T) with Doxorubicin and Cyclophosphamide Followed by Docetaxel and Trastuzumab (AC→TH) with Docetaxel, Carboplatin and Trastuzumab (TCH) in Her2neu Positive Early Breast Cancer Patients: BCIRG 006 Study. *Cancer Research* 69(24 Supplement):62–62.

48. Joensuu H, et al. (2006) Adjuvant Docetaxel or Vinorelbine with or without Trastuzumab for Breast Cancer. *New England Journal of Medicine* 354(8):809–820.

49. Zhang S, et al. (2011) Combating trastuzumab resistance by targeting SRC, a common node downstream of multiple resistance pathways. *Nature Medicine* 17(4):461–469.

50. Shattuck DL, Miller JK, Carraway KL, Sweeney C (2008) Met receptor

contributes to trastuzumab resistance of Her2-overexpressing breast cancer cells. *Cancer Research* 68(5):1471–1477.

51. Nahta R (2005) Insulin-like Growth Factor-I Receptor/Human Epidermal Growth Factor Receptor 2 Heterodimerization Contributes to Trastuzumab Resistance of Breast Cancer Cells. *Cancer Research* 65(23):11118–11128.

52. English DP, Roque DM, Santin AD (2013) HER2 expression beyond breast cancer: therapeutic implications for gynecologic malignancies. *Mol Diagn Ther* 17(2):85–99.

53. Garrett JT, Arteaga CL (2014) Resistance to HER2-directed antibodies and tyrosine kinase inhibitors. *Cancer Biology & Therapy* 11(9):793–800.

54. Gallardo A, et al. (2012) Increased signalling of EGFR and IGF1R, and deregulation of PTEN/PI3K/Akt pathway are related with trastuzumab resistance in HER2 breast carcinomas. *Br J Cancer* 106(8):1367–1373.

55. Swain SM, et al. (2013) Pertuzumab, trastuzumab, and docetaxel for HER2-positive metastatic breast cancer (CLEOPATRA study): overall survival results from a randomised, double-blind, placebo-controlled, phase 3 study. *Lancet Oncol* 14(6):461–471.

56. Baselga J, et al. (2012) Pertuzumab plus Trastuzumab plus Docetaxel for Metastatic Breast Cancer. *New England Journal of Medicine* 366(2):109–119.

57. Ma J, et al. (2010) Mammalian target of rapamycin regulates murine and human cell differentiation through STAT3/p63/Jagged/Notch cascade. *J Clin Invest* 120(1):103–114.

58. André F, et al. (2014) Everolimus for women with trastuzumab-resistant, HER2-positive, advanced breast cancer (BOLERO-3): a randomised, double-blind, placebo-controlled phase 3 trial. *Lancet Oncol* 15(6):580–591.

59. Saal LH, et al. (2005) PIK3CA mutations correlate with hormone receptors, node metastasis, and ERBB2, and are mutually exclusive with PTEN loss in human breast carcinoma. *Cancer Research* 65(7):2554–2559.

60. Pandolfi PP (2004) Breast Cancer — Loss of PTEN Predicts Resistance to Treatment. *New England Journal of Medicine* 351(22):2337–2338.

61. Saura C, et al. (2014) Phase Ib study of Buparlisib plus Trastuzumab in patients with HER2-positive advanced or metastatic breast cancer that has progressed on Trastuzumab-based therapy. *Clin Cancer Res* 20(7):1935–1945.

62. Weigelt B, Peterse JL, van't Veer LJ (2005) Breast cancer metastasis: markers

and models. *Nature Reviews Cancer* 5(8):591–602.

63. Fidler IJ (2003) *The pathogenesis of cancer metastasis: the “seed and soil” hypothesis revisited.* (Nature Publishing Group).

64. Radisky DC (2005) Epithelial-mesenchymal transition. *Journal of Cell Science* 118(19):4325–4326.

65. Thiery JP, Acloque H, Huang RYJ, Nieto MA (2009) Epithelial-Mesenchymal Transitions in Development and Disease. *Cell* 139(5):871–890.

66. Friedl P, Wolf K (2003) Tumour-cell invasion and migration: diversity and escape mechanisms. *Nature Reviews Cancer* 3(5):362–374.

67. Steeg PS (2016) Targeting metastasis. *Nature Reviews Cancer* 16(4):201–218.

68. Chambers AF, Werb Z (2015) Invasion and metastasis--recent advances and future challenges., pp 361–368.

69. Bittner JJ (1936) SOME POSSIBLE EFFECTS OF NURSING ON THE MAMMARY GLAND TUMOR INCIDENCE IN MICE. *Science* 84(2172):162–162.

70. Guy CT, Cardiff RD, Muller WJ (1992) Induction of mammary tumors by expression of polyomavirus middle T oncogene: a transgenic mouse model for metastatic disease. *Molecular and Cellular Biology* 12(3):954–961.

71. Hoess R, Abremski K, Sternberg N (1984) The Nature of the Interaction of the P1 Recombinase Cre with the Recombining Site loxP. *Cold Spring Harbor Symposia on Quantitative Biology* 49(0):761–768.

72. Cardiff RD, Wellings SR (1999) The Comparative Pathology of Human and Mouse Mammary Glands. *Journal of Mammary Gland Biology and Neoplasia* 4(1):105–122.

73. Ursini-Siegel J, Schade B, Cardiff RD, Muller WJ (2007) Insights from transgenic mouse models of ERBB2-induced breast cancer. *Nature Reviews Cancer* 7(5):389–397.

74. Muller WJ, Sinn E, Pattengale PK, Wallace R, Leder P (1988) Single-step induction of mammary adenocarcinoma in transgenic mice bearing the activated c-neu oncogene. *Cell* 54(1):105–115.

75. Siegel PM, Ryan ED, Cardiff RD, Muller WJ (1999) Elevated expression of activated forms of Neu/ErbB-2 and ErbB-3 are involved in the induction of mammary tumors in transgenic mice: implications for human breast cancer. *The EMBO Journal* 18(8):2149–2164.

76. Siegel PM, Muller WJ (1996) Mutations affecting conserved cysteine residues within the extracellular domain of Neu promote receptor dimerization and activation. *Proceedings of the National Academy of Sciences* 93(17):8878–8883.

77. Ursini-Siegel J, et al. (2008) ShcA signalling is essential for tumour progression in mouse models of human breast cancer. *The EMBO Journal* 27(6):910–920.

78. Andrechek ER, et al. (2003) Gene expression profiling of neu-induced mammary tumors from transgenic mice reveals genetic and morphological similarities to ErbB2-expressing human breast cancers. *Cancer Research* 63(16):4920–4926.

79. Hanahan D, Weinberg RA (2000) The hallmarks of cancer. *Cell* 100(1):57–70.

80. Hanahan D, Weinberg RA (2011) Hallmarks of Cancer: The Next Generation. *Cell* 144(5):646–674.

81. Tan M, et al. (2011) Identification of 67 histone marks and histone lysine crotonylation as a new type of histone modification. *Cell* 146(6):1016–1028.

82. Martin C, Zhang Y (2007) Mechanisms of epigenetic inheritance. *Current Opinion in Cell Biology* 19(3):266–272.

83. Ruthenburg AJ, Li H, Patel DJ, David Allis C (2007) Multivalent engagement of chromatin modifications by linked binding modules. *Nat Rev Mol Cell Biol* 8(12):983–994.

84. Kirmizis A (2004) Silencing of human polycomb target genes is associated with methylation of histone H3 Lys 27. *Genes & Development* 18(13):1592–1605.

85. Cao R, et al. (2002) Role of Histone H3 Lysine 27 Methylation in Polycomb-Group Silencing. *Science* 298(5595):1039–1043.

86. Czermin B, et al. (2002) Drosophila Enhancer of Zeste/ESC Complexes Have a Histone H3 Methyltransferase Activity that Marks Chromosomal Polycomb Sites. *Cell* 111(2):185–196.

87. Kuzmichev A, Nishioka K, Erdjument-Bromage H, Tempst P, Reinberg D (2002) Histone methyltransferase activity associated with a human multiprotein complex containing the Enhancer of Zeste protein. *Genes & Development* 16(22):2893–2905.

88. Francis NJ (2004) Chromatin Compaction by a Polycomb Group Protein Complex. *Science* 306(5701):1574–1577.

89. Zhou W, et al. (2008) Histone H2A Monoubiquitination Represses Transcription by Inhibiting RNA Polymerase II Transcriptional Elongation. *Molecular Cell*

29(1):69–80.

90. Boyer LA, et al. (2006) Polycomb complexes repress developmental regulators in murine embryonic stem cells. *Nature* 441(7091):349–353.

91. Ku M, et al. (2008) Genomewide Analysis of PRC1 and PRC2 Occupancy Identifies Two Classes of Bivalent Domains. *PLoS Genetics* 4(10):e1000242.

92. Schoeftner S, et al. (2006) Recruitment of PRC1 function at the initiation of X inactivation independent of PRC2 and silencing. *The EMBO Journal* 25(13):3110–3122.

93. Kalb R, et al. (2014) Histone H2A monoubiquitination promotes histone H3 methylation in Polycomb repression. *Nature Structural & Molecular Biology* 21(6):569–571.

94. Brookes E, et al. (2012) Polycomb associates genome-wide with a specific RNA polymerase II variant, and regulates metabolic genes in ESCs. *Cell Stem Cell* 10(2):157–170.

95. Stock JK, et al. (2007) Ring1-mediated ubiquitination of H2A restrains poised RNA polymerase II at bivalent genes in mouse ES cells. *Nat Cell Biol* 9(12):1428–1435.

96. Pauler FM, et al. (2009) H3K27me3 forms BLOCs over silent genes and intergenic regions and specifies a histone banding pattern on a mouse autosomal chromosome. *Genome Research* 19(2):221–233.

97. Zhao XD, et al. (2007) Whole-Genome Mapping of Histone H3 Lys4 and 27 Trimethylations Reveals Distinct Genomic Compartments in Human Embryonic Stem Cells. *Cell Stem Cell* 1(3):286–298.

98. Squazzo SL, et al. (2006) Suz12 binds to silenced regions of the genome in a cell-type-specific manner. *Genome Research* 16(7):890–900.

99. Hawkins RD, et al. (2010) Distinct epigenomic landscapes of pluripotent and lineage-committed human cells. *Cell Stem Cell* 6(5):479–491.

100. Pan G, et al. (2007) Whole-Genome Analysis of Histone H3 Lysine 4 and Lysine 27 Methylation in Human Embryonic Stem Cells. *Cell Stem Cell* 1(3):299–312.

101. Cui K, et al. (2009) Chromatin Signatures in Multipotent Human Hematopoietic Stem Cells Indicate the Fate of Bivalent Genes during Differentiation. *Cell Stem Cell* 4(1):80–93.

102. Rosenfeld JA, et al. (2009) Determination of enriched histone modifications in non-genic portions of the human genome. *BMC Genomics* 10(1):143.

103. Leeb M, et al. (2010) Polycomb complexes act redundantly to repress genomic repeats and genes. *Genes & Development* 24(3):265–276.

104. Lee TI, et al. (2006) Control of Developmental Regulators by Polycomb in Human Embryonic Stem Cells. *Cell* 125(2):301–313.

105. Cao R, Zhang Y (2004) SUZ12 is required for both the histone methyltransferase activity and the silencing function of the EED-EZH2 complex. *Molecular Cell* 15(1):57–67.

106. Pasini D, Bracken AP, Jensen MR, Lazzerini Denchi E, Helin K (2004) Suz12 is essential for mouse development and for EZH2 histone methyltransferase activity. *The EMBO Journal* 23(20):4061–4071.

107. Margueron R, et al. (2008) Ezh1 and Ezh2 maintain repressive chromatin through different mechanisms. *Molecular Cell* 32(4):503–518.

108. Ezhkova E, et al. (2011) EZH1 and EZH2 cogovern histone H3K27 trimethylation and are essential for hair follicle homeostasis and wound repair. *Genes & Development* 25(5):485–498.

109. Hansen KH, et al. (2008) A model for transmission of the H3K27me3 epigenetic mark. *Nat Cell Biol* 10(11):1291–1300.

110. Margueron R, et al. (2009) Role of the polycomb protein EED in the propagation of repressive histone marks. *Nature* 461(7265):762–767.

111. Xu C, et al. (2010) Binding of different histone marks differentially regulates the activity and specificity of polycomb repressive complex 2 (PRC2). *Proc Natl Acad Sci USA* 107(45):19266–19271.

112. Margueron R, Reinberg D (2011) The Polycomb complex PRC2 and its mark in life. *Nature* 469(7330):343–349.

113. Schmitges FW, et al. (2011) Histone Methylation by PRC2 Is Inhibited by Active Chromatin Marks. *Molecular Cell* 42(3):330–341.

114. Nowak AJ, et al. (2011) Chromatin-modifying Complex Component Nurf55/p55 Associates with Histones H3 and H4 and Polycomb Repressive Complex 2 Subunit Su(z)12 through Partially Overlapping Binding Sites. *Journal of Biological Chemistry* 286(26):23388–23396.

115. Lee MG, et al. (2007) Demethylation of H3K27 Regulates Polycomb Recruitment and H2A Ubiquitination. *Science* 318(5849):447–450.

116. Xiang Y, et al. (2007) JMJD3 is a histone H3K27 demethylase. *Cell Research* 17(10):850–857.

117. Ketel CS, et al. (2005) Subunit Contributions to Histone Methyltransferase Activities of Fly and Worm Polycomb Group Complexes. *Molecular and Cellular Biology* 25(16):6857–6868.

118. Yuan W, et al. (2011) H3K36 Methylation Antagonizes PRC2-mediated H3K27 Methylation. *Journal of Biological Chemistry* 286(10):7983–7989.

119. Pasini D, et al. (2010) Characterization of an antagonistic switch between histone H3 lysine 27 methylation and acetylation in the transcriptional regulation of Polycomb group target genes. *Nucleic Acids Research* 38(15):4958–4969.

120. Yuan W, et al. (2012) Dense Chromatin Activates Polycomb Repressive Complex 2 to Regulate H3 Lysine 27 Methylation. *Science* 337(6097):971–975.

121. Kia SK, Gorski MM, Giannakopoulos S, Verrijzer CP (2008) SWI/SNF Mediates Polycomb Eviction and Epigenetic Reprogramming of the INK4b-ARF-INK4a Locus. *Molecular and Cellular Biology* 28(10):3457–3464.

122. Wilson BG, et al. (2010) Epigenetic antagonism between polycomb and SWI/SNF complexes during oncogenic transformation. *Cancer Cell* 18(4):316–328.

123. Kennison JA, Tamkun JW (1988) Dosage-dependent modifiers of polycomb and antennapedia mutations in Drosophila. *Proceedings of the National Academy of Sciences* 85(21):8136–8140.

124. Gal-Yam EN, et al. (2008) Frequent switching of Polycomb repressive marks and DNA hypermethylation in the PC3 prostate cancer cell line. *Proc Natl Acad Sci USA* 105(35):12979–12984.

125. Schlesinger Y, et al. (2007) Polycomb-mediated methylation on Lys27 of histone H3 pre-marks genes for de novo methylation in cancer. *Nat Genet* 39(2):232–236.

126. Viré E, et al. (2006) The Polycomb group protein EZH2 directly controls DNA methylation. *Nature* 439(7078):871–874.

127. Reddington JP, et al. (2013) Redistribution of H3K27me3 upon DNA hypomethylation results in de-repression of Polycomb target genes. *Genome Biol* 14(3):R25.

128. Wu Z, Luo J, Ge Q, Lu Z (2008) Microarray-based Ms-SNuPE: Near-quantitative analysis for a high-throughput DNA methylation. *Biosensors and Bioelectronics* 23(9):1333–1339.

129. McGarvey KM, Greene E, Fahrner JA, Jenuwein T, Baylin SB (2007) DNA

methylation and complete transcriptional silencing of cancer genes persist after depletion of EZH2. *Cancer Research* 67(11):5097–5102.

130. Brinkman AB, et al. (2012) Sequential ChIP-bisulfite sequencing enables direct genome-scale investigation of chromatin and DNA methylation cross-talk. *Genome Research* 22(6):1128–1138.

131. Cha TL (2005) Akt-Mediated Phosphorylation of EZH2 Suppresses Methylation of Lysine 27 in Histone H3. *Science* 310(5746):306–310.

132. Sahasrabuddhe AA, et al. (2014) Oncogenic Y641 mutations in EZH2 prevent Jak2/β-TrCP-mediated degradation. *Oncogene* 34(4):445–454.

133. Kaneko S, et al. (2010) Phosphorylation of the PRC2 component Ezh2 is cell cycle-regulated and up-regulates its binding to ncRNA. *Genes & Development* 24(23):2615–2620.

134. Chen S, et al. (2010) Cyclin-dependent kinases regulate epigenetic gene silencing through phosphorylation of EZH2. *Nat Cell Biol* 12(11):1108–1114.

135. Wei Y, et al. (2011) CDK1-dependent phosphorylation of EZH2 suppresses methylation of H3K27 and promotes osteogenic differentiation of human mesenchymal stem cells. *Nat Cell Biol* 13(1):87–94.

136. Chu C-S, et al. (2014) O-GlcNAcylation regulates EZH2 protein stability and function. *Proc Natl Acad Sci USA* 111(4):1355–1360.

137. Ciferri C, et al. (2012) Molecular architecture of human polycomb repressive complex 2. *eLife* 1:250.

138. Nekrasov M, et al. (2007) Pcl-PRC2 is needed to generate high levels of H3-K27 trimethylation at Polycomb target genes. *The EMBO Journal* 26(18):4078–4088.

139. Savla U, Benes J, Zhang J, Jones RS (2008) Recruitment of Drosophila Polycomb-group proteins by Polycomblike, a component of a novel protein complex in larvae. *Development* 135(5):813–817.

140. Cai L, et al. (2013) An H3K36 methylation-engaging Tudor motif of polycomb-like proteins mediates PRC2 complex targeting. *Molecular Cell* 49(3):571–582.

141. Musselman CA, et al. (2012) Molecular basis for H3K36me3 recognition by the Tudor domain of PHF1. *Nature Structural & Molecular Biology* 19(12):1266–1272.

142. Landeira D, et al. (2010) Jarid2 is a PRC2 component in embryonic stem cells required for multi-lineage differentiation and recruitment of PRC1 and RNA Polymerase II to developmental regulators. *Nat Cell Biol* 12(6):618–624.

143. Peng JC, et al. (2009) Jarid2/Jumonji coordinates control of PRC2 enzymatic activity and target gene occupancy in pluripotent cells. *Cell* 139(7):1290–1302.

144. Son J, Shen SS, Margueron R, Reinberg D (2013) Nucleosome-binding activities within JARID2 and EZH1 regulate the function of PRC2 on chromatin. *Genes & Development* 27(24):2663–2677.

145. Sanulli S, et al. (2015) Jarid2 Methylation via the PRC2 Complex Regulates H3K27me3 Deposition during Cell Differentiation. *Molecular Cell* 57(5):769–783.

146. Chan CS, Rastelli L, Pirrotta V (1994) A Polycomb response element in the Ubx gene that determines an epigenetically inherited state of repression. *The EMBO Journal* 13(11):2553–2564.

147. Kassis JA (1994) Unusual properties of regulatory DNA from the Drosophila engrailed gene: three “pairing-sensitive” sites within a 1.6-kb region. *Genetics* 136(3):1025–1038.

148. Simon J, Chiang A, Bender W, Shimell MJ, O'Connor M (1993) Elements of the Drosophila Bithorax Complex That Mediate Repression by Polycomb Group Products. *Developmental Biology* 158(1):131–144.

149. Sing A, et al. (2009) A Vertebrate Polycomb Response Element Governs Segmentation of the Posterior Hindbrain. *Cell* 138(5):885–897.

150. Woo CJ, Kharchenko PV, Daheron L, Park PJ, Kingston RE (2010) A Region of the Human HOXD Cluster that Confers Polycomb-Group Responsiveness. *Cell* 140(1):99–110.

151. Mendenhall EM, et al. (2010) GC-rich sequence elements recruit PRC2 in mammalian ES cells. *PLoS Genetics* 6(12):e1001244.

152. Lynch MD, et al. (2012) An interspecies analysis reveals a key role for unmethylated CpG dinucleotides in vertebrate Polycomb complex recruitment. *The EMBO Journal* 31(2):317–329.

153. Vasanthi D, Nagabhushan A, Matharu NK, Mishra RK (2013) A functionally conserved Polycomb response element from mouse HoxD complex responds to heterochromatin factors. *Sci Rep* 3:3011.

154. Riising EM, et al. (2014) Gene Silencing Triggers Polycomb Repressive Complex 2 Recruitment to CpG Islands Genome Wide. *Molecular Cell* 55(3):347–360.

155. Schorderet P, et al. (2013) A genetic approach to the recruitment of PRC2 at the HoxD locus. *PLoS Genetics* 9(11):e1003951.

156. Arnold P, et al. (2013) Modeling of epigenome dynamics identifies transcription factors that mediate Polycomb targeting. *Genome Research* 23(1):60–73.

157. Jermann P, Hoerner L, Burger L, Schübeler D (2014) Short sequences can efficiently recruit histone H3 lysine 27 trimethylation in the absence of enhancer activity and DNA methylation. *Proc Natl Acad Sci USA* 111(33):E3415–21.

158. Klose RJ, Cooper S, Farcas AM, Blackledge NP, Brockdorff N (2013) Chromatin Sampling—An Emerging Perspective on Targeting Polycomb Repressor Proteins. *PLoS Genetics* 9(8):e1003717.

159. Cooper S, et al. (2014) Targeting Polycomb to Pericentric Heterochromatin in Embryonic Stem Cells Reveals a Role for H2AK119u1 in PRC2 Recruitment. *Cell Reports* 7(5):1456–1470.

160. Hagarman JA, Motley MP, Kristjansdottir K, Soloway PD (2013) Coordinate Regulation of DNA Methylation and H3K27me3 in Mouse Embryonic Stem Cells. *PLoS ONE* 8(1):e53880.

161. Kohlmaier A, et al. (2004) A Chromosomal Memory Triggered by Xist Regulates Histone Methylation in X Inactivation. *PLoS Biology* 2(7):e171.

162. Silva J, et al. (2003) Establishment of Histone H3 Methylation on the Inactive X Chromosome Requires Transient Recruitment of Eed-Enx1 Polycomb Group Complexes. *Developmental Cell* 4(4):481–495.

163. Plath K (2003) Role of Histone H3 Lysine 27 Methylation in X Inactivation. *Science* 300(5616):131–135.

164. Okamoto I (2004) Epigenetic Dynamics of Imprinted X Inactivation During Early Mouse Development. *Science* 303(5658):644–649.

165. Rinn JL, et al. (2007) Functional demarcation of active and silent chromatin domains in human HOX loci by noncoding RNAs. *Cell* 129(7):1311–1323.

166. Tsai M-C, et al. (2010) Long noncoding RNA as modular scaffold of histone modification complexes. *Science* 329(5992):689–693.

167. Khalil AM, et al. (2009) Many human large intergenic noncoding RNAs associate with chromatin-modifying complexes and affect gene expression. *Proc Natl Acad Sci USA* 106(28):11667–11672.

168. Zhao J, et al. (2010) Genome-wide Identification of Polycomb-Associated RNAs by RIP-seq. *Molecular Cell* 40(6):939–953.

169. Davidovich C, et al. (2015) Toward a consensus on the binding specificity and promiscuity of PRC2 for RNA. *Molecular Cell* 57(3):552–558.

170. Wang X, et al. (2017) Targeting of Polycomb Repressive Complex 2 to RNA by Short Repeats of Consecutive Guanines. *Molecular Cell* 65(6):1056–1067.e5.

171. Kaneko S, Son J, Bonasio R, Shen SS, Reinberg D (2014) Nascent RNA interaction keeps PRC2 activity poised and in check. *Genes & Development* 28(18):1983–1988.

172. Hauri S, et al. (2016) A High-Density Map for Navigating the Human Polycomb Complexome. *Cell Reports* 17(2):583–595.

173. Herranz N, et al. (2008) Polycomb Complex 2 Is Required for E-cadherin Repression by the Snail1 Transcription Factor. *Molecular and Cellular Biology* 28(15):4772–4781.

174. Lewis EB (2007) A Gene Complex Controlling Segmentation in Drosophila. *Genes, Development, and Cancer* (Springer Netherlands, Dordrecht), pp 229–242.

175. Jürgens G (1985) A group of genes controlling the spatial expression of the bithorax complex in Drosophila. *Nature* 316(6024):153–155.

176. Xie H, et al. (2014) Polycomb repressive complex 2 regulates normal hematopoietic stem cell function in a developmental-stage-specific manner. *Cell Stem Cell* 14(1):68–80.

177. Su I-H, et al. (2003) Ezh2 controls B cell development through histone H3 methylation and Igh rearrangement. *Nat Immunol* 4(2):124–131.

178. Chamberlain SJ, Yee D, Magnuson T (2008) Polycomb repressive complex 2 is dispensable for maintenance of embryonic stem cell pluripotency. *Stem Cells* 26(6):1496–1505.

179. Bracken AP, Dietrich N, Pasini D, Hansen KH, Helin K (2006) Genome-wide mapping of Polycomb target genes unravels their roles in cell fate transitions. *Genes & Development* 20(9):1123–1136.

180. O'Carroll D, et al. (2001) The polycomb-group gene Ezh2 is required for early mouse development. *Molecular and Cellular Biology* 21(13):4330–4336.

181. Faust C, Schumacher A, Holdener B, Magnuson T (1995) The eed mutation disrupts anterior mesoderm production in mice. *Development* 121(2):273–285.

182. Faust C, Lawson KA, Schork NJ, Thiel B, Magnuson T (1998) The Polycomb-group gene eed is required for normal morphogenetic movements during gastrulation in the mouse embryo. *Development* 125(22):4495–4506.

183. Pasini D, Bracken AP, Hansen JB, Capillo M, Helin K (2007) The polycomb

group protein Suz12 is required for embryonic stem cell differentiation. *Molecular and Cellular Biology* 27(10):3769–3779.

184. Shen X, et al. (2008) EZH1 Mediates Methylation on Histone H3 Lysine 27 and Complements EZH2 in Maintaining Stem Cell Identity and Executing Pluripotency. *Molecular Cell* 32(4):491–502.

185. Simon C, et al. (2012) A key role for EZH2 and associated genes in mouse and human adult T-cell acute leukemia. *Genes & Development* 26(7):651–656.

186. Neff T, et al. (2012) Polycomb repressive complex 2 is required for MLL-AF9 leukemia. *Proc Natl Acad Sci USA* 109(13):5028–5033.

187. Mochizuki-Kashio M, et al. (2011) Dependency on the polycomb gene Ezh2 distinguishes fetal from adult hematopoietic stem cells. *Blood* 118(25):6553–6561.

188. Xie H, et al. (2014) Polycomb repressive complex 2 regulates normal hematopoietic stem cell function in a developmental-stage-specific manner. *Cell Stem Cell* 14(1):68–80.

189. Caganova M, et al. (2013) Germinal center dysregulation by histone methyltransferase EZH2 promotes lymphomagenesis. *J Clin Invest* 123(12):5009–5022.

190. Berg T, et al. (2014) A transgenic mouse model demonstrating the oncogenic role of mutations in the polycomb-group gene EZH2 in lymphomagenesis. *Blood* 123(25):3914–3924.

191. Béguelin W, et al. (2013) EZH2 is required for germinal center formation and somatic EZH2 mutations promote lymphoid transformation. *Cancer Cell* 23(5):677–692.

192. Dardenne E, et al. (2016) N-Myc Induces an EZH2-Mediated Transcriptional Program Driving Neuroendocrine Prostate Cancer. *Cancer Cell* 30(4):563–577.

193. Koontz JI, et al. (2001) Frequent fusion of the JAZF1 and JJAZ1 genes in endometrial stromal tumors. *Proceedings of the National Academy of Sciences* 98(11):6348–6353.

194. Ma X, et al. (2017) The JAZF1-SUZ12 fusion protein disrupts PRC2 complexes and impairs chromatin repression during human endometrial stromal tumorogenesis. *Oncotarget* 8(3):4062–4078.

195. Morin RD, et al. (2010) Somatic mutations altering EZH2 (Tyr641) in follicular and diffuse large B-cell lymphomas of germinal-center origin. *Nat Genet*

42(2):181–185.

196. Hodis E, et al. (2012) A landscape of driver mutations in melanoma. *Cell* 150(2):251–263.

197. Souroullas GP, et al. (2016) An oncogenic Ezh2 mutation induces tumors through global redistribution of histone 3 lysine 27 trimethylation. *Nature Medicine* 22(6):632–640.

198. Pugh TJ, et al. (2012) Medulloblastoma exome sequencing uncovers subtype-specific somatic mutations. *Nature* 488(7409):106–110.

199. Waddell N, et al. (2015) Whole genomes redefine the mutational landscape of pancreatic cancer. *Nature* 518(7540):495–501.

200. Dalgliesh GL, et al. (2010) Systematic sequencing of renal carcinoma reveals inactivation of histone modifying genes. *Nature* 463(7279):360–363.

201. Bitler BG, et al. (2015) Synthetic lethality by targeting EZH2 methyltransferase activity in ARID1A-mutated cancers. *Nature Medicine* 153:17.

202. Fillmore CM, et al. (2015) EZH2 inhibition sensitizes BRG1 and EGFR mutant lung tumours to TopoII inhibitors. *Nature* 520(7546):239–242.

203. Lee W, et al. (2014) PRC2 is recurrently inactivated through EED or SUZ12 loss in malignant peripheral nerve sheath tumors. *Nat Genet* 46(11):1227–1232.

204. Zhang M, et al. (2014) Somatic mutations of SUZ12 in malignant peripheral nerve sheath tumors. *Nat Genet* 46(11):1170–1172.

205. Sashida G, et al. (2014) Ezh2 loss promotes development of myelodysplastic syndrome but attenuates its predisposition to leukaemic transformation. *Nat Commun* 5:4177.

206. Abdel-Wahab O, et al. (2012) ASXL1 mutations promote myeloid transformation through loss of PRC2-mediated gene repression. *Cancer Cell* 22(2):180–193.

207. Score J, et al. (2012) Inactivation of polycomb repressive complex 2 components in myeloproliferative and myelodysplastic/myeloproliferative neoplasms. *Blood* 119(5):1208–1213.

208. Ueda T, et al. (2012) EED mutants impair polycomb repressive complex 2 in myelodysplastic syndrome and related neoplasms. *Leukemia* 26(12):2557–2560.

209. Ntziachristos P, et al. (2012) Genetic inactivation of the polycomb repressive complex 2 in T cell acute lymphoblastic leukemia. *Nature Medicine* 18(2):298–

301.

210. Puda A, et al. (2012) Frequent deletions of JARID2 in leukemic transformation of chronic myeloid malignancies. *Am J Hematol* 87(3):245–250.

211. Schwartzentruber J, et al. (2012) Driver mutations in histone H3.3 and chromatin remodelling genes in paediatric glioblastoma. *Nature* 482(7384):226–231.

212. Wu G, et al. (2012) Somatic histone H3 alterations in pediatric diffuse intrinsic pontine gliomas and non-brainstem glioblastomas. *Nat Genet* 44(3):251–253.

213. Bender S, et al. (2013) Reduced H3K27me3 and DNA hypomethylation are major drivers of gene expression in K27M mutant pediatric high-grade gliomas. *Cancer Cell* 24(5):660–672.

214. Lewis PW, et al. (2013) Inhibition of PRC2 activity by a gain-of-function H3 mutation found in pediatric glioblastoma. *Science* 340(6134):857–861.

215. Kim E, et al. (2013) Phosphorylation of EZH2 Activates STAT3 Signaling via STAT3 Methylation and Promotes Tumorigenicity of Glioblastoma Stem-like Cells. *Cancer Cell* 23(6):839–852.

216. Xu K, et al. (2012) EZH2 Oncogenic Activity in Castration-Resistant Prostate Cancer Cells Is Polycomb-Independent. *Science* 338(6113):1465–1469.

217. Gonzalez ME, et al. (2014) EZH2 expands breast stem cells through activation of NOTCH1 signaling. *Proceedings of the National Academy of Sciences* 111(8):3098–3103.

218. Shi B, et al. (2007) Integration of Estrogen and Wnt Signaling Circuits by the Polycomb Group Protein EZH2 in Breast Cancer Cells. *Molecular and Cellular Biology* 27(14):5105–5119.

219. Varambally S, et al. (2002) The polycomb group protein EZH2 is involved in progression of prostate cancer. *Nature* 419(6907):624–629.

220. Bracken AP, et al. (2003) EZH2 is downstream of the pRB-E2F pathway, essential for proliferation and amplified in cancer. *The EMBO Journal* 22(20):5323–5335.

221. Bachmann IM, et al. (2006) EZH2 Expression Is Associated With High Proliferation Rate and Aggressive Tumor Subgroups in Cutaneous Melanoma and Cancers of the Endometrium, Prostate, and Breast. *Journal of Clinical Oncology* 24(2):268–273.

222. Kleer CG, et al. (2011) EZH2 is a marker of aggressive breast cancer and promotes neoplastic transformation of breast epithelial cells. *Proceedings of the*

National Academy of Sciences 100(20):11606–11611.

223. Zingg D, et al. (2015) The epigenetic modifier EZH2 controls melanoma growth and metastasis through silencing of distinct tumour suppressors. *Nat Commun* 6:6051.

224. Abd Al Kader L, et al. (2013) In aggressive variants of non-Hodgkin lymphomas, Ezh2 is strongly expressed and polycomb repressive complex PRC1.4 dominates over PRC1.2. *Virchows Archiv* 463(5):697–711.

225. Yan J, et al. (2013) EZH2 overexpression in natural killer/T-cell lymphoma confers growth advantage independently of histone methyltransferase activity. *Blood* 121(22):4512–4520.

226. Li X, et al. (2009) Targeted overexpression of EZH2 in the mammary gland disrupts ductal morphogenesis and causes epithelial hyperplasia. *The American Journal of Pathology* 175(3):1246–1254.

227. Holm K, et al. (2012) Global H3K27 trimethylation and EZH2 abundance in breast tumor subtypes. *Molecular Oncology* 6(5):494–506.

228. Beca F, et al. (2017) EZH2 protein expression in normal breast epithelium and risk of breast cancer: results from the Nurses' Health Studies. *Breast Cancer Research* 19(1):21.

229. Miranda TB, et al. (2009) DZNep is a global histone methylation inhibitor that reactivates developmental genes not silenced by DNA methylation. *Molecular Cancer Therapeutics* 8(6):1579–1588.

230. Tan J, et al. (2007) Pharmacologic disruption of Polycomb-repressive complex 2-mediated gene repression selectively induces apoptosis in cancer cells. *Genes & Development* 21(9):1050–1063.

231. Knutson SK, et al. (2012) A selective inhibitor of EZH2 blocks H3K27 methylation and kills mutant lymphoma cells. *Nat Chem Biol* 8(11):890–896.

232. McCabe MT, et al. (2012) EZH2 inhibition as a therapeutic strategy for lymphoma with EZH2-activating mutations. *Nature* 492(7427):108–112.

233. Qi W, et al. (2012) Selective inhibition of Ezh2 by a small molecule inhibitor blocks tumor cells proliferation. *Proc Natl Acad Sci USA* 109(52):21360–21365.

234. Konze KD, et al. (2013) An Orally Bioavailable Chemical Probe of the Lysine Methyltransferases EZH2 and EZH1. *ACS Chemical Biology* 8(6):1324–1334.

235. Qi W, et al. (2017) An allosteric PRC2 inhibitor targeting the H3K27me3 binding pocket of EED. *Nat Chem Biol*. doi:10.1038/nchembio.2304.

236. Kim W, et al. (2013) Targeted disruption of the EZH2-EED complex inhibits EZH2-dependent cancer. *Nat Chem Biol* 9(10):643–650.

237. Fujii S, et al. (2011) MEK-ERK pathway regulates EZH2 overexpression in association with aggressive breast cancer subtypes. *Oncogene* 30(39):4118–4128.

238. Chang C-J, et al. (2011) EZH2 promotes expansion of breast tumor initiating cells through activation of RAF1-β-catenin signaling. *Cancer Cell* 19(1):86–100.

239. Derfoul A, et al. (2011) Decreased microRNA-214 levels in breast cancer cells coincides with increased cell proliferation, invasion and accumulation of the Polycomb Ezh2 methyltransferase. *Carcinogenesis* 32(11):1607–1614.

240. Bruggeman SWM (2005) Ink4a and Arf differentially affect cell proliferation and neural stem cell self-renewal in Bmi1-deficient mice. *Genes & Development* 19(12):1438–1443.

241. Fujii S, Ito K, Ito Y, Ochiai A (2008) Enhancer of zeste homologue 2 (EZH2) down-regulates RUNX3 by increasing histone H3 methylation. *Journal of Biological Chemistry* 283(25):17324–17332.

242. Cao Q, et al. (2008) Repression of E-cadherin by the polycomb group protein EZH2 in cancer. *Oncogene* 27(58):7274–7284.

243. Lee ST, et al. (2011) Context-Specific Regulation of NF-κB Target Gene Expression by EZH2 in Breast Cancers. *Molecular Cell* 43(5):798–810.

244. Bae WK, et al. (2014) The methyltransferase EZH2 is not required for mammary cancer development, although high EZH2 and low H3K27me3 correlate with poor prognosis of ER-positive breast cancers. *Molecular Carcinogenesis* 54(10):1172–1180.

245. Wassef M, et al. (2015) Impaired PRC2 activity promotes transcriptional instability and favors breast tumorigenesis. *Genes & Development* 29(24):2547–2562.

246. Koppens M, van Lohuizen M (2015) Context-dependent actions of Polycomb repressors in cancer. *Oncogene* 35(11):1341–1352.

247. Comet I, Riising EM, Leblanc B, Helin K (2016) Maintaining cell identity: PRC2-mediated regulation of transcription and cancer. *Nature Reviews Cancer* 16(12):803–810.

248. Lin EY, et al. (2003) Progression to Malignancy in the Polyoma Middle T Oncoprotein Mouse Breast Cancer Model Provides a Reliable Model for Human

Diseases. *The American Journal of Pathology* 163(5):2113–2126.

249. Pfefferle AD, et al. (2013) Transcriptomic classification of genetically engineered mouse models of breast cancer identifies human subtype counterparts. *Genome Biol* 14(11):R125.

250. Pal B, et al. (2013) Global Changes in the Mammary Epigenome Are Induced by Hormonal Cues and Coordinated by Ezh2. *Cell Reports* 3(2):411–426.

251. Michalak EM, et al. (2013) Polycomb group gene Ezh2 regulates mammary gland morphogenesis and maintains the luminal progenitor pool. *Stem Cells* 31(9):1910–1920.

252. Rao T, et al. (2014) Inducible and coupled expression of the polyomavirus middle T antigen and Cre recombinase in transgenic mice: an in vivo model for synthetic viability in mammary tumour progression. *Breast Cancer Research* 16(1):542.

253. Gunther EJ, et al. (2002) A novel doxycycline-inducible system for the transgenic analysis of mammary gland biology. *FASEB J* 16(3):283–292.

254. Knutson SK, et al. (2013) Durable tumor regression in genetically altered malignant rhabdoid tumors by inhibition of methyltransferase EZH2. *Proceedings of the National Academy of Sciences* 110(19):7922–7927.

255. Knutson SK, et al. (2014) Selective Inhibition of EZH2 by EPZ-6438 Leads to Potent Antitumor Activity in EZH2-Mutant Non-Hodgkin Lymphoma. *Molecular Cancer Therapeutics* 13(4):842–854.

256. Tiwari N, et al. (2013) Sox4 Is a Master Regulator of Epithelial-Mesenchymal Transition by Controlling Ezh2 Expression and Epigenetic Reprogramming. *Cancer Cell* 23(6):768–783.

257. Ikeda K, et al. (2006) Loss of Expression of Type IV Collagen α5 and α6 Chains in Colorectal Cancer Associated with the Hypermethylation of Their Promoter Region. *The American Journal of Pathology* 168(3):856–865.

258. Amenta PS, et al. (2003) Loss of types XV and XIX collagen precedes basement membrane invasion in ductal carcinoma of the female breast. *The Journal of Pathology* 199(3):298–308.

259. Sassano A, et al. (2015) Human Schlafen 5 (SLFN5) Is a Regulator of Motility and Invasiveness of Renal Cell Carcinoma Cells. *Molecular and Cellular Biology* 35(15):2684–2698.

260. Li J, Ye L, G Jiang W (2012) Repulsive Guidance Molecules (RGMs) and Their

Potential Implication in Cancer as Co-receptor of BMPs. *Current Signal Transduction Therapy* 7(2):149–160.

261. Li J, Ye L, Sanders A, Mansel R, Jiang W (2014) The Role of Dragon (Repulsive Guidance Molecule-B, RGM-B) in Human Breast Cancer. *Cancer Research* 69(24 Supplement):6158–6158.

262. He L-H, et al. (2013) CHL1 is involved in human breast tumorigenesis and progression. *Biochemical and Biophysical Research Communications* 438(2):433–438.

263. Szász AM, et al. (2014) Cross-validation of survival associated biomarkers in gastric cancer using transcriptomic data of 1,065 patients. *Oncotarget* 7(31):49322–49333.

264. Ray PS, et al. (2010) FOXC1 Is a Potential Prognostic Biomarker with Functional Significance in Basal-like Breast Cancer. *Cancer Research* 70(10):3870–3876.

265. Wang J, et al. (2012) FOXC1 regulates the functions of human basal-like breast cancer cells by activating NF-κB signaling. *Oncogene* 31(45):4798–4802.

266. DeRose YS, et al. (2011) Tumor grafts derived from women with breast cancer authentically reflect tumor pathology, growth, metastasis and disease outcomes. *Nature Medicine* 17(11):1514–1520.

267. Gough DJ, Messina NL, Clarke CJP, Johnstone RW, Levy DE (2012) Constitutive Type I Interferon Modulates Homeostatic Balance through Tonic Signaling. *Immunity* 36(2):166–174.

268. Hwang SY, et al. (1995) A null mutation in the gene encoding a type I interferon receptor component eliminates antiproliferative and antiviral responses to interferons alpha and beta and alters macrophage responses. *Proceedings of the National Academy of Sciences* 92(24):11284–11288.

269. Chiappinelli KB, et al. (2016) Inhibiting DNA Methylation Causes an Interferon Response in Cancer via dsRNA Including Endogenous Retroviruses. *Cell* 164(5):1073.

270. Roulois D, et al. (2015) DNA-Demethylating Agents Target Colorectal Cancer Cells by Inducing Viral Mimicry by Endogenous Transcripts. *Cell* 162(5):961–973.

271. Naba A, et al. (2012) The matrisome: in silico definition and in vivo characterization by proteomics of normal and tumor extracellular matrices. *Mol Cell Proteomics* 11(4):M111.014647–M111.014647.

272. WHO releases new edition of Model List of Essential Medicines (2015) WHO releases new edition of Model List of Essential Medicines. *PharmacoEconomics & Outcomes News* 728(1):8–8.

273. Luen SJ, et al. (2017) Tumour-infiltrating lymphocytes in advanced HER2-positive breast cancer treated with pertuzumab or placebo in addition to trastuzumab and docetaxel: a retrospective analysis of the CLEOPATRA study. *Lancet Oncol* 18(1):52–62.

274. Gajria D, Chandarlapaty S (2011) HER2-amplified breast cancer: mechanisms of trastuzumab resistance and novel targeted therapies. *Expert Rev Anticancer Ther* 11(2):263–275.

275. Weber J (2010) Immune Checkpoint Proteins: A New Therapeutic Paradigm for Cancer—Preclinical Background: CTLA-4 and PD-1 Blockade. *Seminars in Oncology* 37(5):430–439.

276. Lowenfeld L, et al. (2016) Dendritic Cell Vaccination Enhances Immune Responses and Induces Regression of HER2 posDCIS Independent of Route: Results of Randomized Selection Design Trial. *Clin Cancer Res*. doi:10.1158/1078-0432.CCR-16-1924.

277. Wolpoe ME, et al. (2003) HER-2/neu-specific monoclonal antibodies collaborate with HER-2/neu-targeted granulocyte macrophage colony-stimulating factor secreting whole cell vaccination to augment CD8+ T cell effector function and tumor-free survival in Her-2/neu-transgenic mice. *The Journal of Immunology* 171(4):2161–2169.

278. Ladoire S, et al. (2011) T-bet expression in intratumoral lymphoid structures after neoadjuvant trastuzumab plus docetaxel for HER2-overexpressing breast carcinoma predicts survival. *Br J Cancer* 105(3):366–371.

279. Disis ML, et al. (2009) Concurrent Trastuzumab and HER2/ neu-Specific Vaccination in Patients With Metastatic Breast Cancer. *Journal of Clinical Oncology* 27(28):4685–4692.

280. Disis M, et al. (2014) Phase II Study of a HER-2/Neu (HER2) Intracellular Domain (ICD) Vaccine Given Concurrently with Trastuzumab in Patients with Newly Diagnosed Advanced Stage Breast Cancer. *Cancer Research* 69(24 Supplement):5102–5102.

281. Stagg J, et al. (2011) Anti-ErbB-2 mAb therapy requires type I and II interferons and synergizes with anti-PD-1 or anti-CD137 mAb therapy. *Proc Natl Acad Sci USA* 108(17):7142–7147.

282. Gianni L, et al. (2014) Abstract S6-7: Adaptive immune system and immune

checkpoints are associated with response to pertuzumab (P) and trastuzumab (H) in the NeoSphere study. *Cancer Research* 72(24 Supplement):S6–7–S6–7.

283. Jaime-Ramirez AC, et al. (2011) IL-12 Enhances the Antitumor Actions of Trastuzumab via NK Cell IFN- Production. *The Journal of Immunology* 186(6):3401–3409.

284. Bekaii-Saab TS, et al. (2009) A phase I trial of paclitaxel and trastuzumab in combination with interleukin-12 in patients with HER2/neu-expressing malignancies. *Molecular Cancer Therapeutics* 8(11):2983–2991.

285. Zhang H, et al. (1999) Shared Antigenic Epitopes and Pathobiological Functions of Anti-p185her2/neu Monoclonal Antibodies. *Experimental and Molecular Pathology* 67(1):15–25.

286. Pagès F, et al. (2005) Effector Memory T Cells, Early Metastasis, and Survival in Colorectal Cancer. *New England Journal of Medicine* 353(25):2654–2666.

287. Zhang L, et al. (2003) Intratumoral T Cells, Recurrence, and Survival in Epithelial Ovarian Cancer. *New England Journal of Medicine* 348(3):203–213.

288. Jin Y, et al. (2014) FOXC1 is a critical mediator of EGFR function in human basal-like breast cancer. *Ann Surg Oncol* 21 Suppl 4(S4):S758–66.

289. Sizemore GM, et al. (2013) FOXC1 is enriched in the mammary luminal progenitor population, but is not necessary for mouse mammary ductal morphogenesis. *Biol Reprod* 89(1):10.

290. Jensen TW, et al. (2015) Diagnosis of Basal-Like Breast Cancer Using a FOXC1-Based Assay. *J Natl Cancer Inst* 107(8):djv148–djv148.

291. Mani SA, et al. (2007) Mesenchyme Forkhead 1 (FOXC2) plays a key role in metastasis and is associated with aggressive basal-like breast cancers. *Proceedings of the National Academy of Sciences* 104(24):10069–10074.

292. Seo S, et al. (2006) The forkhead transcription factors, Foxc1 and Foxc2, are required for arterial specification and lymphatic sprouting during vascular development. *Developmental Biology* 294(2):458–470.

293. Somerville TDD, Somervaille TCP (2016) Tissue-inappropriate derepression of FOXC1 is frequent and functional in human acute myeloid leukemia. *Mol Cell Oncol* 3(2):e1131355.

294. Galvis LA, et al. (2015) Repression of Igf1 expression by Ezh2 prevents basal cell differentiation in the developing lung. *Development* 142(8):1458–1469.

295. Ku S-Y, et al. (2017) Rb1 and Trp53 cooperate to suppress prostate cancer

lineage plasticity, metastasis, and antiandrogen resistance. *Science* 355(6320):78–83.

296. Zhang H, et al. (2017) Lkb1 inactivation drives lung cancer lineage switching governed by Polycomb Repressive Complex 2. *Nat Commun* 8:14922.

297. Muggerud AA, et al. (2010) Frequent aberrant DNA methylation of ABCB1, FOXC1, PPP2R2B and PTEN in ductal carcinoma in situ and early invasive breast cancer. *Breast Cancer Research* 12(1):R3.

298. Bartke T, et al. (2010) Nucleosome-Interacting Proteins Regulated by DNA and Histone Methylation. *Cell* 143(3):470–484.

299. Belinsky SA, et al. (1998) Aberrant methylation of p16(INK4a) is an early event in lung cancer and a potential biomarker for early diagnosis. *Proceedings of the National Academy of Sciences* 95(20):11891–11896.

300. McDermott KM, et al. (2006) p16INK4a Prevents Centrosome Dysfunction and Genomic Instability in Primary Cells. *PLoS Biology* 4(3):e51.

301. Reynolds PA, et al. (2006) Tumor Suppressor p16 INK4ARegulates Polycomb-mediated DNA Hypermethylation in Human Mammary Epithelial Cells. *Journal of Biological Chemistry* 281(34):24790–24802.

302. Ezhkova E, et al. (2009) Ezh2 orchestrates gene expression for the stepwise differentiation of tissue-specific stem cells. *Cell* 136(6):1122–1135.

303. Jacobs JJ, Kieboom K, Marino S, DePinho RA, van Lohuizen M (1999) The oncogene and Polycomb-group gene bmi-1 regulates cell proliferation and senescence through the ink4a locus. *Nature* 397(6715):164–168.

304. Bracken AP, et al. (2007) The Polycomb group proteins bind throughout the INK4A-ARF locus and are disassociated in senescent cells. *Genes & Development* 21(5):525–530.

305. Dietrich N, et al. (2007) Bypass of senescence by the polycomb group protein CBX8 through direct binding to the INK4A-ARF locus. *The EMBO Journal* 26(6):1637–1648.

306. Pellacani D, et al. (2016) Analysis of Normal Human Mammary Epigenomes Reveals Cell-Specific Active Enhancer States and Associated Transcription Factor Networks. *Cell Reports* 17(8):2060–2074.

307. Henry MD, Triplett AA, Oh KB, Smith GH, Wagner K-U (2004) Parity-induced mammary epithelial cells facilitate tumorigenesis in MMTV-neu transgenic mice. *Oncogene* 23(41):6980–6985.

308. Lo P-K, et al. (2011) CD49f and CD61 identify Her2/neu-induced mammary tumor-initiating cells that are potentially derived from luminal progenitors and maintained by the integrin–TGFβ signaling. *Oncogene* 31(21):2614–2626.

309. Vaillant F, et al. (2008) The Mammary Progenitor Marker CD61/ 3 Integrin Identifies Cancer Stem Cells in Mouse Models of Mammary Tumorigenesis. *Cancer Research* 68(19):7711–7717.

310. Balkwill F, Watling D, Taylor-Papadimitriou J (1978) Inhibition by lymphoblastoid interferon of growth of cells derived from the human breast. *International Journal of Cancer* 22(3):258–265.

311. Bernardo AR, Cosgaya JM, Aranda A, Jiménez-Lara AM (2013) Synergy between RA and TLR3 promotes type I IFN-dependent apoptosis through upregulation of TRAIL pathway in breast cancer cells. *Cell Death and Disease* 4(1):e479.

312. Macfarlan TS, et al. (2012) Embryonic stem cell potency fluctuates with endogenous retrovirus activity. *Nature* 184:1286.

313. Hutnick LK, Huang X, Loo T-C, Ma Z, Fan G (2010) Repression of Retrotransposal Elements in Mouse Embryonic Stem Cells Is Primarily Mediated by a DNA Methylation-independent Mechanism. *Journal of Biological Chemistry* 285(27):21082–21091.

314. Matsui T, et al. (2010) Proviral silencing in embryonic stem cells requires the histone methyltransferase ESET. *Nature* 464(7290):927–931.

315. Rebollo R, et al. (2012) Epigenetic interplay between mouse endogenous retroviruses and host genes. *Genome Biol* 13(10):R89.

316. Walter M, Teissandier A, Pérez-Palacios R, Bourc'his D (2016) An epigenetic switch ensures transposon repression upon dynamic loss of DNA methylation in embryonic stem cells. *eLife* 5:R87.

317. Ishak CA, et al. (2016) An RB-EZH2 Complex Mediates Silencing of Repetitive DNA Sequences. *Molecular Cell* 64(6):1074–1087.

318. Peng D, et al. (2015) Epigenetic silencing of TH1-type chemokines shapes tumour immunity and immunotherapy. *Nature* 527(7577):249–253.

319. Garcia-Sastre A (2006) Type 1 Interferons and the Virus-Host Relationship: A Lesson in Detente. *Science* 312(5775):879–882.

320. Yang Y, et al. (2012) Exploiting Synthetic Lethality for the Therapy of ABC Diffuse Large B Cell Lymphoma. *Cancer Cell* 21(6):723–737.

321. Maeda S, et al. (2014) Interferon-α acts on the S/G2/M phases to induce apoptosis in the G1 phase of an IFNAR2-expressing hepatocellular carcinoma cell line. *J Biol Chem* 289(34):23786–23795.

322. Parker BS, Rautela J, Hertzog PJ (2016) Antitumour actions of interferons: implications for cancer therapy. *Nature Reviews Cancer* 16(3):131–144.

323. Lee YJ, Holzapfel KL, Zhu J, Jameson SC, Hogquist KA (2013) Steady-state production of IL-4 modulates immunity in mouse strains and is determined by lineage diversity of iNKT cells. *Nat Immunol* 14(11):1146–1154.

324. Weinreich MA, Odumade OA, Jameson SC, Hogquist KA (2010) T cells expressing the transcription factor PLZF regulate the development of memory-like CD8+ T cells. *Nat Immunol* 11(8):709–716.

325. Vasanthakumar A, et al. (2017) A non-canonical function of Ezh2 preserves immune homeostasis. *EMBO Rep* 18(4):619–631.

326. Dobenecker M-W, et al. (2015) Coupling of T cell receptor specificity to natural killer T cell development by bivalent histone H3 methylation. *The Journal of Experimental Medicine* 212(3):297–306.

327. Imai K, Matsuyama S, Miyake S, Suga K, Nakachi K (2000) Natural cytotoxic activity of peripheral-blood lymphocytes and cancer incidence: an 11-year follow-up study of a general population. *Lancet* 356(9244):1795–1799.

328. Yin J, et al. (2015) Ezh2 regulates differentiation and function of natural killer cells through histone methyltransferase activity. *Proc Natl Acad Sci USA* 112(52):15988–15993.

329. Tumes DJ, et al. (2013) The Polycomb Protein Ezh2 Regulates Differentiation and Plasticity of CD4+ T Helper Type 1 and Type 2 Cells. *Immunity* 39(5):819–832.

330. Tong Q, et al. (2014) Ezh2 regulates transcriptional and posttranslational expression of T-bet and promotes Th1 cell responses mediating aplastic anemia in mice. *J Immunol* 192(11):5012–5022.

331. Zhao E, et al. (2016) Cancer mediates effector T cell dysfunction by targeting microRNAs and EZH2 via glycolysis restriction. *Nat Immunol* 17(1):95–103.

332. Vance GH, et al. (2009) Genetic heterogeneity in HER2 testing in breast cancer: panel summary and guidelines. *Arch Pathol Lab Med* 133(4):611–612.

333. Lee HJ, et al. (2014) HER2 heterogeneity affects trastuzumab responses and survival in patients with HER2-positive metastatic breast cancer. *American*

Journal of Clinical Pathology 142(6):755–766.

334. Tubbs RR, et al. (2007) Fluorescence in situ hybridization (FISH) as primary methodology for the assessment of HER2 Status in adenocarcinoma of the breast: a single institution experience. *Diagn Mol Pathol* 16(4):207–210.

335. Lewis JT, et al. (2005) Analysis of Intratumoral Heterogeneity and Amplification Status in Breast Carcinomas With Equivocal (2+) HER-2 Immunostaining. *American Journal of Clinical Pathology* 124(2):273–281.

336. Varadan V, et al. (2016) Immune Signatures Following Single Dose Trastuzumab Predict Pathologic Response to PreoperativeTrastuzumab and Chemotherapy in HER2-Positive Early Breast Cancer. *Clin Cancer Res* 22(13):3249–3259.

337. Mayer EL, et al. (2015) Long-Term Follow-Up After Preoperative Trastuzumab and Chemotherapy for HER2-Overexpressing Breast Cancer. *Clinical Breast Cancer* 15(1):24–30.

338. Wolfe AL, et al. (2014) RNA G-quadruplexes cause eIF4A-dependent oncogene translation in cancer. *Nature* 513(7516):65–70.

339. Van Grembergen O, et al. (2016) Portraying breast cancers with long noncoding RNAs. *Sci Adv* 2(9):e1600220–e1600220.

340. Niknafs YS, et al. (2016) The lncRNA landscape of breast cancer reveals a role for DSCAM-AS1 in breast cancer progression. *Nat Commun* 7:12791.

341. Mentch SJ, et al. (2015) Histone Methylation Dynamics and Gene Regulation Occur through the Sensing of One-Carbon Metabolism. *Cell Metab* 22(5):861–873.

342. Shiraki N, et al. (2014) Methionine metabolism regulates maintenance and differentiation of human pluripotent stem cells. *Cell Metab* 19(5):780–794.

343. Towbin BD, et al. (2012) Step-wise methylation of histone H3K9 positions heterochromatin at the nuclear periphery. *Cell* 150(5):934–947.

344. Kim SK, Jung WH, Koo JS (2014) Differential expression of enzymes associated with serine/glycine metabolism in different breast cancer subtypes. *PLoS ONE* 9(6):e101004.

345. Kawamoto S, et al. (2000) A novel reporter mouse strain that expresses enhanced green fluorescent protein upon Cre-mediated recombination. *FEBS Letters* 470(3):263–268.

346. Amin S, et al. (2015) Hoxa2 Selectively Enhances Meis Binding to Change a

Branchial Arch Ground State. *Developmental Cell* 32(3):265–277.

347. Li H, Durbin R (2009) Fast and accurate short read alignment with Burrows-Wheeler transform. *Bioinformatics* 25(14):1754–1760.

348. Zhang Y, et al. (2008) Model-based Analysis of ChIP-Seq (MACS). *Genome Biol* 9(9):R137.

349. Quinlan AR, Hall IM (2010) BEDTools: a flexible suite of utilities for comparing genomic features. *Bioinformatics* 26(6):841–842.

350. Heinz S, et al. (2010) Simple Combinations of Lineage-Determining Transcription Factors Prime cis-Regulatory Elements Required for Macrophage and B Cell Identities. *Molecular Cell* 38(4):576–589.

351. Chen EY, et al. (2013) Enrichr: interactive and collaborative HTML5 gene list enrichment analysis tool. *BMC Bioinformatics* 14(1):128.

352. Tofigh A, et al. (2014) The Prognostic Ease and Difficulty of Invasive Breast Carcinoma. *Cell Reports* 9(1):129–142.

353. Arqués O, Chicote I, Tenbaum S, Puig I, G Palmer H (2012) Standardized Relative Quantification of Immunofluorescence Tissue Staining. *Protocol Exchange*. doi:10.1038/protex.2012.008.

354. Millar EKA, et al. (2008) BAG-1 predicts patient outcome and tamoxifen responsiveness in ER-positive invasive ductal carcinoma of the breast. *Br J Cancer* 100(1):123–133.

355. Zhu J, et al. (2009) The UCSC Cancer Genomics Browser. *Nature Methods* 6(4):239–240.

356. Győrffy B, et al. (2009) An online survival analysis tool to rapidly assess the effect of 22,277 genes on breast cancer prognosis using microarray data of 1,809 patients. *Breast Cancer Research and Treatment* 123(3):725–731.